UNIKASSEL
VERSITÄT

Photoperiod-dependent plasticity of circadian pacemaker center in the brain of the Madeira cockroach *Rhyparobia maderae*

Dissertation zur Erlangung des akademischen Grades

eines Doktors der Naturwissenschaften (Dr. rer. nat.)

im Fachbereich Mathematik und Naturwissenschaften

der Universität Kassel

vorgelegt von

Hongying Wei

Kassel, September 2012

Vom Fachbereich Mathematik und Naturwissenschaften der Universität Kassel als Dissertation am 05.09.2012 angenommen.

Erstgutachter: Prof. Dr. Monika Stengl

Zweitgutachter: Prof. Dr. Charlotte Helfrich-Förster

Tag der mündlichen Prüfung: 05.11.2012

Erklärung

Hiermit versichere ich, dass ich die vorliegende Dissertation selbständig und ohne unerlaubte Hilfe angefertigt und andere als die in der Dissertation angegebenen Hilfsmittel nicht benutzt habe. Alle Stellen, die wörtlich oder sinngemäß aus veröffentlichten oder unveröffentlichten Schriften entnommen sind, habe ich als solche kenntlich gemacht. Kein Teil dieser Arbeit ist in einem anderen Promotions oder Habilitationsverfahren verwendet worden.

Kassel, September 2012

Hongying Wei

Contents

Summary

To various degrees, insects in nature adapt to and live with two fundamental environmental rhythms around them: (1) the daily rhythm of light and dark, and (2) the yearly seasonal rhythm of the changing photoperiod (length of light per day). It is hypothesized that two biological clocks evolved in organisms on earth which allow them to harmonize successfully with the two environmental rhythms: (1) the circadian clock, which orchestrates circadian rhythms in physiology and behavior, and (2) the photoperiodic clock, which allows for physiological adaptations to changes in photoperiod during the course of the year (insect photoperiodism). The circadian rhythm is endogenous and continues in constant conditions, while photoperiodism requires specific light inputs of a minimal duration. Output pathways from both clocks control neurosecretory cells which regulate growth and reproduction. This dissertation focuses on the question whether different photoperiods change the network and physiology of the circadian clock of an originally equatorial cockroach species. It is assumed that photoperiod-dependent plasticity of the cockroach circadian clock allows for adaptations in physiology and behavior without the need for a separate photoperiodic clock circuit.

The Madeira cockroach *Rhyparobia maderae* is a well established circadian clock model system. Lesion and transplantation studies identified the accessory medulla (aMe), a small neuropil with about 250 neurons, as the cockroach circadian pacemaker. Among them, the pigment-dispersing factor immunoreactive (PDF-ir) neurons anterior to the aMe (aPDFMes) play a key role as inputs to and outputs of the circadian clock system.

The aim of my doctoral thesis was to examine whether and how different photoperiods modify the circadian clock system. With immunocytochemical studies, three-dimensional (3D) reconstruction, standardization and Ca^{2+}-imaging technique, my studies revealed that raising cockroaches in different photoperiods changed the neuronal network of the circadian clock (Wei and Stengl, 2011). In addition, different photoperiods affected the physiology of single, isolated circadian pacemaker neurons. This thesis provides new evidence for the involvement of the circadian clock in insect photoperiodism. The data suggest that the circadian pacemaker system of the Madeira cockroach has the plasticity and potential to allow for physiological adaptations to different photoperiods. Therefore, it may express also properties of a photoperiodic clock.

This doctoral thesis consists of 6 chapters, focusing on 4 main research themes:

(1) Spatial reconstruction and analysis of the structural changes of PDF-ir circadian pacemaker neurons in response to different photoperiods. (Chapter I and II).
(2) Identification of ion channels producing and underlying spontaneous activity of the aMe neurons and analysis of physiological responses of circadian clock neurons to different photoperiods. (Chapter III and V).
(3) Determination of the role of the neurotransmitters acetycholine (ACh) and histamine in the circadian clock and the modulation of ACh-responses via photoperiod (Chapter IV and V).
(4) Assessment of the suitability of terminated ultrananocrystalline diamond surfaces for the cockroach circadian pacemaker cell cultures as a prerequisite to the development of long-term recording devices. (Chapter VI).

Chapter I: Implementation of pigment-dispersing factor-immunoreactive neurons in a standardized atlas of the brain of the cockroach *Leucophaea maderae*

Chapter I describes and analyses the spatial distribution of neuropils in the Madeira cockroach brain and the PDF-ir circadian pacemaker neurons. To facilitate understanding and comparison of the connectivity patterns of circadian pacemaker neurons, a standardized three-dimensional (3D) atlas of the cockroach brain comprising 21 neuropils was generated. Two different standardization protocols were employed: (1) the virtual insect brain protocol (VIB) using global and local rigid transformations followed by local non-rigid transformations, and (2) the iterative shape averaging (ISA) method employing image-intensity-based iterative non-rigid registrations after an affine transformation. While the VIB protocol can be used to determine time- or stimulus-dependent differences in the individual brain, the ISA protocol is designed to maximize the entropy-based normalized mutual information to obtain an intensity-based average brain for neuronal implementation. Quantitative analysis of 20 individual cockroach brains revealed that volumes of the aMe are significantly correlated with the volumes of the medulla, the protocerebral bridge, and the upper division of the central body. These quantitative relationships between the neuropils suggest functional connections between them. In a second step, the branching pattern of PDF-ir circadian pacemaker neurons was implemented into the ISA standard brain. The 3D reconstruction of the network of the PDF-ir neurons reveals two new features of the PDF-ir branching pattern: (1) two PDF-ir arborization areas, the plexus1 and the anterior fiber plexus (AFP), are highly interconnected with other PDF-ir projection sites, which might allow for information exchange between the anterior and posterior commissures (AOC and POC). (2) The distances between PDF-ir branching sites show specific numerical relationships, reminiscent of delay lines employed in temporal encoding schemes in the auditory cortex. This suggests that the timing of parallel outputs of the PDF-ir neurons may maintain defined phase-differences in the respective postsynaptic neurons.

Chapter II: Light affects the branching pattern of peptidergic circadian pacemaker neurons in the brain of the cockroach *Leucophaea maderae*

Chapter II determines whether and how light affects the neuronal circuits of circadian pacemaker neurons of the Madeira cockroach. The cockroaches were raised in different photoperiods (6:18 light:dark LD, 12:12, or 18:6), or in different T-cycles (with different hours per day) (11:11, 12:12 or 13:13). The cockroach brains from different groups were immunostained with antisera against PDF and/or orcokinin. Orcokinin is assumed to be involved in the light-entrainment pathway to the circadian clock. Photoperiod with long day (18:6) increased the number of large- and medium-sized aPDFMes, while short day (6:18) only decreased the medium-sized aPDFMes. In LD 11:11 cycles, only the number of medium-sized specifically decreased, while it increased in 13:13. Moreover, the PDF-ir fibers in the AOC and orcokinin-ir fibers both in AOC and POC were sensitive to different

photoperiods. Thus, light affected the number and branching pattern of PDF-ir neurons, especially the medium-sized aPDFMes, which colocalize orcokinin-immunoreactivity and which could respond to photoperiod specifically. In addition, the different photoperiods changed the numerical relationships of distances between PDF-ir branching sites, which could possibly allow for temporal encoding of different photoperiods. The data suggested that the same neuronal circuits which constitute a circadian pacemaker center could also serve for photoperiodic adaptations.

Chapter III: Ca^{2+}-dependent ion channels underlying spontaneous activity in insect circadian pacemaker neurons

Chapter III identifies pacemaker channels and ionic mechanisms controlling spontaneous Ca^{2+} transients of cultured circadian pacemaker neurons of the Madeira cockroach, using Ca^{2+}-imaging combined with pharmacology. The fast spontaneous Ca^{2+} transients characterized by a rapid increase in intracellular Ca^{2+} concentration and a double exponential decay, occurred in about 26% of the cultured aMe cells. The tetrodotoxin (TTX) blockable fast spontaneous Ca^{2+} transients in the cultured aMe neurons accompany the TTX-sensitive spontaneous spiking activity. Thus, spontaneous Ca^{2+} transients are indicative of spontaneous action potential activity. Spontaneous activity is predominantly driven by mibefradil-sensitive, low-voltage-activated Ca^{2+} channels (L-VACC) and DK-AH269-sensitive hyperpolarization-activated, cyclic nucleotide-gated (HCN) cation channels, but not by TTX-sensitive sustained Na^{+} channels. The excitatory drive from such “pacemaker channels” (L-VACCs and HCNs) activate the voltage-activated Na^{+} channels and nifedipine-sensitive high- VACCs. Together with Ca^{2+} rises, resulting depolarizations open small conduction Ca^{2+}-dependent K^{+} channels (SKs). The P/Q-type VACCs couple to large-conduction Ca^{2+}-dependent K^{+} channels (BKs), which could override pacemaker channels and promote input-dependent inhibition of the spontaneous activity.

Chapter IV: Calcium responses of circadian pacemaker neurons of the cockroach *Rhyparobia maderae* to acetylcholine and histamine

Chapter IV summarizes the Ca^{2+} responses of cultured circadian pacemaker neurons of the Madeira cockroach to the neurotransmitters acetylcholine (ACh) and histamine (HA). The ACh, as a prominent excitatory neurotransmitter, increased the intracellular Ca^{2+} levels of the aMe cells in a dose-dependent manner via nicotinic receptors. The HA, as a prominent inhibitory neurotransmitter, decreased intracellular Ca^{2+} levels of the aMe cells. Moreover, in contrast to ACh, the sustained HA response remained for several minutes after washout. These data suggest that ACh and HA act as neurotransmitters in the Madeira cockroach circadian system and may play a role in the light entrainment pathway (ACh) or in a non-photic input pathway (HA) to the circadian clock.

Chapter V: Photoperiod affects the physiological responses of cultured circadian pacemaker neurons in the Madeira cockroach *Rhyparobia maderae*

Chapter V presents evidence that physiological responses of circadian pacemaker neurons of the Madeira cockroach are photoperiod-sensitive. The spontaneous activity of cultured aMe circadian pacemaker neurons changed in response to increases in the extracellular Ca^{2+} concentration. According to presence or absence of spontaneous activity in salines with low, normal, and high Ca^{2+} levels, different physiological response types of the aMe cells from the same cockroach were distinguished. The cockroaches reared in different photoperiods (6:18, 12:12, or 18:6) showed different percentage distributions of different response types (type-percentage vectors). The type-percentage vectors are highly reproducible and photoperiod-specific. The data suggested that the ion channel composition of the cultured cockroach circadian pacemaker neurons could encode photoperiodic information, and therefore, could be involved in photoperiod-dependent adaptations of behavior and/or physiology. In addition, to test a possibly role of ACh in photoperiod-dependent plasticity, the effect of ACh on intracellular Ca^{2+} levels of the culture aMe neurons from different photoperiodic cockroach groups were compared and analyzed. Comparison of the ACh effect on all tested aMe cells did not provide evidences for the change of ACh-sensitivity of cultured aMe cells by photoperiods. However, it cannot be excluded that ACh relays photoperiodic information only to a small minority of aMe cells.

Chapter VI: Influence of the surface termination of ultrananocrystalline diamond/amorphous carbon composite films on their interaction with neurons

Chapter VI assesses of the suitability of terminated ultrananocrystalline diamond (UNCD) surfaces for the cockroach circadian pacemaker cell cultures. The H-, OH- and NH_2 terminated UNCD surfaces (produced by Alexandra Voss, Institute of Nanostructure Technologies and Analytics, University of Kassel) were used to generate the aMe cell cultures. The OH- and NH_2 terminated UNCD surfaces allow for a faster, stronger attachment of neurons without compromising their viability. Thus, the UNCD surfaces can be used as basic cell adhesive surface for the cultured insect neurons. In the future we want to employ these new surfaces for the development of long-term recording devises of the circadian pacemaker neurons.

Contribution Statement

My contributions for each chapter will be stated clearly as follows.

Chapter I: Implementation of pigment-dispersing factor immunoreactive neurons in a standardized atlas of the brain of the cockroach *Leucophaea maderae*

- Designed and conducted experiments, data analysis
- The double immunostaining of brains were carried out during my master thesis "Three dimensional distribution of pigment dispersing factor in a standard brain of the cockroach *Leucophaea maderae*", Marburg, 2008. The standardization processes and statistical analyses were performed during the dissertation.
- Wrote the manuscript together with Prof. Dr. Monika Stengl, Dr. Basil el Jundi and Prof. Dr. Uwe Homberg
- This manuscript is published in:
  Wei HY, el Jundi B, Homberg U, and Stengl M. (2010)
  J Comp Neurol 518: 4113-4133.

Chapter II: Light affects the branching pattern of peptidergic circadian pacemaker neurons in the brain of the cockroach *Leucophaea maderae*

- Designed and conducted experiments, data analysis
- Wrote the manuscript together with Prof. Dr. Monika Stengl
- This manuscript is published in:
  Wei HY, and Stengl M. (2011)
  J Biol Rhythms 26: 507–517.

Chapter III: Ca^{2+}-dependent ion channels underlying spontaneous activity in insect circadian pacemaker neurons

- Designed and conducted experiments, data analysis
- Wrote the manuscript together with Prof. Dr. Monika Stengl
- This manuscript is published in:
  Wei HY, and Stengl M. (2012)
  Eur J Neurosci. doi:10.1111/j.1460-9568.2012.08227.x.

Chapter IV: Calcium responses of circadian pacemaker neurons of the cockroach *Rhyparobia maderae* to acetylcholine and histamine

- Designed and conducted experiments, data analysis for the acetylcholine dose response curve together with Johannes Grosshans. The acetylcholine pharmacology was performed together with El-Sayed Baz. The histamin response experiments were carried out by El-Sayed Baz.
- Wrote the manuscript together with Prof. Dr. Monika Stengl and El-Sayed Baz
- This manuscript has been submitted in the Journal of Experimental Biology.

Chapter V: Photoperiod affects physiological responses of cultured circadian pacemaker neurons in the Madeira cockroach *Rhyparobia maderae*

- Designed and conducted experiments, data analysis for the response types and type-percentage vectors. The acetylcholine response analyses were carried out by El-Sayed Baz.
- Wrote the manuscript together with Prof. Dr. Monika Stengl and El-Sayed Baz
- This manuscript will be submitted in the Journal of Biological Rhythms.

Chapter VI: Influence of the surface termination of ultrananocrystalline diamond/amorphous carbon composite films on their interaction with neurons

- Cell culture preparation, Calcium imaging experiments, statistical analysis for the cell density, potassium chloride responses and spontaneous activity of the cell cultures by candidate.
- Wrote the neuronal parts in manuscript together with Prof. Dr. Monika Stengl.
- This manuscript is published in:
  Voss A, Wei HY, Müller C, Popov C, Kulisch W, Ceccone G, Ziegler C, Stengl M, and Reithmaier JP. (2012)
  Diamond and Related Materials 26: 60-65.

Introduction

Insect photoperiodism

Like all planets in the solar system, the earth revolves around the sun in an elliptical orbit, which gives rise to the procession of seasonal changes. The 23.5 degrees inclination of the earth's axis with respect to the plane of its orbit determines the seasonal differences in the length of the light/dark (LD) cycles (photoperiod). **The Photoperiod** (the length of the light phase per day = daylength) changes systematically throughout the year, becoming longer during the summer and shorter during the winter (Fig.1). For equator-distant organisms, higher latitudes express remarkable seasonal changes in climate, with winters becoming colder and longer. To survive the cold and unfavorable environmental conditions, the majority of insects have evolved several strategies of adaptation. **Photoperiodism** is defined as a change of physiology and/or behavior in response to changes in photoperiod. For example night-active rodents and insects extend their activity phase during short-day conditions, while they shorten it during long-day conditions. Swarming and migration to the south could be a photoperiod-induced change of behavior. Photoperiod-dependent changes in physiology are e.g. the short day-dependent initiation of diapause. Insects living at temperate and polar climate zones (latitudes) initiate a cascade of hormonal changes that culminate in diapause. Diapause is a stage of developmental arrest with interruptions or alteration of neuroendocrine activity. Depending on the species, diapause can occur at any developmental stage, from embryo to adult. Embryonic diapause is an arrest of embryogenesis. Pupal and larval diapause is an arrest of growth and differentiation at the pupal or larval stages, respectively. Adult diapause is characterized by absence of reproductive activity and reduced female ovarian development. Other photoperiodic physiological adaptations are production of "antifreeze"-molecules in the hemolymph or increase of energy reservoirs.

The photoperiod-dependent change in locomotor behavior may be a direct light stimulus-dependent response. Alternatively, it may be controlled by an endogenous clock which is photoperiod-sensitive. Currently, it is generally assumed that an endogenous **photoperiodic clock** underlies photoperiodism. Its relationship to endogenous circadian clocks is under discussion.

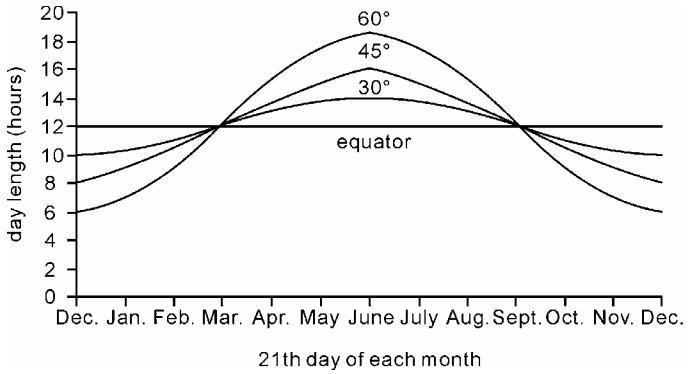

Figure 1. Day length (hours) over the course of a year at different latitudes (Redrawn after Palmer, 1976).

Structure and function of photoperiodic systems in insects

The photoperiodic system of insects is hypothesized to consist of three components: a photoperiod-sensitive photoreceptor/mechanism (e.g. light input pathway, or light-sensitive enzymes), the photoperiodic clock (core mechanism), and outputs to behavior and/or control of hormone release (hormonal effectors) (Fig.2) (Emerson et al., 2009; Vladimir, 2011).

(A) Reported **photoperiod-sensitive photoreceptors/mechanisms** were located in the brain (extraretinal photoreceptors) and in the compound eyes (retinal photoreceptors). Both types of photoreception vary in different species and appear to be cooperatively involved in the input pathway of photoperiodism. In adults of the bug *Plautia crossota stali* removal of the compound eyes terminated their diapause, however, could not delete the photoperiodic response completely (Morita and Numata, 1999). Thus, in *P. crossota stali* next to the predominant role of compound eyes, also extraretinal photoreception in the brain appears to exist. In larvae of the butterfly *Pieris brassicae*, in contrast, the brain plays the predominant role in photoperiodic photoreception. Their stemmata are only subordinate photoreceptors for photoperiodism (Seuge and Veith, 1976). In insects, pigments with a caroteniod-derived chromophore coupled to opsin were shown to be involved in photoperiodism (Numata et al., 1997). In the aphid *Megoura viciae*, using immunocytochemistry with antibodies against different opsins, the photoperiodic photoreceptor in the brain was located to an anterior ventral neuropil region of the protocerebrum (Gao et al., 1999). In the larval brain of the silkworm *Bombyx mori*, the cerebral opsin (boceropsin) labeled cells were found in four regions: the dorsal anterior protocerebrum, the ventral anterior protocerebrum, the dorsal posterior protocerebrum and the lateral posterior tritocerebrum (Shimizu et al., 2001).

(B) The core **photoperiodic clock** for photoperiodism is hypothesized to consist of a "**photoperiodic timer**" and a "**photoperiodic counter**" of non-defined cellular nature (Emersion et al., 2009). The "photoperiodic timer" can distinguish different photoperiods. It is either identical with (A), the photoperiodic photoreceptor, or it receives input from a photoperiodic photoreceptor/mechanism which measures actual duration of daylength. Furthermore, it can distinguish whether the day is either "long" or "short". Depending on its distinction it initiates differential outputs such as an increase or a decrease in action potential frequency. In most insect species, a minimum number of long- or short days are required to initiate a photoperiodic response. Thus, a "photoperiodic counter" was suggested to "count" the number of consecutive short or long days. Then, after a certain number of days e.g. diapause is initiated. Under the assumption that the photoperiodic counter has to store the information from the photoperiodic timer for a certain number of days, Ikeda et al. (2005) tested whether the mushroom bodies (MB), which are the memory center of insect brains, were involved in the counter system. Ablation of the MB of blow flies *Protophormia terraenovae* did not prevent their adult diapause. Thus, the MB is not required for photoperiodism in this insect species.

Still, the cellular nature of the various photoperiodic clock components remains to

be identified. Several studies have indicated that the photoperiodic clock is probably based upon damping circadian oscillators (Saunders, 2010a). The possible relationships between photoperiodic and circadian clocks will be discussed in a later chapter of my thesis.

(C) The photoperiodic clock initiates behavioral and physiological changes via outputs to **locomotor control centers** and to **hormonal effectors**. Known locomotor control centers are the neural circuits of the central complex in the middle of the insect brain. In addition, locomotor control centers are located in less well characterized regions of the protocerebrum which connect to descending neurons which relay information to central pattern generators in the thoracic ganglia. Furthermore, neurosecretory cells in the *pars intercerebralis* (PI) and *pars lateralis* (PL) of the insect dorsal and lateral protocerebrum are the most likely hormonal effectors targeted by the photoperiodic clock. These neurons release neuropeptides (e.g. prothoracicotropic neurohormone PTTH, allatostatins, allatotropins, and insulin-like peptides). Or they use direct axonal connections to control the activity of neurohemal organs, such as the *corpora cardiaca* (CC), the *corpora allata* (CA), and endocrine glands such as the prothoracic gland, which all release key hormones for insect development and physiology. In adult diapause, the biosynthesis of juvenile hormone (JH) in CA is reduced, which leads to reduced ovarian development in females of different species (Matsuo et al., 1997; Shiga et al., 2003). Furthermore, Horseman et al. (1994) showed that electrical stimulation of PL neurons significantly suppressed the JH synthesis in locusts *Locusta migratoria*. The connections of PI and PL neurons with the CA and CC were described in several insect species, such as the Colorado potato beetle (Khan et al., 1986) and the blow fly *P. terraenovae* (Shiga and Numata, 2000). Ablation experiments showed that PI and PL are involved also in ovarian development and diapause induction in the linden bug *Pyrrhocoris apterus* (Hodkova, 1976) and the blow fly *P. terraenovae* (Shiga and Numata, 2000). Furthermore, ecdysteroids are also fundamentally important hormones for the regulation of adult diapause in dipterans (Brown et al., 1998; Richard et al., 1998; Raikhel et al., 2005). Biosynthesis and release of ecdysteroids from the prothoracic gland can terminate pupal and larval diapause (Denlinger et al., 2005). In the tobacco hornworm *Manduca sexta* PTTH of PL neurons stimulated production of ecdysteroids in the prothoracic gland (Agui et al., 1979; Shiga et al., 2003; Siegmund and Korge, 2001). In contrast, embryonic diapause in silkmoth *B. mori* is under maternal control. The diapause hormone from neurosecretory cells in the subesophageal ganglion of the mother can induce embryonic diapause of the next generation (Sato et al., 1994; Yamashita, 1996).

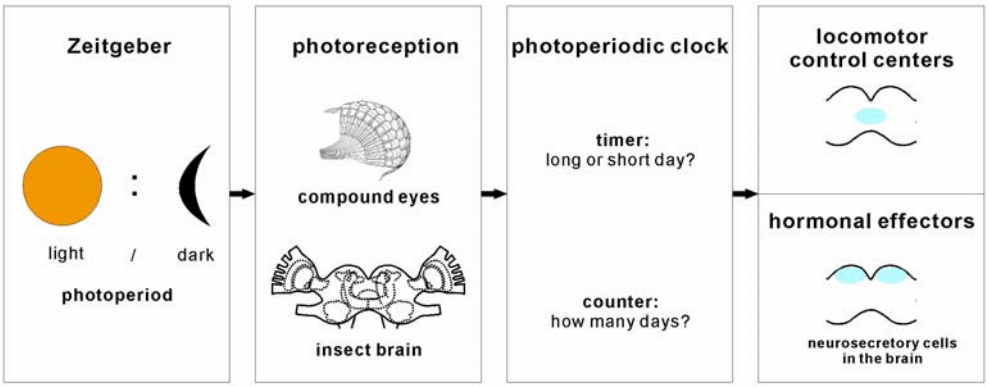

Figure 2. Scheme of insect photoperiodism. Photoperiodic information (light/dark cycle) from Zeitgeber is received by the insect brain or compound eye (photoreception) and then transmitted to a proposed photoperiodic clock neural network. A **photoperiodic timer** decides whether the day is either "long" or "short". A **photoperiodic counter** counts the consecutive photoperiodic cycles. Output pathways connect the photoperiodic clock to locomotor control centers and hormonal effectors, which release specific neurohormones or neurotransmitters. They control the synthesis and release of developmental hormones, which decide over the development state (development or diapause).

The circadian clock system of *Drosophila melanogaster*

There is another fundamental rhythm of light that insects encounter: next to the photoperiod, the circadian rhythm, which is caused by the rotation of the earth about its axis. The term "circadian" is derived from the Latin "circa", meaning "approximately", and "dies", meaning "day". A circadian rhythm is any biological process/oscillation with an about-24-hour period, driven by an endogenous circadian clock. Circadian rhythms can be entrained by external Zeitgeber, such as rhythmic changes in light and temperature. The Zeitgeber rhythm and the internal circadian rhythm of the organism maintain a fixed phase relationship forced by the Zeitgeber. **Phase** is defined as any defined state (the amplitude) of the rhythm such as the beginning of locomotor activity for the circadian locomotor activity rhythm. **Period** (τ = tau, duration of rhythm) is the shortest distance between same phases of a rhythm. The period is temperature-compensated over a wide temperature range and is genetically determined for the respective species.

Circadian systems are organized into three components: (A) Input pathways (entrainment pathways) synchronize the clock to the environmental rhythm or Zeitgeber via respective **photoreceptors**. (B) An intrinsic, self-sustained **circadian clock** (oscillator, pacemaker center) maintains the endogenous rhythm. (C) Output pathways control downstream oscillators or/and **effectors** such as control centers of locomotion or hormone release centers (effector pathways). The outputs temporally organize the molecular, cellular, physiological and behavioral responses relative to one another. The three components are not necessarily separate neuronal circuits or cells. The effectors also feed-back to the core clock and entrainment pathways (Fig.3).

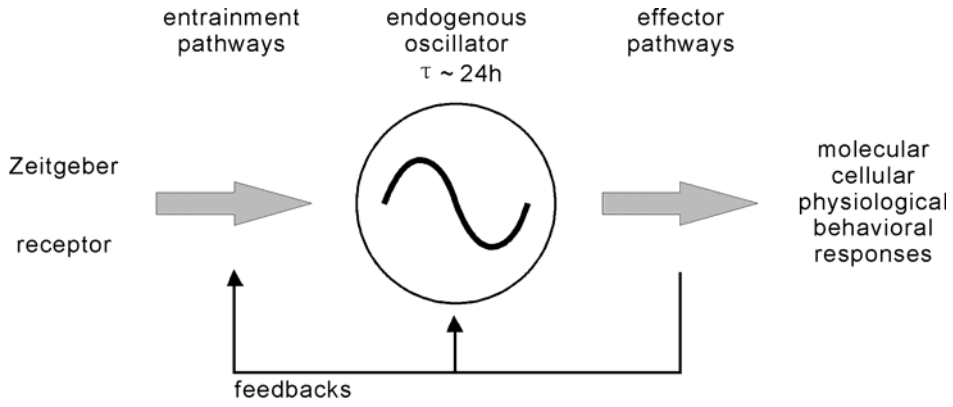

Figure 3. Schematic structure of the circadian clock system. It consists of an endogenous clock with an endogenous period of approximately 24 hours. The **circadian clock** is synchronized with external rhythms (Zeitgeber) via **entrainment pathways**, and controls the molecular, cellular, physiological, and behavioral responses via **effector pathways**, which feed-back to clock and entrainment pathways.

Molecular clockwork in the brain of D. melanogaster

The circadian pacemaker neurons express a molecular circadian clockwork, here defined as **nuclear circadian clock**. Extensive studies were carried out in the fruit fly *D. melanogaster*, the best established insect model for genetic studies. Since the 1990s, many clock genes were discovered (Table1) (Allada et al., 1998; Edery, 2000; Williams et al., 2001; Cyran, 2003). The nuclear circadian clock generates circadian rhythms in clock gene expression, resulting in circadian rhythms of mRNA and protein concentrations in the cytoplasm. The clock genes *period* (*per*) and *timeless* (*tim*), which code for the clock proteins PERIOD (PER) and TIMELESS (TIM) respectively, form an integral transcriptional-translational feedback loop which is interlaced with other feedback loops of other circadian clock genes. While the *per/tim* mRNA levels peak during the early subjective night, their protein levels are maximal during the late night. Two nuclear clock proteins CLOCK-CYCLE (CLK-CYC) heterodimerize in the nucleus to promote *per* and *tim* transcription. In the early night, the *per* and *tim* mRNAs are transported to the cytoplasm and translated into their respective proteins PER and TIM. In the cytoplasm TIM forms heterodimers with PER and, thereby, protects it from degradation. Starting in the early night and peaking in the late night, PER and TIM move back into the nucleus apparently as heterodimers as well as independently of each other. Inside the nucleus, PER-TIM might dissociate. There, PER directly inhibits its own as well as *tim* transcription via interference with the transcription factors CLK-CYC. This process leads to lower *per* and *tim* mRNA transcription levels. Nuclear PER then is degraded, resulting in derepression of *per* and *tim* transcription. In the presence of light, the blue light photoreceptor protein CRYPTOCHROME (CRY) binds TIM, prevents its dimerization with PER, and subsequently leads to TIM degradation. PER dissociates and enters into the nucleus. (Tomioka and Matsumoto, 2010; Peschel and Helfrich-Förster, 2011) (Fig.4).

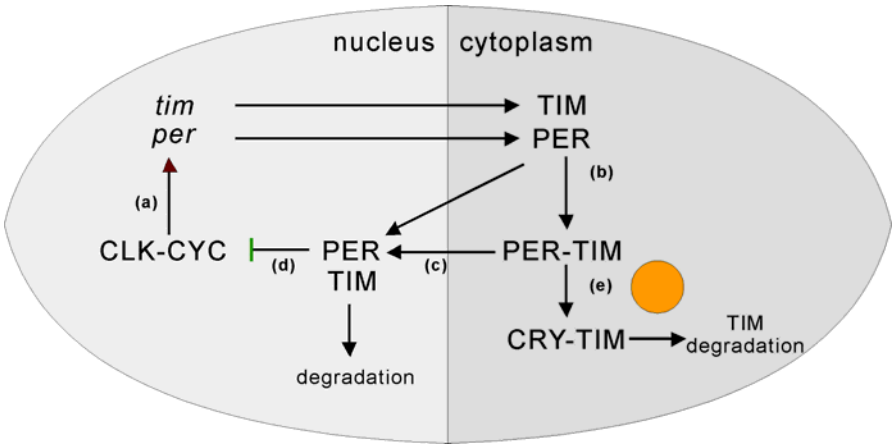

Figure 4. Simplified schematic structure of *period-timeless* circadian clockwork in the *Drosophila* circadian pacemaker neurons. (a) The CLOCK-CYCLE (CLK-CYC) heterodimer is a transcription factor for *period* and *timeless* (*per*, *tim*) transcription. (b) In the early night, *per* and *tim* mRNAs are transported to the cytoplasm and translated into proteins PERIOD (PER) and TIMELESS (TIM), respectively, which start moving into the nucleus. (b) PER heterodimerizes with TIM and, therefore, is stabilized. (c) Starting in the early night and peaking in the late night, PER and TIM moved back into the nucleus apparently as heterodimer as well as independently of each other. (d) Nuclear PER inhibits the transcription factors CLK-CYC, and, therefore inhibits *per* and *tim* transcription. (e) In addition, morning light promotes the binding of photoreceptor CRYPTOCHROME (CRY) with TIM in the cytoplasm. PER dissociates and enters into the nucleus. (modified from Emerson et al, 2009)

Table1. Circadian clock genes in *Drosophila melanogaster*

Gene	Clock role	references
period (per)	negative regulator of Clk Cyc	Konopka et al., 1971
timeless (tim)	negative regulator of Clk Cyc light sensitive	Sehgal et al., 1994
clock (clk)	positive regulator of *per tim*	Allada et al., 1998
cycle (cyc)	positive regulator of *per tim*	Allada et al., 1998
doubletime	phosphorylates PER protein	Price et al., 1998
vrille	blocks per and tim expression	Blau et al., 1999
cryptochrome	Photoreceptor input pathway	Stanewsky et al., 1998

Cellular circuit of circadian pacemaker neurons in the brain of D. melanogaster

In the brain of *D. melanogaster* seven clusters of circadian clock neurons have been characterized: the large and small ventrolateral neurons (l-LNv, s-LNv), the dorsal lateral neurons (LNd), the lateral posterior neurons (LPN) and there groups of dorsal neurons (DN_1, DN_2, DN_3). Among the DN_1s, a pair of cells lies more anterior and therefore they are called $DN_{1anterior}$ (DN_{1a}). The remaining DN_1s lie more posterior and are called $DN_{1posterior}$ (DN_{1p}) (Fig.5). Photoreceptors of the compound eyes, the Hofbauer-Bucher

(H-B) eyelet (adults) or Bolwig`s organ (larvae) are involved in entrainment pathways (Helfrich-Förster et al., 2001). The protein CRY plays an important role in rapid, light-dependent TIM degradation, which is the main regulator for the phase-synchronization of the circadian clock with the environmental light dark cycle. The s-LNv neurons receive light information directly from the H-B eyelet, and the l-LNv neurons from the compound eyes (Helfrich-Förster et al., 2001; Collins et al., 2005). Pigment-dispersing factor (PDF), the insect homologue of the decapods pigment-dispersing hormone, is a well-characterized output signal from the circadian clock. The LNv neurons (s-LNv and l-LNv, except 5th s-LNv) express PDF under the control of clock genes (Helfrich-Förster, 1995; Park et al., 2000). However, the ectopic expression of PDF does not influence the circadian expression of clock genes (Helfrich-Förster et al., 2000). Apart from l-LNv neurons, apparently all clock neurons contain the G-protein-coupled PDF receptor (Shafer et al., 2008) (Fig.6). In addition, using immunocytochemistry, visualization of PER, TIM, and PDF showed that all clock neurons appear to be connected and project to the dorsal protocerebrum and to the optic lobes (Kaneko and Hall, 2000). PDF is released to act as output signal, synchronizes the individual clock neurons, transfers the information to downstream neurons, and controls different aspects of the physiological and behavioral activity rhythms (Peng et al., 2003; Lin et al., 2004, Nitabach et al., 2006; Yoshii et al., 2009).

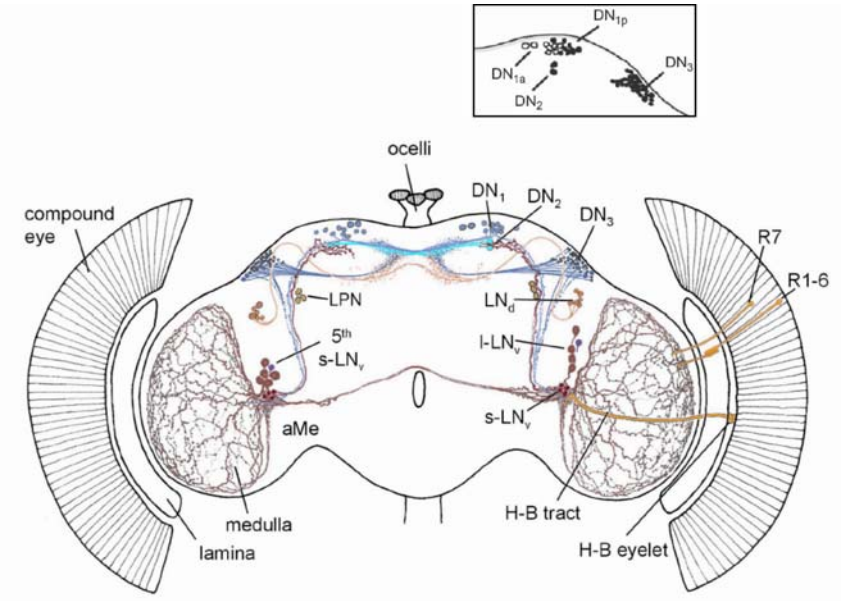

Figure 5. Circadian pacemaker neurons and their projection areas in the brain of *Drosophila melanogaster*. They express circadian clock genes and consist of seven clusters: the large and small ventrolateral neurons (l-LNv and s-LNv), the dorsal lateral neurons (LNd), the lateral posterior neurons (LPN) and dorsal neurons 1-3 (DN_1, DN_2, DN_3). According to the location, DN_1s are subdivided into anterior DN_1s (DN_{1a}) and posterior DN_1s (DN_{1p}). The circadian pacemaker center, the accessory medulla (aMe) is innervated by projections from s-LNs (except 5th s-LNs), l-LNv, DN1 and DN3. Except l-LNv, all the other clock neurons project their axons into the dorsal photocerebrum. Light information is transmitted from photoreceptor cells R1-6 and R7/8 of the compound eye and from the four Hofbauer-Buchner (H-B) eyelet cells to the circadian system. (modified from Helfrich-Förster et al., 2007 and Yoshii et al., 2012)

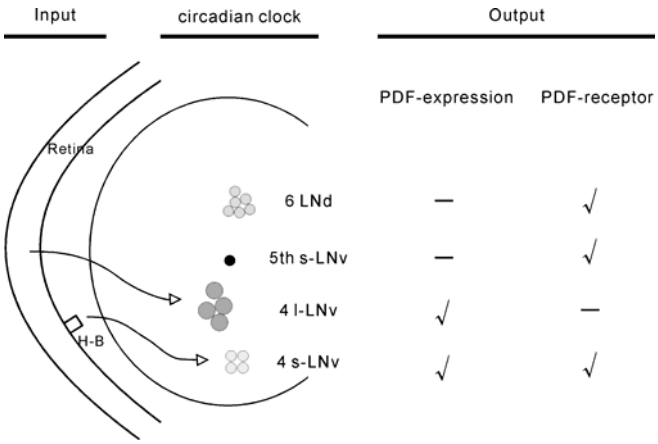

Figure 6. Simplified schematic structure of the dorsal lateral neurons (LNd) and ventral lateral neurons (LNv) of *Drosophila melanogaster*. According to their size, LNv neurons are subdivided into 4 large and 5 small ventrolateral neurons (l-LNv and s-LNv). The 4 l-LNv neurons and 4 s-LNv receive the light input from the compound eye and the Hofbauer-Bucher (H-B) eyelet, respectively. Pigment-dispersing factor (PDF), the well identified output neuropeptide, is expressed in 4 l-LNv and 4 s-LNv, but not in the 5th s-LNv and 6LNd. Apart from 4 l-LNv neurons, all clock neurons contain the G-protein-coupled PDF receptor (strong modified from Helfrich-Förster, 2009).

Morning and Evening Oscillator Model in the brain of D. melanogaster

Typically, the fruit fly *D. melanogaster* shows bimodal locomotor activity rhythmus with an activity peak in the morning associated with light-on and an activity peak in the evening associated with light-off (Helfrich-Förster, 2009). Helfrich-Förster (2001) based upon a model by Pittendrigh and Daan (1976) suggested a Zeitgeber-dependent dual-oscillator system consisting of morning oscillator (M-cells) and evening oscillator (E-cells), which underlie the light-on morning and light-off evening activity peaks. Later, two research groups (Grima et al., 2004; Stoleru et al., 2004) suggested that the M and E cells are located in specific clock neurons separately: the M oscillator in s-LNv and the E oscillator in LNd. In addition, DNs seem to contain M and E oscillators (Stoleru et al., 2004). Further analysis of the M-E oscillator system resulted in a better identification of M and E cells and further improvement of the original model (Rieger et al., 2006; Bachleiter et al., 2007; Murad et al., 2007; Picot et al., 2007; Cusumano et al., 2009; Helfrich-Förster, 2009; Zhang et al., 2010; Yoshii et al. 2012). Figure 7 summarizes the M and E cells in the *Drosophila* brain. The **M cells** are: 4s-LNv neurons and CRY-positive DN_{1p}s. The **E cells** are: the 5th s-LNv, 3 CRY-positive LNd neurons and perhaps the CRY-negative DN_{1p}s. The M and E cells could be mutual regulated and functionally coupled (Stoleru et al., 2005; Murad et al., 2007; Picot et al., 2007; Stoleru et al., 2007; Parisky et al., 2008; Helfrich-Förster, 2009; Rieger et al., 2009; Sheeba et al., 2010). The M cells appear to be regulated by l-LNv neurons via PDF, which receive the light information from the compound eye (Shafer et al., 2008; Sheeba et al., 2008a, 2008b; Wülbeck et al., 2008). The regulatory function of PDF for the E cells was confirmed by Cusumano et al. (2009). Duvall and Taghert (2012) showed the PDF-signaling in M and E cells was different. While

the PDF-signaling in the M cells couples preferentially to a single adenylate cyclase (AC3), the PDF-signal activates other AC(s).

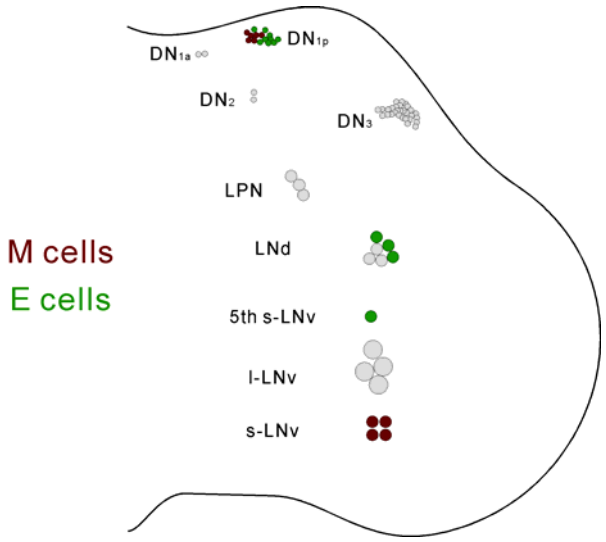

Figure 7. Schematic representation of morning (M) and evening (E) cells in the brain of *Drosophila melanogaster*. The M cells are 4 small ventrolateral neurons (s-LNv) and CRYPTOCHROME (CRY)-positive neurons in posterior dorsal neuron group1 (DN_{1p}s). The E cells are three CRY-positive dorsal lateral neurons (LNd), the 5th s-LNv and the CRY-negative DN_{1p}s. The large ventrolateral neurons (l-LNv) receive and transfer light information from the compound eye to the M cells via pigment dispersing factor (PDF). LPN, lateral posterior neurons. DN_2, dorsal neuron group 2. DN_3, dorsal neuron group 3. (modified from Yoshii et al., 2012)

Circadian clock system in Madeira cockroach *Rhyparobia maderae*

While the fruit fly is an important model organism for molecular genetic studies, the Madeira cockroach *Rhyparobia maderae* (Syn.: *Leucophaea maderae*) is well suited for anatomical, physiological, and behavioral studies of the circadian clock system.

The Madeira cockroach was the first animal where lesion studies located an endogenous circadian pacemaker in the brain. The accessory medulla (aMe) with associated neurons is the circadian pacemaker controlling circadian locomotor activity (Nishiitsutsuji-Uwo and Pittendrigh, 1968; Roberts, 1974; Sokolove, 1975; Page, 1982; Stengl and Homberg, 1994; Reischig and Stengl, 2003a). The aMe is a small pear-shaped neuropil at the anterior-proximal edge of the medulla in the optic lobes. The aMe shows a clear non-retinotopical neuroarchitecture and consists of nodular and internodular neuropil, next to a shell region. Seven soma groups with about 250 neurons are associated with the aMe. They are defined as: anterior neurons (ANes), distal and medial groups of fronto-ventral neurons (DFVNes, MFVNes), median neurons (MNes), ventral neurons (VNes), ventromedian neurons (VMNes), and ventro-posterior neurons (VPNes), according to their position relative to the aMe (Reischig and Stengl, 1996, 2003b; Söhler et al., 2008) (Fig.8).

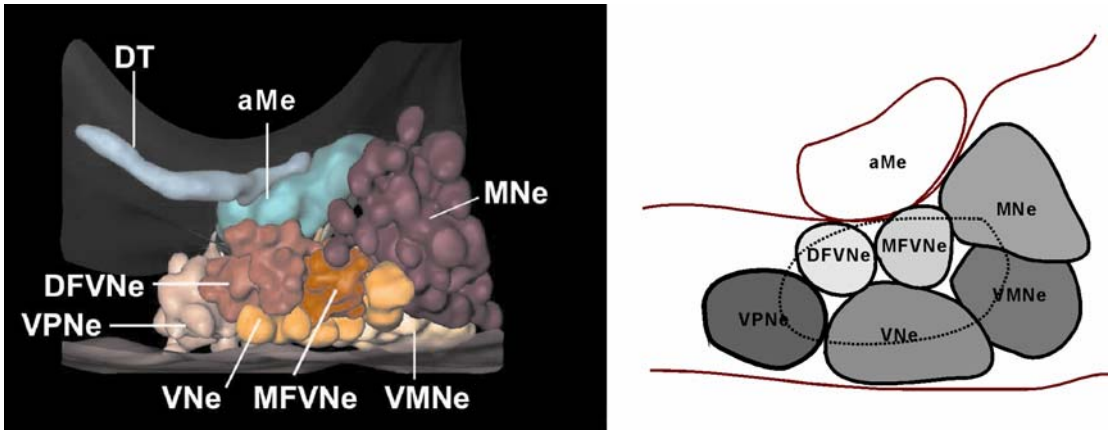

Figure 8. The accessory medulla (aMe) is associated with seven soma groups in the brain of *Rhyparobia maderae.* The noduli of the aMe are connected to the distal tract (DT), which projects to the medulla. The seven soma groups are named, according to their position relative to the aMe: anterior neurons (ANes), distal and medial groups of fronto-ventral neurons (DFVNes, MFVNes), median neurons (MNes), ventral neurons (VNes), ventromedian neurons (VMNes), and ventro-posterior neurons (VPNes). The ANes are symbolized by a dashed circle. Scale bar: 100 µm. (modified from Reischig and Stengl, 2003b)

Immunocytochemical studies and matrix-assisted laser desorption/ionization time of flight (MALDI-TOF) analysis showed that neurons of the aMe are packed with an unusually high density of dense-core vesicles, which contains abundant in partly colocalized neuropeptides. To date, ten different neuropeptides have been detected in aMe neurons: allatostatin, allatotropin, baratin, corazonin, different FMRFamid-related peptides, such as leucomyosuppression and short neuropeptide F, gastrin, leucokinin, myoinhibitory peptides, orcokinin, and PDF (Petri et al., 1995; Reischig and Stengl, 1996, 2003b; Nässel et al., 1991, 1992, 2000; Hofer and Homberg, 2006a, b; Soehler et al., 2007, 2008, 2011; Schulze et al., 2012). Moreover, the neurotransmitters gamma-aminobutyric acid (GABA), histamine and serotonin were also located in the aMe (Petri et al., 1995, 2002; Loesel and Homberg, 1999). Among these, the structure of the PDF-immunoreactive (PDF-ir) neurons has been studied best. In the cockroach brain, two PDF-ir neuron groups are located at the posterior dorsal and posterior ventral edge of the lamina (dPDFLa, vPDFLa), 12 anterior PDF-ir neurons are located near the aMe (aPDFMe), and 6 posterior PDF-ir neurons (pPDFMe) lie in the posterior cell cortex of the medulla (Petri et al., 1995; Reischig and Stengl, 1996, 2003b). The 12 aPDFMe comprise 4 large, 4 medium-sized, and 4 small PDF-ir neurons. The 4 large and 4 medium-sized aPDFMes belong to the VNes, while the 4 small aPDFMes are assigned to the DFVNes. The aPDFMes connect the aMe to the medulla and lamina via two distinct pathways, the anterior fiber fan and the median layer fiber system of the medulla. While the branching patterns of any single aPDFMe are not known, some general morphological features can be analyzed and predicted, according to backfill experiments combined with immunocytochemistry (Söhler et al., 2011). The fibers of large aPDFMes arborize in the anterior and shell neuropil of the aMe, which are the input and output regions connecting optic lobe and midbrain neuropils. The fibers of the medium-sized aPDFMe largely

innervate in the internodular and, to a lesser extent, the nodular neuropil of the aMe (Reishig and Stengl, 2003b). The largest aPDFMe connects both bilaterally aMae via the anterior and posterior optic commissures (AOC, POC) and projects to all PDF-ir targets in the midbrain (i.e. the superior lateral, superior medial, inferior lateral and ventrolateral protocerebrum). Besides the largest aPDFMe, 3 medium-sized aPDFMes, which contain also orcokinin and FMRFaminde, also form a coupling pathway between the bilateral aMae, however, only via the AOC, but not the POC. The large and medium-sized aPDFMes send their processes to different midbrain targets via the AOC and/or the POC. The small aPDFMes, appear to be local neurons. They are restricted to the aMe and possibly to other neuropils in the ipsilateral optic lobe (Fig.9).

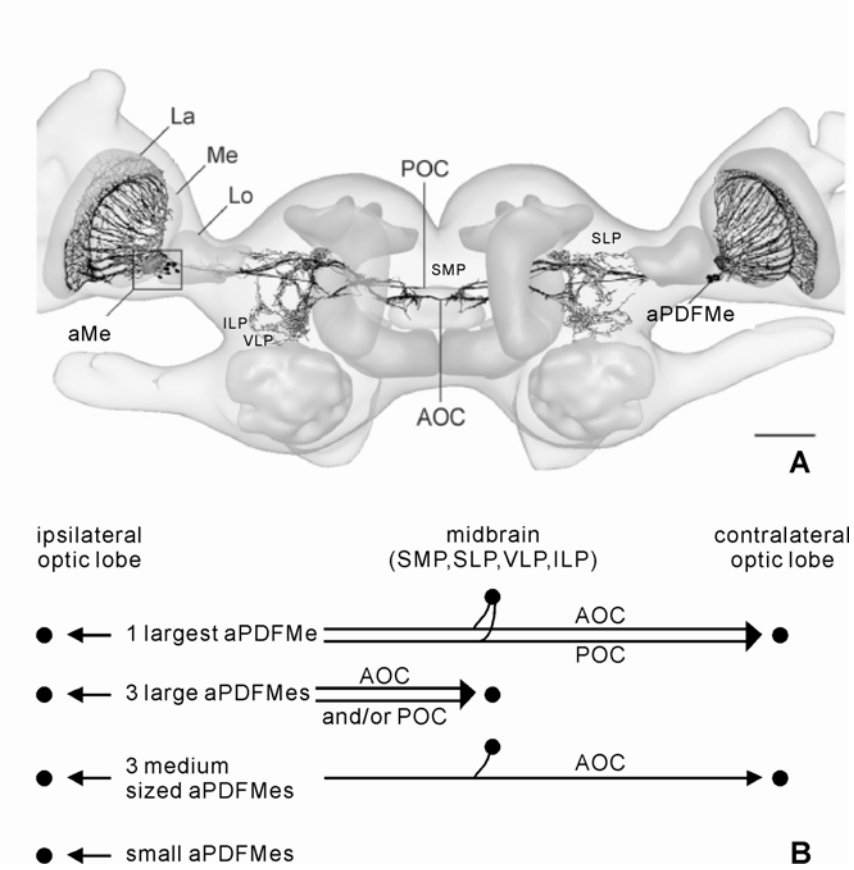

Figure 9 A,B. Reconstruction (A) and schematic arborization pattern (B) of anterior pigment-dispersing factor (PDF)-immunoreactive(ir) neurons (aPDFMes) next to the accessory medulla (aMe). A.The PDF targets in the midbrain are: the superior lateral (SLP), superior medial (SMP), inferior lateral (ILP), and ventrolateral protocerebrum (VLP). The aPDFMes can be further devided according to soma sizes. One largest aPDFMe sends its process to all PDF-ir midbrain targets. In addition, it branches in neuropils of the contralateral optic lobe via processes in the anterior and posterior optic commissures (AOC, POC). The remaining 3 large aPDFMes send process to midbrain targets via AOC and/or POC, but not to the contralateral aMe. Three medium-sized aPDFMes connect both aMae via the AOC. The small aPDFMes appear to be local neurons of the ipsilateral optic lobe. La, lamina. Lo, lobula. Me, medulla. Scale bar: 200 µm (reconstruction modified after Homberg et al., 2003).

Light-entrainment pathways to the circadian clock in the Madeira cockroach

In the Madeira cockroach *R. maderae*, light entrainment of the circadian clock occurs through photoreceptors in or near the compound eyes, while each of the two bilateral pacemakers receives photic information not only from ipsilateral, but also from the contralateral compound eye (Robert, 1974; Page et al., 1977; Page, 1978). The photic entrainment pathways to the aMe are largely unknown. Immunocytochemical staining against histamine, the transmitter of retinal axons in insects, showed no direct inputs from histaminergic ommatidial photoreceptors into the aMe (Loesel and Homberg, 1999). Therefore, light information must be transmitted indirectly via interneurons from the photoreceptors to the aMe. The GABA-ir distal tract is a good candidate for the light entrainment pathway into the aMe since it connects the noduli of the aMe with the medulla and possibly also with the lamina. Injections of GABA, allatotropin, and orcokinin into the vicinity of the aMe resulted in light-like phase response curves (PRC) and suggested that neurons expressing these substances are involved in the light entrainment pathway. Since both GABA-ir and allatotropin-ir neurons densely innervate the noduli of the aMe (Petri et al., 1995, 2002; Reischig and Stengl, 2003b) it was suggested that ipsilateral light entrainment is processed in the noduli of the aMe. This assumption was supported via intracellular recordings which stained light-sensitive neurons which connected the noduli of the aMe via the anterior fiber fan with the distal lamina (Loesel and Homberg, 2001). Light information from the contralateral compound eye reaches the internodular region of the aMe apparently via orcokinin-ir VMNes projecting via the POC.

Coupling- and output pathways of the circadian clock in the Madeira cockroach

Dextran and neurobiotin backfills combined with double-staining of commissural neurons with PDF antisera showed that the largest aPDFMe and 3 medium-sized aPDFMes connect both bilaterally symmetric aMae (Plural of aMe) via branches mostly in the internodular neuropil and to a lesser extend in the noduli (Petri, 1998; Reischig and Stengl 2002, 2003b; Söhler et al. 2011). However, since PDF-injections resulted in a monophasic all-delay PRC (Petri and Stengl 1997, 2001) it was assumed that PDF does not transmit contralateral light information but forms a direct coupling pathway between both aMae (Petri, 1998; Reischig and Stengl, 2002; Söhler et al., 2011). Computer models of coupled PER/TIM feedback loops suggested that only two antagonistic coupling forces together can explain experimental observations in the cockroach (Stengl and Homberg 1994; Petri and Stengl, 2001). This phase-advancing coupling pathway remains to be identified.

In addition to being a coupling input signal into the contralateral aMe PDF also forms several output pathways from the aMe to different targets in the optic lobes and in the midbrain. The PDF-ir neurons branch in the superior lateral protocerebrum (SLP), the superior medial (SMP), inferior lateral (ILP), and ventrolateral protocerebrum (VLP) to control physiological and behavioral activity rhythms (Fig. 10).

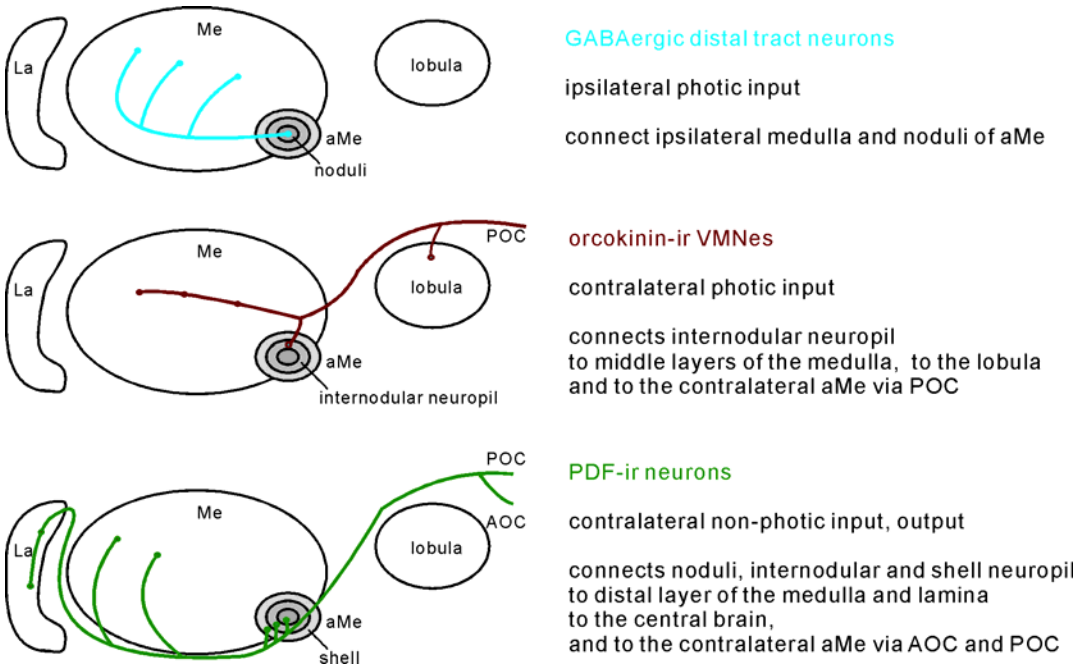

Figure 10. Scheme of hypothesized input and output pathways of the circadian clock. The scheme shows a horizontal view of the optic lobe neuropils lamina (La), medulla (Me), and accessory medulla (aMe). It is hypothesized that GABAergic distal tract neurons provide photic input from the medulla and possibly also from the distal lamina of the ipsilateral compound eye to the noduli of the aMe. Orcokinin-immunoreactive (ir) ventromedian (VMNes) neurons are suggested to provide contralateral light input via the posterior optic commissure (POC). They connect the internodular neuropil of the aMe to middle layers of the medulla, to the lobula of the ipsilateral optic lobe, and to the contralateral aMe. The PDF-ir neurons play a key role as contralateral non-photic inputs and outputs controlling locomotor activity rhythms. They connect the aMe via the fiber fan to the distal lamina and distal medulla. PDF-ir outputs to the various central brain regions and to the contralateral aMe project via the anterior and posterior optic commissures (AOC, POC).

Circadian pacemaker neurons of the aMe are spontaneously active in the gamma frequency band

Extracellular recordings from the aMe *in vitro* and *in vivo* revealed that the large majority of aMe neurons are spontaneously active. The membrane potential of the excised aMe oscillates with ultradian periods in the gamma frequency range of 20-70 Hz (Schneider and Stengl, 2005, 2006, 2007). The aMe neurons are synchronized and form different assemblies of cells, apparently via GABAergic interneurons. The cells within an assembly express the same ultradian period and the same phase. Period defined as interspike interval, the phase is defined as the time of action potential occurrence. Cells between assemblies differ in phase, but not in period. The aMe neurons are coupled via gap junctions to maintain synchronous firing with the same frequency. However, the gap-junction-dependently synchronized cells remain at a stable phase difference if not synchronized to zero phase difference by e.g. GABAergic interneurons (Schneider and Stengl, 2005, 2006). Application of PDF formed a new, transient ensemble of aMe

neurons, via synchronization to zero phase difference. It is hypothesized that this PDF-dependent phase synchronization gates locomotor activity rhythms via activation of downstream neurons (Schneider and Stengl, 2005).

Ion channels underlying spontaneous activity in the SCN

Molecular genetic studies of *D. melanogaster* increased greatly our understanding of the molecular circadian clockwork (Tomioka and Matsumoto, 2010; Peschel and Helfrich-Förster, 2011). However, still it is not understood how the molecular clock based upon feed-back cycles of circadian gene expression signals to the plasma membrane, or couples endogenous membrane potential oscillations, to generate circadian rhythms in action potential activity. It has been suggested by some studies and questioned by others that electrical membrane activity is coupled to circadian clock gene expression in the nucleus of *D. melanogaster* (Nitabach et al., 2005; Sheeba et al., 2008b; Fogle et al., 2011; Depetris-Chauvin et al., 2011). More is known about electrophysiological rhythms in vertebrates (Colwell, 2011).

The suprachiasmatic nucleus (SCN) of the hypothalamus is the primary circadian pacemaker generating circadian rhythms in mammals. The SCN neurons generate circadian rhythms in their electrical activity. They are electrically active in the day with peaks of around 6-10Hz and silent during the night (Yamaguchi et al., 2003; Schaap et al., 2003; Kuhlman and Mcmahon 2006; Ko et al., 2009; Colwell 2011). Even about 60%-70% of the isolated single SCN neurons in primary cultures exhibit a rhythm in firing rate (Aton et al., 2005; Webb et al., 2009). In recent years, the understanding of the ion channels responsible for the spontaneous circadian rhythms in electrical activity in the SCN neurons has been much improved (Colwell, 2001). Conceptually, the spontaneous circadian membrane activity needs two kinds of ion channels: the "**pacemakers**" and the "**circadian modulators**" (Table.2).

The "**pacemakers**" provide the excitatory drive of the hyperpolarized neurons at rest and amplify the depolarization for generation of spontaneous action potentials. The hyperpolarization-activated, cyclic nucleotide-gated cation channel (HCN) is a well known pacemaker channel. The HCN channels are activated at hyperpolarizing potentials (half-maximal activation potentials: -70 to -140 mV) and do not display voltage-dependent inactivation. They are modulated by cAMP, which facilitates the channel opening (de Jeu and Pennartz, 1997; Atkinson et al., 2011). Another pacemaker channel is the persistent sodium (Na^+) channels (Nav 1.5 and Nav 1.6). Their activation is in the subthreshold region with threshold between -65 mV and -60 mV and is maximal at about -45 mV. They express slow inactivation kinetics and thereby produce "persistent" Na^+ currents (Jackson et al., 2004; Panda et al., 2002; Kononenko et al., 2004).

The "**circadian modulators**" with circadian properties are the primary determinant of circadian rhythmicity. They are membrane targets directly responsible for circadian modulation of firing rate and are transcribed in a circadian rhythm. The voltage-activated calcium channels (VACCs) are "day modulators" involved in the high firing rate during the day. Firing rate increase during the day is accompanied by a Ca^{2+} baseline increase

which could be caused by the VACCs (Colwell, 2000). T-type VACC channels (Cav3) are low voltage-activated Ca^{2+} channels which are activated at hyperpolarized potentials (Akasu et al., 1993; Huang, 1993; Kim et al., 2005). Circadian rhythmic expression of their transcripts was shown previously (Nahm et al., 2005). Thereby, the magnitude of the L-type VACC channels Cav1.3 displays a circadian rhythm. The Cav1.3 blocker nimodipine caused a reduction in firing rate during the day, but not during the night (Pennartz et al., 2002). Vandael et al. (2010) showed that Cav1.3 blocker could reduce not only Ca^{2+} currents but also Ca^{2+} activated potassium currents. Apparently, both currents were coupled and determine circadian rhythmicity. Other targets for circadian modulation are different potassium channel families. The fast delayed rectifier K^+ channels (Kv3.1 Kv3.2) with their positive shifted voltage-dependence and fast deactivation rates are activated specifically during repolarization without compromising threshold, rise time or height (Rudy and Mcbain, 2001). The K^+ currents during the day are larger than those recorded during the night. Immunocytochemistry showed a higher expression of the Kv3.1 and Kv3.2 channels during the day (Itri et al., 2005). Therefore, the fast delayed rectifier K^+ channels (Kv3.1 Kv3.2) are “day modulator” involved in the high firing rate during the day. The A-type K^+ channels (Kv4.1 Kv4.2) with a higher magnitude of current during the day, could also act as “day modulators” (Itri et al., 2010). Anderson et al. (2010) showed the Kv 4.2 complex can be regulated by T-type VACCs (Cav3.1). The large-conductance Ca^{2+} activated K^+ channels (BK) drive the membrane hyperpolarization during the night. The magnitude of the BK current is higher during the night than during the day. In situ hybridization studies showed a higher expression of mRNA during the night (Pitts et al., 2006). The BK channel knockout-mice increased action potential firing rate selectively at night (Meredith et al., 2006). Therefore, the BK channels are “night modulators” responsible for the nightly silencing of firing rate. Also, a novel set of subthreshold voltage-dependent cation channels (SVC) was found to be responsible for circadian modulation (Kononenko, 2011). The SVCs are active at resting potential and increase their open probability with membrane depolarization. They regulate circadian activity rhythms of SCN neurons since they are expressed in a circadian manner.

Table 2. Ion channels responsible for spontaneous circadian membrane activity in the suprachiasmatic nucleus.

function		current	Channels
Pacemakers		hyperpolarization-activited, cyclic nucleotide-gated cation channel (HCN)	HCN1 HCN2
		persistent Na^+	Nav1.8 Nav1.9
Circadian modulators	day	T-type Ca^{2+}	Cav3
		L-type Ca^{2+}	Cav1.3
		fast delayed K^+ rectifier	Kv3.1 Kv3.2
		A-type K^+	Kv4.1 Kv4.2
		subthreshold voltage dependent cation channels (SVC)	?
	night	large-conductance Ca^{2+} activated K^+ channels (BK)	BK

Relationships between the photoperiodic clock and the circadian clock

Firstly, it is important to mention that at first the photoperiodic clock and the circadian clock were studied independently with different approaches and aims. The photoperiodic clock system with a photoperiodic timer and a photoperiodic counter was studied to understand season-dependent phenotypes (e.g. diapause). In contrast, the circadian clock system was firstly studied mostly at the molecular level in the fruitfly *D. melanogaster* to search for the molecular mechanisms of circadian time-keeping. Behavioral studies combined with lesions established the Madeira cockroach as an adept model system for cellular analysis of the insect circadian clock (Nishiitsutsji-Uwo and Pittendrigh, 1968; Page, 1982). Later, lesion and transplantation studies in the Madeira cockroach revealed the cellular nature of the circadian pacemaker located in the aMe with associated PDF-ir neurons (Stengl and Homberg 1994; Reischig and Stengl 2003a).

In recent years, ample evidence suggested that daily and seasonal timing systems send outputs to the same effectors. The output signals from the two systems finally converge on neurosecretory cells which release various neurotransmitters and neuropeptides to control physiology. Synthesis and release of insect hormones are under strict circadian control (Jackson et al., 2001; Zhao and Zera, 2004; Vafopoulou and Steel, 2009; Vafopoulou et al., 2010). For instance, in the bug *Rhodnius prolixus*, immunohistochemistry study showed that the PTTH releasing neurons in the lateral protocerebrum receive projections from the PDF-ir lateral clock neurons, apparently controlling circadian release of PTTH (Vafopoulou and Steel, 1996; Vafopoulou et al., 2007, 2010). In the fruitfly *D. melanogaster*, the axonal arborizations from s-LNv neurons overlap with five peptidergic neurons that directly innervate the prothoracic gland or *corpora allata* (CA) cells of the larval ring gland (Siegmund and Korge, 2001). In the blow fly *P. terraenovae*, synaptic connections between clock neurons and neurons in PL have been detected, which are indispensable for diapause induction (Hamanaka et al., 2005). These anatomical studies provided direct evidence that circadian clock neurons control hormone release.

To explain the relationships between the photoperiodic clock and the circadian clock, several models have been postulated based on experimental results in different insect species. They can be divided into three major formal hypotheses:

(A) Circadian clock neurons are “photoperiodic timers” (Fig.11). Bünning in 1960 first suggested that photoperiodic timer measurement in insects depends on the circadian system. In his model (**Bünning hypothesis**), a short day was detected when the light was restricted to the endogenous subjective day and a long day was measured when the light was extended to the subjective night. Later, the photoperiodic time measurement was suggested to use one or two circadian oscillator systems. The “**external coincidence**” model by Pittendrigh and Minis (1964) determined a specific light sensitive phase in the circadian oscillators (photoinducible phase of the circadian clock). The day is “short”, when the photoinducible phase is in darkness, while the day is “long”, when the photoinducible phase coincides with the light phase. In the “**internal coincidence**” model Tyshchenko (1966), the short or long day is determined by the phase relationship between two endogenous circadian oscillators. One is

entrained by dawn and the other by dusk. Helfrich-Förster (2001) developed a two oscillator model (morning cells = M oscillator, evening oscillator = E cells) for the bimodal locomotor rhythms of *Drosophila*. Stoleru et al. (2007) suggested that M-cells dominate the network in darkness and E cells dominate the circadian network during the light phase allowing for behavioral adjustment to changes in photoperiods. The M and E oscillators were suggested to couple either to dawn or dusk to measure the day or the night length and underlie the bimodal rhythms under different photoperiods (Rieger et al., 2006; Bachleiter et al., 2007; Picot et al., 2007; Cusumano et al., 2009; Helfrich-Förster, 2009; Yoshii et al. 2012). In the blow fly *P. terraenovae*, Shiga and Numata (2009) showed that bilateral ablation of the PDF-ir s-LNvs resulted in the loss of photoperiodic discrimination. The diapause occurred in 48% of the flies under long-day conditions and in 55% under short day conditions. They demonstrated that the PDF-ir circadian pacemaker neurons s-LNvs are necessary for the photoperiodism. Furthermore, Potdar and Sheeba (2012) suggested that the light-sensitive lLNvs enable flies to adjust to different photoperiods via maintaining the phase relationships between M and E-oscillators, possibly via direct connections to the sLNvs.

(B) Alternatively, Lees (1973) developed the "**hourglass model**", in which the circadian clock and photoperiodic clock are independent. In the aphid *M. viciae*, the photoperiodism of parthenogenetic or bisexual forms is regulated by the absolute duration of the dark length. Varying light cycle of circadian system did not influence the photoperiodism of the aphid. The model considers the photoperiodic clock as a sequence of biochemical reactions that must be finished in the darkness. If the duration of darkness is not long enough these reactions cannot be finished and no output occurs.

The independence of the photoperiodic clock and the circadian clock is further supported by the observation that the damping rate of the photoperiodic oscillators is much higher as compared to circadian oscillators. In addition, the circadian clock receives light information mainly via CRY, while the rhodopsins probably play the primary role in the light input pathway to the photoperiodic clock.

(C) Alternatively, the „**damped oscillator model**" describes cooperation between the photoperiodic clock and the circadian clock (Saunders, 2010a). The two systems are physically separated, but work in cooperation. Both of them are regulated possibly by clock genes based on the circadian oscillator principle. Using mathematical modeling based on respective experiments, Saunder suggested that the previously described competing models (in A and B) are not mutually exclusive, because the "hourglass model" could be based upon heavily damped circadian oscillators (Saunders, 2005, 2007, 2009, 2010a, b). Comparing *per* mutants with wild type *D. melanogaster*, Saunders et al., (1989) demonstrated that photoperiod-induced adult diapause is independent of *per* genes. Several recent studies have raised the possibility that *tim* plays a role in the photoperiodic clock system (Goto and Denlinger, 2002; Shafer et al., 2004; Pavelka et al., 2003). In the flies, *Sarcophaga crassipalpis* and *D. melanogaster*, under long-day conditions, the mRNA or protein levels of *tim* are significantly lower than those measured under short-day conditions. This sensitivity to photoperiod was not found in clock gene *per* (Goto and Denlinger, 2002; Shafer et al., 2004). In contrast,

tim appears to be involved in the diapause of another drosophilid fly *Chymomyza costata*. Disrupting *tim* transcription using RNA interference method could result in the loss of diapause (Riihimaa and Kimura, 1988). Using the different *tim* transgenic *D. melanogaster*, Sandrelli et al. (2007) suggested the *tim* effect on the diapause is independent of the circadian clock. TIM could then provide the downstream signal for hormonal control of diapause.

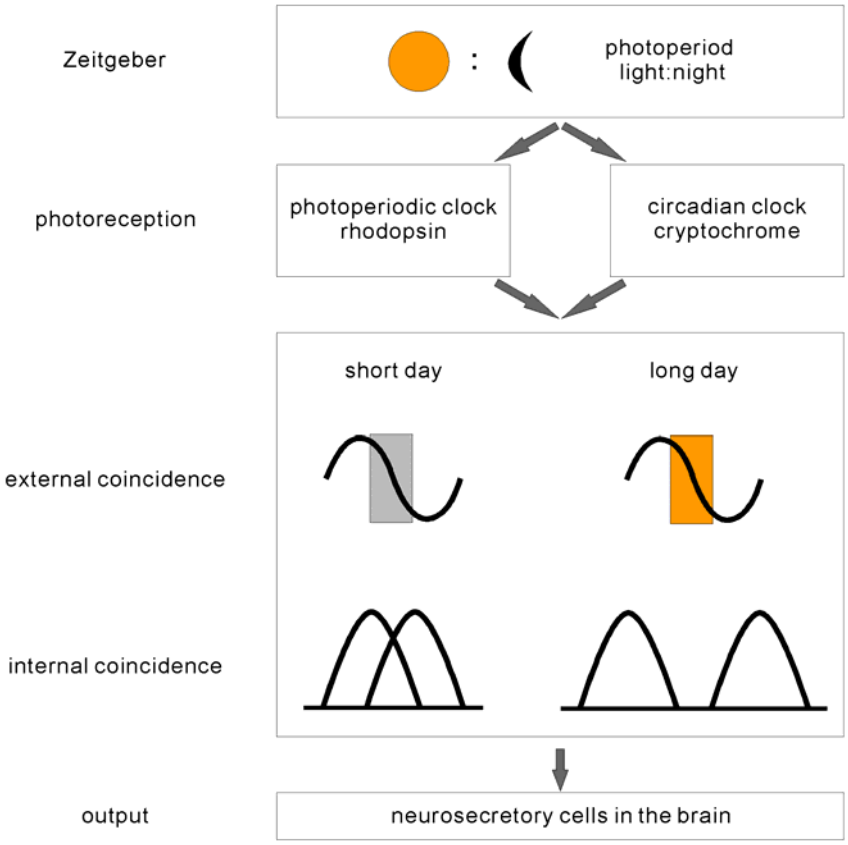

Figure 11. Two models of photoperiodic time measurement. **A.** The photoreceptive systems of the photoperiodic clock and the circadian clock are separate. The circadian clock receives light information mainly via CRYPTOCHROME (CRY), while the rhodopsins probably play a primary role as the light input pathway of the photoperiodic clock. Still, the photoperiodic time could be measured by circadian clock neurons. **B.** In the external conincidence model, circadian clock neurons have a specific light sensitive phase. The day is sensed as being long, when the sensitive phase coincides with the light phase. In contrast, short days are detected, when the sensitive phase coincides with the dark phase of the Zeitgeber. **C.** In the internal coincidence model, photoperiodic time is measured by the phase difference of two circadian oscillators. One is entrained by dawn and the other by dusk. **D.** Output signals of both clocks are transmitted to neurosecretory cells which release various neurotransmitters and neuropeptides to control the physiology of the organism.

Aims and major findings

Nowadays, it is generally accepted that the circadian clock neurons are involved in insect photoperiodism since they control photoperiod-dependent changes in locomotor activity. However, it is still not known whether there is a particular neuropil which fulfills properties of a photoperiodic clock as a photoperiodic timer and counter only in insects evolved in temperate zones. Alternatively, it is conceivable that the brain of insects is adaptive enough to adjust to changing photoperiods and changing environmental conditions without the need of a specialized photoperiod circuit. Here I concentrate my studies on the examination of the plasticity of the circadian system. For my Ph.D. work I selected an originally non-photoperiodic species, the Madeira cockroach *Rhyparobia maderae* (*Leucophaea* maderae) which originated near the equator in Africa where it is not exposed to changes in photoperiod. Since at least two hundred years it can also be found in other geographical regions such as Portugal (latitude 40° north) and England (latitude 51°north) via sea-trade of fruits. The Madeira cockroach is an ancient, astoundingly adaptive species which survived extreme environmental changes since the Karbon (about 350 million years ago). This cockroach species is long-living with a life span of about 2.5 years appears to have highly adaptive brain circuits which appear to adjust to the changes of photoperiodic information. Moreover, the Madeira cockroach is well established as circadian clock model for basic research on the circadian clock mechanisms. Due to its large size, the Madeira cockroach is well suited for electrophysiological studies. Therefore, the Madeira cockroach could be a rewarding model system for both circadian and photoperiodic responses of the clocks.

To determine whether the PDF-ir circadian clock neurons are affected by different lengths of the light phase the Madeira cockroaches were reared under different photoperiods 6:18 (short day), 12:12 (control group) or 18:6 (long day) LD cycles. The aim of this doctoral thesis is to examine whether and how the different photoperiodic conditions modify the circadian clock architecture and the physiology of circadian pacemaker aMe neurons in the primary cell cultures, with immunocytochemical studies, 3D reconstruction, standardization and Ca^{2+}-imaging techniques.

To facilitate understanding and comparison of the spatial distribution of circadian pacemaker neurons in the cockroach, a 3D standard atlas of the control group (LD 12:12) was generated. The standard brain comprises of atlases of 21 neuropils, calculated from 20 individual immunostained wholemount brains. The branching pattern of PDF-ir neurons was implemented into the control standard brain and statistically analyzed with new details. The distances between PDF-ir branching areas show specific numerical relationships (Chapter I) as known for delay lines in the auditory cortex. These relationships of distances were changed by the different photoperiods. The number of specific groups of PDF-ir and orcokinin-ir circadian pacemaker neurons and their connections were also affected by rearing in different photoperiods (Chapter II). Thus, the PDF-ir circadian pacemaker neurons are sensitive to photoperiodic change and could be involved in photoperiodic time measurement.

To analyze the physiological response of the circadian clock neurons to the different photoperiods, the aMe with associated soma groups from different cockroach

photoperiodic groups were dispersed to obtain primary cell cultures. Using Ca^{2+}-imaging, spontaneous intracellular Ca^{2+} transients (activity) were measured as indication of spontaneous action potential activity. For better understanding of the ion channel composition of the circadian clocks, Ca^{2+}-imaging combined with pharmacology was employed to analyze ion channels underlying spontaneous activity in the cultured circadian pacemaker neurons under control conditions (LD 12:12 extracellular Ca^{2+} concentration = 1 mM). The mibefradil-sensitive, low-voltage VACCs and HCNs appear to be “pacemakers” of the cockroach circadian clock neurons. The P/Q VACCs coupled to BKs appear to be involved in input-dependent activity (Chapter III). The spontaneous intracellular Ca^{2+} activity of aMe neurons was changed in response to changes in the extracellular Ca^{2+} concentration mimicking different conditions of input-dependent depolarization. According to the presence or absence of intracellular Ca^{2+} activity (= spontaneous action potential activity) in 3 different extracellular Ca^{2+} concentrations (1 µM = presumed hyperpolarization, 1 mM = control, and 6 mM = presumed depolarization), the aMe cells were assigned to different physiological cell types. Using vector analyses it was shown that the different photoperiods could change the percentage of physiological response-types of cultured circadian clock neurons significantly (Chapter V). Thus, it was shown that the physiological parameters which determine spontaneous activity of circadian pacemaker neurons are sensitive to changes in photoperiod.

Next, it was examined which neurotransmitter could be involved in relaying photic input to aMe neurons. Previously, it was shown that cholinergic input from the H-B eyelet of *D. melanogaster* controls circadian photosensitivity and clock gene expression (Lelito and Shafer, 2012; Veleri et al., 2007). Thus, in the Madeira cockroach acetylcholine (ACh) responses of cultured circadian clock neurons from different photoperiodic groups were compared. Using Ca^{2+}-imaging combined with pharmacology, it was shown that ACh increased the intracellular Ca^{2+} level of the aMe cells from control group (LD 12:12) via nicotinic ACh-receptors in a dose-dependent manner (Chapter IV). The effect of ACh on intracellular Ca^{2+} levels of the culture aMe neurons from cockroaches raised in different photoperiods were compared and analyzed. At the ACh concentrations tested, no evidences for a change in ACh-sensitivity of cultured aMe cells by photoperiods was detected. (Chapter V). Although comparison of the ACh effect on all pooled aMe cells did not show any obvious difference between experimental groups, it could not be excluded that ACh could relay photoperiodic information only to a small group of cells which was overlooked via pooling all physiological response types. Other neurotransmitters, such as glutamate or GABA need to be tested in the future.

To improve the primary cell culture techniques and to develop a multielectrode array assay for circadian pacemaker cells, different terminated ultrananocrystalline diamond surfaces (UNCD) (produced by Alexandra Voss, Institute of Nanostructure Technologies and Analytics, University of Kassel) were tested. It is shown the diamond surfaces allow for a faster, stronger attachment of neurons without compromising their viability. The UNCD surfaces can be used as basic cell adhesive surface for the cultured insect neurons in the further. (Chapter VI).

In summery, this doctoral thesis reveals that raising Madeira cockroaches *R. maderae* under different photoperiods changes the neuronal circuit of the PDF-ir circadian

pacemaker neurons as well as the physiology of cultured aMe neurons. These results indicate that the neuronal circuit of the circadian clock could at least partially serve as photoperiodic clock, which detects changes in day length. Whether it can also control photoperiodic adaptations (photoperiodism) in the Madeira cockroach remains to be studied.

Abbreviations

AC	adenylate cyclase
ACh	acetylcholine
aMe	accessory medulla
ANe	anterior neuron
AOC	anterior optic commissure
aPDFMe	anterior PDF- immunoreactive neuron
BK	large-conductance Ca^{2+} activated K^{+} channel
CA	*corpora allata*
CC	*corpora cardiaca*
CLK-CYC	CLOCK-CYCLE
CRY	CRYPTOCHROME
DFVNe	distal group of fronto-ventral neurons
DN_1, DN_2, DN_3	dorsal neuron group 1-3
DN_{1a}	anterior dorsal neuron group1
DN_{1p}	posterior dorsal neuron group1
dPDFLa	PDF-immunoreactive neuron at the posterior dorsal edge of the lamina
DT	distal tract
E-cell	evening oscillator
GABA	gamma-aminobutyric acid
H-B eyelet	Hofbauer-Bucher eyelet
HCN	hyperpolarization-activated, cyclic nucleotide-gated cation channel
ILP	inferior lateral protocerebrum
ir	immunoreactive
JH	juvenile hormone
La	lamina
LD	light/dark
l-LNv	large ventrolateral neuron
LNd	dorsal lateral neuron
LPN	lateral posterior neuron
MALDI-TOF	matrix-assisted laser desorption/ionization time of flight
MB	mushroom body
M-cell	morning oscillator
Me	medulla
MFVNe	medial group of fronto-ventral neurons
MNe	median neuron

per /PER	*period* / PERIOD
PDF	pigment dispersing factor
PI	*pars intercerebralis*
PL	*pars lateralis*
POC	posterior optic commissure
pPDFMe	posterior PDF- immunoreactive neuron
PRC	phase response curve
PTTH	prothoracicotropic neurohormone
SCN	suprachiasmatic nucleus
s-LNv	small ventrolateral neuron
SLP	superior lateral protocerebrum
SMP	superior medial protocerebrum
SVC	subthreshold voltage-dependent cation channel
tim /TIM	*timeless* / TIMELESS
UNCD	ultrananocrystalline diamond surfaces
VACC	voltage-activated calcium channel
VLP	ventrolateral protocerebrum
VMNe	ventromedian neuron
VNe	ventral neuron
vPDFLa	PDF-immunoreactive neuron at the posterior ventral edge of the lamina
VPNe	ventro-posterior neuron

References

Agui, N., Granger, N.A., Gilbert, L.I., Bollenbacher, W.E., 1979. Cellular localization of the insect prothoracicotropic hormone: in vitro assay of a single neurosecretory cell. Proceedings of the National Academy of Sciences of the USA 76, 5694–5698.

Akasu, T., Shoji, S., Hasuo, H., 1993. Inward rectifier and low-threshold calcium currents contribute to the spontaneous firing mechanism in neurons of the rat suprachiasmatic nucleus. Pflügers Archiv 425, 109-116.

Allada, R., White, NE., So, WV., Hall, JC., Rosbash, M., 1998. A mutant Drosophila homolog of mammalian clock disrupts circadian rhythms and transcription of period and timeless. Cell 93, 791-804.

Anderson, D., Rehak, R., Hameed, S., Mehaffey, W.H., Zamponi, G.W., Turner, R.W., 2010. Regulation of the $K_V4.2$ complex by $Ca_V3.1$ calcium channels. Channels (Austin) 4, 163-7.

Atkinson, S.E., Maywood, E.S., Chesham, J.E., Wozny, C., Colwell, C.S., Hastings, M.H., Williams, S.R., 2011. Cyclic AMP signalling controls action potential firing rate and molecular circadian pacemaking in the suprachiasmatic nucleus. Journal of Biological Rhythms 26, 210–220.

Aton, S.J., Colwell, C.S., Harmar, A.J., Waschek, J., Herzog, E.D., 2005. Vasoactive intestinal polypeptide mediates circadian rhythmicity and synchrony in mammalian clock neurons. Nature Neuroscience 8, 476–483.

Bachleitner, W., Kempinger, L., Wülbeck, C., Rieger, D., Helfrich-Förster, C., 2007. Moonlight shifts the endogenous clock of *Drosophila melanogaster*. Proceedings of the National Academy of Sciences of

the USA 104, 3538-3543.

Blau, J., Young, M.W., 1999. Cycling vrille expression is required for a functional Drosophila clock. Cell 99, 661–671.

Brown, M.R., Graf, R., Swiderek, K.M., Fendeley, D., Stracker, T.H., Champagne, D.E., Lea, A.O., 1998. Identification of a steroidogenic neurohomone in female mosquitoes. Journal of Biological Chemistry 273, 3967–3971.

Bünning, E., 1960. Circadian rhythms and time measurement in photoperiodism. Cold Spring Harbor Symposium on Quantitative Biology 25, 249–256.

Collins, B.H., Dissel, S., Gaten, E., Rosato, E., Kyriacou, C.P., 2005. Disruption of Cryptochrome partially restores circadian rhythmicity to the arrhytmic period mutant of Drosophila. Proceedings of the National Academy of Sciences of the USA 102, 19012–19026.

Colwell, C. S., 2000. Circadian modulation of calcium levels in cells in the suprachiasmatic nucleus. European Journal of Neuroscience 12, 571–576.

Colwell, C. S., 2011. Linking neural activity and molecular oscillations in the SCN. Nature Reviews Neuroscience 12, 553-569.

Cusumano, P., Klarsfeld, A., Chelot, E., Picot, M., Richier, B., 2009. PDF modulated visual inputs and cryptochrome define diurnal behavior in *Drosophila*. Nature Neuroscience 12, 1431–1437.

Cyran, S., 2003. *Vrille, pdpl,* and *dClock* from a second feedback loop in the *Drosophila* circadian clock. Cell 112, 329-341.

de Jeu, M. T., Pennartz, C. M., 1997. Functional characterization of the H-current in SCN neurons in subjective day and night: a whole-cell patch-clamp study in acutely prepared brain slices. Brain Research 767, 72–80.

Denlinger, D.L., Yocum, G.D., Rinehart, J.P., 2005. Hormonal control of diapause. In: Gilbert, L.I., Iatrou, K., Gill, S.S. (Eds.), Comperehensive Molecular Insect Science Endocrinology, vol. 3. Elsevier, Amsterdam, pp. 615–650.

Depetris-Chauvin, A., Berni, J., Aranovich, E.J., Muraro, N.I., Beckwith, E.J., Ceriani, M.F., 2011. Adult-specific electrical silencing of pacemaker neurons uncouples molecular clock from circadian outputs. Current Biology 21, 1783-1793.

Duvall, L.B., Taghert, P.H., 2012. The circadian neuropeptide PDF signals preferentially through a specific adenylate cyclase isoform AC3 in M pacemakers of Drosophila. PLoS Biology 10(6): e1001337. doi:10.1371/journal.pbio.1001337.

Edery, I., 2000. Circadian rhythms in a nutshell. Physiological Genomics 3, 59-74.

Emerson, K.J., Bradshaw, W.E., Holzapfel, C.M., 2009. Complications of complexity: integrating environmental, genetic and hormonal control of insect diapause. Trends in Genetics 25, 217–225.

Fogle, K. J., Parson, K.G., Dahm, N.A., Holmes, T.C., 2011. Cryptochrome is a blue-light sensor that regulates neuronal firing rate. Science 331, 1409-1413.

Gao, N., Von Schantz, M., Foster, R.G., Hardie, J., 1999. The putative brain photoperiodic photoreceptors in the vetch aphid, Megoura viciae. Journal of Insect Physiology 45, 1011–1019.

Goto, S.S, Denlinger, D.L., 2002. Short-day and long-day expression patterns of genes involved in the flesh fly clock mechanism: period, timeless, cycle and cryptochrome. Journal of Insect Physiology 48, 803–816.

Grima, B., Chelot, E., Xia, R., Rouyer, F., 2004. Morning and evening peaks of activity rely on different clock neurons of the Drosophila brain. Nature 431, 869–873.

Hamanaka, Y., Yasuyama, K., Numata, H., Shiga, S., 2005. Synaptic connections between

pigment-dispersing factor-immunoreactive neurons and neurons in the pars lateralis of the blow fly Protophormia terranovae. Journal of Comparative Neurology 491, 390–399.

Helfrich-Förster, C., 1995. The period gene is expressed in CNS neurons which also produce a neuropeptide that reveals the projections of circadian pacemaker cells within the brain of *Drosophila melanogaster*. Proceedings of the National Academy of Sciences USA 92, 612–616.

Helfrich-Förster, C., 2001. The locomotor activity rhythm of *Drosophila melanogaster* is controlled by a dual oscillator system. Journal of Insect Physiology 47, 877–887.

Helfrich-Förster, C., 2009. Does the morning and evening oscillator model fit better for flies or mice? Journal of Biological Rhythms 24, 259–270.

Helfrich-Förster, C., Shafer, O.T., Wülbeck, C., Grieshaber, E., Rieger, D., Taghert, P., 2007. Development and Morphology of the Clock-Gene-Expressing Lateral Neurons of *Drosophila melanogaster*. Journal of Comparative Neurology 500, 47-70.

Helfrich-Förster, C., Täuber, C.M., Park,J.H., Mühlig-Versen, M, Schneuwly, S., 2000. Ectopic expression of the neuropeptide pigment-dispersing factor alters the rhythm of locomotor activity in *Drosophila melanogaster*. Journal of Neuroscience 20, 3339–3353.

Helfrich-Förster, C., Winter, C., Hofbauer, A., Hall, J.C., Stanewsky, R., 2001. The circadian clock of fruit flies is blind after elimination of all known photoreceptors. Neuron 30, 249–261.

Hodkova, M., 1976. Nervous inhibition of corpora allata by photoperiod in *Pyrrhocoris apterus*. Nature 263, 521–523.

Hofer, S., Homberg, U., 2006a. Evidence for a role of orcokinin-related peptides in the circadian clock controlling locomotor activity of the cockroach *Leucophaea maderae*. Journal of Experimental Biology 209, 2794-2803.

Hofer, S., Homberg, U., 2006b. Orcokinin immunoreactivity in the accessory medulla of the cockroach *Leucophaea maderae*. Cell and Tissue Research 325, 589-600.

Homberg, U., Reischig, T., Stengl, M., 2003. Neural organization of the circadian system of the cockroach *Leucophaea maderae*. Chronobiology International 20, 577-590.

Horseman, G., Hartmann, R., Virant-Doberlet, M., Loher, W., Huber, F., 1994. Nervous control of juvenile hormone biosynthesis in Locusta migratoria. Proceedings of the National Academy of Sciences USA 91, 2960–2964.

Huang, R.H., 1993. Sodium and calcium currents in acutely dissociated neurons from rat suprachiasmatic nucleus. Journal of Neurophysiology 70, 1692-1703.

Ikeda, K., Numata, H., Shiga, S., 2005. Roles of the mushroom bodies in olfactory learning and photoperiodism in the blow fly *Protophormia terraenovae*. Journal of insect physiology 51, 669–680.

Itri, J.N., Michel, S., Vansteensel, M.J., Meijer, J.H., Colwell, C.S., 2005. Fast delayed rectifier potassium current is required for circadian neural activity. Nature Neuroscience. 8, 650-656.

Itri, J.N., Vosko, A.M., Schroeder, A., Dragich, J.M., Michel, S., Colwell, C.S., 2010. Circadian regulation of A-type potassium currents in the suprachiasmatic nucleus. Journal of Neurophysiology 103, 632-640.

Jackson, F.R., Schroeder, A.J., Roberts, M.A., McNeil, G.P., Kume, K., Akten, B., 2001. Cellular and molecular mechanisms of circadian control in insects. Journal of Insect Physiology 47, 833–842.

Jackson, A. C., Yao, G. L., Bean, B. P., 2004. Mechanism of spontaneous firing in dorsomedial suprachiasmatic nucleus neurons. Journal of Neuroscience 24, 7985–7998.

Kaneko, M., Hall, J.C., 2000. Neuroanatomy of cells expressing clock genes in *Drosophila*: transgenic manipulation of the period and timeless genes to mark the perikarya of circadian pacemaker neurons

and their projections. Journal of Comparative Neurology 422, 66–94.

Khan, M. A., Romberg-Privee, H.M., Koopmanschap, A.B., 1986. Location of allatostatic centers in the pars lateralis regions of the brain of the Colorado potato beetle. Experientia 42, 836–838.

Kim, D.Y., Choi, H.J., Kim, J.S., Kim, Y.S., Jeong, D.U., Shin, H.C., Kim, M.J., Han, H.C., Hong, S.K., Kim, Y.I., 2005. Voltage-gated calcium channels play crucial roles in the glutamate-induced phase shifts of the rat suprachiasmatic circadian clock. European Journal of Neuroscience 21, 1215–1222.

Ko, G., Shi, L., Ko, M., 2009. Circadian regulation of ion channels and their functions. Journal of Neurochemistry 110, 1150–1169.

Kononenko, N.I., 2011. Searching membrane target for mammalian circadianclock responsible fro circadian modulation of firing rate. In Golvkin, L., Maliszkewicz, A. (Eds), Circadian Rhythms: Biology, Cognition and Disorders. Nova Science Publishers Inc., NY, pp. 29-56.

Kononenko, N. I., Shao, L. R., Dudek, F. E., 2004. Riluzole-sensitive slowly inactivating sodium current in rat suprachiasmatic nucleus neurons. Journal of Neurophysiology 91, 710–718.

Konopka, R.T., Benzer, S., 1971. Clock mutants of *Drosophila melanogaster*. Proceedings of the National Academy of Sciences of the USA 68, 2112-2116.

Kuhlman, S.J., Mcmahon, D.G., 2006. Encoding the Ins and Outs of circadian pacemaking. Journal of Biological Rhythms 21, 470-481.

Lees, A.D., 1973. Photoperiodic time measurement in the aphid Megoura viciae. Journal of Insect Physiology 19, 2279–2316.

Lelito, K.R., Shafer, O.T., 2012. Reciprocal cholinergic and GABAergic modulation of the small ventrolateral pacemaker neurons of *Drosophila*'s circadian clock neuron network. Journal of Neurophysiology 107, 2096-2108.

Lin, Y., Stormo, G.D., Taghert, P.H., 2004. The neuropeptide pigment-dispersing factor coordinates pacemaker interactions in the Drosophila circadian system. Journal of Neuroscience 24, 7951–7957.

Loesel, R., Homberg, U., 1999. Histamine-immunoreactive neurons in the brain of the cockroach *Leucophaea maderae*. Brain Research 842, 408-418.

Loesel, R., Homberg, U., 2001. Anatomy and physiology of neurons with processes in the accessory medulla of the cockroach *Leucophaea maderae*. Journal of Comparative Neurology 439, 193-207.

Matsuo, J., Nakayama, S., Numata, H., 1997. Role of the corpus allatum in the control of adult diapause in the blow fly, *Protophormia terraenovae*. Journal of insect physiology 43, 211–216.

Meredith, A.L., Wiler, S.W., Miller, B.H., Takahashi, J.S., Fodor, A.A., Ruby, N.F., Aldrich, R.W., 2006. BK calcium-activated potassium channels regulate circadian behavioral rhythms and pacemaker output. Nature Neuroscience 9, 1041-1049.

Morita, A., Numata, H., 1999. Localization of photoreceptor for photoperiodism in the stink bug Plautia crossota stali. Physiological Entomology 24, 190–196.

Murad, A., Emery-Le, M., Emery, P., 2007. A subset of dorsal neurons modulates circadian behavior and light responses in *Drosophila*. Neuron 53, 689-701.

Nahm, S.S., Farnell, Y.Z., Griffith, W., Earnest, D.J., 2005. Circadian regulation and function of voltage-dependent calcium channels in the suprachiasmatic nucleus. Journal of Neuroscience 25, 9304-9308.

Nässel, D.R., Cantera, R., Karlsson, A., 1992. Neurons in the cockroach nervous system reacting with antisera to the neuropeptide leucokinin-I. Journal of Comparative Neurology 322, 45-67.

Nässel, D.R., Persson, M.G., Muren, J.E., 2000. Baratin, a nonamidated neurostimulating neuropeptide, isolated from cockroach brain: distribution and actions in the cockroach and locust nervous systems.

Journal of Comparative Neurology 422, 267-286.

Nässel, D.R., Shiga, S., Wikstrand, E.M., Rao, K.R., 1991. Pigment-dispersing hormone-immunoreactive neurons in the blowfly and cockroach visual system. Cell and Tissue Research 266, 511-523.

Nishiitsutsuji-Uwo, J., Pittendrigh, C.S., 1968. Central nervous system control of circadian rhythmicity in the cockroach: III. The optic lobes, locus of the driving oscillation? Zeitschrift für vergleichende Physiologie 58, 14-46.

Nitabach, M.N., Sheeba, V., Vera, D.A., Blau, J., Holmes, T.C., 2005. Membrane electrical excitability is necessary for the free-running larval *Drosophila* circadian clock. Journal of Neurobiology 62, 1–13.

Nitabach, M.N., Wu, Y., Sheeba, V., Lemon, W.C., Strumbos, J., Zelensky, P.K., White, B.H., Holmes, T.C., 2006. Electrical hyperexcitation of lateral ventral pacemaker neurons desynchronizes downstream circadian oscillators in the fly circadian circuit and induces multiple behavioural periods. Journal of Neuroscience 26, 479–489.

Numata, H., Shiga, S., Morita, A., 1997. Photoperiodic receptors in arthropods. Zoological Science 14, 187–197.

Page, T.L., 1978. Interactions between bilaterally paired components of the cockroach circadian system. Journal of Comparative Physiology A 124, 225-236.

Page, T.L., 1982. Transplantation of the cockroach circadian pacemaker. Science 216, 73-75.

Page, T.L., Caldarola, P., Pittendrigh, C., 1977. Mutual entrainmant of bilaterally distributed circadian pacemakers. Phyiological Sciences 74, 1277-1281.

Palmer, J.D. (1976) An introduction to biological rhythms. Academic Press, New York.

Panda, S., Antoch, M.P., Miller, B.H., Su, A.I., Schook, A.B., Straume, M., Schultz, P.G., Kay, S.A., Takahashi, J.S., Hogenesch, J.B., 2002. Coordinated transcription of key pathways in the mouse by the circadian clock. Cell 109, 307-320.

Parisky, K.M., Agosto, J., Pulver, S.R., Shang, Y., Kuklin, E., Hodge, J.J., Kang, K., Liu, X., Garrity, P.A., Rosbach, M., Griffith, L.C., 2008. PDF cells are a GABA-responsive wake-promoting component of the Drosophila sleep circuit. Neuron 60, 672–682.

Park, J., Helfrich-Förster, H., Lee, C., Liu, G., Rosbach, M.L., Hall, J.C., 2000. Differential regulation of circadian pacemaker output by separate clock genes in *Drosophila*. Proceedings of the National Academy of Sciences of the USA 97, 3608–3613.

Pavelka, J., Shimada, K., Kostal, V., 2003. TIMELESS: a link between fly's circadian and photoperiodic clocks? European Journal of Entomology 100, 255–265.

Peng, Y., Stoleru, D., Levine, J.D., Hall, J.C., Rosbach, M., 2003. Drosophila free-running rhythms require intercellular communication. PLoS Biology 1, e13. doi:10.1371/journal.pbio.0000013.

Pennartz, C.M., de Jeu M.T., Bos N.P., Schaap J., Geurtsen A.M., 2002. Diurnal modulation of pacemaker potentials and calcium current in the mammalian circadian clock. Nature 416, 286-290.

Peschel, N., Helfrich-Förster, C., 2011. Setting the clock by nature: circadian rhythm in the fruitfly *Drosophila melanogaster*. FEBS Letters 585, 1435-1442.

Petri, B., 1998. Neuronal organisation of a circadian clock. Analysis of the clock which controls circadian locomotor behaviour of the cockroach *Leucophaea maderae.* Dissertation: University of Regensburg, Germany.

Petri, B., Homberg, U., Loesel, R., Stengl, M., 2002. Evidence for a role of GABA and Mas-allatotropin in photic entrainment of the circadian clock of the cockroach *Leucophaea maderae*. Journal of Experimental Biology 205, 1459-1469.

Petri, B., Stengl, M., 1997. Pigment-dispersing hormone shifts the phase of the circadian pacemaker of

the cockroach *Leucophaea maderae*. Journal of Neuroscience 17, 4087-4093.

Petri, B., Stengl, M., 2001. Phase response curves of a molecular model oscillator: implications for mutual coupling of paired oscillators. Journal of Biological Rhythms 16, 125-141.

Petri, B., Stengl, M., Würden, S., Homberg, U., 1995. Immunocytochemical characterization of the accessory medulla in the cockroach *Leucophaea maderae*. Cell and Tissue Research 282, 3-19.

Picot, M., Cusumano, P., Klarsfeld, A., Ueda, R., Rouyer, F., 2007. Light activates output from evening neurons and inhibits output from morning neurons in the *Drosophila* circadian clock. PLoS Biology 5, e315. doi:10.1371/journal.pbio.0050315.

Pittendrigh, C.S., Daan, S., 1976. A functional analysis of circadian pacemakers in nocturnal rodents V. Pacemaker structure: a clock for all seasons. Journal of Comparative Physiology 106, 333–355.

Pittendrigh, C.S., Minis, D.H., 1964. The entrainment of circadian oscillations by light and their role as photoperiodic clocks. American Naturalist 98, 261–294.

Pitts, G.R., Ohta, H., McMahon, D.G., 2006. Daily rhythmicity of large-conductance Ca^{2+}-activated K^{+} currents in suprachiasmatic nucleus neurons. Brain Research 1071, 54-62.

Potdar, S., Sheeba, V., 2012. Large Ventral Lateral Neurons Determine the Phase of Evening Activity Peak across Photoperiods in *Drosophila melanogaster. J*ournal of *Biolo*gical *Rhythms* 27, 267-279.

Price, J.L., Blau, J., Rothenfluh, A., Abodeely, M., Kloss, B., Young, M.W., 1998. *Double-time* is a novel *Drosophila* clock gene that regulates PERIOD protein accumulation. Cell 94, 83–95.

Raikhel, A. S., Brown, M.R., Belles, C., 2005. Hormonal control of reproductive process. In: Gilbert, L.I., Iatrou, K., Gill, S.S. (Eds.), Comperehensive Molecular Insect Science Endocrinology, vol. 3. Elsevier, Amsterdam, pp. 433–491.

Reischig, T., Stengl, M., 1996. Morphology and pigment-dispersing hormone (PDH)-immunocytochemistry of the accessory medulla, the presumptive circadian pacemaker of the cockroach *Leucophaea maderae*: a light- and electron-microscopical study. Cell and Tissue Research 255, 305-319.

Reischig, T., Stengl, M., 2002. Optic lobe commissures in a three-dimensional brain model of the cockroach *Leucophaea maderae*: A search for the circadian coupling pathways. Journal of Comparative Neurology 443, 388-400.

Reischig, T., Stengl, M., 2003a. Ectopic transplantation of the accessory medulla restores circadian locomotor rhythms in arrhythmic cockroaches (*Leucophaea maderae*). Journal of Experimental Biology 206, 1877-1886.

Reischig, T., Stengl, M., 2003b. Ultrastructure of pigment-dispersing hormone-immunoreactive neurons in a threedimensional model of the accessory medulla of the cockroach *Leucophaea maderae*. Cell and Tissue Research 314, 421-435.

Richard, D. S., Watkins, N.L., Serafin, R.B., Gilbert, L.I., 1998. Ecdysteroids regulate yolk protein uptake by *Drosophila melanogaster* oocytes. Journal of insect physiology 44, 637–644.

Rieger, D., Shafer, O.T., Tomioka, K., Helfrich-Förster, C., 2006. Functional analysis of circadian pacemaker neurons in Drosophila melanogaster. Journal of Neuroscience 26, 2531–2543.

Rieger, D., Wülbeck, C., Rouyer, F., Helfrich-Förster, C., 2009. Period gene expression in four neurons is sufficient for rhythmic activity of *Drosophila melanogaster* under dim light conditions. Journal of Biological Rhythms 24, 271–282.

Riihimaa, A.J., Kimura, M., 1988. A mutant strain of Chymomyza costata (Diptera: Drosophilidae) insensitive to diapause-inducing action of photoperiod. Physiological Entomology 13, 441–445.

Roberts, S.K., 1974. Circadian rhythms in cockroaches: effects of optic lobe lesions. Journal of

Comparative Physiology A 88, 21-30.

Rudy, B., McBain, C., 2001. Kv3 channels: voltage-gated K+ channels designed for high-frequency repetitive firing. Trends in Neuroscience 24, 517–526.

Sandrelli, F., Tauber, E., Pegoraro, M., Mazzotta, G., Cisotto, P., Landskron, J., Stanewsky, R., Piccin, A., Rosato, E., Zordan, M., Costa, R., Kyriacou, C.P., 2007. A molecular basis for natural selection at the timeless locus in *Drosophila melanogaster*. Science 316, 1898–1900.

Sato, Y., Ikeda, M., Yamashita, O., 1994. Neurosecretory cells expressing the gene for common precursor for diapause hormone and pheromone biosynthesis-activating neuropeptide in the subesophageal ganglion of the silkworm, *Bombyx mori*. General and Comparative Endocrinology 96, 27–36.

Saunders, D.S., 2005. Erwin Bünning and Tony Lees, two giants of chronobiology, and the problem of time measurement in insect photoperiodism. Journal of Insect Physiology 51, 599–608.

Saunders, D.S, 2007. Photoperiodism in insects and other animals. In: Bjorn, L.O. (Ed.), Photobiology: The Science of Life and Light. 2nd ed. Springer, New York, pp. 389–416.

Saunders, D.S., 2009. Circadian rhythms and the evolution of photoperiodic timing in insects. Physiological Entomology 34, 301–308.

Saunders, D.S., 2010a. Photoperiodism in insects: migration and diapause responses Photoperiodism. In: Nelson, R.J., Denlinger, D.L., Somers, D.E. (Eds.), The Biological Calendar. Oxford University Press, Oxford, pp. 218–257.

Saunders, D.S., 2010b. Controversial aspects of photoperiodism in insects and mites. Journal of Insect Physiology 56, 1491–1502.

Saunders, D.S., Henrich, V.C., Gilbert, L.I., 1989. Induction of diapause in *Drosophila melanogaster*: Photoperiodic regulation and the impact of arrhythmic clock mutations on time measurement. Proceedings of the National Academy of Sciences of the USA 86, 3748–3752.

Schaap, J., Albus, H., VanderLeest, H.T., Eilers, P.H., Detari, L., Meijer, J.H., 2003. Heterogeneity of rhythmic suprachiasmatic nucleus neurons: implications for circadian waveform and photoperiodic encoding. Proceedings of the National Academy of Sciences USA 100, 15994–15999.

Schneider, N.L., Stengl, M., 2005. Pigment-dispersing factor and GABA synchronize cells of the isolated circadian clock of the cockroach *Leucophaea maderae*. Journal of Neuroscience 25, 5138-5147.

Schneider, N.L., Stengl, M., 2006. Gap junctions between accessory medulla neurons appear to synchronize circadian clock cells of the cockroach *Leucophaea maderae*. Journal of Neurophysiology 95, 1996-2002.

Schneider, N.L., Stengl, M., 2007. Extracellular long-term recordings of the isolated accessory medulla, the circadian pacemaker center of the cockroach *Leucophaea maderae*, reveal ultradian and hint circadian rhythms. Journal of Comparative Physiology A 193, 35-42.

Schulze, J., Neupert, S., Schmidt, L., Predel, R., Lamkemeyer, T., Homberg, U., Stengl, M., 2012. Myoinhibitory peptides in the brain of the cockroach *Leucophaea maderae* and colocalization with pigment-dispersing factor in circadian peacemaker cells. Journal of Comparative Neurology 520, 1078-1097.

Sehgal, A., Price, JL., Man,B., 1994. Loss of circadian behavioral rhythms and per RNA oscillations in the Drosophila mutants timeless. Science 263, 1603-1606.

Seuge, J., Veith, K., 1976. Diapause de *Pieris brassicae*: Role des photorecepteurs cephaliques, etude des carotenoides cerebraux. Journal of insect physiology 22, 1229–1235.

Shafer, O.T., Kim, D.J., Dunbar-Yaffe, E., Nikolaev, V.O., Lohse, M.J., Taghert, P.H., 2008. Widespread

receptivity to neuropeptide PDF throughout the neuronal circadian clock network of Drosophila revealed by realtime cyclic AMP imaging. Neuron 58, 223–237.

Shafer, O.T., Levine, J.D., Truman, J.W., Hall, J.C., 2004. Flies by night: effects of changing day length on Drosophila's circadian clock. Current Biology 14, 424–432.

Sheeba, V., Fogle, K.J., Holmes, T.C., 2010. Persistence of morning anticipation behavior and high amplitude morning startle response following functional loss of small ventral lateral neurons in *Drosophila*. PLoS One 5, e11628. doi:10.1371/journal.pone.0011628

Sheeba, V., Fogle, K.J., Kaneko, M., Rashid, S., Chou, Y.T., Sharma, V.K., Holmes, T.C., 2008a. Large ventral lateral neurons modulate arousal and sleep in *Drosophila*. Current Biology 18, 1537-1545.

Sheeba, V., Gu, H., Sharma, V.K., O'Dowd, D.K., Holmes, T.C., 2008b. Circadian- and light-dependent regulation of resting membrane potential and spontaneous action potential firing of *Drosophila* circadian pacemaker neurons. Journal of Neurophysiology 99, 976-988.

Shiga, S., Davis, N.T., Hildebrand, J.G., 2003. Role of neurosecretory cells in the photoperiodic induction of pupal diapause of the tobacco hornworm *Manduca sexta*. Journal of Comparative Neurology 447, 366–380.

Shiga, S., Numata, H., 2000. The role of neurosecretory neurons in the pars intercerebralis and pars lateralis in reproductive diapause of the blow fly, *Protophormia terranovae*. Naturwissenschaften 87, 125–128.

Shiga, S., Numata, H., 2009. Roles of PER immunoreactive neurons in circadian rhythms and photoperiodism in the blow fly, *Protophormia terraenovae*. Journal of Experimental Biology 212, 867-877.

Shimizu, I., Yamanaka, Y., Shimazaki, Y., Iwasa, T., 2001. Molecular cloning of Bombyx cerebral opsin (Boceropsin) and cellular localization of the expression in the silkworm brain. Biochemical and Biophysical Research Communications 287, 27–34.

Siegmund, T., Korge, G., 2001. Innervation of the ring gland of *Drosophila*. Journal of Comparative Neurology 431, 481–491.

Söhler, S., Neupert, S., Predel, R., Nichols, R., Stengl, M., 2007. Localization of leucomyosuppressin in the brain and circadian clock of the cockroach *Leucophaea maderae*. Cell and Tissue Research 328, 443-452.

Söhler, S., Neupert, S., Predel, R., Stengl, M., 2008. Examination of the role of FMRFamide-related peptides in the circadian clock of the cockroach *Leucophaea maderae*. Cell and Tissue Research 332, 257-269.

Söhler, S., Stengl, M., Reischig, T., 2011. Circadian pacemaker coupling by multi-peptidergic neurons in the cockroach *Leucophaea maderae.* Cell and Tissue Research 343, 559-577.

Sokolove, P.G., 1975. Localization of the cockroach optic lobe circadian pacemaker with microlesions. Brain Research 87, 13-21.

Stanewsky, R., Kaneko, M., Emery, P., Beretta, B., Wager-Smith, K., Kay, S. A., Rosbash, M., Hall, J. C., 1998. The cryb mutation identifies cryptochrome as a circadian photoreceptor in *Drosophila*. Cell 95, 681-692.

Stengl, M., Homberg, U., 1994. Pigment-Dispersing Hormone-Immunoreactive Neurons in the cockroach *Leucophaea maderae* Share Properties with Circadian Pacemaker Neurons. Journal of Comparative Physiology A 175, 203-213.

Stoleru, D., Nawathean, P., Paz Fernandez, M., de la Menet, J.S., Ceriani, M.F., Rosbach, M., 2007. The Drosophila circadian network is a seasonal timer. Cell 129, 207–219.

Stoleru, D., Peng, Y., Agosto, J., Rosbach, M., 2004. Coupled oscillators control morning and evening locomotor behaviour of Drosophila. Nature 431, 862–868.

Stoleru, D., Peng, Y., Nawathean, P., Rosbach, M., 2005. A resetting signal between *Drosophila* pacemakers synchronizes morning and evening activity. Nature 438, 238–242.

Tomioka, K., Matsumoto, A., 2010. A comparative view of insect circadian clock systems. Cellular and Moledular Life Sciences 67*:* 1397-1406*.*

Tyshchenko, V. P., 1966. Two-oscillatory model of the physiological mechanism of insect photoperiodic reaction. Zhurnal Obshchei Biologii 27, 209–222.

Vafopoulou, X., Steel, C.G.H., 1996. The insect neuropeptide prothoracicotropic hormone is released with a daily rhythm: re-evaluation of its role in development. Proceedings of the National Academy of Sciences of the USA 93, 3368–3372.

Vafopoulou, X., Steel, C.G.H., 2009. Circadian organization of the endocrine system. In: Gilbert, L.I. (Ed.), Insect Development. Elsevier, Oxford, pp. 395–458.

Vafopoulou, X., Steel, C.G.H., Terry, K.L., 2007. Neuroanatomical relations of prothoracicotropic hormone neurons with the circadian timekeeping system in the brain of larval and adult Rhodnius prolixus (Hemiptera). Journal of Comparative Neurology 503, 511–524.

Vafopoulou, X., Terry, K.L., Steel, C.G.H., 2010. The circadian timing system in the brain of the fifth larval instar of Rhodnius prolixus (Hemiptera). Journal of Comparative Neurology 518, 1264–1282.

Vandael, D.H., Marcantoni, A., Mahapatra, S., Caro, A., Ruth, P., Zuccotti, A., Knipper, M., Carbone, E., 2010. Ca(v)1.3 and BK channels for timing and regulating cell firing. Molecular Neurobiology 42, 185–198.

Veleri, S., Rieger, D., Helfrich-Förster, C., Stanewsky, R., 2007. Hofbauer-Buchner eyelet affects circadian photosensitivity and coordinates TIM and PER expression in *Drosophila* clock neurons. Journal Biological Rhythms 22, 29-42.

Vladimir, K., 2011. Insect photoperiodic calendar and circadian clock: independence, cooperation or unity? Journal of insect physiology 57, 538-556.

Webb, A. B., Angelo, N., Huettner, J. E., Herzog, E. D., 2009. Intrinsic, nondeterministic circadian rhythm generation in identified mammalian neurons. Proceedings of the National Academy of Sciences of the USA 106, 16493–16498.

Williams, J. A., Su, H. S., Bernards, A., Field, J., Sehgal, A., 2001. A circadian out in *Drosophila* mediated by neurofibromatosis-1 and Ras/MAPK. Science 293, 2251-2256.

Wülbeck, C., Grieshaber, E., Helfrich-Förster, C., 2008. Pigment-dispersing factor (PDF) has different effects on *Drosophila's* circadian clocks in the accessory medulla and in the dorsal brain. Journal of Biological Rhythms 23, 409-424.

Yamaguchi, S., Isejima, H., Matsuo, T., Okura, R., Yagita, K., Kobayashi, M., Okamura, H., 2003. Synchronization of cellular clocks in the suprachiasmatic nucleus. Science 302, 1408-1412.

Yamashita, O., 1996. Diapause hormone of the silkworm, *Bombyx mori*: structure, gene expression and function. Journal of Insect Physiology 42, 669–679.

Yoshii, T., Rieger, D., Helfrich-Förster, C., 2012. Two clocks in the brain – an update of the Morning and Evening oscillator model in *Drosophila.* Progress in Brain Research 199, 59-82.

Yoshii, T., Wülbeck, C., Sehadova, H., Veleri, S., Bichler, D., Stanewsky, R., Helfrich-Förster, C., 2009. The neuropeptide Pigment-dispersing factor adjusts period and phase of Drosophila's clock. Journal of Neuroscience 25, 2597–2610.

Zhang, L., Chung, B. Y., Lear, B. C., Kilman, V. L., Liu, Y., Mahesh, G., 2010. DN1(p) circadian neurons

coordinate acute light and PDF inputs to produce robust daily behavior in Drosophila. Current Biology 20, 591–599.

Zhao, Z., Zera, A.J., 2004. The hemolymph JH titer exhibits a large-amplitude. morph-dependent, daily cycle in the wing-polymorphic cricket *Gryllus firmus*. Journal of Insect Physiology 49, 137–148.

Chapter I

Implementation of pigment-dispersing factor-immunoreactive neurons in a standardized atlas of the brain of the cockroach *Leucophaea maderae*

Wei HY, el Jundi B, Homberg U, and Stengl M. 2010.
This manuscript is published in J Comp Neurol 518: 4113-4133.

Implementation of Pigment-Dispersing Factor-Immunoreactive Neurons in a Standardized Atlas of the Brain of the Cockroach *Leucophaea maderae*

Hongying Wei,[1] Basil el Jundi,[2] Uwe Homberg,[2] and Monika Stengl[1]*

[1]Animal Physiology, FB18, University of Kassel, 34132 Kassel, Germany
[2]Animal Physiology, Philipps-University of Marburg, 35032 Marburg, Germany

ABSTRACT

The cockroach *Leucophaea maderae* is an established model in circadian rhythm research. Its circadian clock is located in the accessory medulla of the brain. Pigment-dispersing factor-immunoreactive (PDF-ir) neurons of the accessory medulla act as circadian pacemakers controlling locomotor activity rhythms. To characterize the neuronal network of the circadian system in *L. maderae*, the PDF-ir neurons were implemented into a standardized three-dimensional atlas of the cockroach brain. Serial confocal images from 20 wholemount brains were used for the construction of the atlas comprising 21 neuropils. Two different standardization protocols were employed: the iterative shape averaging (ISA) procedure using an affine transformation followed by iterative non-rigid registrations, and the virtual insect brain (VIB) protocol employing local non-rigid transformations after global and local rigid transformations. Quantitative analysis of the 20 brains revealed that volumes of the accessory medulla are directly correlated with the volumes of the medulla, the protocerebral bridge, and the upper division of the central body, suggesting functional connections among these neuropils. For a standardized reconstruction of the circadian pacemaker network, the ISA protocol was used to register PDF-ir neurons in the standard cockroach brain. The registration revealed that two PDF-ir arborization areas in the brain are highly interconnected with other PDF-ir projection sites and appear to be contacted both by fibers in the posterior and the anterior optic commissures. The distances between PDF-ir branching areas show specific numerical relationships that might be physiologically relevant for temporal encoding. J. Comp. Neurol. 518:4113–4133, 2010.

INDEXING TERMS: circadian pacemaker; neuropeptides; insect brain; neural networks

Geophysical rhythms such as the 24-hour light-dark cycle allowed for the evolution of circadian clocks in apparently all life on earth. The cockroach *Leucophaea maderae* is an established model system for research on circadian rhythms. Nishiitsutsuji-Uwo and Pittendrigh (1968) showed that a circadian clock located in the optic lobe controls locomotor activity rhythms in the cockroach. Lesion and transplantation studies identified the accessory medulla (aMe), a small neuropil with about 250 associated neurons at the ventromedial edge of the medulla, as the circadian pacemaker (Stengl and Homberg, 1994; Reischig and Stengl, 2003a). Unlike other optic lobe neuropils, the aMe is not retinotopically organized but consists of noduli, an internodular region, a shell, and an anterior fiber network (Reischig and Stengl, 1996, 2002, 2003b, 2004; Petri et al., 2002).

Neurons of the aMe are packed with an unusually high density of dense-core vesicles, which contain neuropeptides. Among these peptidergic cells are pigment-dispersing factor-immunoreactive (PDF-ir) neurons, which control locomotor activity rhythms (for reviews, see Helfrich-Förster et al., 1998; Homberg et al., 2003). In the cockroach brain, two groups of PDF-ir neurons are located

Additional Supporting Information may be found in the online version of this article.

Grant sponsor: Deutsche Forschungsgemeinschaft; Grant number: HO 950/14 (to U.H.).

*CORRESPONDENCE TO: Monika Stengl, Biology, Animal Physiology, FB18, University of Kassel, 34132 Kassel, Germany. E-mail: stengl@uni-kassel.de

Received November 25, 2009; Revised April 27, 2010; Accepted May 19, 2010
DOI 10.1002/cne.22471
Published online July 26, 2010 in Wiley Online Library (wileyonlinelibrary.com)

next to the lamina (d- and vPDFLa), 12 anterior PDF-ir neurons are located near the aMe (aPDFMe), and 6 posterior PDF-ir cells (pPDFMe) lie in the posterior cell cortex of the medulla (Petri et al., 1995; Reischig and Stengl, 1996, 2003b). The aPDFMe cells comprise four large, four medium-sized, and four small PDF-ir neurons. Electron microscopy combined with PDF immunocytochemistry revealed that the large PDF-ir cells largely arborize in the shell and anterior region of the aMe. This is the input and output region of the circadian clock, connecting it to optic lobe and midbrain neuropils (Reischig and Stengl, 2003b). In contrast, the medium-sized aPDFMe innervate the internodular and, to a lesser extent, the nodular neuropil of the aMe. The small aPDFMe are local neurons of the aMe. It is not known whether they branch in both the internodular and the nodular neuropil of the aMe. In the nodular neuropil, visual information is provided by γ-aminobutyric acid (GABA)-ir distal-tract terminals from the medulla and is processed by allatotropin-ir local interneurons of the aMe (Reischig and Stengl, 2003b; Petri et al., 2002).

Thus, the aPDFMe neurons contribute to different functional circuits in the aMe. They process ipsi- and possibly contralateral visual information in the noduli/internoduli and provide output/input circuits to midbrain and optic lobe neuropils (for review, see Homberg et al., 2003). Backfills from the contralateral aMe showed that at least three aPDFMe neurons (the largest and medium-sized aPDFMe) connect both aMae via the anterior and posterior optic commissures (Reischig and Stengl, 2002, 2004). Electrophysiological studies indicated that aMe cells generate regular action potentials in the gamma frequency range (Schneider and Stengl, 2005). Gap junctions between aMe neurons maintain defined phase differences between the neurons' spontaneous action potentials (Schneider and Stengl, 2006), and synaptic interactions via GABAergic interneurons result in different ensembles of synchronized cells that all fire at the same phase. These ensembles of cells were rearranged into new ensembles by PDF application (Schneider and Stengl, 2005). Schneider and Stengl (2005, 2006, 2007) hypothesized that PDF released from circadian pacemaker neurons of the aMe control more than one functional output via ensemble formation. Which of these outputs and postsynaptic targets of PDF-ir neurons, however, are essential for the control of locomotor activity rhythms is still unknown. In addition, the arborization patterns of the different PDF-ir neurons and their axonal pathways to the brain remain to be elucidated. Lesion studies indicated that one optic lobe circadian clock not only controls locomotor activity rhythms via ipsi- and contralateral outputs, but also provides coupling output to the contralateral optic lobe pacemaker and receives ipsi- and contralateral light entrainment input (Page, 1984).

To facilitate understanding of the connectivity patterns of circadian pacemaker neurons in the cockroach, we have generated in the present study a 3D standard atlas of the cockroach brain, following two established procedures, the virtual insect brain (VIB) protocol and the iterative shape averaging (ISA) method. The VIB protocol has been used to create standardized brains of the fruit fly *Drosophila* (Rein et al., 2002; Jenett et al., 2006), the desert locust *Schistocerca gregaria* (Kurylas et al., 2008), and the giant sphinx moth *Manduca sexta* (el Jundi et al., 2009), whereas the ISA method has been used in the honeybee (Rohlfing et al., 2001; Brandt et al., 2005), the desert locust (Kurylas et al., 2008), and the noctuid moth *Heliothis virescens* (Kvello et al., 2009). Whereas the VIB protocol can be used to determine time- or stimulus-dependent differences in the individual brains, the ISA protocol is designed to eliminate these differences to obtain an average brain for implementation of identified neurons. The two standard cockroach brains described here comprise atlases of 21 neuropils, calculated from 20 individual immunostained wholemount brains. The quality of the two standardization procedures is evaluated with respect to neuropil sizes and their relative positions. Based on our data set of 20 individual brains, we determined significant volumetric relationships among certain brain neuropils.

In a second step, the branching pattern of PDF-ir neurons was implemented into the ISA standard brain atlas. New details on the branching pattern of the PDF-ir cells are presented and statistically analyzed. Two highly interconnected PDF-ir branching sites are identified that might allow for information exchange between the posterior and anterior optic commissures. In addition, unexpected

Abbreviations

a1–2	area 1–2
AFP	anterior fiber plexus
aMe	accessory medulla
aPDFMe	anterior PDF neurons of the medulla
AOC	anterior optic commissure
3D	three-dimensional
dPDFLa	dorsal PDF neurons of the lamina
ir	immunoreactive
ILP	inferior lateral protocerebrum
ISA	iterative shape averaging
LVT	lobula valley tract
p1–p5	plexus 1–5
PBS	phosphate-buffered saline
PBT	phosphate-buffered saline containing Triton X-100
PDF	pigment-dispersing factor
PDH	pigment-dispersing hormone
POC	posterior optic commissure
POTu	posterior optic tubercle
pPDFMe	posterior PDF neurons of the medulla
SLP	superior lateral protocerebrum
SMP	superior median protocerebrum
VIB	virtual insect brain
VLP	ventrolateral protocerebrum
vPDFLa	ventral PDF neurons of the lamina

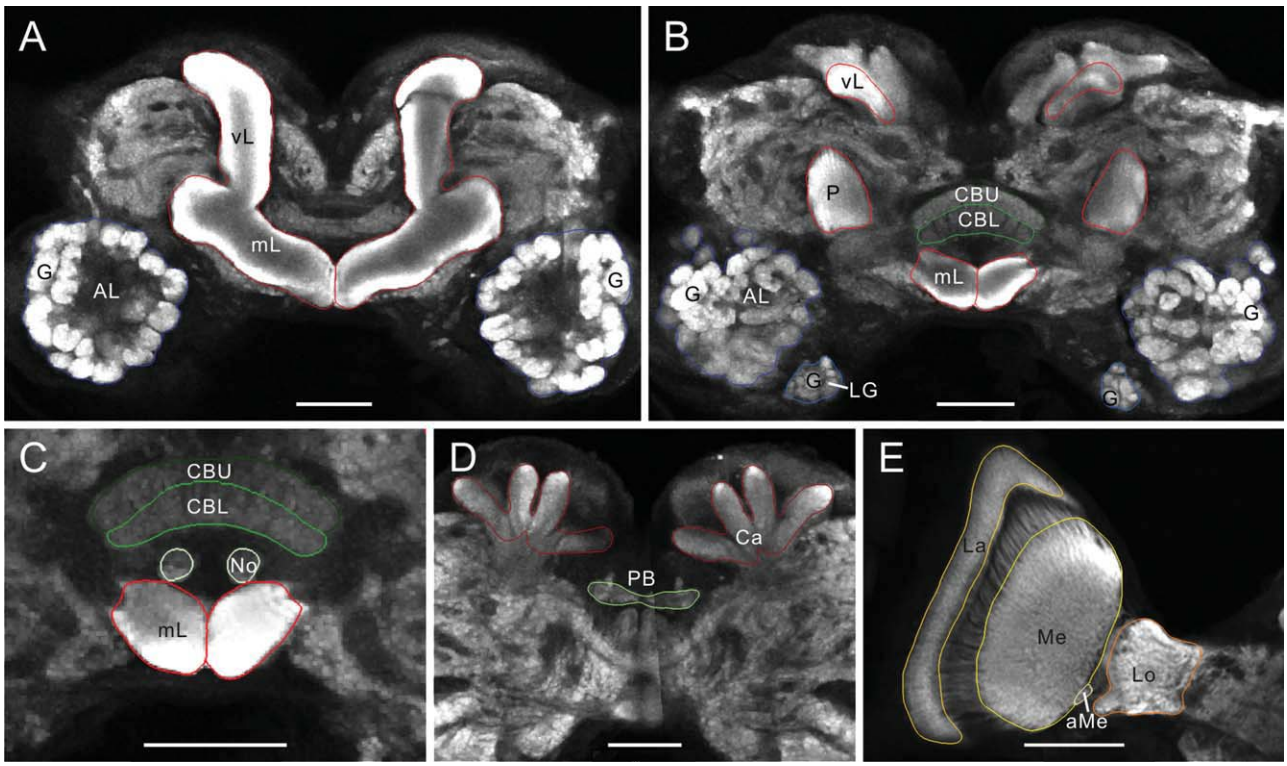

Figure 1. Confocal images from a cockroach brain immunostained with an antibody against the presynaptic vesicle protein synapsin I. Neuropils were labeled manually for three-dimensional surface reconstruction. **A–D:** The most conspicuous neuropils of the protocerebrum are the mushroom bodies with the calyx (Ca), the pedunculus (P), the vertical and median lobes (vL, mL), and the central complex consisting of the protocerebral bridge (PB), the upper and lower divisions of the central body (CBU, CBL), and the noduli (No). In the deutocerebrum the antennal lobes (AL) and in the tritocerebrum the lobus glomerulatus (LG) were labeled individually. Both are subdivided into many glomeruli (G). **E:** The optic lobe contains the retinotopically organized lamina (La), medulla (Me), and lobula (Lo), whereas the accessory medulla (aMe) has a non-retinotopic nodular appearance. The sections were taken at a depth of about 195 μm (A), 273 μm (B), 316 μm (C), 390 μm (D), and 450 μm (E) from the anterior surface of the brain. Scale bar = 200 μm in A–E.

numerical relationships of the distances between the PDF-ir branching sites were found. These findings allow for a better understanding of the spatial distribution of circadian pacemaker neurons in the brain of the cockroach and considerably facilitate further physiological studies of the circadian system of the cockroach *L. maderae*.

MATERIALS AND METHODS

Animals

Experiments were performed on 20 adult male cockroaches (*Leucophaea maderae*) from laboratory colonies at the University of Marburg. Animals were reared at 27°C under a light-dark cycle of 12:12-hours (lights on at 8 a.m.). All brains were dissected at noon.

Characterization of primary antibodies

To label the neuropil structures of the brain, we used a monoclonal mouse anti-synapsin antibody (SYNORF1, 3C11, #151101 (13.12.06) kindly provided by Dr. E. Buchner, University of Würzburg, Germany). Selective neuropil staining by the SYNORF1 antibody has previously been demonstrated in several insect species (Brandt et al., 2005; Kurylas et al., 2008; el Jundi et al., 2009; Kvello et al., 2009). It was raised against a 66-kDa fusion protein comprising glutathione-S-transferase (GST) fused to the first amino acids of the presynaptic vesicle protein synapsin I coded by its 5′ fragment (nucleotide sequence 621–1967, shown in Fig. 1 of Klagges et al., 1996). Thereby, four or five synapsin isoforms (protein bands of 70, 74, 80, and ~143 kDa molecular weight) can be detected on a Western blot of *Drosophila* head homogenates (Klagges et al., 1996). Immunohistochemistry showed no synapsin detection by the SYNORF1 antibody in a *Drosophila* synapsin null mutant, syn^{79} (Godenschwege et al., 2004).

To label the PDF-ir network in the cockroach brain, we used an affinity-purified rabbit antiserum against β-pigment-dispersing hormone (PDH; #3B3), provided by Dr. H. Dircksen (University of Stockholm, Sweden). The antiserum was raised against conjugates of synthetic *Uca*

TABLE 1.
Primary Antibodies Used

Antibody	Working dilution	Source	Immunogen
Anti-synapsin	1:50	Dr. E. Buchner (Würzburg, Germany)	Recombinant glutathione-S-transferase (GST)-synapsin fusion protein
Anti-pigment-dispersing hormone (PDH)	1:20,000	Dr. H. Dircksen (Stockholm, Sweden)	Conjugates of synthetic *Uca pugilator/Cancer magister* fl-PDH and bovine thyroglobulin

pugilator/Cancer magister PDH (NSELINSILGLPKVMN-DAa) and bovine thyroglobulin (Dircksen et al., 1987). Immunodot-blotting analysis of high-pressure liquid chromatography (HPLC)-separated crustacean sinus-gland extracts showed PDH immunostaining only in biologically active peak fractions (Dircksen et al., 1987). In *L. maderae*, preadsorption of the diluted antiserum with 10 μm PDH completely abolished immunostaining (Stengl and Homberg, 1994).

Double immunostaining of wholemount brains

The generation of the cockroach standard brains is based on immunostainings of wholemount cockroach brains. To minimize tissue distortions, brains were dissected out of the head capsule in saline containing 156 mM NaCl, 4 mM KCl, 6 mM $CaCl_2$, and 5 mM glucose (Schneider and Stengl, 2005). Brains were fixed overnight at 4°C in 4% paraformaldehyde in 0.1 M phosphate-buffered saline (0.1 M PBS, pH 7.4). They were subsequently washed 5 times for 15 minutes in 0.1 M PBS and were treated with 1 mg/ml collagenase in 0.05 M Tris buffer for 1 hour at room temperature to make the ganglionic sheath permeable. Afterwards, the brains were rinsed six times for 2 hours with 0.1 M PBS containing 0.5% Triton X-100 (0.1 M PBT) and were preincubated overnight at 4°C with 5% normal goat serum (NGS; Jackson ImmunoResearch, Westgrove, PA) in 0.1 M PBT containing 0.02% sodium azide. Brains were incubated for 5 days at 4°C with the two primary antibodies (Table 1), anti-synapsin (1:50) and anti-PDH (1:20,000), in 0.1 M PBT containing 1% NGS and 0.02% sodium azide. After extensive washing with 0.1 M PBT over 2 hours, the brains were incubated for 4 days at 4°C in secondary antibodies, goat anti-mouse conjugated to Cy5 (cat. no. 115-175-146 Jackson ImmunoResearch) and goat anti-rabbit conjugated to Cy3 (cat. no. 111-165-003 Jackson ImmunoResearch). Both antisera were diluted 1:300 in 0.1 M PBT containing 1% NGS and 0.02% sodium azide. After this staining step, the brains were rinsed 6 times for 20 minutes in 0.1 M PBT and were dehydrated in an increasing ethanol series (50%, 70%, 90%, 95%, 100%, 15 minutes each). The brains were cleared in a solution of 50% ethanol/50% methyl salicylate for 15 minutes and subsequently for 40 minutes in 100% methyl salicylate (Merck, Darmstadt, Germany). Finally, the brains were embedded in Permount (Fisher Scientific, Pittsburgh, PA) between two coverslips using eight spacers (Zweckform, Oberlaindern, Germany) to prevent compressions.

Confocal microscopy

Brains were imaged with a confocal laser scanning microscope (Leica TCS SP2) using a 10× oil objective (HC PL APO 10×/0.4 Imm Corr CS; Leica, Bensheim, Germany). The fluorescence signals of Cy5 and Cy3 were detected with an HeNe laser (633 nm) for the anti-synapsin staining and an Ar laser (543 nm) for the anti-PDF staining. The wholemount brains were scanned at a resolution of 512 × 512 pixels in the xy direction and a step size of 2 μm in the axial direction. This resulted in a voxel size of the image stacks of 2.93 × 2.93 × 2 μm. Because of the thickness and width of the brains and the limitation of the working distance of the 10× oil objective, each brain was scanned in four image stacks, two from anterior and two from posterior.

Reconstruction of neuropils in the cockroach brains

Neuropil reconstructions were performed with Amira 3.1 and 4.1 (Visage Imaging, Fürth, Germany) on a personal computer (Inter Pentium D945 2x3.4GHz, 2048MB RAM, running Windows XP). The four anti-synapsin image stacks were oriented based on gray values and were merged following translation, rotation, and scaling. The same transformation parameters were used for alignment of the corresponding image stacks showing anti-PDF staining. Brain areas were labeled based on the image stacks by using the segmentation editor in Amira. Therefore, reconstruction of brain areas was performed by labeling the neuropils in selected frontal, sagittal, and axial slices. A 3D structure was then calculated by using the function “wrap.” As a result, a “labelfield” for an individual brain with all labeled neuropils could be generated.

Generation of the standard brain

Two different protocols for registration of a 3D insect standard brain have been established: the virtual insect brain protocol (VIB; Rein et al., 2002; Jenett et al., 2006)

and the iterative shape averaging method (ISA; Rohlfing et al., 2001; Brandt et al., 2005). We followed both procedures and created two 3D standard brains of the cockroach based on the same set of 20 individual brains by using the VIB protocol and the ISA method. Both methods require selection of an individual brain as a template on which the other individual brains are registered. To choose an ideal template brain, we calculated for each brain the relative positions and volumes of all reconstructed neuropils. The brain with the smallest volume and position differences to the mean volume and to the mean distances was chosen as the template brain for registration.

The creation of the VIB standard brain consisted of three transformation steps. At first, the reconstructed brain areas were transformed by a global rigid transformation (translation, rotation, and isotropic scaling). Next, the brains were transformed by using a local rigid transformation, and the overlaps of the volumes of the individual neuropils were maximized for each labeled structure without influence from the other labeled neuropils (Jenett et al., 2006). Finally, after a non-rigid transformation with a diffusion algorithm, the relative positions between neuropils were corrected according to the template.

In contrast to the VIB standard brain, the ISA standard brain was calculated based on the image stacks. Thereby, an intensity-based affine transformation and iterative non-rigid transformations were carried out to maximize the entropy-based normalized mutual information (Rohlfing et al., 2001). By using affine transformation, the image stacks were transformed with respect to translation, rotation, anisotropic scaling, and shearing. During the iterative averaging process, the images were segmented into third-order 3D B-splines and were transformed iteratively four times by using a non-rigid elastic algorithm.

Reconstruction and registration of the PDF-ir neurons

The PDF-ir neurons from one of the 20 individual cockroach brains whose fine PDF-ir fiber projections could be completely resolved was reconstructed and fitted into the ISA standard brain.

For better structural analysis, the PDF-ir neurons were scanned and reconstructed with a voxel size of $1.46 \times 1.46 \times 2$ µm. The 3D reconstruction of the PDF-ir neuronal network was accomplished by a custom module in Amira 3.1, the "skeleton reconstruction" tool (Schmitt et al., 2004; Evers et al., 2005). The beginning, branching, and end points of stained fibers were selected manually. For surface reconstructions, the midline and diameter of each neuronal branch were automatically determined by means of local staining intensity gradients.

Because the relative position between the neuropils and PDF-ir neurons should be preserved, the implementation was based on the volumes and centers of gravity of 21 neuropils comprising the PDF-ir network. The registration procedure using Amira 4.1 is described in detail in Kurylas et al. (2008) and el Jundi et al. (2010). The labeled neuropils of the individual brain were transformed into the standard brain by using an affine transformation, followed by an elastic transformation. The resulting transformation matrix and the deformation field (vector field) of both transferring steps were then used to register the PDF-ir neurons into the standard brain. Because of the complexity of the widespread PDF-ir fiber connections, all 21 neuropils had to be registered into the ISA standard brain in one process. Owing to limited computer resources and to limitations of the software available, the neuropil images had to be downsampled to a voxel size of $8 \times 8 \times 8$ µm during the elastic transformation. However, the resolution of PDF-ir neurons retained the voxel size of $1.46 \times 1.46 \times 2$ µm, which allowed for detailed analysis of their fiber processes.

Photomicrograph production was obtained with AMIRA only. For size adjustment, inclusion of symbols and letters, and constructions of schemes (see Fig. 11A,B). Corel Draw X3 was employed. Figures 10 and 12 were designed with Microsoft Office Excel.

Statistics

Based on the data from the 20 individual brains (neuropil sizes and centers of gravity), statistical studies were performed by using Microsoft Office Excel and SPSS 13.0. To test whether the cockroach brain is bilaterally symmetric, we compared volumes and relative positions in transferred coordinates of corresponding left and right neuropils by using paired t-tests. Linear regression analyses in SPSS were performed to analyze pairs of selected neuropils for correlations in volumes. As a positive control, we examined whether the lamina, medulla, and lobula were correlated in volume size. The quality of standardization was evaluated by one-sample t-tests. This test determined whether the standard atlas represented the average shape, size, and relative positions of neuropils of the 20 individual brains. To evaluate the quality of the ISA standard brain, we compared the distances of the non-rigid deformations between the 20 individual brains and the ISA standard brain and between each individual brain and 5 randomly selected individual brains (Suppl. Fig. 7).

To determine whether there were statistically significant differences in the size and position of aPDFMe-ir and pPDFMe-ir somata, the diameter of the PDF-ir cell bodies and the distances of their centers to the border of the aMe were measured. The relationship between size and position of PDF-ir somata was studied by using linear

regression in SPSS. PDF-ir arborization sites were named "area" if more than one PDF-ir axon bundle contributed fibers. A site was called "plexus" if it was supplied by fibers from one axon bundle only. To analyze the morphology of the PDF-ir neuronal system, the distances between all PDF-ir arborization sites were measured in 10 cockroach brains. To examine whether the PDF-ir arborization sites were arranged in identical distances to each other or in multiples thereof, we evaluated the relationships between the respective distances with Origin 6.0 (Microcal Software, Northampton, MA).

RESULTS

Reconstructed neuropils of the cockroach brain

Immunocytochemistry using the antibody SYNORF1 revealed intense immunostaining in synaptic neuropils in the cockroach brain, whereas somata and tracts remained unstained (Fig. 1A–E). Based on distinct immunostaining, 21 neuropils were segmented from stacks of confocal images. In the central brain, subcompartments of the mushroom bodies and central complex were reconstructed. In the mushroom bodies, which are implicated in associative olfactory learning and memory, sensory filtering, motor control, and place memory (Mizunami et al., 1998; Menzel and Giurfa, 2006; Liu and Davis, 2006), the paired cup-shaped calyces and the combined pedunculus/vertical and medial lobe were reconstructed separately (Fig. 1A,B). In the central complex, which is involved in spatial orientation, locomotor control, and visual object recognition (Strauss, 2002; Liu et al., 2006; Heinze and Homberg, 2007), the protocerebral bridge, the upper and lower divisions of the central body, and the pair of noduli were reconstructed separately (Fig. 1B–D).

Anteroventrally in the deutocerebrum, the antennal lobes are the primary olfactory centers of the insect brain (Fig. 1A,B). In the antennal lobe, about 100 glomeruli could be distinguished. Also encoding chemosensory information, the lobus glomerulatus (Fig. 1B) of the tritocerebrum is a gustatory neuropil (Ernst et al., 1977; Ignell et al., 2000). In *L. maderae* it consists of about 15 spherical glomeruli. For the purpose of whole-brain reconstruction, the antennal lobe and the lobus glomerulatus were segmented as single entities. The optic lobes are the primary processing centers of visual information from both compound eyes. In the optic lobe, the three retinotopically organized neuropils, the lamina, the medulla (Me), and the lobula and the non-retinotopically organized accessory medulla (aMe) were segmented individually (Fig. 1E). The aMe is located anteriorly at the ventromedian border of the medulla (Reischig et al., 2003a,b). The stained neuropil structures of an individual cockroach brain can be downloaded and visualized using AMIRA software. The Amira file and movie file are available online (Suppl. Figs. 1, 2).

Morphometric analysis of neuropils

Table 2 shows a volumetric analysis of all labeled neuropils from the 20 individual brains. Statistical analysis of the volumetric relationships between the labeled neuropils provided several results:

1. Comparison of volumes and relative positions of corresponding neuropils in the right and left hemispheres revealed that the cockroach brain is bilaterally symmetric ($P > 0.05$, paired t-test). Thus, no evidence for side-specific processing was found.
2. The size of several neuropils showed a significant linear correlation. A linear relationship of volumes was found among all retinotopically organized neuropils of the optic lobe, lamina, medulla, and lobula. This means that a brain with a larger lamina volume than a reference brain had a correspondingly larger medulla and lobula volume ($P < 0.05$, linear regression; Table 3). Whereas a significant volumetric relationship also occurred between the calyx and the pedunculus/lobes of the mushroom body, this was not true for the four central-complex neuropils ($P > 0.05$, linear regression). Correspondingly, there was significantly less variability in the volumes of the mushroom bodies (9.13% left; 9.36% right mushroom body) than in the volumes of the central complex (15.53%) and all other neuropils measured. A linear volumetric relationship was also found between the antennal lobe and the mushroom body, but not between the lobus glomerulatus or the optic-lobe neuropils and the mushroom body. Interestingly, the volume of the aMe was linearly correlated with the volume of the medulla, but not with that of the lamina or lobula. In addition, the volume of the aMe was proportional to the volume of the upper division of the central body and the protocerebral bridge ($P < 0.05$, linear regression), but not to that of the lower division or the noduli of the central complex, to the antennal lobe or the lobus glomerulatus (Table 3).

Standardized neuropils of the cockroach brain

Two standard brains of the cockroach were calculated, one using the VIB procotol (Fig. 2A–J) and the other using the ISA method (Fig. 3A–H). Surface reconstructions of 21 neuropils show the location and size of most neuropil regions of the cockroach brain equally well with both standardization procedures (Figs. 2A–D, 3A–D). A

TABLE 2.

Volume of Neuropil Structures in the Brain of the Cockroach *Leucophaea maderae* (N = 20)

							ISA	
Structure	MV (μm^3)	Rel. vol. (%)	SD (μm^3)	Rel. SD (%)	SE (μm^3)	Rel. SE (%)	Volume (μm^3)	Rel. vol (%)
Lamina (left)	8.27×10^6	4.90	2.78×10^6	33.55	6.21×10^5	7.50	8.19×10^6	4.86
Lamina (right)	8.66×10^6	5.13	2.95×10^6	34.03	6.59×10^5	7.61	8.22×10^6	4.87
Medulla (left)	1.34×10^7	7.91	1.91×10^6	14.28	4.26×10^5	3.19	1.38×10^7	8.17
Medulla (right)	1.30×10^7	7.71	2.35×10^6	18.06	5.26×10^5	4.04	1.38×10^7	8.18
Lobula (left)	4.30×10^6	2.55	8.35×10^5	19.44	1.87×10^5	4.35	4.28×10^6	2.54
Lobula (right)	4.22×10^6	2.50	5.85×10^5	13.88	1.31×10^5	3.10	4.38×10^6	2.60
Accessory medulla (left)	1.09×10^5	0.06	2.66×10^4	24.31	5.95×10^3	5.43	1.02×10^5	0.06
Accessory medulla (right)	1.08×10^5	0.06	2.22×10^4	20.63	4.96×10^3	4.61	9.98×10^4	0.06
Calyx (left)	9.13×10^6	5.41	1.08×10^6	11.85	2.42×10^5	2.65	9.22×10^6	5.47
Calyx (right)	9.41×10^6	5.57	7.57×10^5	8.04	1.69×10^5	1.80	9.47×10^6	5.61
Pedunculus/lobes (left)	1.92×10^7	11.37	1.23×10^6	6.42	2.76×10^5	1.44	1.94×10^7	11.51
Pedunculus/lobes (right)	1.87×10^7	11.05	1.99×10^6	10.69	4.46×10^5	2.39	1.90×10^7	11.28
Upper division of CB	1.90×10^6	1.13	3.10×10^5	16.30	6.94×10^4	3.64	1.80×10^6	1.07
Lower division of CB	1.32×10^6	0.78	1.96×10^5	14.77	4.37×10^4	3.30	1.28×10^6	0.76
Protocerebral bridge	9.13×10^5	0.54	1.09×10^5	11.93	2.44×10^4	2.67	9.01×10^5	0.53
Nodulus (left)	9.12×10^4	0.05	1.90×10^4	20.80	4.24×10^3	4.65	8.95×10^4	0.05
Nodulus (right)	9.62×10^4	0.06	2.25×10^4	23.43	5.04×10^3	5.24	9.03×10^4	0.05
Lobus glomerulatus (left)	9.69×10^5	0.57	1.67×10^5	17.20	3.73×10^4	3.85	9.95×10^5	0.59
Lobus glomerulatus (right)	1.12×10^6	0.66	1.80×10^5	16.10	4.03×10^4	3.60	1.04×10^6	0.62
Antennal lobe (left)	2.70×10^7	15.99	3.98×10^6	14.74	8.90×10^5	3.30	2.63×10^7	15.62
Antennal lobe (right)	2.70×10^7	15.99	3.59×10^6	13.30	8.03×10^5	2.97	2.61×10^7	15.50

Volume and relative volume (Rel. vol.) of the ISA-derived standard neuropils are shown on the right side. Abbreviations: CB, central body; MV, mean volume; SD, standard deviation; Rel. SD, relative SD; SE, standard error; Rel. SE, relative SE of 21 segmented neuropils in the cockroach brain (n = 20).

TABLE 3.

Linear Regression Analysis (y = Ax + B) for Correlation of Volumes Between Pairs of Selected Neuropils

y	x	R^2	*P* value	B	A
Lamina	Medulla	0.434	0.002	-2.98×10^6	0.87
Lobula	Medulla	0.670	0.000	8.02×10^5	0.26
Pedunculus/lobes	Calyx	0.251	0.024	1.08×10^7	0.87
Upper division of CB	Lower division of CB	0.049	0.346	–	–
Protocerebral bridge	Lower division of CB	0.016	0.597	–	–
Noduli	Lower division of CB	0.001	0.892	–	–
Optic lobe	Mushroom body	0.095	0.188	–	–
Central complex	Mushroom body	0.047	0.360	–	–
Antennal lobe	Mushroom body	0.219	0.038	3.23×10^6	0.42
Lobus glomerulatus	Mushroom body	0.172	0.069	–	–
Lamina	Accessory medulla	0.071	0.256	–	–
Medulla	Accessory medulla	0.205	0.045	7.47×10^6	52.65
Lobula	Accessory medulla	0.026	0.497	–	–
Lower division of CB	Accessory medulla	0.093	0.192	–	–
Upper division of CB	Accessory medulla	0.206	0.044	2.79×10^6	−8.16
Protocerebral bridge	Accessory medulla	0.218	0.038	1.23×10^6	−2.95
Noduli	Accessory medulla	0.014	0.623	–	–
Antennal lobe	Accessory medulla	0.063	0.287	–	–
Lobus glomerulatus	Accessory medulla	0.007	0.727	–	–

Abbreviation: CB, central body.

comparison of the average images between both methods showed a better signal-to-noise ratio for the ISA method (Figs. 2J, 3E–H). The ISA standard brain (AMIRA file and movie file), and movies of the average neuropil images in xy and xz planes can be downloaded online (Suppl. Figs. 3–6).

The quality of the standardization of the neuropils was scrutinized statistically and revealed the following results:

1. The volumes of most neuropils in the standard brain derived by the ISA procedure or VIB protocol did not differ significantly from the mean neuropil volumes of the individual brains and from each other ($P >$

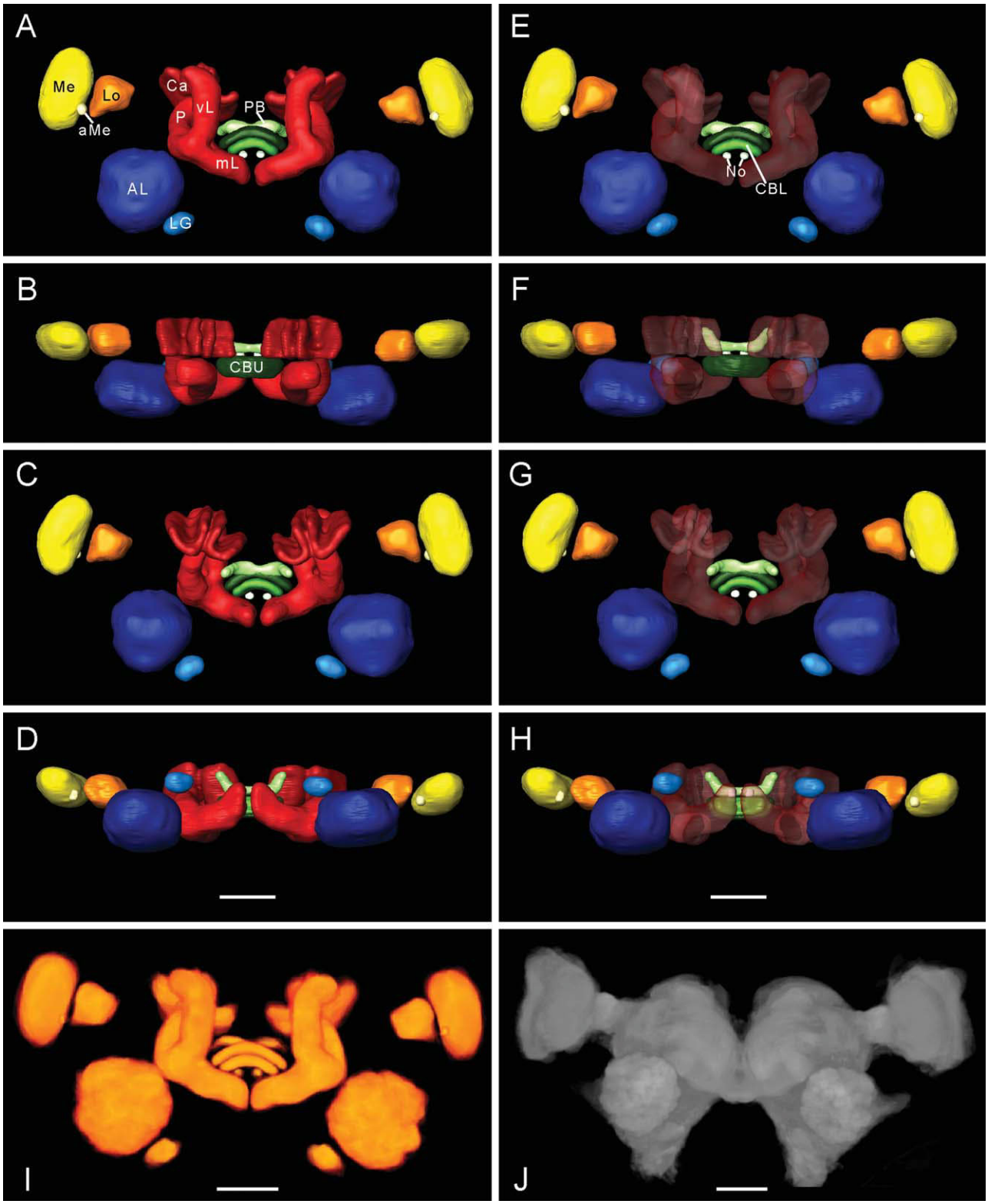

Figure 2. The cockroach standard brain with standardized neuropils calculated with the VIB protocol. A–D: Surface reconstructions. E–H: The same views with the mushroom bodies rendered transparent. **A,E:** Frontal view. **B,F:** Dorsal view. **C,G:** Posterior view. **D,H:** Ventral view. **I,J:** Direct volume rendering of the average labels and average images, respectively. Scale bar = 300 μm in D (applies to A–D), H (applies to E–H), I,J.

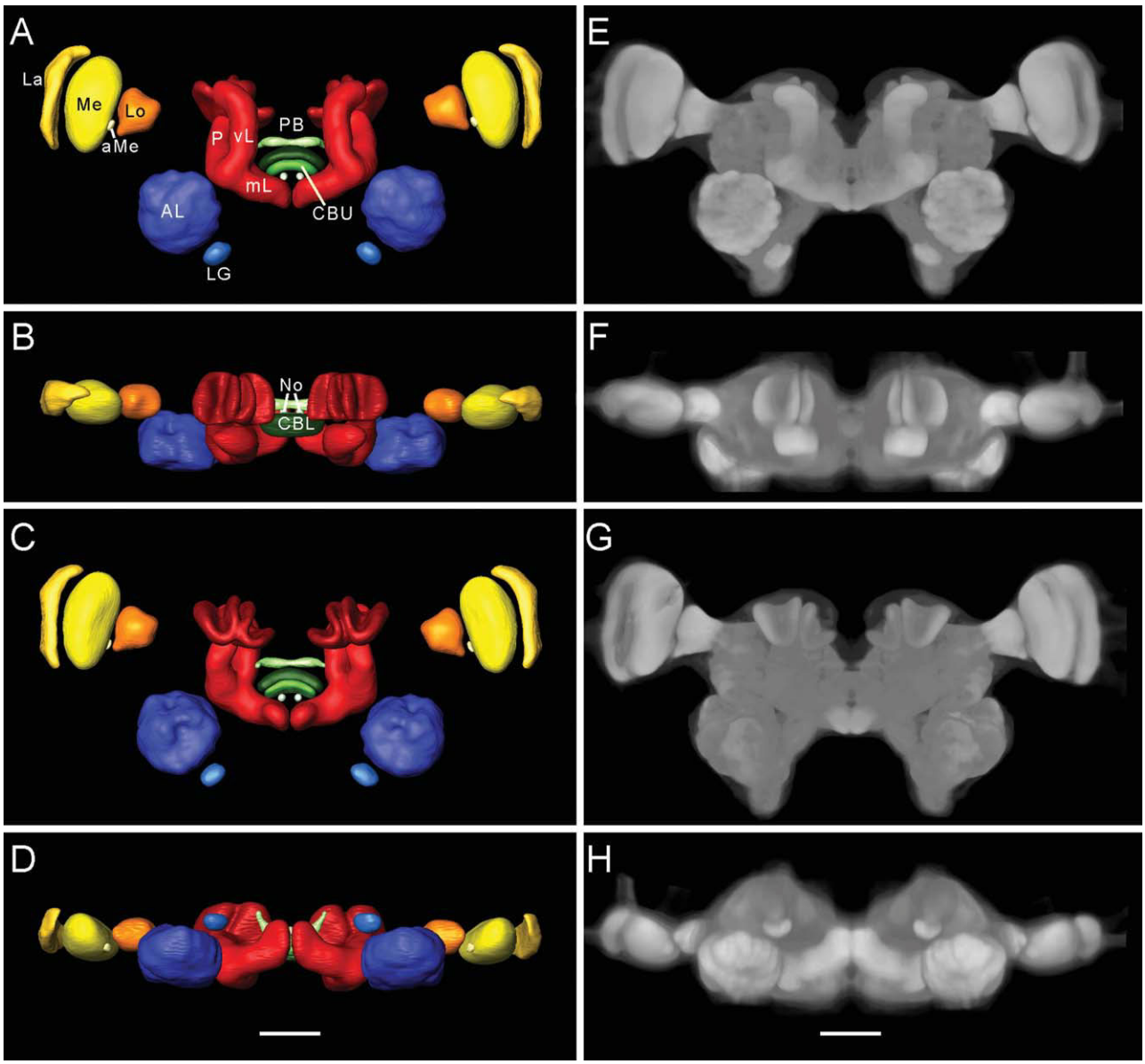

Figure 3. The cockroach standard brain calculated using the ISA method. The left panels (A–D) show surface reconstructions and the right panels (E–H) show the direct volume rendering of the corresponding views. The images needed to be obtained with a 10× objective and thus appear fuzzy. **A,E:** Frontal view. **B,F:** Dorsal view. **C,G:** Posterior view. **D,H:** Ventral view. Scale bar = 300 µm in D (applies to A–D) and H (applies to E–H).

0.05, one-sample t-test). Therefore, both standard brains represent the average shapes and sizes of neuropils in the cockroach brain. The only exception was the lamina of the VIB standard brain. The standard error of the mean of the laminae was very large (33.79%). Because the visualized lamina could not represent the individual laminae, the lamina was omitted from the VIB standard brain.

2. The spatial coordinates (x,y,z) of the centers of gravity of the neuropils in the standard brains did not differ significantly from their average coordinates calculated from 20 individuals ($P > 0.05$, one-sample t-test).

These findings demonstrate that the standard brains maintained the relative positions between the neuropils found in the individual brains.

Finally, the mean volumes of neuropils were computed and their percentages relative to all computed neuropil volumes were calculated (Table 2) to allow for comparisons with corresponding neuropils in standardized brains of other species.

The quality of the ISA standard brain was evaluated by using comparison of the non-rigid deformation differences between the 20 individual brains and the ISA standard brain and between each individual brain and 5

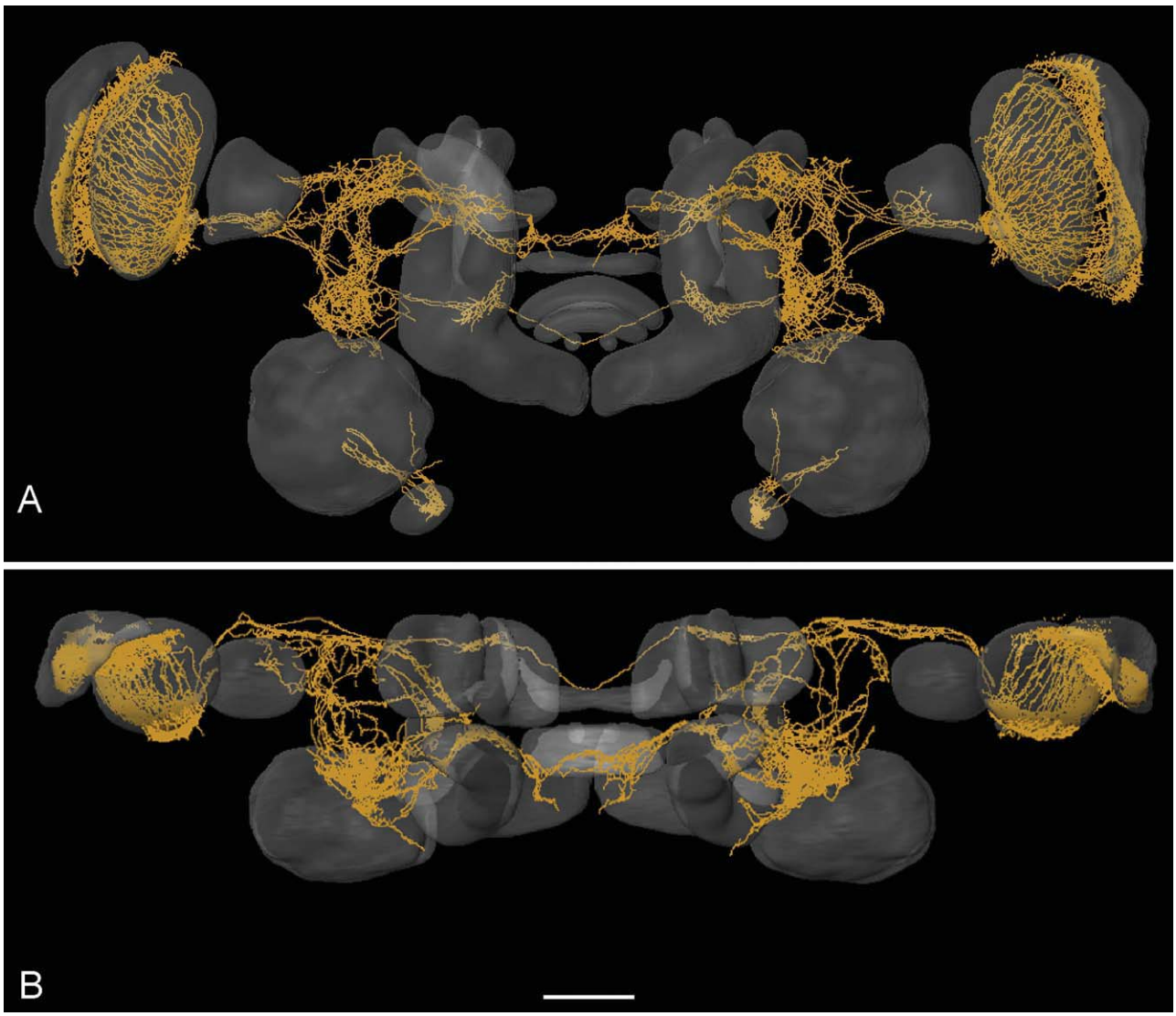

Figure 4. Skeleton graph of 3D reconstruction of PDF-ir neurons registered into the ISA standard brain. **A:** Frontal view. **B:** Dorsal view. Scale bar = 300 μm in B (applies to A,B).

randomly selected individual brains (Suppl. Fig. 7). The non-rigid deformation distance of each individual brain to the standard brain is smaller than the mean deformation between any two individual brains. When these data are taken together, this analysis suggests that the ISA standard brain of *L. maderae* is an ideal averaged platform for neuronal network analysis.

Three-dimensional reconstruction of PDF-ir neurons in the standard brain

For detailed morphological analysis and visualization, the arborizations of PDF-ir neurons of an individual brain were reconstructed and transformed into the ISA-derived standard cockroach brain (Fig. 4A,B). The resulting 3D image provided several novel findings on the neuroarchitecture of the PDF-ir neural network. In addition, a number of quantitative measurements were performed on PDF-ir neurons from 10 preparations.

PDF-ir somata and fibers in the optic lobes

Four PDF-ir soma groups were identified according to their location as the anterior and posterior medulla neurons (aPDFMes, pPDFMes) and the dorsal and ventral lamina neurons (dPDFLas, vPDFLas; Fig. 5A–E). All of the four soma groups appeared to contribute to immunostaining in the aMe. The aPDFMes could be subdivided into three groups according to soma size and staining intensity. Each of these groups consisted of four somata (Fig. 5A–D). The large aPDFMes were stained most intensely and included a single, particularly large soma

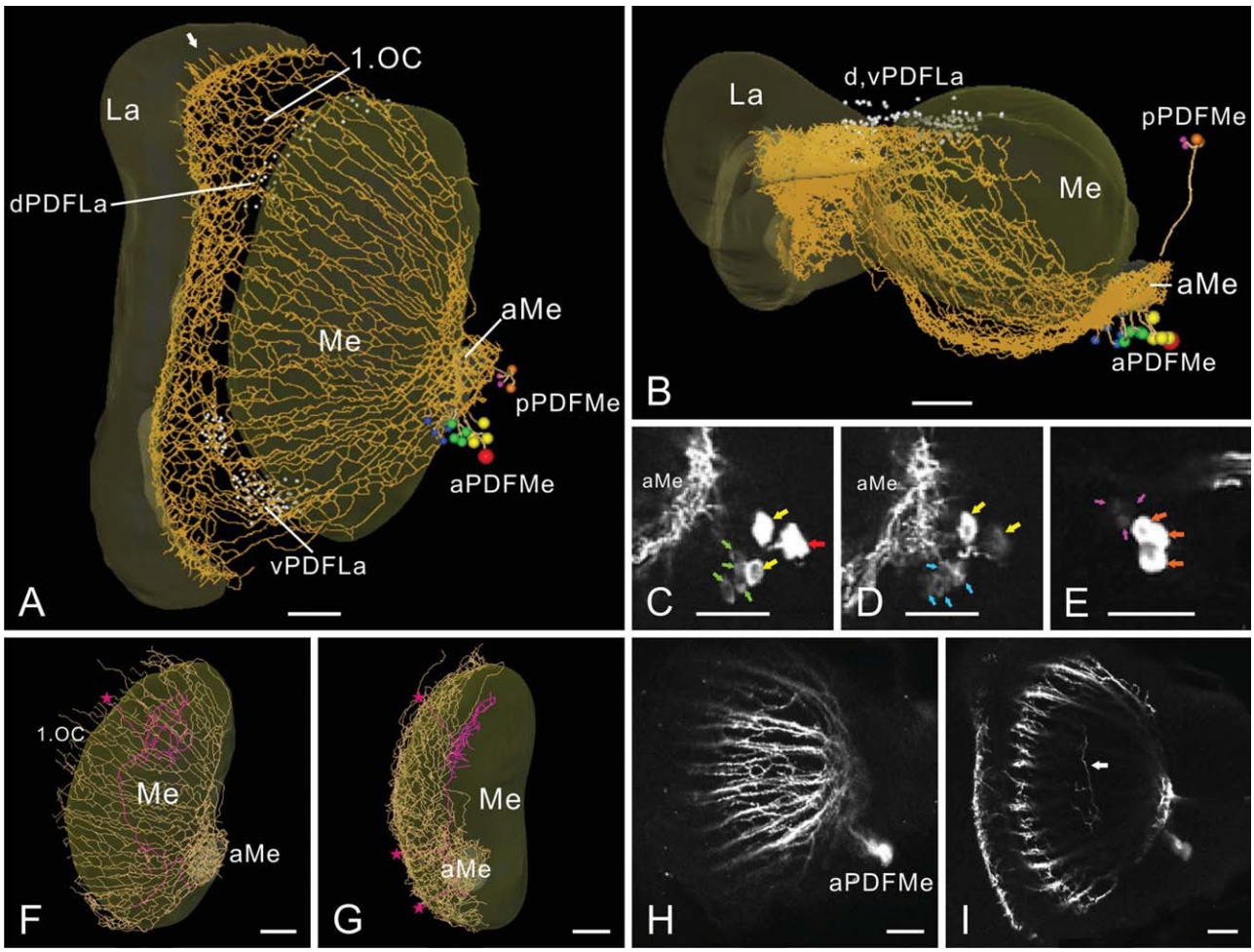

Figure 5. PDF-ir somata and fibers in the optic lobe. **A–E:** Anterior and posterior medulla (Me) neurons (aPDFMe, pPDFMe), and dorsal and ventral lamina (La) neurons (dPDFLa, vPDFLa). The aPDFMe are composed of three subgroups of somata: the large somata (A,B: in yellow, C,D: yellow arrows) including one particularly large soma (A,B: in red, C: red arrow), the medium-sized somata (A,B: in light green, C: light green arrows), and the small somata (A,B: in blue, D: light blue arrow). The pPDFMe consists of five large (A,B: in orange, E: orange arrows) and three small somata (A,B: in violet, E: violet arrows). The dPDFLa and vPDFLa are shown in white (A,B). Some fibers from the first optic chiasma (1. OC) enter the distal layer of the La (arrow in A). **F–I:** The anterior fiber fan (F,G: in dark yellow) and the median layer fiber system (F,G: in violet, I: arrow). The median layer system is connected with the anterior fiber fan and the 1.OC by neural processes (violet stars in F,G). aMe, accessory medulla. Scale bar = 50 μm in A–I.

(21.01 ± 1.94 μm), which was always recognized individually, and three slightly smaller cells (16.84 ± 1.68 μm). The four medium-sized, less intensely stained somata (13.99 ± 1.38 μm), and the four small, faintly stained somata (9.50 ± 0.98 μm), could not always be clearly distinguished from the three large somata of the aPDFMes. In contrast, the somata of the pPDFMes could be separated reliably into two subgroups according to size, staining intensity, and position. Five large, intensely stained pPDFMes (13.82 ± 2.73 μm) were positioned farther away from the aMe than three smaller, faintly stained pPDFMes (9.34 ± 1.47 μm; Fig. 5A,B,E, Table 4). Both dPDFLas and vPDFLas consisted of 50–70 somata proximal to the posterior edge of lamina and sent their primary neurites toward the first optic chiasma (Fig. 5A,B). There was a significant relationship between the size of the aPDFMe somata and their distance to the aMe. The largest aPDFMe was always furthest away, and the small aPDFMes were always closest to the aMe. In contrast, there was no linear relationship between the size of pPDFMes and their distance to the aMe (Table 4).

The aPDFMes connected the aMe to the medulla and lamina in both optic lobes via two distinct pathways, the anterior fiber fan, which innervated the distalmost layer of the medulla (Fig. 5A,F–I), and the median layer fiber system of the medulla (Fig. 5F,G, violet branches; I, arrow). A few fibers from the anterior fiber fan ran perpendicularly into a median layer of the medulla and ramified there (violet stars and fibers in Fig. 5F,G). Some branches projected into the first optic chiasma (Fig. 5F,G). Dense

TABLE 4.

Diameters of Somata in the Different PDF-ir Soma Groups (in μm) and Their Distances to the Accessory Medulla (aMe) Calculated From Nine Optic Lobes of Five Cockroaches[1]

		Diameters of somata			Distances between somata and aMe		
Neuron group	No.	Mean (μm)	SD (μm)	Normalized mean (%)	Mean (μm)	SD (μm)	Normalized mean (%)
Largest aPDFMe neuron	9	21.01	1.94	100	56.18	11.58	100
Large aPDFMe neurons	27	16.84	1.68	80.49	40.18	9.41	72.51
Medium-sized aPDFMe neurons	31	13.99	1.38	66.88	29.27	4.90	54.53
Small aPDFMe neurons	12	9.50	0.98	48.40	21.52	7.17	47.90
Large pPDFMe neurons	23	13.82	2.73	66.54	93.05	15.07	179.52
Small pPDFMe neurons	16	9.34	1.47	44.78	67.38	10.87	130.96
dPDFLa neurons	16	9.34	0.55		–		
vPDFLa neurons	16	9.36	0.40		–		

[1]The diameter and distance of the largest soma was 100% for the normalization of the neuronal soma sizes and their positions. Abbreviations: aPDFMe and pPDFMe, anterior and posterior medulla neurons; dPDFLa and vPDFLa, dorsal and ventral lamina neurons.

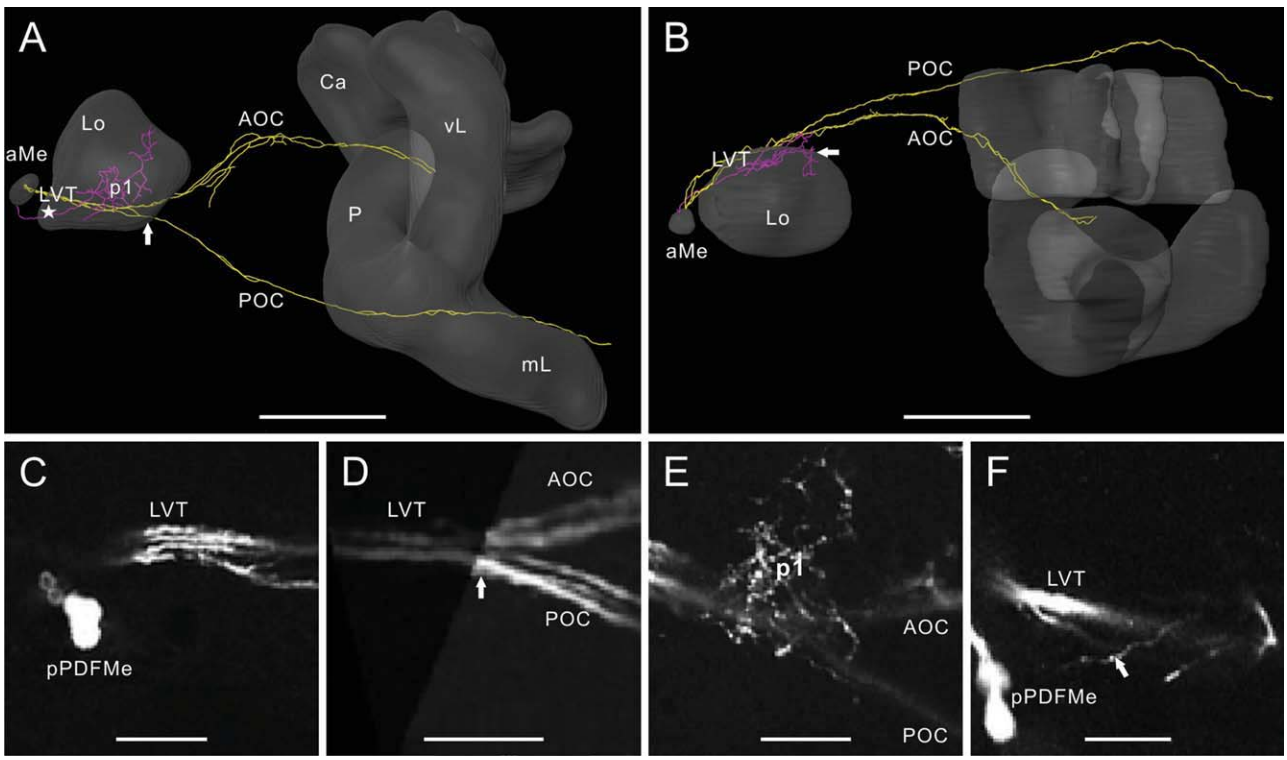

Figure 6. PDF-ir fibers in the lobula valley tract (LVT) posterior to the lobula (Lo) **A–F:** Four major PDF-ir fibers run in the LVT and bifurcate into the anterior and posterior optic commissures (AOC, POC) (A,D: arrow, B,E). PDF-ir fibers from the LVT form plexus 1 (p1, violet fibers) at the posterior face of the Lo (A,B,E). Some branches of p1 enter the Lo (B, arrow). Plexus 1 is connected directly with the aMe by the fiber shown in A (star) and F (arrow). The confocal images were pixellated because they were zoomed to reveal details of the neurites. Scale bar = 200 in A,B; 50 μm in C–F.

fibers from the anterior fiber fan ran from the first optic chiasma along the proximal edge of the lamina in an anterior direction and formed a sheet-like fiber meshwork along the inner face of the lamina. Some fibers even entered the distal layer of the lamina (Fig. 5A, arrow). Thus, although apparently all aPDFMes (Fig. 5C,D), and possibly also all pPDFMes (Fig. 5E) and PDFLas (Fig. 5A,B), connected the aMe with the medulla and distal lamina via the anterior fiber fan, only a few of them projected into the median layer system of the medulla.

At least four major and several smaller PDF-ir fibers originating from ipsi- and contralateral aPDFMes ran posterior to the aMe in the lobula valley tract (LVT). They fasciculated and formed a common bundle that ran along the posterior face of the lobula (Fig. 6A–F). The bundle bifurcated at the border between the lobula and the median

protocerebrum (Fig. 6A,B,D,E). At least two large PDF-ir fibers projected to the posterior optic commissure (POC), whereas two other large fibers and several smaller ones entered the anterior optic commissure (AOC; Fig. 6A,B,D,E). Near the bifurcation, some side branches from apparently all four major fiber extended in a dorsal direction and gave rise to a small plexus of arborizations, termed plexus 1 (p1; Fig. 6A,B,E). Plexi were defined as branching sites of side branches from major fibers running in the POC or AOC. An arborization area is a meeting point of different fiber bundles. Fiber terminals extended into the proximal posterior lobula (Fig. 6B, arrow). A faint PDF-ir fiber from the aMe ran through the lobula and reached p1 directly (Fig. 6A, star; F, arrow). This fiber was distinct from the four major fibers in the LVT and established direct contact between the aMe and p1 (Fig. 6A, star; F, arrow).

PDF-ir fibers in the POC and its associated plexi

PDF-ir fibers in the POC connected both aMae via the LVTs and formed several branching sites along their way (Fig. 7). Some branches innervated the posterior optic tubercle (POTu), which lies posteriorly from the medial lobe of the mushroom body (Fig. 7A,B,E). Several side branches ramified extensively in a plexus (plexus 2 [p2]), which lay more proximally to the optic lobe than the POTu (Fig. 7A,C,D). Two to four fibers from p2 projected parallel to the two major fibers in the POC and connected p2 and POTu directly (green fibers in Fig. 7A; arrow in Fig. 7I). A PDF-ir fiber bundle originating from p1 bifurcated into two fascicles at the ventrolateral side of p2 (Fig. 7B, arrow; H, arrow). One fascicle extended posteriorly into p2. The other fascicle projected anteriorly through the inferior lateral protocerebrum (ILP), and then into the ventrolateral protocerebrum (VLP), where it split into several branches (Fig. 7B,C,G). The fiber branches in the VLP sent off several processes to an “anterior fiber plexus” (AFP) laterally to the vertical lobe of the mushroom body. Wide ramifications of PDF-ir fibers in the AFP extended to the frontal face of the protocerebrum and contributed to a superficial layer of neuropil lateral to the vertical lobe (Fig. 7B,C,F,J,K). A PDF-ir fiber originating from the aMe ran parallel to the four main fibers in the LVT to the midbrain (Fig. 7J–N, arrows). It left the LVT near p1 and projected anteriorly through the lobula (Fig. 7J–M). The fiber bifurcated into two branches that reached the AFP directly (Fig. 7N).

PDF-ir fibers in the AOC and its associated plexi

The second branch from the LVT separated into four to six main fibers. They crossed the brain midline via the AOC. Along their way, they gave rise to side branches which formed plexi 3–5 (p3–p5), arborization areas 1 and 2 (a1, a2), and wide ramifications in the superior lateral (SLP) and superior median protocerebrum (SMP) (Fig. 8A–K). The main fibers in the AOC bypassed the peduncle of the mushroom body anteriorly and arborized most densely in area 1 (a1) between the vertical lobe and the pedunculus of the mushroom body (Fig. 8A–C,E). Four fiber fascicles originating in a1 extended along the posterior surface of the vertical lobe in anterior direction (Fig. 8C, arrows; E, arrows). Two fascicles made a lateral turn anteriorly and provided a connection with the lateral AFP (Fig. 8B,C,F). The other two fascicles continued toward the contralateral hemisphere and merged in area 2 (a2) medially from the vertical lobe in the SMP (Fig. 8A,F). Four to six PDF-ir fibers from a2 crossed the brain midline in the AOC anterior to the protocerebral bridge and superior to the central body to the contralateral hemisphere (Fig. 8I–K). The main fibers in the AOC gave rise to three small fiber plexi interconnected by several fine fibers: plexus 3 (p3) near p1, plexus 5 (p5) near a1, and plexus 4 (p4) between p5 and p3 (Fig. 8A,C,D,G). Neurites from p1, p3, and p5 extended anterior-superiorly and formed overlapping arborizations in the SLP (Fig. 8B,C). Two fibers originated from the main fibers in the AOC between plexus 3 and plexus 4. They ran anterior-superiorly and reached the fiber layer in the SLP (Fig. 8D, arrows). Several processes extended from the SLP anteriorly and fused with the AFP (Fig. 8B,C).

PDF-ir fibers in the deuto- and tritocerebrum

PDF immunoreactivity was not detected in somata of the deuto- and tritocerebrum. However, an area posterior to the lobus glomerulatus in the tritocerebrum showed dense PDF-ir ramifications (Fig. 9A–D). Three fiber bundles extended from this area. A fiber bundle with three to five faintly PDF-immunostained fibers (Fig. 9D) ran in an anterior-superior-lateral direction and terminated near the posterior surface of the antennal lobe in the deutocerebrum (Fig. 9B). The other two faintly stained fiber bundles extended in a posterior-superior-lateral direction and reached the posterior surface of the brain.

Distances between PDF-ir arborization sites

The corresponding distances in the left and right brain hemispheres were compared by means of paired t-tests. If the regularly active PDF-ir neurons and their postsynaptic neurons use phase information between spikes as an encoding scheme, it might be important to ensure that the same or a specifically different phase is maintained in the different output regions. This should be reflected in the arborization scheme of the PDF-ir neurons. For an estimation of conduction times of action potentials

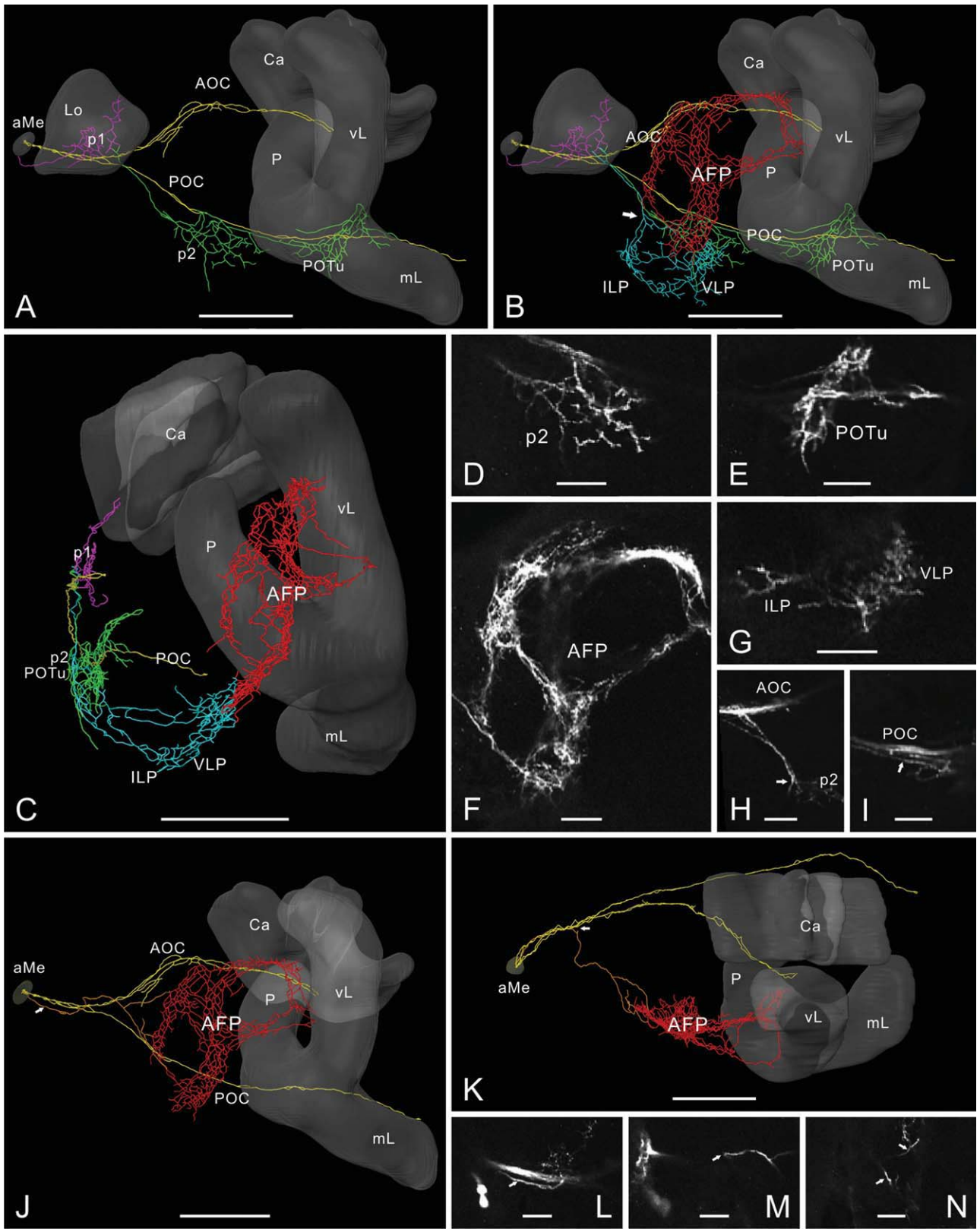

Figure 7. PDF-ir fibers in the posterior optic commissure (POC) and associated arborization sites. **A–I:** The posterior optic tubercle (POTu) is located posteriorly from the median lobe (mL) whereas plexus 2 (p2) is situated more proximally to the optic lobe (A–C: green, D,E). Both PDF-ir arborization sites are connected by two major fibers in the POC and by two additional fibers (A, green; I, arrow). A PDF-ir fiber from plexus1 (A–C, violet) runs anteriorly and bifurcates ventrally to p2 (B; H, arrow). One branch projects into p2. The other branch runs anteriorly through the inferior lateral protocerebrum (ILP), the ventrolateral protocerebrum (VLP) (B,C light blue; G), and into the anterior fiber plexus (AFP) (B,C,J,K, red; F). **J–N:** One fiber connects the aMe and the AFP directly (orange in J,K). The fiber runs parallel to the lobula valley tract (L, arrow) and extends anteriorly at an angle of about 90 degrees (K; M, arrow). It bifurcates into two branches (N, arrows), which reach the AFP. Scale bar = 200 μm in A,B,C,J,K; 50 μm in D–I, L–N.

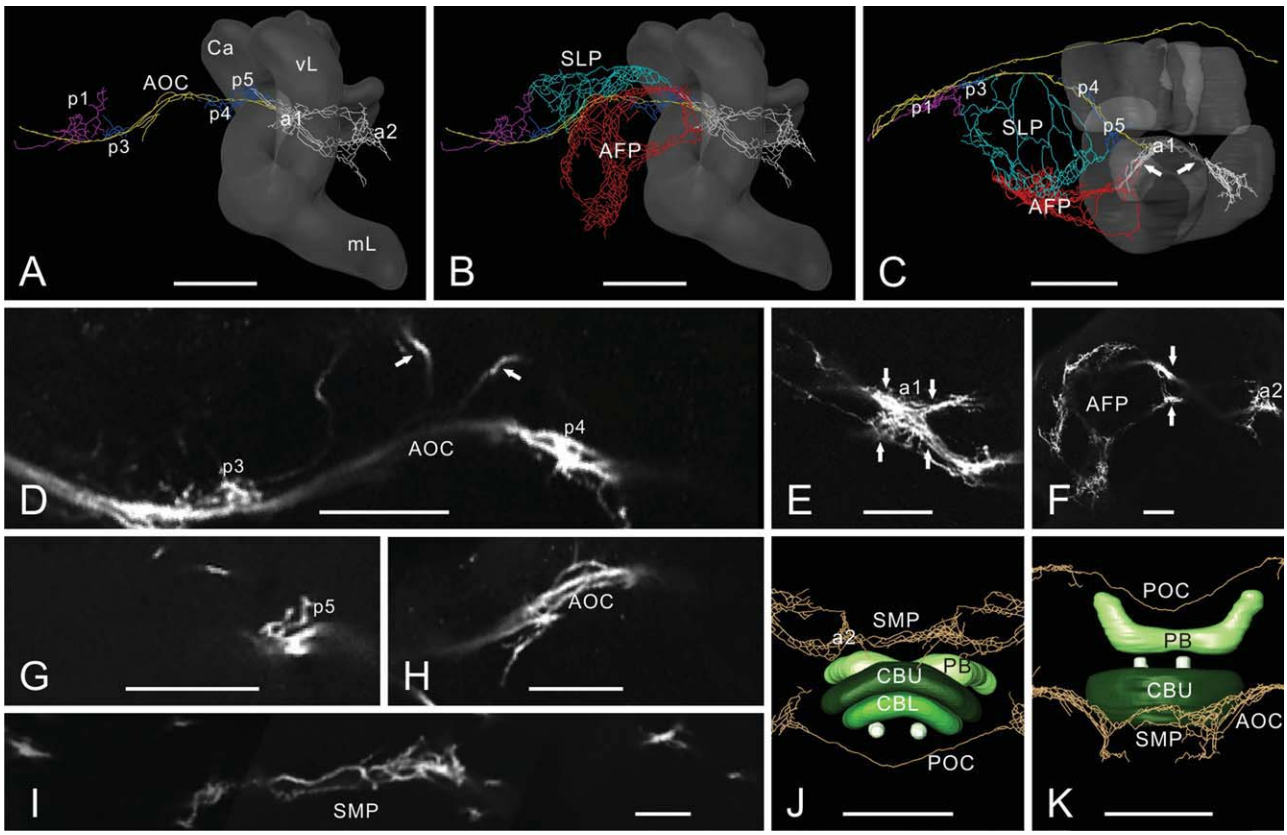

Figure 8. PDF-ir fibers in the anterior optic commissure (AOC) and associated plexi. **A–K:** There are four to six main fibers in the AOC (A–C yellow; H). They run anteriorly toward area one (a1) with dense fibers between the vertical lobe (vL) and the pedunculus (P) (A,C,E). Four fiber fascicles from a1 extend in an anterior direction (C; E, arrows). Two laterally directed fascicles provide a connection with the AFP (B; F, arrows). The other two fascicles project medially and merge in area 2 (a2) (A,F). Four to six fibers anterior to the protocerebral bridge (PB) and superior to the central body connect the two hemispheres (I–K). The p3, p4, p5 (A,C dark blue, D,G), and two fibers from the AOC (D, arrows) run toward the superior lateral protocerebrum (SLP) (B; C light blue). The arborizations in the SLP extend into the anterior fiber plexus (AFP) (B,C in red). Scale bar = 200 μm in A–C,J,K; 80 μm in D–I.

between the different PDF-ir arborization sites, we calculated the distances between neighboring PDF-ir arborization sites in the AMe, the five plexi (p1–p5), the POTu, and the two arborization areas (a1, a2) from all 10 animals (Figs. 10, 11, Suppl. Table 1). Arborization sites in the SLP, SMP, and AFP were not included in the analysis because they were less confined. The PDF-ir neuronal processes in the left and right hemisphere were symmetrically organized ($P > 0.05$, paired t-test). Distances between p1 and p3, between p4 and p5, and between p5 and a1, were not significantly different from each other (Fig. 10). Linear regression analysis showed that the relative distances of several other PDF-ir arborization areas were integer multiples of these short distances (Suppl. Table 1, Fig. 11A).

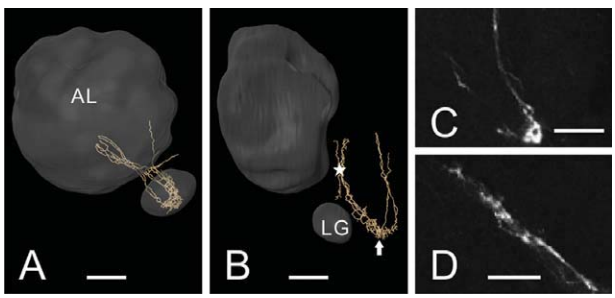

Figure 9. A few PDF-ir fibers from a non-identified soma arborize in the deuto- and tritocerebrum. **A–D:** An area posterior to the lobus glomerulatus (LG) in the tritocerebrum shows fibrous PDF immunostaining (A; B, arrow; C). A fiber bundle runs anteriorly, enters the deutocerebrum, and terminates near the posterior surface of the antennal lobe (AL) (B, star; D). Scale bar = 100 μm in A–D.

Two highly interconnected PDF-ir areas

Two arborization areas of PDF-ir fibers, p1 and the AFP, were highly interconnected with other PDF-ir branching sites (Fig. 11B–F). Plexus 1 was formed by ramifications of the four major fibers in the LVT. It was directly connected with: 1) the aMe; 2) p2 in the POC; 3) p3 in the AOC; 4) the main fibers in the AOC; 5) the SLP, ILP, and

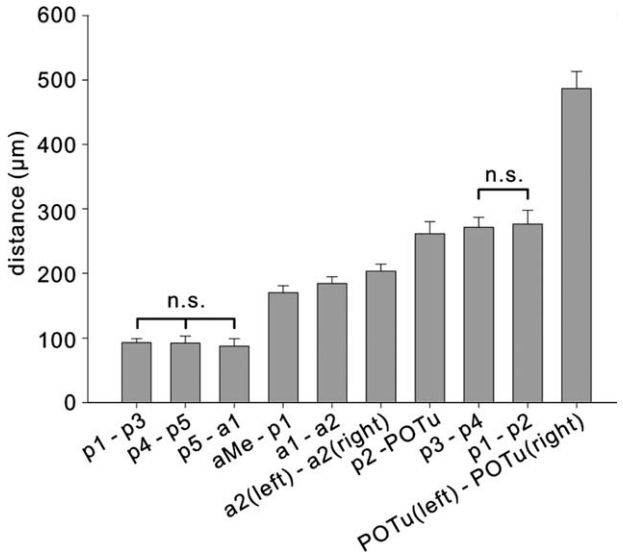

Figure 10. Mean distances between five PDF-ir plexi (p1–p5), the posterior optic turbercle (POTu), and two PDF-ir areas (a1, a2) calculated from 10 cockroaches (bars, standard deviation). The distances p1–p3, p4–p5, and p5–a1 were not significantly different from each other ($P > 0.05$, one-way ANOVA; n.s., not significant). The distance between p5 and a1 was the smallest and was defined as 1. In addition, the distances p1–p2 and p3–p4 were not significantly different from each other. They were 3.1 × the distance of p5–a1, whereas p2–POTu was 3.0 × the distance of p5–a1. Finally, the distance between aMe–p1 was 1.9 × and the distance a1–a2 was 2 × the distance of p5–a1. aMe, accessory medulla.

VLP; and 6) the AFP. The AFP was formed by fibers originating from: 1) the aMe; 2) p1 in the LVT; 3) p2 in the POC; 4) the main fibers in the AOC; 5) a1; 6) p3; and 7) p5 in the AOC. These highly interconnected areas are described here for the first time and allow for direct exchange of information between the AOC and the POC.

A comparison of different standardized insect brains

In a comparison of the relative mean neuropil volumes (%) between different insects with standardized brains (Fig. 12, Suppl. Table 2) it becomes apparent that in the cockroach *L. maderae* the distribution of relative mean volumes of the standardized neuropils differ from the other insects studied so far. In the cockroach the relative mean volumes of the optic lobes are relatively smaller and those of the antennal lobes are relatively larger compared with other insects. As in *A. mellifera*. but in contrast to *D. melanogaster*, *S. gregaria*, *M. sexta*, and *H. virescens*, the mean volume of the mushroom bodies of the cockroach is relatively large. In all insects studied so far, the relative mean volumes of the central body are very similar.

DISCUSSION

To facilitate the morphological and physiological analysis of the circadian pacemaker network in the cockroach *L. maderae*, we employed two different procedures to obtain a 3D standard brain. With the VIB and the ISA protocols, anti-synapsin-stained adult brains of male *L. maderae* were successfully standardized. Morphometric analysis revealed linear relationships between the sizes of several labeled neuropils. Interestingly, the size of the cockroach's circadian pacemaker center, the aMe, was linearly correlated with the size of the medulla, the protocerebral bridge, and the upper division of the central body. For better visualization and statistical analysis, the branching pattern of PDF-ir neurons, circadian pacemaker neurons controlling locomotor activity rhythms (Helfrich-Förster et al., 1998; Homberg et al., 2003), were registered into the standard cockroach brain. Several new features of the aPDFMes were identified, such as two highly interconnected PDF-ir branching sites, p1 and AFP, which appear to be composed of processes from the AOC and the POC. In addition, we found numerical relationships between the distances of several PDF-ir branching sites.

Comparison of the VIB- and ISA-derived standard cockroach brains

Statistical comparison of all standardized neuropils with the neuropils of the individual brains and a comparison of both procedures showed that the VIB and the ISA protocols revealed equally well-defined locations and volumes of the 21 neuropils examined. Only the lamina could not be standardized satisfactorily with the VIB protocol, owing to high variability resulting from distortions of photoreceptor axon bundles during brain dissection. The VIB protocol is preferable for comparison of neuropil volumes, e.g., between cockroaches raised at different light conditions, because it takes only about 10% of the time of the ISA procedure and can be employed with smaller voxel sizes (Jenett et al., 2006; Kurylas et al., 2008; el Jundi et al., 2009). In addition, it does not change the volumes of neuropils, whereas the ISA protocol averages volume differences. In contrast to the ISA protocol, the VIB protocol depends on the quality of the label fields (Rohlfing et al., 2001; Brandt et al., 2005). Thus, when variable, poorly defined neuropils are evaluated, it is preferable to employ the ISA procedure, which is based upon confocal images. The quality of both standardization methods depends on the template brain employed for alignment. Because our template was carefully selected as the brain with the least differences from the mean of all individual brains, it is a valid standard for *L. maderae*. For reconstruction of the circadian

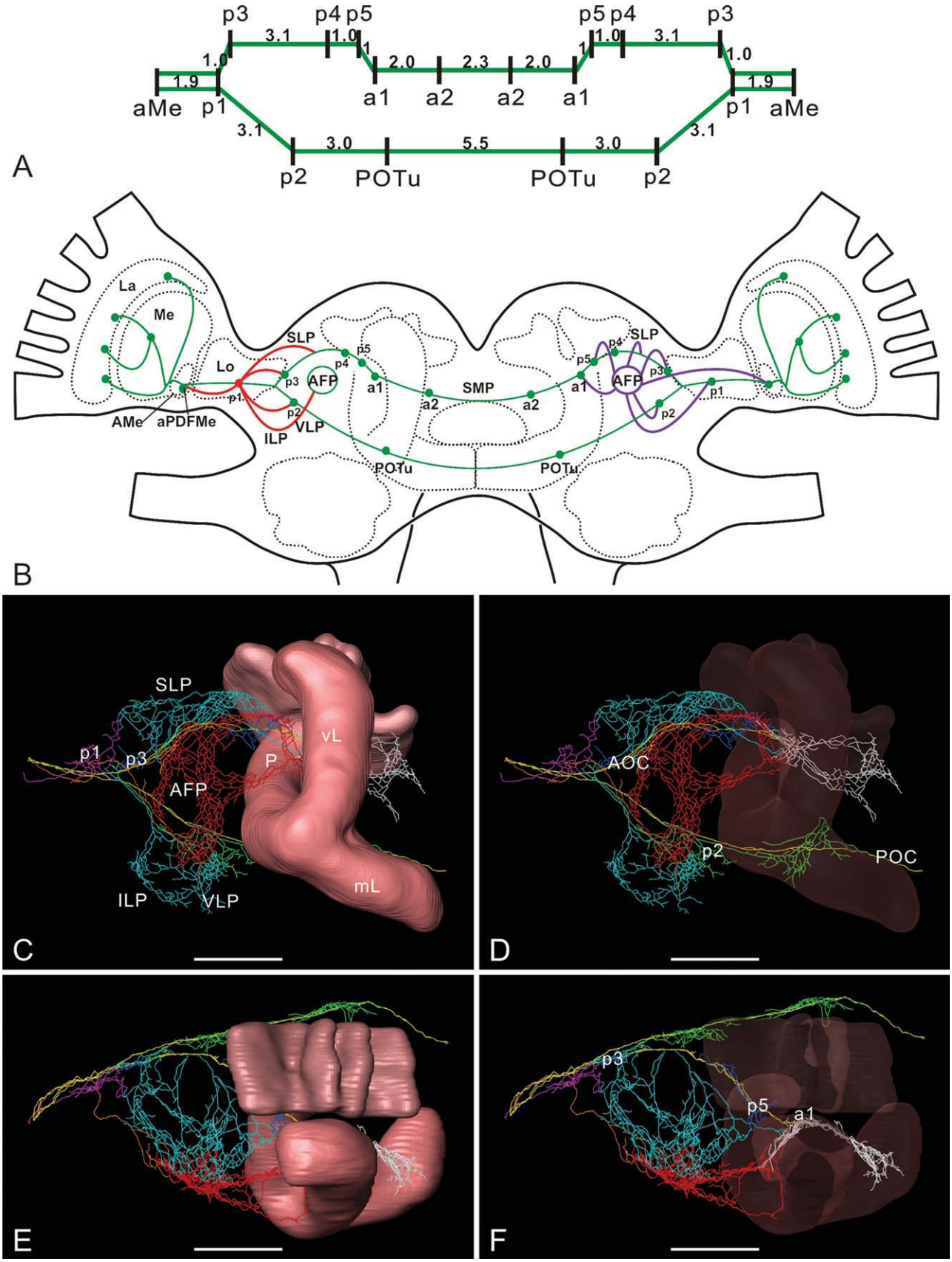

Figure 11. The 3D reconstructions identified numerical relationships between distances of PDF-ir arborization sites and described for the first time highly interconnected association areas. **A:** Relative positions of all PDF-ir arborization sites. The distance between p5 and area a1 was defined as "1". The other distances were integer multiples of p5–a1. **B–F:** Two sites, p1 and the anterior fiber plexus (AFP), are highly interconnected. P1 (C–F in violet) is connected with the aMe, with p2 (C–F in green), with p3 (C–F in dark blue), with the AFP (C–F in red), and with the main fibers in the AOC (C–F in yellow). The AFP is formed by fibers from the aMe, p1, p2, p3, p5, and a1 (C–F in white), and from the main fibers in the AOC. C,D: Frontal view. E,F: Dorsal view. B, modified from Reischig and Stengl, 2002. Scale bar = 200 μm in A–F.

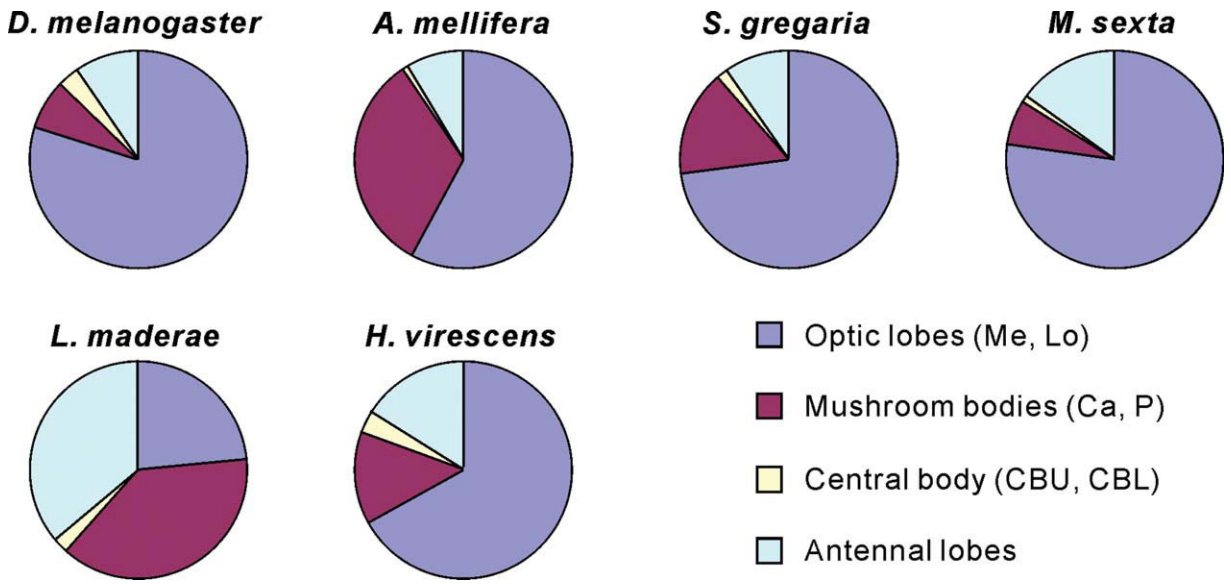

Figure 12. Relative mean volumes (%) of selected neuropils in six different insect species: *Drosophila melanogaster*, *Apis mellifera*, *Schistocerca gregaria*, *Manduca sexta* males (el Jundi et al., 2009); *Heliothis virescens* (Kvello et al., 2009); and *Leucophaea maderae* (this study). Only neuropils that were analyzed in all six species were selected: optic lobes comprising medulla (Me) and lobula complex (Lo), mushroom bodies consisting of calyces (Ca) and pedunculi/lobes (P), upper and lower division of the central body (CBU, CBL), and antennal lobes.

pacemaker network in a 3D standard brain of *L. maderae*, the ISA method is more appropriate, because it averages individual differences and provides a better signal-to-noise ratio for visualization of the neuropils (Rohlfing et al., 2001).

3D standardization not only greatly improved the visualization and understanding of the location of neuropils in the brain, but also allowed for statistical analysis of neuropil volumes within and between individual brains. We show that the volumes of the antennal lobe and mushroom body and those of the lamina, medulla, and lobula are directly correlated within each brain. It is not completely clear what this correlation means. It can be hypothesized that neuropils that analyze the same sensory information to about the same extent are correlated in volume. This hypothesis is confirmed by the observed correlations among the neuropil volumes of the lamina, medulla, and lobula. It is well known from physiological and anatomical studies that the lamina, medulla, and lobula maintain a retinotopic map of the visual surround, while processing visual stimuli with adjacent receptive fields. Because the volume of the aMe was linearly correlated only with the volume of the medulla, but was independent of the volumes of the lamina and lobula, it is expected that the aMe receives direct visual entrainment only via the medulla. This hypothesis is supported by the finding that distal tract neurons carry visual information from the medulla to the noduli of the aMe (Reischig and Stengl, 1996; Loesel and Homberg, 2001; Petri et al., 2002).

Thus, the PDF-ir arborizations in the lamina might rather be an output than an input pathway of the clock. Linear correlations of the volumes of the aMe, the protocerebral bridge, and the upper division of the central complex hinted at functional connections among these neuropils. The posterior optic tubercles, prominent target sites of PDF-ir projections, are directly connected to the protocerebral bridge in locusts (Heinze and Homberg, 2007). Based on evidence for a role of the central complex as an internal sky compass, Homberg et al. (2004) have promoted the idea that circadian timing information may enter the central complex via this pathway for time compensation in spatial navigation. In addition, the central complex is implicated in the control of locomotor behavior (for review, see Strauss, 2002). It is known from several studies that PDF-ir neurons in the fruitfly and the cockroach *L. maderae* control locomotor activity rhythms (fruitfly: Helfrich-Förster, 2009; Helfrich-Förster et al., 1998; cockroach: Stengl and Homberg, 1994; Petri and Stengl, 1997; Reischig and Stengl, 2003a). In the fruitfly, PDF-ir neurons connect in the superior median protocerebrum to locomotor control centers (Helfrich-Förster, 1998; Park et al., 2000). It is unknown whether there are functional connections between the superior median protocerebrum and the central complex in the fruitfly. Because linear correlations of the volumes of the aMe,

the protocerebral bridge, and the upper division of the central complex were found in the cockroach, it is possible that PDF-ir neurons control locomotor activity via postsynaptic pathways including the upper division of the central complex.

A comparative volumetric analysis indicates that *L. maderae* relies more heavily on chemosensory than on visual information than all other species studied (*Drosophila melanogaster*: Rein et al., 2002; *Apis mellifera*: Brandt et al., 2005; *Schistocerca gregaria*: Kurylas et al., 2008; *Manduca sexta*: el Jundi et al., 2009; *Heliothis virescens*: Kvello et al., 2009), and that *L. maderae* has relatively smaller optic lobes, the largest antennal lobe, and the largest mushroom body. Chemosensory input appears to be the main input to the mushroom bodies, as suggested by linear regression analysis (Table 3). Because the nocturnal, social cockroach is active at very low light levels, it is likely that it relies more heavily on chemosensory and mechanosensory cues than on vision. The crepuscular, fast flying moth *M. sexta*, in contrast, has much larger optic lobes and a much smaller mushroom body than *L. maderae* but a similarly sized central complex (el Jundi et al., 2009).

We did not find a linear correlation between the volumes of the lobus glomerulatus and the mushroom body, suggesting that its contribution to computation in the mushroom body may be less prominent than in the locust and cricket (Homberg et al., 2004; Frambach and Schürmann 2004). The lobus glomerulatus, a chemosensory neuropil in the tritocerebrum, has only about 15 glomeruli in *L. maderae*, whereas about 40 glomeruli were counted in *Diploptera punctata* (Chiang et al., 2001). The lobus glomerulatus has not yet been well characterized. It appears to receive input from sensory neurons of the maxillary palps and from interneurons of the deutocerebrum and appears to be involved in the chemosensory control of feeding (Ernst et al., 1977).

New features of PDF-ir circadian pacemaker neurons

PDF-ir neurons are circadian pacemakers that control locomotor activity rhythms in the fruitfly *D. melanogaster* and the cockroach *L. maderae* (for reviews, see Helfrich-Förster et al., 1998; Homberg et al., 2003; Helfrich-Förster, 2009). However, in both species, the number of different functional circuits in which the PDF-ir neurons play a role is still unknown. To facilitate neuroanatomical and physiological studies on the functions of the PDF-ir circadian pacemaker neurons in the cockroach, they were implemented in the standard cockroach brain by employing the ISA protocol.

To characterize the neuronal processes in detail, the individual PDF-ir neurons were reconstructed at a high voxel resolution ($1.46 \times 1.46 \times 2$ μm). The available software and the computer resources allowed for a maximal spatial resolution of only $8 \times 8 \times 8$ μm for deformation registration. This resolution was still sufficient to characterize the general localization of the different branching sites of the PDF-ir neurons with respect to surrounding neuropils. The data from PDF-ir fiber reconstructions of individual brains were used to analyze the relative positions and distances between PDF-ir arborization sites (Suppl. Table 1). Registration of the neurons in brain regions that have poorly defined boundaries with other neuropil structures is a general problem that can only be solved with further improvement and development of the respective softwares. Imprecision in the registration in poorly defined regions also persists at higher spatial resolution (el Jundi et al., 2010). In forthcoming triple-label studies, we will improve the resolution of PDF-ir arborization sites in comparison with other labeled cells in brain regions of interest.

Registration and statistical analysis of the PDF-ir cells revealed several new and interesting features. The distances of the aPDFMes to the border of the aMe were not randomly distributed but were directly correlated to soma size. Therefore, it is likely that all aPDFMes are sequential offsprings of the same neuroblast, with the largest soma being the first descendant. In addition, the distance to the aMe can now be used for identification of the three aPDFMe soma groups that cannot always be easily distinguished otherwise. A correlation between soma size and distance to the aMe was not found in the eight pPDFMes. In this group two subgroups could easily be distinguished based on a prominent difference in soma size.

Two distinctly different branching patterns of the PDF-ir neurons in the optic lobe have already been observed by Reischig and Stengl (2002). The present study revealed that at least one PDF-ir neuron contributes to both the PDF-ir fiber fan and the medium layer fiber system.

Varicose fiber specializations suggested that PDF is released via branching sites in the lamina, the aMe, p1–p5, a1 and a2, the posterior optic tubercle, the SLP, the SMP, and the AFP. Two specific features were especially remarkable: 1) apparently, all of the central PDF-ir branching sites are connected with each other either directly or via two highly interconnected branch points in p1 and AFP, thereby allowing for negative feedback and for mixing of information from AOC and POC projecting fibers; and 2) several PDF-ir branching sites showed equal distances or integer multiples thereof. Extracellular analysis indicated that aMe neurons form an electrically coupled network of phase-coupled ensembles that can

be synchronized and differently grouped via GABA and neuropeptide applications. These specific morphological features hint that phase-information and temporal processing (Ivry and Schlerf, 2008) might be a specifically important feature of the circadian pacemaker neurons (Schneider and Stengl, 2005, 2006, 2007). It remains to be studied whether the specific distances of the PDF-ir branching sites contribute to different delay lines that might allow for measurements of phase differences in postsynaptic neurons. In addition, it remains to be examined whether the feedback connections between different PDF-ir branching sites guarantee synchronization of phases of action potential output at these sites. Future studies have still to reveal the branching patterns of individual aPDFMes and their respective postsynaptic neurons.

Because peptidergic neurons do not necessarily release their peptides at synaptic sites to close neighbors only, the peptides could target distant cells with the respective receptors if the peptide is not degraded quickly. Therefore, it will be important to identify neurons in the cockroach brain carrying PDF receptors, as was accomplished in the fruitfly (Hyun et al., 2005; Mertens et al., 2005; Shafer et al., 2008; Lear et al., 2005, 2009). Because in *D. melanogaster*, all PDF-sensitive postsynaptic cells appear to express circadian clock genes, it is likely that period-ir neurons in the cockroach midbrain will also be targeted by PDF. Current studies are testing this hypothesis.

ACKNOWLEDGMENTS

We are grateful to Drs. E. Buchner and H. Dircksen for the generous supply of antibodies, and to Dr. Torsten Rohlfing for providing ISA tools and for assistance in registration. Registration tools used in this work are available in source code as part of the Computational Morphometry Toolkit (CMTK), which is available at http://nitrc.org/projects/cmtk/. We thank unknown referees and the editor for constructive suggestions that considerably improved our manuscript.

LITERATURE CITED

Brandt R, Rohlfing T, Rybak J, Krofczik S, Maye A, Westerhoff M, Hege HC, Menzel R. 2005. Three-dimensional average-shape atlas of the honeybee brain and its applications. J Comp Neurol 492:1–19.

Chiang AS, Liu YC, Chiu SL, Hu SH, Huang CY, Hsieh CH. 2001. Three-dimensional mapping of brain neuropils in the cockroach, *Diploptera punctata*. J Comp Neurol 440:1–11.

Dircksen H, Zahnow CA, Gaus G, Keller R, Rao KR, Riehm JP. 1987. The ultrastructure of nerve endings containing pigment-dispersing hormone (PDH) in crustacean sinus glands: identification by an antiserum against synthetic PDH. Cell Tissue Res 250:377–387.

el Jundi B, Huetteroth W, Kurylas AE, Schachtner J. 2009. Anisometric brain dimorphism revisited: implementation of a volumetric 3D standard brain in *Manduca sexta*. J Comp Neurol 517:210–225.

el Jundi B, Heinze S, Lenschow C, Kurylas A, Rohlfing T, Homberg U. 2010. The locust standard brain: a 3D standard of the central complex as a platform for neural network analysis. Front Syst Neurosci 3:21.

Ernst KD, Boeckh J, Boeckh V. 1977. A neuroanatomical study on the organization of the central antennal pathways in insects. Cell Tissue Res 176:285–308.

Evers JF, Schmitt S, Sibila M, Duch C. 2005. Progress in functional neuroanatomy: precise automatic geometric reconstruction of neuronal morphology from confocal image stacks. J Neurophysiol 93:2331–2342.

Frambach I, Schürmann FW. 2004. Separate distribution of deutocerebral projection neurons in the mushroom bodies of the cricket brain. Acta Biol Hung 55:21–92.

Godenschwege TA, Reisch D, Diegelmann S, Eberle K, Funk N, Heisenberg M, Hoppe V, Hoppe J, Klagges BRE, Martin JR. 2004. Flies lacking all synapsins are unexpectedly healthy but are impaired in complex behavior. Eur J Neurosci 20: 611–622.

Heinze S, Homberg U. 2007. Map-like representation of celestial *E*-vector orientations in the brain of an insect. Science 315:995–997.

Helfrich-Förster C. 1998. Robust circadian rhythmicity of *Drosophila melanogaster* requires the presence of lateral neurons: a brain-behavioral study of disconnected mutants. J Comp Physiol A 182:435–453.

Helfrich-Förster C. 2009. Does the morning and evening oscillator model fit better for flies or mice? J Biol Rhythms 24: 259–70.

Helfrich-Förster C, Stengl M, Homberg U. 1998. Organization of the circadian system in insects. Chronobiol Int 15:567–594.

Homberg U, Reischig T, Stengl M. 2003. Neural organization of the circadian system of the cockroach *Leucophaea maderae*. Chronobiol Int 20:577–591.

Homberg U, Brandl C, Clynen E, Schoofs L, Veenstra JA. 2004. Mas-allatotropin/Lom-AG-myotropin I immunostaining in the brain of the locust, *Schistocerca gregaria*. Cell Tissue Res 318:439–457.

Hyun S, Lee Y, Hong ST, Bang S, Paik D, Kang J, Shin J, Lee J, Jeon K, Hwang S, Bae E, Kim J. 2005. *Drosophila* GPCR Han is a receptor for the circadian clock neuropeptide PDF. Neuron 48:267–278.

Ignell R, Anton S, Hansson BS. 2000. The maxillary palp sensory pathway of Orthoptera. Arthropod Struct Dev 29: 295–305.

Ivry RB, Schlerf JE. 2008. Dedicated and intrinsic models of time perception. Trends Cogn Sci 12:273–280.

Jenett A, Schindelin JE, Heisenberg M. 2006. The virtual insect brain protocol: creating and comparing standardized neuroanatomy. BMC Bioinform 7:544.

Klagges B, Heimbeck G, Godenschwege TA, Hofbauer A, Pflugfelder GO, Reifegerste R, Reisch D, Schaupp M, Buchner S, Buchner E. 1996. Invertebrate synapsins: a single gene codes for several isoforms in *Drosophila*. J Neurosci 16: 3154–3165.

Kurylas AE, Rohlfing T, Krofczik S, Jenett A, Homberg U. 2008. Standardized atlas of the brain of the desert locust, *Schistocerca gregaria*. Cell Tissue Res 333:125–145.

Kvello P, Lofaldli BB, Rybak J, Menzel R, Mustaparta H. 2009. Digital, three-dimensional average shaped atlas of the *Heliothis virescens* brain with integrated gustatory and olfactory neurons. Front Syst Neurosci 3:14.

Lear BC, Merrill CE, Lin JM, Schroeder A, Zhang L, Allada R. 2005. A G protein-coupled receptor, groom-of-PDF, is required for PDF neuron action in circadian behavior. Neuron 48:221–227.

Lear BC, Zhang L, Allada R. 2009. The neuropeptide PDF acts directly on evening pacemaker neurons to regulate multiple features of circadian behavior. PLoS Biol 7:e1000154.

Liu X, Davis RL. 2006. Insect olfactory memory in time and space. Curr Opin Neurobiol 16:679–685.

Liu G, Seiler H, Wen A, Zars T, Ito K, Wolf R, Heisenberg M, Liu L. 2006. Distinct memory traces for two visual features in the *Drosophila* brain. Nature 439:551–556.

Loesel R, Homberg U. 2001. Anatomy and physiology of neurons with processes in the accessory medulla of the cockroach *Leucophaea maderae*. J Comp Neurol 439:193–207.

Menzel R, Giurfa M. 2006. Dimensions of cognition in an insect, the honeybee. Behav Cogn Neurosci Rev 5:24–40.

Mertens I, Vandingenen A, Johnson EC, Shafer OT, Li W, Trigg JS, De Loof A, Schoofs L, Taghert PH. 2005. PDF receptor signaling in *Drosophila* contributes to both circadian and geotactic behaviors. Neuron 48:213–219.

Mizunami M, Okada R, Li YS, Strausfeld NJ. 1998. Mushroom bodies of the cockroach: activity and identities of neurons recorded in freely moving animals. J Comp Neurol 402: 501–519.

Nishiitsutsuji-Uwo J, Pittendrigh CS. 1968. Central nervous system control of circadian rhythmicity in the cockroach: III. The optic lobes, locus of the driving oscillation? Z Vgl Physiol 58:14–46.

Page TL. 1984. Neural organization of a circadian clock in the cockroach *Leucophaea maderae*. In: Porter R, Collins GM, editors. Photoperiodic regulation of insect and molluscan hormones. London: Pitman. p115–135.

Park JH, Helfrich-Förster C, Lee G, Liu L, Rosbash M, Hall JC. 2000. Differential regulation of circadian pacemaker output by separate clock genes in *Drosophila*. Proc Natl Acad Sci U S A 97:3608–3613.

Petri B, Stengl M, Würden S, Homberg U. 1995. Immunocytochemical characterization of the accessory medulla in the cockroach *Leucophaea maderae*. Cell Tissue Res 282:3–19.

Petri B, Stengl M. 1997. Pigment-dispersing hormone phase-shifts the circadian pacemaker of the cockroach *Leucophaea maderae*. J Neurosci 17:4087–4093.

Petri B, Homberg U, Loesel R, Stengl M. 2002. Evidence for a role of GABA and Mas-allatotropin in photic entrainment of the circadian clock of the cockroach *Leucophaea maderae*. J Exp Biol 205:1459–1469.

Rein K, Zöckler M, Mader MT, Grübel C, Heisenberg M. 2002. The *Drosophila* standard brain. Curr Biol 12:227–231.

Reischig T, Stengl M. 1996. Morphology and pigment-dispersing hormone (PDH)-immunocytochemistry of the accessory medulla, the presumptive circadian pacemaker of the cockroach *Leucophaea maderae*: a light- and electron-microscopical study. Cell Tissue Res 255: 305–319.

Reischig T, Stengl M. 2002. Optic lobe commissures in a three-dimensional brain model of the cockroach *Leucophaea maderae*: a search for the circadian coupling pathway. J Comp Neurol 443:388–400.

Reischig T, Stengl M. 2003a. Ectopic transplantation of the accessory medulla restores circadian locomotor rhythms in arrhythmic cockroaches (*Leucophaea maderae*). J Exp Biol 206:1877–1886.

Reischig T, Stengl M. 2003b. Ultrastructure of pigment-dispersing hormone-immunoreactive neurons in a three-dimensional model of the accessory medulla of the cockroach *Leucophaea maderae*. Cell Tissue Res 314:421–435.

Reischig T, Stengl M. 2004. Pigment-dispersing hormone (PDH)-immunoreactive neurons form direct coupling pathways between the bilateral symmetric circadian pacemakers of the cockroach *Leucophaea maderae*. Cell Tissue Res 318:553–564.

Rohlfing T, Brandt R, Maurer CR Jr, Menzel R. 2001. Bee brains, B-splines and computational democracy: generating an average shape atlas. Proc IEEE Workshop on Mathematical Methods in Biomedical Image Analysis, MMBIA, Kauai, Hawaii, December, 2001. p 187–194.

Schmitt S, Evers JF, Duch C, Scholz M, Obermayer K. 2004. New methods for the computer-assisted 3-D reconstruction of neurons from confocal image stacks. Neuroimage 23:1283–1298.

Schneider NL, Stengl M. 2005. Pigment-dispersing factor and GABA synchronize cells of the isolated circadian clock of the cockroach *Leucophaea maderae*. J Neurosci 25: 5138–5147.

Schneider NL, Stengl M. 2006. Gap junctions between accessory medulla neurons appear to synchronize circadian clock cells of the cockroach *Leucophaea maderae*. J Neurophysiol 95:1996–2002.

Schneider NL, Stengl M. 2007. Extracellular long-term recordings of the isolated accessory medulla, the circadian pacemaker center of the cockroach *Leucophaea maderae*, reveal ultradian and hint circadian rhythms. J Comp Physiol A 193:35–42.

Shafer OT, Kim DJ, Dunbar-Yaffe R, Nikolaev VO, Lohse MJ, Taghert PH. 2008. Widespread receptivity to neuropeptide PDF throughout the neuronal circadian clock network of *Drosophila* revealed by real-time cyclic AMP imaging. Neuron 58:223–237.

Stengl M, Homberg U. 1994. Pigment-dispersing hormone-immunoreactive neurons in the cockroach *Leucophaea maderae* share properties with circadian pacemaker neurons. J Comp Physiol A 175:203–213.

Strauss R. 2002. The central complex and the genetic dissection of locomotor behaviour. Curr Opin Neurobiol 12: 633–638.

Chapter II

Light affects the branching pattern of peptidergic circadian pacemaker neurons in the brain of the cockroach *Leucophaea maderae*

Wei HY, and Stengl M. 2011.
This manuscript is published in J Biol Rhythms 26: 507–517.

Light Affects the Branching Pattern of Peptidergic Circadian Pacemaker Neurons in the Brain of the Cockroach *Leucophaea maderae*

Hongying Wei and Monika Stengl[1]
University of Kassel, FB 10, Biology, Animal Physiology, Kassel, Germany

Abstract Pigment-dispersing factor–immunoreactive neurons anterior to the accessory medulla (aPDFMes) in the optic lobes of insects are circadian pacemaker neurons in cockroaches and fruit flies. The authors examined whether any of the aPDFMes of the cockroach *Leucophaea maderae* are sensitive to changes in period and photoperiod of light/dark (LD) cycles as a prerequisite to adapt to changes in external rhythms. Cockroaches were raised in LD cycles of 11:11, 13:13, 12:12, 6:18, or 18:6 h, and the brains of the adults were examined with immunocytochemistry employing antisera against PDF and orcokinin. Indeed, in 11:11 LD cycles, only the number of medium-sized aPDFMes specifically decreased, while it increased in 13:13. In addition, 18:6 LD cycles increased the number of large- and medium-sized aPDFMes, as well as the posterior pPDFMes, while 6:18 LD cycles only decreased the number of medium-sized aPDFMes. Furthermore, PDF-immunoreactive fibers in the anterior optic commissure and orcokinin-immunoreactive fibers in both the anterior and posterior optic commissures were affected by different lengths of light cycles. Thus, apparently different groups of the PDFMes, most of all the medium-sized aPDFMes, which colocalize orcokinin, respond to changes in period and photoperiod and could possibly allow for the adjustment to different photoperiods.

Key words circadian pacemakers; orcokinin; pigment-dispersing factor; PDF; photoperiod; brain plasticity

For equator-distant organisms, the length of the light/dark (LD) cycles varies regularly during the course of the year because of the inclination of the Earth's axis. In addition, because of the gravitational pull of the moon on the Earth's oceans, the rotation of the Earth around its axis is gradually slowed, causing the length of a day to change since the first organisms inhabited the Earth. Thus, a main task of endogenous clocks such as circadian clocks and photoperiodic clocks is to allow for entrainment to changing external geophysical rhythms. Accordingly, photoperiodic clocks not only entrain to but also appear to measure the duration of the photophase ("photoperiodic timer") and appear to count the number of consecutive long or short days ("photoperiodic counter") before they initiate photoperiodic adaptations such as pupal diapause (Shiga et al., 2003; Emerson et al., 2009). It is under debate whether photoperiodic clocks and circadian clocks are constituted by the same cellular circuits. In mammals and insects, a dual circadian oscillator model was proposed previously to explain adjustment of locomotor rhythms to different

1. To whom all correspondence should be addressed: Monika Stengl, FB 10, Biology, Animal Physiology, University of Kassel, Heinrich-Plett-Str. 40, 34132 Kassel, Germany; e-mail: stengl@uni-kassel.de.

JOURNAL OF BIOLOGICAL RHYTHMS, Vol. 26 No. 6, December 2011 507-517
DOI: 10.1177/0748730411419968

photoperiods (Pittendrigh and Daan, 1976). Recently, in the fruit fly *Drosophila melanogaster*, it was suggested that a zeitgeber-dependently environmentally modifiable network of circadian clock-gene-expressing neuronal groups in the brain is responsible for either controlling the morning (M-cells) or the evening (E-cells) peak of locomotor activity (Helfrich-Förster, 2009). While in the fruit fly, the pigment-dispersing factor–immunoreactive (PDF-ir) small ventral lateral neurons (sLN_v) are assumed to be M-cells, which are phase advanced by light at the late night, in the cockroach *Leucophaea maderae*, PDF-ir neurons are also known while the nature of M- and E-cells remains to be discerned.

In the cockroach *L. maderae* (= *Rhyparobia maderae*), lesion and transplantation experiments located the circadian pacemaker, which controls locomotor activity rhythms to the optic lobes' accessory medulla (aMe) with associated PDF-ir neurons (Stengl and Homberg, 1994; Reischig and Stengl, 2003a). The about 12 PDF-ir neurons anterior to the aMe (aPDFMes) can be subgrouped according to soma size into 4 small, 4 medium-sized, and 4 large aPDFMes. Posterior to the aMe are the less well-described 2 small and 2 large posterior PDF-ir neurons (pPDFMes). The respective functions of the different PDF-ir neurons in different neuronal circuits are not well understood. However, backfill studies combined with immunocytochemistry suggested that the 4 medium-sized aPDFMes colocalize orcokinin and FMRFamide-immunoreactivity and project via the anterior optic commissure (AOC) to ipsi- and contralateral midbrain targets. Three of them reach as far as into the contralateral optic lobe (Reischig and Stengl, 2004; Soehler et al., 2008). The 4 large aPDFMes do not colocalize orcokinin or FMRFamide. They project via the lobula valley tract to the AOC and posterior optic commissure (POC) and branch in different ipsilateral and/or contralateral midbrain targets, and only one of them (the conspicuously largest) reaches into the contralateral optic lobe (Soehler et al., 2008). The 4 pPDFMes are assumed to restrict their arborizations to optic lobe neuropils while not projecting to the midbrain. Their respective branching pattern within the aMe neuropil is not known. The small PDFMes appear to be local neurons of the aMe and are not well characterized due to their low level of PDF-immunoreactivity (Reischig and Stengl, 2003b). Therefore, they are not taken into account in this study.

In the Madeira cockroach, PDF is an input and output signal of the circadian clock (Petri and Stengl, 1997), while in the German cockroach, PDF is necessary for circadian rhythmicity (Lee et al., 2009), and in the cricket *Gryllus bimaculatus*, PDF plays a role for photic entrainment next to additional functions in the clock (Abdelsalam et al., 2008; Hassaneen et al., 2011). In the Madeira cockroach, orcokinin and not PDF is assumed to play a role in photic entrainment because orcokinin injections produce a light-like phase response curve with delays at the early night and advances at the late night (Hofer and Homberg, 2006a). Whether light or darkness is an input signal to PDF-dependent neuronal circuits in the brain of the Madeira cockroach is not known. Furthermore, while PDF-ir circadian pacemaker neurons are assumed to play a role in photoperiod-controlled behaviors in flies (Hamanaka et al., 2007; Shiga and Numata, 2009), this is not known for the Madeira cockroach.

Here we examined in *L. maderae* whether PDF-ir neurons are sensitive to changes in photoperiod (the duration of the photophase) and period (the number of hours per day) of LD cycles. On the basis of previous work (Barrett and Page, 1989; Page and Barrett, 1989), we tested whether the PDF-ir branching pattern or the number of their respective PDF-ir somata was changed via different LD regimes during development: 11:11 (T22), 12:12 (T24), 13:13 (T26), 18:6 (long days), and 6:18 (short days). Indeed, changes in LD regimes during development affected primarily the number of PDF-ir medium-sized aPDFMes, which colocalize orcokinin and project via the AOC to the contralateral aMe. Thus, light regimes either affect the survival of PDFMes or the expression of PDF in PDFMes during development. This indicates that even the circadian system of a tropical species without immediate need to adjust to changes in photoperiod has the plasticity to allow for radiation into different climatic zones.

MATERIALS AND METHODS

Animals

Adult male cockroaches (*L. maderae*) were reared at constant conditions: temperature 26 °C and humidity 60%, with 5 different light/dark cycles—that is, 11 h light–11 h dark (LD 11:11), 12 h light–12 h dark (LD 12:12), 13 h light–13 h dark (LD 13:13), 6 h light–18 h dark (LD 6:18), and 18 h light–6 h dark (LD 18:6). All brains were dissected at about the same zeitgeber time (ZT) 1:00 to avoid ZT-dependent effects.

Primary Antisera

The anti-β-PDH antiserum (#3B3), an affinity-purified rabbit antiserum against synthetic *Uca pugilator* β-PDH, was generated by Dr. H. Dircksen (University of Stockholm, Sweden) (Dircksen et al., 1987). Its specificity was shown by immunodot-blotting assays of high-pressure liquid chromatography (HPLC)–separated crude sinus gland extracts (Dircksen et al., 1987; Mangerich et al., 1987). The specificity of the antiserum for cockroach PDF has been demonstrated through preadsorption controls (Stengl and Homberg, 1994; Petri et al., 1995; Reischig and Stengl, 1996). The monoclonal anti-*Drosophila*-PDF (#C7) antibody raised in mouse was provided by the Developmental Studies Hybridoma Bank. To examine its specificity, the PDF-ir network in the cockroach wholemount brain was labeled by using anti-β-PDH antiserum diluted at 1:20,000 and anti-*Drosophila*-PDF diluted at 1:5 simultaneously. Both antisera labeled the same neuronal structures (data not shown). The anti-Asn^{13}-orcokinin antiserum (provided by Dr. H. Dircksen) was raised in rabbits. Its specificity on cockroach brain sections was determined using liquid-phase preadsorption by Hofer and Homberg (2006b).

Immunocytochemistry on Paraffin Sections

The brains of cockroaches raised in LD 11:11 (T22; n = 29) and LD 13:13 (T26; n = 34) hours were processed for immunocytochemistry on paraffin sections. The immunocytochemical staining protocol was performed as described before (Reischig and Stengl, 2003b). The brains were dissected from the head capsule and fixed overnight in 4% paraformaldehyde (PFA) at 4 °C. Subsequently, they were washed (3 times for 10 min) with 0.1 M phosphate-buffered saline (0.1 M PBS, pH 7.4) and dehydrated in an ethanol series and embedded in paraffin (Paraplast plus; Sigma-Aldrich, Deisenhofen, Germany). Serial frontal 10-µm sections were cut with a rotary microtome and mounted on microscope slides. Afterwards, the samples were deparaffinized with xylene and rehydrated using graded ethanol concentrations. The brain sections were stained with anti-β-PDH for 18 to 24 h diluted at 1:3000 in 0.1 M PBS containing 0.5% Triton X-100 (0.1 M PBT) and 1% normal goat serum (NGS; Jackson ImmunoResearch, West Grove, PA). Immunoreactive cells were detected by using a 3-step peroxidase technique (Sternberger, 1979; Reischig and Stengl, 1996). After a thorough rinsing with PBT (3 times for 10 min), the sections were incubated for 1 h in goat-anti-rabbit IgG diluted at 1:100 and for 1 h in rabbit PAP (DAKO, Hamburg, Germany) at a dilution of 1:300. After washing again, the brains were stained with 0.03% 3,3'-diaminobenzidine tetrahydrochloride (DAB; Sigma-Aldrich) and 0.015% H_2O_2 in 0.1 M PBS for 10 min. To visualize the neuropils of the brain, the sections were counterstained with 1% methylene blue.

Double-Staining on Sections

Double-staining experiments with the anti-Asn^{13}-orcokinin and the monoclonal anti-*Drosophila*-PDF were performed with cockroaches, reared in short day lengths (LD 6:18; n = 20), normal day lengths (LD 12:12; n = 20), and long day lengths (LD 18:6; n = 20). The brains were dissected and fixed as described above. After fixation, the brains were embedded in a gelatine/albumin mixture (4.8% gelatine and 12% ovalbumin in demineralized water), postfixed in 8% formalin, and sectioned using a vibratome (Leica, Nussloch, Germany) in a frontal plane of 200 µm thickness. The free-floating sections were washed for 10 min in 0.1 M PBT for 6 times and preincubated for 3 h with 5% NGS and 0.02% sodium azide in 0.1 M PBT at room temperature. The primary antisera anti-Asn^{13}-orcokinin (from rabbit) and anti-*Drosophila*-PDF (from mouse) were diluted at 1:4000 and 1:5 in 0.1 M PBT containing 1% NGS and 0.02% sodium azide and were incubated on sections for 3 days. After 6 consecutive washes in 0.1 M PBT for 10 min each, the sections were stained with a Cy2-conjugated goat anti-mouse secondary antibody (Cy2-GAM; Jackson ImmunoResearch) and a Cy3-conjugated goat anti-rabbit secondary antibody (Cy3-GAR; Jackson ImmunoResearch) (diluted in 1:300) in 0.1 M PBT containing 1% NGS and 0.02% sodium azide for 2 days. The sections were washed before dehydration in an increasing ethanol series (0%, 50%, 70%, 90%, 95%, 100%, 5 min each). They were precleared in a mixture of 50% methyl salicylate (MS; Merck, Darmstadt, Germany) and 50% ethanol for 5 min and cleared with MS for 15 min. Finally, to prevent compressions, the sections were mounted in Permount (Fisher Scientific, Pittsburgh, PA) in the center of 3 spacers between 2 coverslips (Zweckform, Oberlaindern, Germany).

Immunocytochemistry for Wholemount Brains

To determine the developmental plasticity of the PDF-ir network regarding the different day and night lengths, the wholemount brains of the cockroaches reared in LD 6:18 (n = 16), LD 12:12 (n = 18), and LD 18:6 (n = 18) were stained with anti-β-PDH antiserum. The procedure was described previously in detail (Wei et al., 2010). Briefly, dissected brains were fixed as described above. The brains were washed in 0.1 M PBS 5 times for 15 min each before treating with 1 mg/mL collagenase for 1 h. After washing 6 times with 0.1 M PBT for 20 min, the brains were preincubated overnight at 4 °C with 5% NGS and 0.02% sodium azide in 0.1 M PBT. The brains were incubated in anti-β-PDH antiserum diluted at 1:20,000 in 0.1 M PBT containing 1% NGS and 0.02% sodium azide for 5 days at 4 °C. After another washing step with 0.1 M PBT over 2 h, the primary antibody was detected by Cy3-GAR diluted at 1:300 in 0.1 M PBT containing 1% NGS and 0.02% sodium azide for 4 days at 4 °C. After washing again, the brains were dehydrated in an increasing series of ethanol, precleared in a mixture of 50% methyl salicylate and 50% ethanol, and cleared with methyl salicylate for 40 min. Finally, the wholemounts were mounted in Permount.

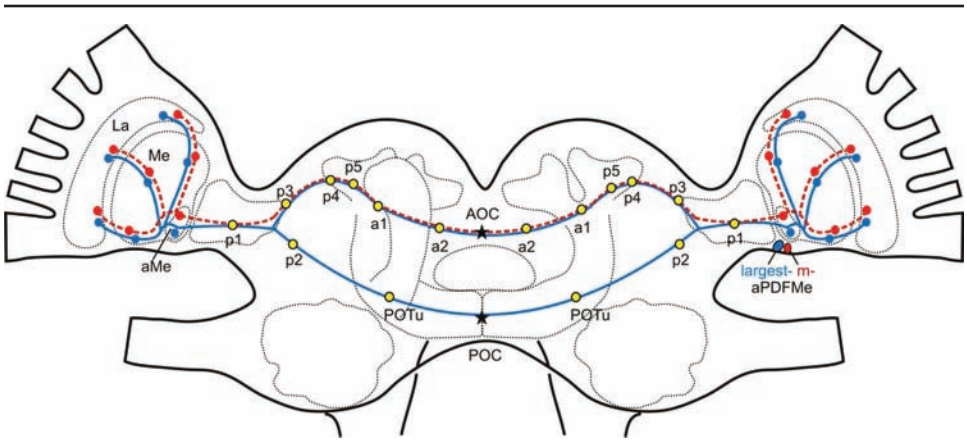

Figure 1. Arborization pattern of the pigment-dispersing factor–immunoreactive (PDF-ir) neurons connecting the ipsi- and contralateral optic lobe is shown in a brain model of the cockroach *L. maderae*. One particularly large PDF-ir neuron (blue) anterior to the medulla (aPDFMe) connected both optic lobes via the anterior and posterior optic commissures (AOC, POC). Three medium-sized PDF-ir neurons (red) cross the brain midline via the AOC. Along their way, they gave rise to several branching sites: 5 plexi (p1-5), 2 areas (a1-2), and the posterior optic tubercle (POTu). Stars mark the sites of fiber counts taken. La = lamina; aMe = accessory medulla; Me = medulla.

Visualization and Evaluation

The PDF-ir structures in paraffin sections were observed using a Zeiss microscope (Zeiss Axio Scope A1). A confocal laser-scanning microscope (Leica TCS SP5) was employed to image the 200 µm sections and wholemounts. The fluorescence signals of Cy3 were excited with a helium/neon laser at 543 nm and detected between 560 nm and 580 nm. Cy2 fluorescence was excited with a 488 nm argon laser and detected between 500 nm and 520 nm. The orcokinin-ir and PDF-ir structures were consecutively photographed using a 20x objective at a resolution of 1024 × 1024 pixels in the x-y plane and an interslice interval of 0.5 µm (axial distance). Due to the thickness and width of the wholemounts, they were scanned in 8 image stacks that were combined using Amira 3.1 and 4.1 (Visage Imaging, Fürth, Germany). For better structural analysis, the orcokinin-ir fibers in one optic lobe were three-dimensionally reconstructed with the "skeleton reconstruction" tool in Amira 3.1 (Wei et al., 2010).

To determine whether different LD cycles cause environmentally induced plasticity of the PDF-ir network, the somata of large- and medium-sized anterior PDF-ir somata next to the medulla (aPDFMes) and of the posterior PDF-ir neurons next to the medulla (pPDFMes) were counted in all experimental groups. In addition, the number of PDF-ir fibers in the AOC and POC was counted (Fig. 1). Furthermore, the length of the AOC and POC and the distances between all PDF-ir arborization sites in animals with LD 6:18, 12:12, and 18:6 were measured (n = 10). Finally, the number of orcokinin-ir fibers in the orcokinin-ir AOC and POC was counted in all 3 experimental groups. The data were compared and analyzed using SPSS 13.0 and Origin 6.0.

RESULTS

To determine whether different photoperiods and different T cycles affect PDFMes, we examined whether rearing in different light regimes changes PDF-ir circadian pacemaker neurons associated with the

accessory medulla (aMe) in *L. maderae*. We hypothesized that circadian pacemaker neurons with long endogenous periods are more activated via long-period T cycles compared to short-period T cycles and that light-sensitive cells are more activated via long photoperiods compared to short photoperiods. Since activation of neurons during development affects survival, we expected to see changes in the number of respectively affected cells. Furthermore, we wanted to distinguish pacemaker neurons that are affected by light and darkness equally or not equally. Therefore, cockroaches were raised in non-24-h LD (T) cycles 11:11 (T22; $n = 29$) and 13:13 (T26; $n = 34$) as well as in different photoperiods with long days (18:6; $n = 18$) or short days (6:18; $n = 16$). Then, the brains of the adult cockroaches were processed for PDF-immuno-cytochemistry. Double-labeling with anti-orcokinin together with anti-PDF antibodies was only performed in animals raised under different photoperiods ($n = 20$). The number of different groups of PDF-ir neuronal cells anterior or posterior to the aMe (aPDFMes, pPDFMes), as well as the number and length of PDF- or orcokinin-ir processes in optic lobe commissures, was evaluated. Then, the different experimental groups were compared to cockroaches raised in 12:12 (T24 = control; $n = 18$) LD cycles.

Different T Cycles Only Changed Medium-Sized aPDFMes

The number of immunoreactive somata of large aPDFMes and pPDFMes in cockroaches reared under the 3 different T cycles showed no significant difference (analysis of variance [ANOVA] least significant difference [LSD] $p > 0.05$). However, the number of somata of medium-sized aPDFMes in T22 animals ($n = 29$) was significantly smaller, and in T26 animals ($n = 34$), it was significantly higher as compared to T24 animals ($n = 18$) (ANOVA LSD $p < 0.05$) (Fig. 2A). The number of the PDF-ir fibers in the AOC in T22 and T24 animals showed no significant difference (ANOVA LSD $p > 0.05$). In contrast, the number of the PDF-ir fibers in T26 animals was higher in the AOC than in T22 or T24 animals (ANOVA LSD $p < 0.05$). The number of the PDF-ir fibers in the POC was not affected by changes in zeitgeber period (ANOVA LSD $p > 0.05$) (Fig. 2B).

Different Photoperiods Changed All Groups of PDFMes Differentially

The number of immunoreactive somata of the large aPDFMes and of the pPDFMes did not differ significantly in cockroaches raised in LD 6:18 ($n = 16$) and 12:12 ($n = 18$) (ANOVA LSD $p > 0.05$), while fewer medium-sized aPDFMes were counted in short day-rearing conditions (ANOVA LSD $p < 0.05$) (Fig. 3A). The cockroaches raised in LD 18:6 ($n = 18$) maintained significantly more somata of large- and medium-sized aPDFMes and of pPDFMes than those raised under LD 6:18 or 12:12 (ANOVA LSD $p < 0.05$) (Fig. 3A). The number of PDF-ir fibers in the AOC and POC showed no significant difference among the 3

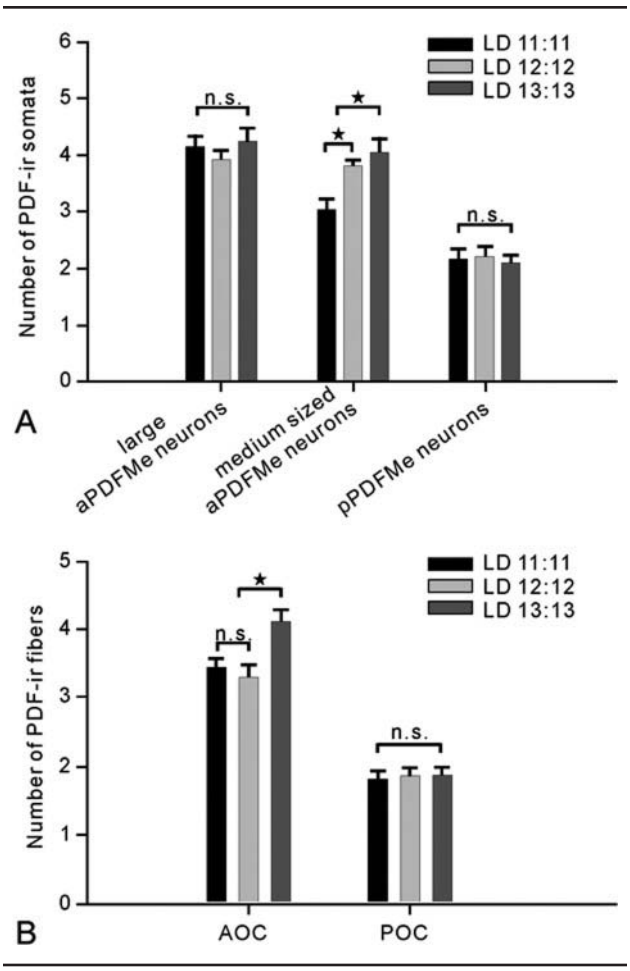

Figure 2. (A, B) Cockroaches raised in different light/dark (LD) time (T) cycles: 11:11 (T22; $n = 29$), 12:12 (T24; $n = 18$), and 13:13 (T26; $n = 34$) showed differences in the number of pigment-dispersing factor–immunoreactive (PDF-ir) somata and commissural processes (bars, standard error). The different light and dark regimes did not affect the soma numbers of large anterior PDF-ir neurons (aPDFMes) or of posterior PDF-ir neurons (pPDFMes), nor did they affect the number of PDF-ir fibers in the posterior optic commissures (POC) (ANOVA LSD $p > 0.05$; n.s. = not significant). However, the number of medium-sized aPDFMes in T24 animals was significantly higher than in T22 and lower than in cockroaches raised in T26 (ANOVA LSD $p < 0.05$, star). T26 animals displayed a significantly higher number of PDF-ir fibers in the anterior optic commissures (AOC) than T22 and T24 animals (ANOVA LSD $p < 0.05$, star).

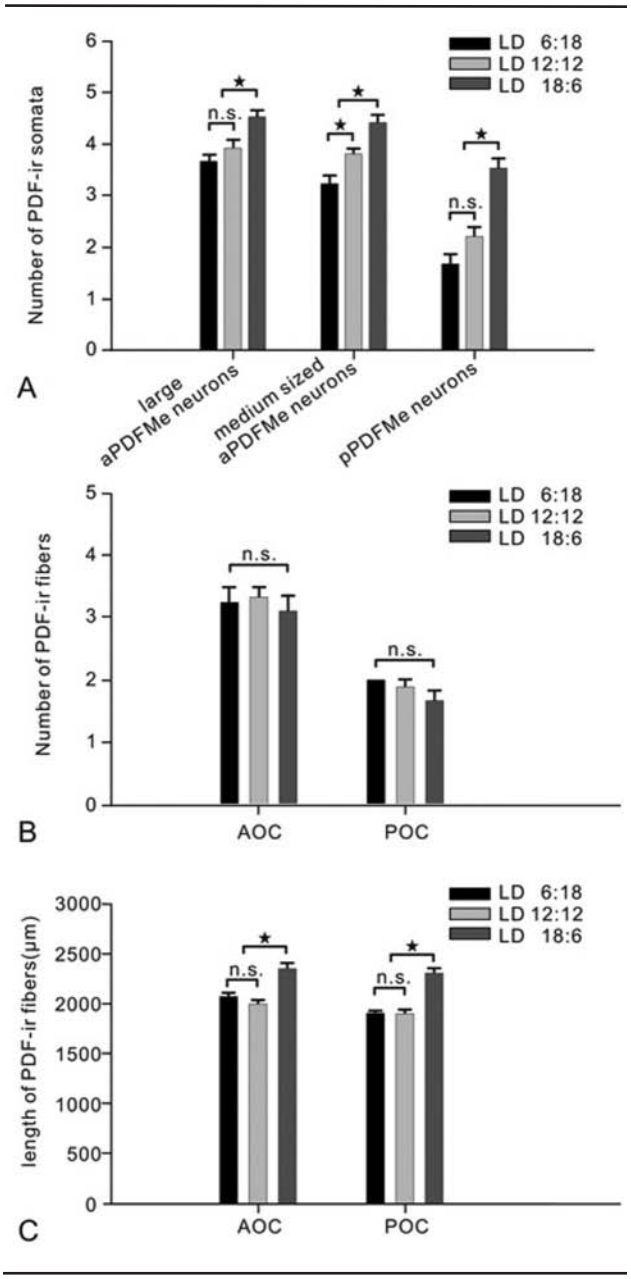

Figure 3. (A-C) Cockroaches reared in light/dark (LD) cycles 6:18 (n = 16), 12:12 (n = 18), and 18:6 (n = 18) showed significant differences in the number of the pigment-dispersing factor–immunoreactive (PDF-ir) somata as well as in the length of commissural processes (bars, standard error). More large- and medium-sized anterior PDF-ir neurons (aPDFMes) as well as more posterior PDF-ir neurons (pPDFMes) occurred in cockroaches with LD 18:6 compared to animals raised in LD 6:18 and 12:12. In the 6:18 light regime, only medium-sized aPDFMes decreased in number as compared to the other experimental groups (ANOVA LSD $p < 0.05$, A star). The number of PDF-ir fibers in the anterior and posterior commissures (AOC, POC) showed no significant difference among the 3 animal groups (ANOVA LSD $p > 0.05$ B, n.s. = not significant). The longer PDF-ir fibers in the AOC and POC occurred in animals under LD 18:6 and were absent in those animals under LD 6:18 and 12:12 (ANOVA LSD $p < 0.05$, C star, n = 10).

experimental groups (ANOVA LSD $p > 0.05$) (Fig. 3B). The length of the PDF-ir fibers in the AOC and POC did not show a significant difference between the cockroaches raised in LD 6:18 and 12:12 (ANOVA LSD $p > 0.05$; n = 10). However, the cockroaches raised in LD 18:6 exhibited significantly longer fibers in the AOC and POC compared to those raised in LD 6:18 or 12:12 (ANOVA LSD $p < 0.05$; n = 10) (Fig. 3C). Linear regression analysis (n = 10) showed that the relative distances of the different PDF-ir arborization sites in the aMe, the 5 plexi (p1-p5), the posterior optic tubercle (POTu), and the 2 arborization areas (a1, a2) were regulated by different photoperiods (Fig. 4) (Wei et al., 2010).

Different Photoperiods Changed the Orcokinin-ir Network

Next to the network of PDFMes, orcokinin-ir neurons were further examined (n = 20) because all medium-sized aPDFMes colocalize orcokinin and PDF immunoreactivity (Soehler et al., 2011). In addition, orcokinin appears to act in the light-entrainment pathway of the circadian clock (Hofer and Homberg, 2006b; Soehler et al., 2011). Our results confirmed previous findings of orcokinin-ir branching patterns in the cockroach brain (n = 20). However, at least 3 new observations were reported in this study, based on 20 preparations examined.

First, at least 3 of the 4 medium-sized aPDFMes differentially colocalized PDF with orcokinin immunoreactivity (n = 20). Always, 1 soma contained relatively stronger PDF immunoreactivity as compared to weaker orcokinin immunoreactivity. In contrast, always the other 2 somata expressed strong orcokinin and weaker PDF immunostaining (Fig. 5A).

Second, the PDF-ir fibers from the anterior aMe projected toward the medulla and lamina via 2 distinct pathways: the anterior fiber fan covering the anterior and distal surface of the medulla (Fig. 5B1-B2, yellow star) and the median layer fiber system in the medulla (Fig. 5B2, yellow arrow). In contrast, the orcokinin-ir fibers from the posterior aMe extended into the medulla and ramified extensively in a proximal-median layer of the medulla (Fig. 5B1, B3-B4, white star). Dense orcokinin-ir fibers ran in a distal-posterior direction and gave rise to a fiber meshwork parallel to the distal surface of the medulla (Fig. 5B2, B3-B4, blue star). Despite the colocalization of both peptides in apparently all medium-sized

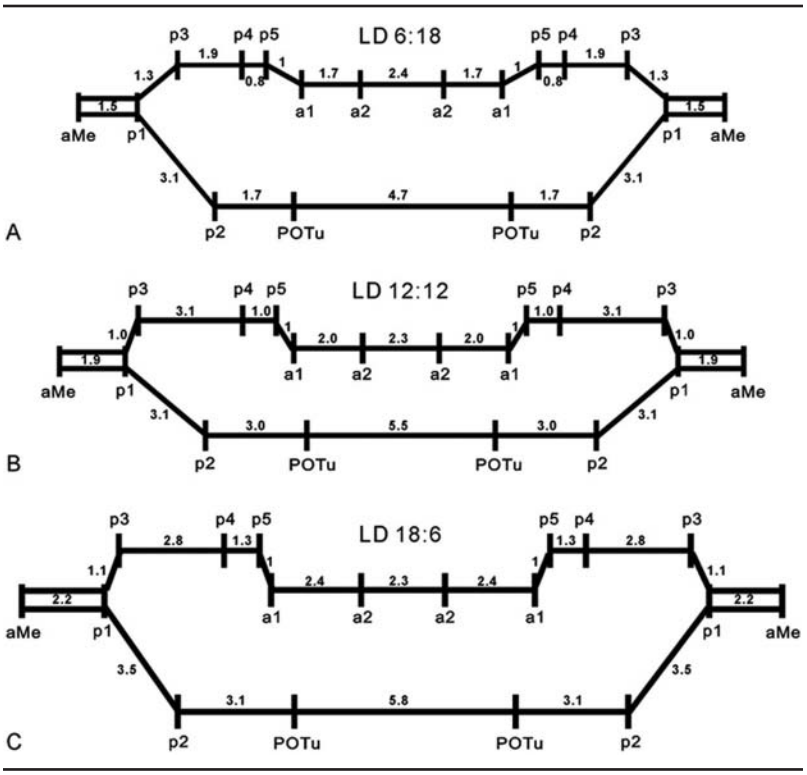

Figure 4. (A-C) The light/dark regimes (LD 6:18 in A, 12:12 in B, and 18:6 in C) changed the distances between pigment-dispersing factor–immunoreactive (PDF-ir) arborization sites (n = 10): 5 plexi (p1-5), 2 areas (a1-2), and posterior optic tubercle (POTu). The distance between p5 and area a1 was defined as "1." Linear regression analysis calculated the respective multiples of this distance for the other connections. These were changed under different LD conditions.

aPDFMe somata of the ventral neurons next to the aMe, the median layer fiber system of the PDF-ir neurons and the fiber meshwork of the orcokinin-ir cells arborized in the same layer of the medulla without expressing any colocalization (Fig. 5B2). Clearly, colocalization of PDF and orcokinin immunoreactivity could not be observed in any of the described PDF-ir branching sites (n = 20) (Wei et al., 2010; Soehler et al., 2011).

Third, two distinguishable orcokinin-ir fiber fascicles crossed the brain midline via the AOC (Fig. 5C1, D1). Animals raised in LD 6:18 or LD 18:6 exhibited either fewer or more fibers in both bundles as compared to cockroaches raised under LD 12:12 (ANOVA LSD $p < 0.05$) (Fig. 6). The PDF-ir fibers in the AOC ran near the upper orcokinin-ir fiber bundle (Fig. 5C1), and 2 fiber bundles (middle and lower POC in Fig. 5D2) with dense orcokinin immunoreactivity connected both aMae via the POC. Several faint orcokinin-ir fibers were found superior to these 2 fiber bundles in the POC (upper POC in Fig. 5D2). The number of fibers in the middle bundle showed significant changes in response to LD environmental changes. Lengthening the light phase and shortening the dark phase (LD 18:6) induced a significant increase of the orcokinin-ir fibers in the middle bundle, while shortening the light phase and increasing the dark phase (LD 6:18) decreased the number of orcokinin-ir fibers in the middle bundle (ANOVA LSD $p < 0.05$) (Fig. 6). The number of fibers in the upper bundle and lower bundle showed no significant difference among the 3 experimental groups. Generally, only 2 orcokinin-ir fibers projected via the lower bundle. The orcokinin-ir fibers in the POC did not show colocalization with PDF immunoreactivity (Fig. 5C2).

DISCUSSION

To determine whether PDF-ir circadian pacemaker circuits are sensitive to different photoperiods and T cycles, rearing in different light cycles was combined with immunocytochemistry employing antisera against PDF and orcokinin. After raising cockroaches *L. maderae* in different light regimes, T22, T24, T26, 6:18, and 18:6 LD, it was found that non-24-h periods as well as different length of the light phase in T24 animals changed the soma number and branching pattern of immunoreactive PDFMes specifically, with the medium-sized aPDFMes, which project via the AOC, being the most LD-regime responsive among the PDF-ir neurons. In all cases, we were not able to distinguish whether the number of immunoreactive cells changed in the different light regimes due to regulated survival of neurons or due to regulated PDF or orcokinin expression in the respective cells. This, however, would not affect the main conclusions concerning light responsiveness of the circadian pacemaker neurons.

Plasticity of the Optic Lobes

In accordance with our findings, it was known from previous studies in vertebrates as well as in invertebrates that light-dependent neuronal activity shapes neuronal circuits in the visual system (reviews: Hirsch et al., 1995; Heisenberg et al., 1995; Aamodt and

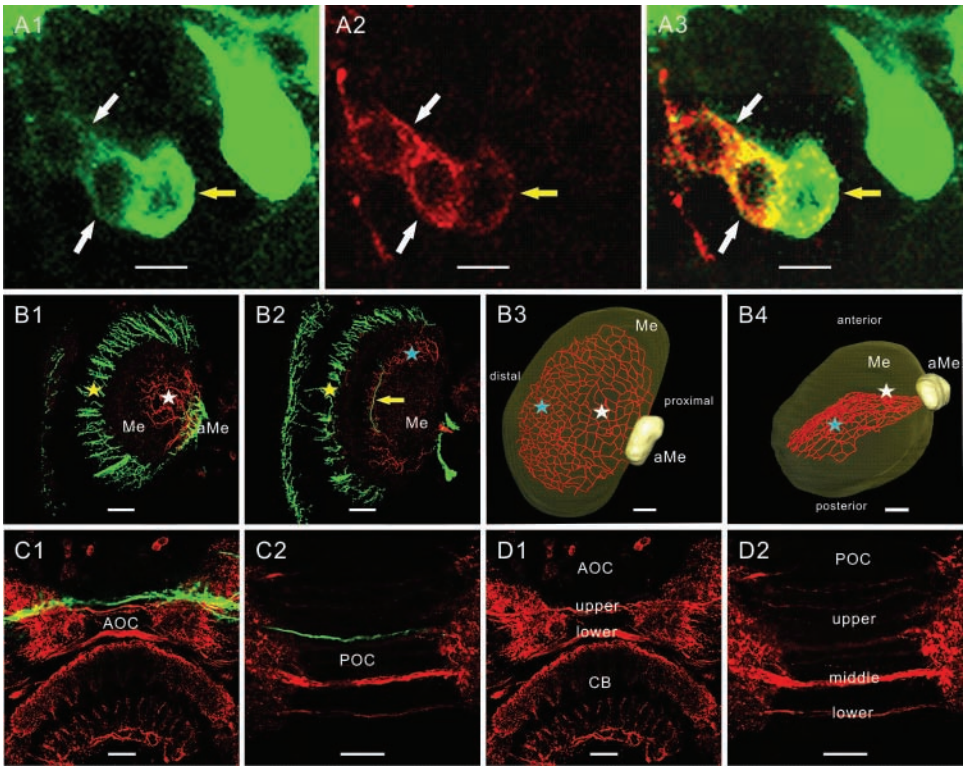

Figure 5. (A-D) Orcokinin-immunoreactive (orcokinin-ir) and pigment-dispersing factor–immunoreactive (PDF-ir) fibers in the optic lobes (A, B) and at the level of the anterior and posterior optic commissures (AOC, POC) (C, D). PDF immunoreactivity is shown in green and orcokinin immunoreactivity is shown in red. (A1-A3) Three medium-sized anterior PDF-ir neurons (aPDFMes) expressed colocalization and always differential intensity of staining with both peptide antisera (n = 20). Always 1 soma showed stronger PDF and weaker orcokinin immunoreactivity (yellow arrow), while the other 2 somata expressed more orcokinin and less PDF immunoreactivity (white arrows). The overlay image in A3 proved the colocalization of both peptides. (B1-B4) Orcokinin- and PDF-ir fibers in the optic lobes do not express colocalization of both peptides. The PDF-ir neurons connected the accessory medulla (aMe), the medulla (Me), and the lamina via the anterior fiber fan (B1, B2, yellow star) and via the median layer fiber system (B2, yellow arrow). The orcokinin-ir fibers ran from the posterior aMe, fasciculated in a proximal-median layer of the medulla (B1, B3, B4, white stars), and projected distal-posteriorly in a layer of the medulla toward the first optic chiasma (B2, B3, B4, blue stars). They formed a fiber network covering at least one complete layer in the medulla. The median layer fiber system of the PDF-ir neurons (B2, yellow arrow) and the fiber meshwork of the orcokinin-ir cells (B2, blue star) arborized in the same layer of the medulla. (C1-D2) No colocalization occurred in the upper and lower fiber bundles in the AOC or in the upper, middle, and lower fiber bundles in the POC. CB = central body. Scale bar = 10 m in A, 50 m in B-D

Constantine-Paton, 1999). In *D. melanogaster*, changes in light levels changed the volume of light-dependent neuropils in the brain (Barth and Heisenberg, 1997). The lamina and medulla were largest in flies raised in constant light (LL) and smallest in flies reared in constant darkness (DD), mainly due to changes in the volume of photoreceptor cell terminals (Barth et al., 1997). The activity-dependent morphological changes in the optic lobes also were accompanied by changes in the physiology, such as altered contrast sensitivity (Deimel and Kral, 1992; Kral and Meinertzhagen, 1989). The experience-dependent plasticity in the optic lobes was interpreted as a form of long-term memory that allows adaptation to varying environmental conditions. Thus, it is very likely that in the cockroach, the light-dependent change in the length of the PDF-ir processes reflects respective light-dependent changes in the volume of PDF-ir neuropils. It is not completely resolved how light affects the PDF-ir l-LNvs to control PDF release at dawn in the fruit fly to elicit arousal (Parisky et al., 2008; Park and Griffith, 2006). Even less is known about the pre- and postsynaptic cells of the PDF-ir neurons in the cockroach.

Light Affects PDF-ir Neurons Differentially in the Cockroach *L. maderae*

Our studies show that the medium-sized aPDFMes, which project via the AOC, are affected via different T cycles and different length of the light phase during different photoperiods. One possible explanation would be that the medium-sized aPDFMes have longer endogenous periods and couple better to long T cycles as compared to short T cycles. Alternatively or additionally, the about 4 medium-sized aPDFMes are a diverse group of cells. Most of them are activated more by light than inhibited by darkness, and at least one is inhibited more by darkness than activated by light. Alternatively, only light or darkness of a minimum duration activates or inhibits the medium-sized aPDFMes ZT-independently. As the most likely hypothesis, we suggest that the medium-sized aPDFMes are only activated by light and inhibited by darkness

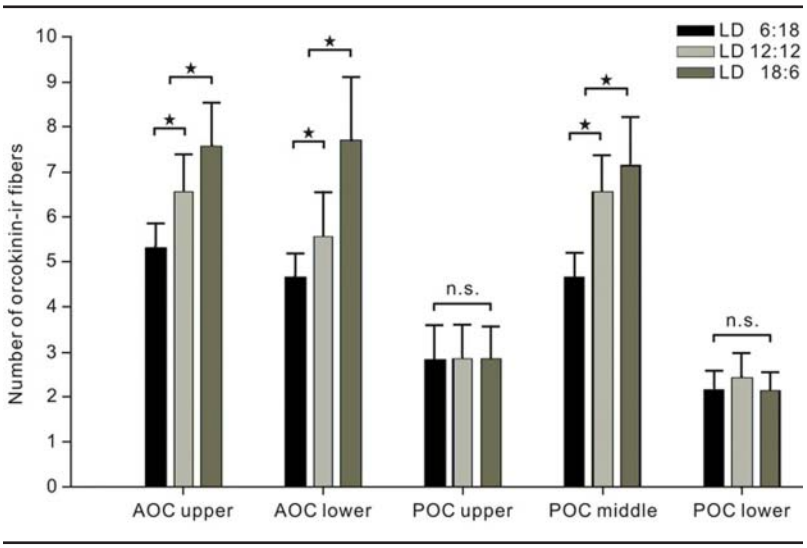

Figure 6. Cockroaches raised in light/dark (LD) 6:18, 12:12, and 18:6 showed differences in the amount of orcokinin-immunoreactive (orcokinin-ir) commissural fibers (n = 20; bars, standard error). The number of the orcokinin-ir fibers in the upper and lower fiber bundles in the anterior optic commissure (AOC) as well as in the middle fiber bundle in the posterior optic commissure (POC) increased significantly with lengthening of the light phase while shortening the dark phase (ANOVA LSD $p < 0.05$, star, n = 20). The number of fibers in the upper and lower bundles in the POC showed no significant correlation with the different LD conditions (ANOVA LSD $p > 0.05$, n.s. = not significant, n = 20).

during ZT 11-13 but are not affected via photic stimuli at other zeitgeber times. In contrast, the large aPDFMes and the pPDFMes appear to receive balanced activity by light and inhibition by darkness since the different T cycles did not affect them. However, apparently a longer light duration compared to the dark phase appears to activate these cells. Alternatively, we find it most likely that these cells are only light-responsive during a time window between ZT 13 and 18. Because the number of PDF-ir fibers in the AOC increased in T26 but did not increase in 18:6 LD cycles, possibly some of the contralaterally projecting medium-sized aPDFMes are activated by light while others are inhibited by decreases in the duration of darkness.

How light reaches the PDF-ir circuits in the cockroach is not completely clear. Lesion studies revealed that photoreceptors in or near the compound eyes provide light entrainment of locomotor activity rhythms (Nishiitsutsuji-Uwo and Pittendrigh, 1968; Roberts, 1965, 1974). Anti-histamine immunocytochemistry revealed that there is no direct photoreceptor input to the aMe, and the photoreceptors terminate in the lamina and a distal layer of the medulla (Loesel and Homberg, 2001). Light input to the circadian clock appears to be relayed via the GABAergic distal tract, which projects over the distal face of the medulla to the noduli of the aMe (Petri et al., 2002). In addition, intracellular recordings identified a light-excited GABAergic neuron next to the aMe with tangential projections to a median layer of the medulla, arborizations in the noduli of the aMe, and projections to accessory neuropils of the lamina via the fiber fan over the anterior face of the medulla (Loesel and Homberg, 2001). Contralateral light input appears to reach the noduli of the aMe via 3 orcokinin-immunoreactive ventromedian neurons, which are excited by light and are polarization sensitive (Loesel and Homberg, 2001; Hofer and Homberg, 2006a, 2006b). They connect both aMae with a median layer of both medullae via the POC (Loesel and Homberg, 2001). Possibly, the processes of these light-sensitive orcokinin-ir ventromedian neurons project via the middle bundle in the POC, which changed in fiber number light-regime-dependently. Furthermore, injection studies combined with locomotor activity assays support a role of orcokinin, next to allatotropin and GABA in the processing of photic inputs via the noduli of the aMe (Petri et al., 2002; Hofer and Homberg, 2006a). Orcokinin, allatotropin, and GABA injections into the vicinity of the aMe shifted locomotor activity daytime-dependently. Because their respective phase response curves resembled light-dependent biphasic phase response curves, in contrast to PDF (Petri and Stengl, 1997), it was assumed that the respective orcokinin-, allatotropin-, and GABA-ir cells are part of the light entrainment pathway. Finally, centrifugal neurons with processes in the median protocerebrum, which are inhibited by light, send axonal arborizations to the aMe (Loesel and Homberg, 2001). Whether there is also light input via extraocular photoreceptors from the cryptochrome-positive lamina and lobula organs remains to be examined (Fleissner et al., 2001).

Previous studies examined how light affects circadian pacemaker development in *L. maderae* raised in non-24-h light rhythms (Barrett and Page, 1989; Page and Barrett, 1989). It was shown that raising cockroaches in 11:11 LD (T22) cycles throughout their development caused a significant reduction in the delay portion of the light-dependent

phase response curve in addition to a shortening of their endogenous period (τ). In contrast, in cockroaches raised in 13:13 LD (T26), the advance portion of the light-dependent phase response curve was significantly reduced and τ lengthened. The cellular basis of the experience-dependent plasticity of the circadian system remained unknown. In addition, it was unknown whether clock genes affect circadian system plasticity as described in the fruit fly by Fernández et al. (2008). Our data suggest that the medium-sized aPDFMes might at least partly relay light-dependent phase delays and might possibly also inhibit light-dependent phase advances. Therefore, medium-sized aPDFMes might be part of the neuronal circuit, which encodes light-dependent phase delays of locomotor activity at the end of the day and the beginning of the night, possibly via long endogenous pacemaker periods. Thus, the medium-sized aPDFMes are candidates for an E oscillator circuit in the Madeira cockroach, different from the PDF-ir sLN_vs in *D. melanogaster*. Since PDF injections cause phase delays of locomotor activity at the late day and because the number of medium-sized aPDFMes decreased in T22 cycles, this assumption is in accordance with previous evidence (Barrett and Page, 1989; Page and Barrett, 1989; Petri and Stengl, 1997; Schneider and Stengl, 2005). Whether the decrease in the light-dependent advances of locomotor activity in T26 cycles at least partly depends on the increase in the number of immunoreactive medium-sized and large posterior PDFMes remains to be examined further. Thus, our data add further evidence to the assumption that even in a tropical species, the pacemaker center in the aMe not only regulates 24-h rhythms. It also has the potential to control ultradian rhythms of action potentials in the gamma frequency range (Schneider and Stengl, 2007) and might even allow for adaptation to photoperiodic cycles during the course of the year.

ACKNOWLEDGMENTS

We are grateful to Dr. H. Dircksen for the generous supply with antibodies and to Johannes Grosshans for preparation of the antiserum-labeled sections. Dr. Thomas Reischig and Rita Zintl provided some of the preparations in different day lengths. In addition, we thank our referees, which considerably improved our manuscript. Supported by DFG grants STE 531/15, STE 531/18, and STE 531/21.

CONFLICT OF INTEREST STATEMENT

The author(s) have no potential conflicts of interest with respect to the research, authorship, and/or publication of this article.

REFERENCES

Aamodt SM and Constantine-Paton M (1999) The role of neural activity in synaptic development and its implications for adult brain function. Adv Neurol 79:133-144.

Abdelsalam, S, Uemura H, Umezaki Y, Saifullah ASM, Shimohigashi M, and Tomioka K (2008) Characterization of PDF-immunoreactive neurons in the optic lobe and cerebral lobe of the cricket, *Gryllus bimaculatus*. J Insect Physiol 54:1205-1212.

Barrett R and Page T (1989) Effects of light on circadian pacemaker development I: The freerunning period. J Comp Physiol A 165:41-49.

Barth M and Heisenberg M (1997) Vision affects mushroom bodies and central complex in *Drosophila melanogaster*. Learn Mem 4:219-229.

Barth M, Hirsch HVB, Meinertzhagen IA, and Heisenberg M (1997) Experience-dependent developmental plasticity in the optic lobe of *Drosophila melanogaster*. J Neurosci 17:1493-1504.

Deimel E and Kral K (1992) Long-term sensitivity adjustment of the compound eyes of the housefly *Musca domestica* during early adult life. J Insect Physiol 38:425-430.

Dircksen H, Zahnow CA, Gaus G, Keller R, Rao KR, and Riehm JP (1987) The ultrastructure of nerve endings containing pigment-dispersing hormone (PDH) in crustacean sinus glands: Identification by an antiserum against synthetic PDH. Cell Tissue Res 250:377-387.

Emerson KKJ, Bradshoaw WE, and Holzapfel CM (2009) Complications of complexity: Integrating environmental, genetic and hormonal control of insect diapause. Trends Genet 25:217-225.

Fernández MP, Berni J, and Ceriani MF (2008) Circadian remodeling of neuronal circuits involved in rhythmic behavior. PLoS Biol 6(3):e69.

Fleissner G, Loesel R, Fleissner G, Waterkamp M, Kleiner O, Batschauer A, and Homberg U (2001) Candidates for extraocular photoreceptors in the cockroach suggest homology to the lamina and lobula organs in beetles. J Comp Neurol 433:401-414.

Hamanaka Y, Tanaka S, Numata H, and Shiga S (2007) Peptide immunocytochemistry of neurons projecting to the retrocerebral complex in the blow fly, *Protophormia terraenovae*. Cell Tissue Res 329:581-593.

Hassaneen E, Sallam AE-D, Abo-Ghalia A, Moriyama Y, Karpova SG, Abdelsalam S, Matsushima A, Shimohigashi Y, and Tomioka K (2011) Pigment-dispersing factor affects nocturnal activity rhythms, photic entrainment, and the free-running period of the circadian clock in the cricket *Gryllus bimaculatus*. J Biol Rhythms 26:3-13.

Heisenberg M, Heusipp M, and Wanke T (1995) Structural plasticity in the *Drosophila* brain. J Neurosci 15:1951-1960.

Helfrich-Förster C (2009) Does the morning and evening oscillator model fit better for flies or mice? J Biol Rhythms 24:259-270.

Hirsch HVB, Barth M, Luo S, Sambaziotis H, Huber M, Possidente D, Ghiradella H, and Tompkins L (1995) Early visual experience affects mate choice in *Drosophila melanogaster*. Anim Behav 50:1211-1217.

Hofer S and Homberg U (2006a) Evidence for a role of orcokinin-related peptides in the circadian clock controlling locomotor activity of the cockroach *Leucophaea maderae*. J Exp Biol 209:2794-2803.

Hofer S and Homberg U (2006b) Orcokinin immunoreactivity in the accessory medulla of the cockroach *Leucophaea maderae*. Cell Tissue Res 325:589-600.

Kral K and Meinertzhagen I (1989) Anatomical plasticity of synapsis in the lamina of the optic lobe of the fly. Philos Trans R Soc Lond B 323:155-183.

Lee C-M, Su M-T, and Lee H-J (2009) Pigment dispersing factor: An output regulator of the circadian clock in the German cockroach. J Biol Rhythms 24:35-43.

Loesel R and Homberg U (2001) Anatomy and physiology of neurons with processes in the accessory medulla of the cockroach *Leucophaea maderae*. J Comp Neurol 439:193-207.

Mangerich S, Keller R, Dircksen H, Rat KR, and Riehm JP (1987) Immunocytochemical localization of pigment-dispersing hormone (PDH) and its coexistence with FMRFamide-immunoreactive material in the eyestalks of the decapod crustaceans *Carcinus maenas* and *Orconectes limosus*. Cell Tissue Res 250:365-375.

Nishiitsutsuji-Uwo J and Pittendrigh CS (1968) Central nervous system control of circadian rhythmicity in the cockroach: III. The optic lobes, locus of the driving oscillation? Z Vgl Physiol 58:14-46.

Page T and Barrett R (1989) Effects of light on circadian pacemaker development: II. Responses to light. J Comp Physiol A 165:51-59.

Parisky K, Agosto J, Pulver S, Shang Y, Kuklin E, Hodge J, Kang K, Liu X, Garrity P, Rosbash M, et al. (2008) PDF cells are a GABA-responsive wake-promoting component of the *Drosophila* sleep circuit. Neuron 60:672-682.

Park D and Griffith LC (2006) Electrophysiological and anatomical characterization of PDF-positive clock neurons in the intact adult *Drosophila* brain. J Neurophysiol 95:3955-3960.

Petri B, Homberg U, Loesel R, and Stengl M (2002) Evidence for a role of GABA and Mas-allatotropin in photic entrainment of the circadian clock of the cockroach *Leucophaea maderae*. J Exp Biol 205:1459-1469.

Petri B and Stengl M (1997) Pigment-dispersing hormone phase-shifts the circadian pacemaker of the cockroach *Leucophaea maderae*. J Neurosci 17:4087-4093.

Petri B, Stengl M, Würden S, and Homberg U (1995) Immunocytochemical characterization of the accessory medulla in the cockroach *Leucophaea maderae*. Cell Tissue Res 282:3-19.

Pittendrigh CS and Daan S (1976) A functional analysis of circadian pacemakers in nocturnal rodents: V. Pacemaker structure: a clock for all seasons. J Comp Physiol A Neuroethol Sens Neural Behav Physiol 106:333-355.

Reischig T and Stengl M (1996) Morphology and pigment-dispersing hormone (PDH)–immunocytochemistry of the accessory medulla, the presumptive circadian pacemaker of the cockroach *Leucophaea maderae*: a light- and electron-microscopical study. Cell Tissue Res 255:305-319.

Reischig T and Stengl M (2003a) Ectopic transplantation of the accessory medulla restores circadian locomotor rhythms in arrhythmic cockroaches (*Leucophaea maderae*). J Exp Biol 206:1877-1886.

Reischig T and Stengl M (2003b) Ultrastructure of pigment-dispersing hormone-immunoreactive neurons in a three-dimensional model of the accessory medulla of the cockroach *Leucophaea maderae*. Cell Tissue Res 314:421-435.

Reischig T and Stengl M (2004) Pigment-dispersing hormone (PDH)–immunoreactive neurons form direct coupling pathways between the bilateral symmetric circadian pacemakers of the cockroach *Leucophaea maderae*. Cell Tissue Res 318:553-564.

Roberts SK (1965) Photoreception and entrainment of cockroach activity rhythms. Science 148:958-959.

Roberts SK (1974) Circadian rhythms in cockroaches: Effects of optic lobe lesions. J Comp Physiol 88:21-30.

Schneider NL and Stengl M (2005) Pigment-dispersing factor and GABA synchronize cells of the isolated circadian clock of the cockroach *Leucophaea maderae*. J Neurosci 25:5138-5147.

Schneider NL and Stengl M (2007) Long-term recordings of the isolated circadian pacemaker center of the cockroach *Leucophaea maderae* reveals circadian and ultradian rhythms. J Comp Physiol A 193:35-42.

Shiga S and Numata H (2009) Roles of PER immunoreactive neurons in circadian rhythms and photoperiodism in the blow fly, *Protophormia terraenovae*. J Exp Biol 212:867-877.

Shiga S, Toyoda I, and Numata H (2003) Role of neurosecretory cells in the photoperiodic induction of pupal diapause of the tobacco hornworm *Manduca sexta*. J Comp Neurol 462:275-285.

Soehler S, Neupert S, Predel R, and Stengl M (2008) Examination of the role of FMRFamide-related peptides in the circadian clock of the cockroach *Leucophaea maderae*. Cell Tissue Res 332:257-269.

Soehler S, Stengl M, and Reischig T (2011) Circadian pacemaker coupling by multi-peptidergic neurons in the cockroach *Leucophaea maderae*. Cell Tissue Res 343:559-577.

Stengl M and Homberg U (1994) Pigment-dispersing hormone-immunoreactive neurons in the cockroach *Leucophaea maderae* share properties with circadian pacemaker neurons. J Comp Physiol A 175:203-213.

Sternberger LA (1979) *Immunocytochemistry*. New York: John Wiley.

Wei H, El Jundi B, Homberg U, and Stengl M (2010) Implementation of pigment-dispersing factor-immunoreactive neurons in a standardized atlas of the brain of the cockroach *Leucophaea maderae*. J Comp Neurol 518:4114-4133.

Chapter III

Ca^{2+}-dependent ion channels underlying spontaneous activity in insect circadian pacemaker neurons

Wei HY, and Stengl M. 2012.
This manuscript is published in Eur J Neurosci.
doi: 10.1111/j.1460-9568.2012.08227.x.

EJN fens EUROPEAN JOURNAL OF NEUROSCIENCE

doi:10.1111/j.1460-9568.2012.08227.x

Ca^{2+}-dependent ion channels underlying spontaneous activity in insect circadian pacemaker neurons

Hongying Wei and Monika Stengl
FB 10, Biology, Animal Physiology, University of Kassel, Heinrich Plett Str. 40, 34132 Kassel, Germany

Keywords: circadian pacemaker, gamma band oscillations, *Rhyparobia* (*Leucophaea) maderae*, spontaneous Ca^{2+} transients

Abstract

Electrical activity in the gamma frequency range is instrumental for temporal encoding on the millisecond scale in attentive vertebrate brains. Surprisingly, also circadian pacemaker neurons in the cockroach *Rhyparobia maderae* (*Leucophaea maderae*) employ fast spontaneous rhythmic activity in the gamma band frequency range (20–70 Hz) together with slow rhythmic activity. The ionic conductances controlling this fast spontaneous activity are still unknown. Here, Ca^{2+} imaging combined with pharmacology was employed to analyse ion channels underlying spontaneous activity in dispersed circadian pacemakers of the adult accessory medulla, which controls circadian locomotor activity rhythms. Fast spontaneous Ca^{2+} transients in circadian pacemakers accompany tetrodotoxin (TTX)-blockable spontaneous action potentials. In contrast to vertebrate pacemakers, the spontaneous depolarisations from rest appear to be rarely initiated via TTX-sensitive sustained Na^+ channels. Instead, they are predominantly driven by mibefradil-sensitive, low-voltage-activated Ca^{2+} channels and DK-AH269-sensitive hyperpolarisation-activated, cyclic nucleotide-gated cation channels. Rhythmic depolarisations activate voltage-gated Na^+ channels and nifedipine-sensitive high-voltage-activated Ca^{2+} channels. Together with Ca^{2+} rises, the depolarisations open repolarising small-conductance but not large-conductance Ca^{2+}-dependent K^+ channels. In contrast, we hypothesise that P/Q-type Ca^{2+} channels coupled to large-conductance Ca^{2+}-dependent K^+ channels are involved in input-dependent activity.

Introduction

Circadian pacemakers control the temporal order of physiological processes and behavior in organisms in synchrony with geophysical rhythms on earth. The circadian pacemaker center of the Madeira cockroach *Rhyparobia* (*Leucophaea) maderae* was the first circadian clock to be localised in a general brain region's neuronal circuit (Nishiitsutsuji-Uwo & Pittendrigh, 1968; Homberg *et al.*, 2003). The accessory medulla (aMe) with associated pigment-dispersing factor-immunoreactive neurons is the circadian clock that controls activity rhythms in the Madeira cockroach and the fruit fly *Drosophila melanogaster* via circadian release of pigment-dispersing factor and other neuropeptides (Stengl & Homberg, 1994; Helfrich-Forster, 1995; Park *et al.*, 2000; Homberg *et al.*, 2003; Reischig & Stengl, 2003a; Peschel & Helfrich-Forster, 2011). The large majority of aMe neurons are spontaneously active both *in vivo* and *in vitro*. In isolated aMae, they express both circadian and ultradian rhythms in their action potential (AP) activity (Schneider & Stengl, 2007). The ultradian rhythms are in the gamma band frequency range (20–70 Hz), as employed for temporal encoding in attentive vertebrate brains (Nadasdy, 2010). Also, in the vertebrate circadian pacemaker center, the suprachiasmatic nucleus (SCN), pacemaker neurons express not only slow circadian but also fast ultradian AP rhythms (Brown & Piggins, 2007; Maywood *et al.*, 2007; Colwell, 2011; Kononenko, 2011). Although it has been suggested by some studies that electrical membrane activity is coupled to circadian clock gene expression in the nucleus (Nitabach *et al.*, 2002, 2005; Lundkvist *et al.*, 2005; Harrisingh *et al.*, 2007; Sheeba *et al.*, 2008; Fogle *et al.*, 2011), the functional mechanisms of this interdependence are not understood and are still under debate (Depetris-Chauvin *et al.*, 2011). In addition, it is not known whether circadian clocks that time the phase of physiological processes on the 24-h circadian time scale also time outputs precisely on the ultradian scale of milliseconds, seconds, and minutes, as was suggested by preliminary experiments in the cockroach circadian clock (Schneider & Stengl, 2007).

Ca^{2+} imaging is a major optical tool used to investigate neuronal activity. Ca^{2+} signals accompany APs, owing to the voltage dependence of Ca^{2+}-permeable ion channels. Thus, rapid, high-amplitude Ca^{2+} signals can be interpreted to indicate spiking activity, whereas slow, low-amplitude Ca^{2+} concentration changes are coupled to subthreshold voltage events (Moreaux & Laurent, 2007, 2008). For further analysis of spontaneous membrane potential oscillation, here it was examined, with Ca^{2+}-imaging studies combined with pharmacology, which Ca^{2+}-dependent ion channels are responsible for spontaneous Ca^{2+} transients indicative of spiking activity of aMe neurons in primary cell culture. We focused on hyperpolarisation-activated, cyclic nucleotide-gated cation channels (HCNs), voltage-activated Ca^{2+} channels (VACCs), and Ca^{2+}-dependent K^+ channels (Hille, 2001). We found that mostly low-voltage-activated (LVA) VACCs, as well as HCNs, are pacemaker channels underlying pacemaking depolarisations. Spontaneous Ca^{2+} transients are triggered via tetro-

Correspondence: M. Stengl, as above.
E-mail: stengl@uni-kassel.de

Received 27 March 2012, revised 12 June 2012, accepted 20 June 2012

dotoxin (TTX)-sensitive Na^+-based APs and mediated via high-voltage-activated (HVA) VACCs coupled to small-conductance Ca^{2+}-dependent K^+ channels (SKs). In contrast, we hypothesise that P/Q-type VACCs coupled to large-conductance Ca^{2+}-dependent K^+ channels (BKs) are involved in stimulation-dependent activity.

Materials and methods

Primary cell culture

All experiments were performed on primary cell cultures of the aMe isolated from adult males of the cockroach *R. maderae (L. maderae)*, reared in laboratory colonies at 26 °C with 60% humidity. A cycle of 12 h of light/12 h of darkness was used to entrain the circadian system (lights on from 08:00 h to 20:00 h).

Primary cell cultures of the aMe were generated under sterile conditions by mechanical dissociation and enzymatic treatment, as previously described (Petri & Stengl, 1999). The cell suspension was plated on no. 1 glass coverslips (Thermo Scientific) coated with the cellular adhesive concanavalin A (Sigma). The cell cultures were maintained at 20 °C in a humidified incubator in constant darkness for approximately 24 h before Ca^{2+}-imaging experiments were carried out.

Ca^{2+} imaging

For loading of the Ca^{2+} indicator, 1 mg of Fura-2 acetoxymethyl ester (Fura-2 AM; Molecular Probes) was diluted in 1 mL of dimethylsulfoxide (Sigma). After vortexing, aliquots of 40 μL were stored at −20 °C. Before the loading, this stock solution was immediately diluted 250-fold in standard saline containing 156 mM NaCl, 4 mM KCl, 1 mM $CaCl_2$, 10 mM Hepes and 5 mM glucose (pH 7.1; osmolarity, 380 mOsm), and had a final concentration of 4 μM. The cells were loaded with 2 mL of loading solution for 40 min at 24–26 °C, and then transferred to a recording chamber on the stage of an Examiner D1 microscope (Zeiss, Germany) with a × 20 objective (W N-Achroplan, NA 1.0). Ca^{2+} imaging recordings (Till Photonics imaging system) were performed during continuous superfusion. Excitation wavelengths for Fura-2 fluorescence were 340 nm (exposure time, 15 ms) and 380 nm (exposure time, 10 ms) with 400-ms intervals (Polychrome 5000 monochromator; Till Photonics). Emission fluorescence (at 510 nm) was recorded with a CCD camera (Andor 885). The cell bodies were defined for the region of interest, in which the Fura-2 fluorescence intensities F^{340} and F^{380} were measured and their ratio was calculated with Till-Photonics software (TILLVISION 4.0). The background (between cells) was subtracted from each image before calculation of the ratio.

The intracellular Ca^{2+} concentration ($[Ca^{2+}]_i$) was calculated by use of the Grynkiewicz equation, which links the fluorescence ratios to the Ca^{2+} concentration (Grynkiewicz *et al.*, 1985):

$$[Ca^{2+}]_i = K_d(R - R_{min}/R_{max} - R)(F^{380}_{min}/F^{380}_{max})$$

R is the ratio of fluorescence intensity (F^{340}/F^{380}) measured during the experiment, and F_{min} and F_{max} are the fluorescence intensities in the absence of Ca^{2+} or in the presence of a saturating concentration of Ca^{2+}, respectively. $F^{380}_{min}, R_{min}(F^{340}_{min}/F^{380}_{min}), F^{380}_{max}$ and $R_{max}(F^{380}_{max}/\ F^{380}_{max})$were obtained after the experiments by incubation of the cells with standard saline solution containing 0 mM Ca^{2+}, 2 μM ionomycin (Sigma) and 5 mM EGTA, and 10 mM Ca^{2+} and 2 μM ionomycin, respectively. The dissociation constant for Fura-2 (K_d) under our experimental conditions was determined by using the calibration saline containing 2 μM ionomycin and 0.2, 1, 10, 30, 40 and 50 μM Ca^{2+}. The K_d of 2.66 μM was obtained by use of linear regression analyses in ORIGIN 6.0 (Microcal Software, Northampton, MA, USA).

The ion channel antagonists TTX (100 nM final concentration, blocks Na^+ channels in cockroach aMe neurons) (Schneider & Stengl, 2007), mibefradil (10 μM, blocks mostly LVA and, to a lesser extent, HVA Ca^{2+} channels in embryonic cockroach neurons) (Benquet *et al.*, 2000, 2002), nifedipine (20 μM, blocks L-type HVA Ca^{2+} channels in motor and embryonic neurons in the cockroach) (Mills & Pitman, 1997; Benquet *et al.*, 2002), ω-agatoxin IVA (50 nM, blocks P/Q-type HVA Ca^{2+} channels in cockroach dorsal unpaired median neurons) (Benquet *et al.*, 1999), iberiotoxin (100 nM, blocks BKs in cockroach dorsal unpaired median neurons) (Gautier *et al.*, 2008), nimodipine (10 μM, blocks L-type HVA Ca^{2+} channels; Cav1.3 in SCN neurons) (Cloues & Sather, 2003), DK-AH 269 (10 μM, blocks HCN channels in SCN neurons) (Atkinson *et al.*, 2011) and apamin (100 nM, blocks SKs in SCN neurons) (Cloues & Sather, 2003) were purchased from Sigma Aldrich and washed into the bath to replace the bath solution by use of 1-mL syringes. The concentrations of the antagonists were taken from the literature cited above. Responses to the antagonists or mixtures of blockers were analysed after 10 min of incubation at each drug concentration. For Na^+-free saline, NaCl was replaced with an equal concentration of choline chloride (Sigma).

Statistical analyses

Data are given as means ± standard errors of the mean. The amplitudes of the Ca^{2+} transients were calculated with software written in-house using C++ (Table 1). The Kolmogorov–Smirnov test was used for normality test. The amplitudes of Ca^{2+} transients in the same cells before and after blocker treatment were compared by use of the paired *t*-test. The statistical studies were performed with SPSS 19.0. For all cultures, only cells with spontaneous activity (with fast Ca^{2+} transients) were analysed (Table 1).

Results

As a first step towards the functional analysis of spontaneous gamma frequency membrane potential oscillation, Ca^{2+} currents underlying the spontaneous activity of neuropeptidergic insect circadian pacemaker cells were examined with Ca^{2+} imaging combined with pharmacology. The focus was on the analysis of pacemaker channels that affect baseline Ca^{2+} levels and of ion channels that underlie spontaneous Ca^{2+} transients in isolated, adult circadian pacemaker cells of the Madeira cockroach.

Cultured aMe cells generate spontaneous Ca^{2+} transients

It was reported previously that > 80% of all extracellular recordings of the isolated circadian pacemaker center of the Madeira cockroach show regular, fast AP activity together with slow circadian activity rhythms. The aMe neurons generate spontaneous AP rhythms in the gamma frequency range that are blocked by the Na^+-channel antagonist TTX (Schneider & Stengl, 2005, 2006, 2007). Here, it was examined with Ca^{2+} imaging combined with pharmacology which ion channels underlie spontaneous Ca^{2+} transients that might accompany TTX-blockable AP activity in isolated cockroach circadian pacemakers.

Spontaneous elevations in $[Ca^{2+}]_i$ were observed in primary cell cultures of adult male cockroach aMe cells loaded with Fura-2. These fluctuations in $[Ca^{2+}]_i$ occurred as either rapid Ca^{2+} transients in 26%

TABLE 1. Summary of dose-dependent effect of channel blockers on the amplitude of Ca^{2+} transients

Experimental condition	Amplitude of Ca^{2+} transients (nM)	Normality test [$P_{(K–S)}$]	n	P (paired t-test)			
				Groups compared	t	d.f.	P
TTX							
Control	182 ± 11	0.445	41	Control, 10 nM drug	3.543	40	0.001
10 nM	170 ± 11	0.502		10 nM, 100 nM drug	5.795	40	0.000
100 nM	97 ± 14	0.093		Control, 100 nM drug	6.097	40	0.000
DK-AH 269							
Control	170 ± 15	0.462	39	Control, 1 μM drug	2.139	38	0.039
1 μM	157 ± 14	0.514		1 μM, 10 μM drug	3.150	38	0.003
10 μM	132 ± 16	0.408		Control, 10 μM drug	3.225	38	0.003
Mibefradil							
Control	201 ± 13	0.163	37	Control, 1 μM drug	3.434	36	0.002
1 μM	182 ± 13	0.220		1 μM, 10 μM drug	7.864	36	0.000
10 μM	72 ± 10	0.065		Control, 10 μM drug	8.535	36	0.000
Nifedipine							
Control	197 ± 13	0.182	56	Control, 5 μM drug	2.469	55	0.017
5 μM	186 ± 12	0.080		5 μM, 20 μM drug	6.562	55	0.000
20 μM	115 ± 13	0.052		Control, 20 μM drug	6.288	55	0.000
ω-Agatoxin IVA							
Control	198 ± 15	0.444	29	Control, 10 nM drug	3.325	28	0.002
10 nM	176 ± 15	0.298		10 nM, 50 nM drug	5.566	28	0.000
50 nM	129 ± 12	0.937		Control, 50 nM drug	6.768	28	0.000
Apamin							
Control	193 ± 15	0.902	32	Control, 10 nM drug	3.147	31	0.004
10 nM	183 ± 15	0.526		10 nM, 100 nM drug	6.973	31	0.000
100 nM	138 ± 11	0.780		Control, 100 nM drug	8.918	31	0.000

The amplitudes of Ca^{2+} transients are given as means ± standard error of the mean. The Kolmogorov–Smirnov (K–S) test was used as the normality test. All $P_{(K–S)}$ values being > 0.05 showed that the data had a normal distribution. The amplitudes of Ca^{2+} transients in the same cells before and after blocker treatment were compared by use of the paired t-test. $P_{(paired\text{-}t)}$ (< 0.05) indicated a significant difference in the amplitude of Ca^{2+} transients between the control, the lower drug concentrations, and the higher drug concentrations, respectively. n, number of spontaneously active cells examined.

of the cultured cells or as slow Ca^{2+} waves in 36% of the cultured cells (n = 2666). The Ca^{2+} transients were defined as a rapid increase (within 10 s from baseline to peak) in $[Ca^{2+}]_i$ and a characteristic double exponential decay. Their amplitude ranged from 120 to 400% of baseline levels. In contrast, Ca^{2+} waves showed a slow gradual increase, requiring more than 40 s followed by a decay of several minutes. An aMe cell with one or more spontaneous Ca^{2+} transients was defined as spontaneously active.

Spontaneous Ca^{2+} transients are mediated by voltage-activated Na^+ channels (VASCs) and sodium ions are needed for maintaining resting $[Ca^{2+}]_i$

To determine whether spontaneous Ca^{2+} transients are related to the AP activity of circadian pacemaker neurons, the effect of the VASC blocker TTX was examined. Spontaneous Ca^{2+} transients were eliminated by TTX in a dose-dependent manner in all spontaneously active neurons (n = 80) (Fig. 1A–D; Table 1). Application of 10 nM TTX was capable of abolishing the Ca^{2+} transients, and decreased the amplitude and frequency of Ca^{2+} transients in 56% of the active aMe cells *in vitro* (n = 80). A higher concentration of TTX (50 nM) more reliably decreased the frequency and amplitude of the Ca^{2+} transients while still not affecting baseline $[Ca^{2+}]_i$ (73% of n = 80). Finally, at 100 nM TTX, Ca^{2+} transients were almost completely abolished in all tested active cells. However, 100 nM TTX did not affect the baseline $[Ca^{2+}]_i$ in 89% of the active cells with TTX-dependently blocked transients (71 of 80) (Fig. 1A). In a small minority (11%), the baseline Ca^{2+} concentrations were slightly reduced (data not shown). Subsequent application of the Ca^{2+}-channel antagonist mibefradil (10 μM) in the presence of 100 nM TTX decreased baseline $[Ca^{2+}]_i$ significantly in all experiments (n = 26) (Fig. 1B). These data suggest that the VASCs that underlie the fast upstroke of the APs trigger transient VACCs and thus elicit fast Ca^{2+} transients. In SCN neurons, a TTX-sensitive sustained, slowly inactivating Na^+ channel was suggested as a pacemaker channel that could regulate the pacemaker oscillations (Kononenko *et al.*, 2004). However, TTX-sensitive Na^+ channels do not contribute to baseline $[Ca_{2+}]_i$ in the large majority of spontaneously active cockroach aMe neurons. Thus, in circadian pacemakers of the Madeira cockroach a sustained Na^+ pacemaker channel does not play a predominant role in spontaneous subthreshold membrane potential oscillations.

To further examine the contribution of Na^+ to the generation of Ca^{2+} transients, Na^+ concentrations were changed in the extracellular saline, which usually contained 156 mM NaCl. Perfusion with Na^+-free saline rapidly induced a large $[Ca^{2+}]_i$ increase, indicating that Na^+ either blocks a Ca^{2+}-permeable ion channel or activates a hyperpolarising current. In 45% of the recorded cells, $[Ca^{2+}]_i$ transiently decreased shortly after the first Ca^{2+} increases (Fig. 1C), and then immediately reached a high steady state, accompanied by rapid Ca^{2+} oscillations (Fig. 1C; n = 165). This high $[Ca^{2+}]_i$ was reduced by

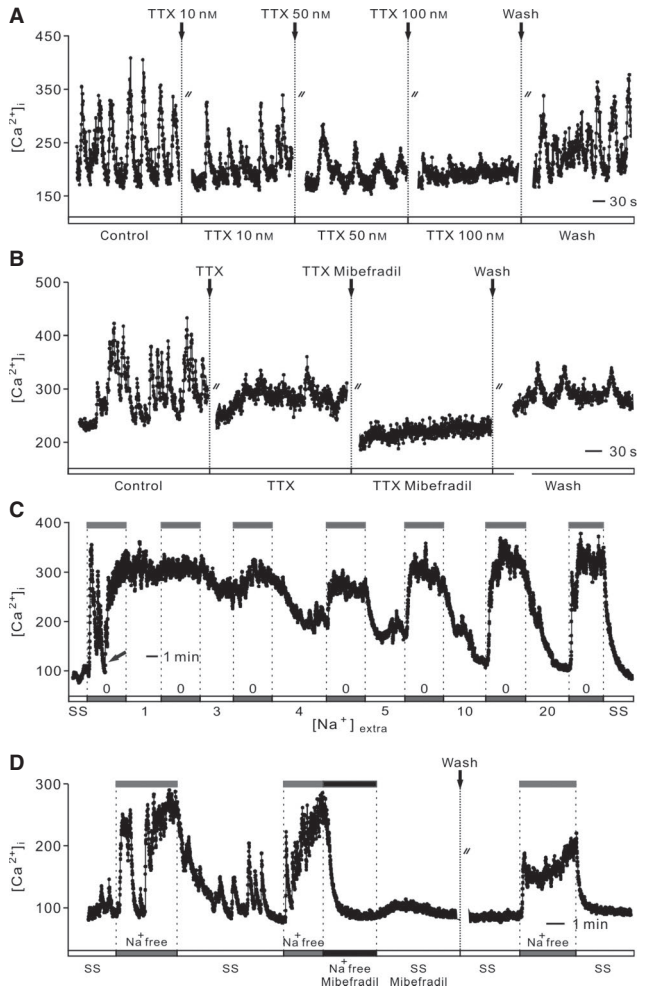

FIG. 1. Circadian pacemaker neurons of the aMe of the Madeira cockroach generate TTX-blockable spontaneous APs, which generate fast Ca^{2+} transients. VASCs do not contribute to baseline Ca^{2+} levels, but sodium ions affect Ca^{2+}-permeable ion channels. (A) Primary cell cultures of aMe neurons generate TTX-blockable fast Ca^{2+} transients. In Fura-2 Ca^{2+}-imaging experiments, perfusion with standard saline (SS) (with 1 mM Ca^{2+}) containing TTX (10 nM, 50 nM, and 100 nM; 10 min of preincubation) reduced the frequency and amplitude of spontaneous Ca^{2+} transients in a dose-dependent manner (n = 80). Baseline $[Ca_{2+}]_i$ was not affected by TTX at all concentrations tested in 89% of the recordings (n = 80). In these cells, no TTX-dependent slowly inactivating pacemaker Na^+ current was present. However, additional application of 10 μM mibefradil in SS containing 100 nM TTX always decreased baseline $[Ca_{2+}]_i$ (n = 26). (B) The effect of antagonists was partially reversible after a 10-min washout. (C) The replacement of external sodium ions with choline caused a large increase in $[Ca^{2+}]_i$ with rapid Ca^{2+} oscillations (grey rectangles). Some cells showed a transient decrease shortly after the first Ca^{2+} increase (arrow). High $[Ca_{2+}]_i$ were reduced after perfusion of saline containing sodium ions in a concentration-dependent manner. (D) The effects of Na^+ removal were abolished by10 μM mibefradil Black rectangles: Na^+ free+mibefradil.

perfusion of Na^+-containing saline in a concentration-dependent manner. Saline containing 3 mM Na^+ was able to only slightly inhibit the high $[Ca^{2+}]_i$ caused by Na^+-free saline. The $[Ca^{2+}]_i$ returned to its normal resting value after bath application of saline containing 10 mM Na^+ (Fig. 1C). The effects of Na^+ removal were completely blocked by application of the Ca^{2+} channel blocker mibefradil (10 μM) in Na^+-free saline (Fig. 1D; n = 21), indicating that sodium ions modulate VACCs rather than a hyperpolarising anionic current. These results demonstrate that at least a small number of sodium ions are needed for the maintenance of resting $[Ca^{2+}]_i$, but very likely not via a non-inactivating TTX-sensitive Na^+ pacemaker current.

Baseline $[Ca_{2+}]_i$ and spontaneous Ca^{2+} transients are mediated by VACCs and HCN pacemaker channels

Next, we searched for pacemaker channels that activate at rest and affect baseline Ca^{2+} levels. In addition, we examined whether these pacemaker channels might cause strong enough depolarisations to activate VACCs underlying Ca^{2+} transients. The most likely candidates for pacemaker channels are HCN ion channels and LVA-type VACCs. Pharmacological block with the reversible HCN channel antagonist DK-AH269 (10 μM) (Atkinson *et al.*, 2011) decreased baseline $[Ca_{2+}]_i$ and suppressed spontaneous Ca^{2+} transients in 64% of all active adult pacemaker neurons *in vitro* (n = 39) (Fig. 2A; Table 1). Mibefradil, which blocks mostly LVA-type VACCs but also, to a lesser extent, HVA-type VACCs (Benquet *et al.*, 2000, 2002), was employed. In 96% of the aMe cells (n = 57), addition of mibefradil (10 μM) reduced baseline $[Ca^{2+}]_i$ and also inhibited spontaneous Ca^{2+} transients (Fig. 2B; Table 1). Thus, most or all active aMe neurons contain LVA VACCs. After blocking of HVA L-type Ca^{2+} channels with nifedipine (20 μM) (Mills & Pitman, 1997; Benquet *et al.*, 2002) spontaneous Ca^{2+} transients disappeared in approximately 50% (n = 105) of all recorded cells (Fig. 2C; Table 1). However, the baseline Ca^{2+} level was not affected significantly in 88% of nifedipine-sensitive cells. Nimodipine (1 μM and 10 μM), another L-type Ca^{2+} channel (Cav1.3) blocker (Cloues & Sather, 2003), did not significantly affect the spontaneous Ca^{2+} transients of the active cells (n = 26, data not shown). In contrast, the antagonist of HVA P/Q-type VACCs ω-agatoxin IVA (50 nM) (Benquet *et al.*, 1999) increased the frequency of Ca^{2+} transients and increased the baseline Ca^{2+} concentration in approximately 64% of cultured aMe cells (n = 33) (Fig. 2D).

Spontaneous Ca^{2+} transients are mediated by SKs, but not by BKs

Next, the contribution of SKs or BKs to the generation of spontaneous Ca^{2+} transients was examined. In approximately 93% of all active pacemaker neurons (n = 41), inhibition of SKs by 100 nM apamin (Cloues & Sather, 2003) increased baseline $[Ca_{2+}]_i$ (Fig. 3A). This was accompanied by an increase in the frequency and a decrease in the amplitude of spontaneous Ca^{2+} transients (Fig. 3A; Table 1). Thus, SKs were necessary for restraining the activity of aMe neurons. Iberiotoxin (100 nM)-dependent (Gautier *et al.*, 2008) block of BKs did not significantly affect the patterns of spontaneous Ca^{2+} transients in all active cells recorded (n = 31; Fig. 3B). However, in all inactive cells, iberiotoxin (100 nM) induced Ca^{2+} transients and elevation of baseline $[Ca_{2+}]_i$ (n = 26; Fig. 3C). This indicated that BKs did not underlie spontaneous Ca^{2+} transients, and that opening of BKs abolished spontaneous Ca^{2+} transients via potent hyperpolarisations.

P/Q-type VACCs appear to couple to BKs

Changes in the extracelluar Ca^{2+} concentration were combined with pharmacology to determine whether specific VACCs couple to SKs or BKs. Increasing the extracellular Ca^{2+} concentration from 1 μM to 1 mM increased baseline $[Ca^{2+}]_i$ via increased influx of Ca^{2+}. This increase in extracellular Ca^{2+} concentrations resulted in an increase in the frequency of Ca^{2+} transients in 41% of the cells and a decrease in 15% (n = 116) (Fig. 4A). In the remaining 44% of active cells, the

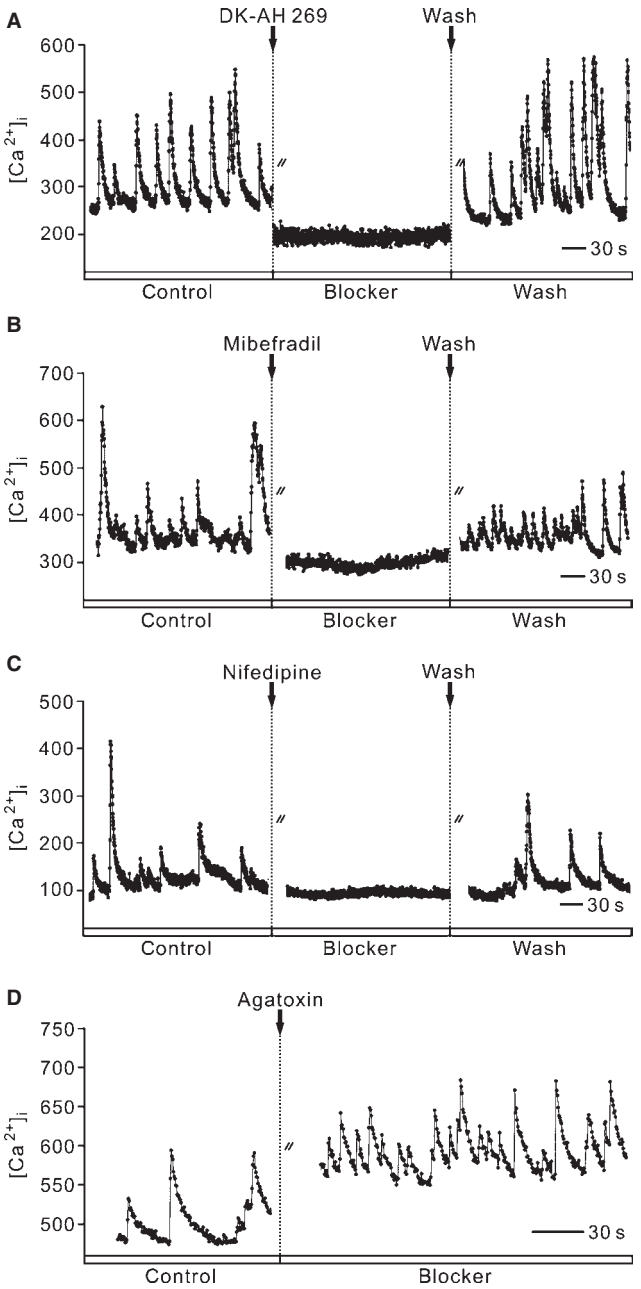

FIG. 2. HCN channels and VACCs contribute to spontaneous Ca^{2+} transients. After a 10-min incubation of the HCN channel antagonist DK-AH 269 (10 μM) (A), spontaneous Ca^{2+} transients were reversibly blocked and baseline $[Ca_{2+}]_i$ were reduced in 64% of all aMe cells *in vitro* (n = 39). After a 10-min incubation with the general VACC antagonist mibefradil (10 μM) (B), spontaneous Ca^{2+} transients were reversibly blocked in 96% of all aMe neurons (n = 57). Furthermore, baseline $[Ca_{2+}]_i$ were always reduced. After a 10-min incubation with the L-type VACC antagonist nifedipine (20 μM) (C), spontaneous Ca^{2+} transients were inhibited, but baseline $[Ca^{2+}]_i$ was not reduced, in 50% of all aMe cells examined (n = 105). A 15-min washout of the antagonists with standard saline (containing 1 mM Ca^{2+}) resulted in partial recovery of the spontaneous Ca^{2+} transients (A–C). In contrast, the P/Q-type VACC antagonist ω-agatoxin IVA (50 nM) (10 min of preincubation) caused increases in the frequency of Ca^{2+} transients and baseline $[Ca^{2+}]_i$ in 64% of all aMe cells examined (n = 33) (D). Continuous records are shown, with interruptions of 10 min.

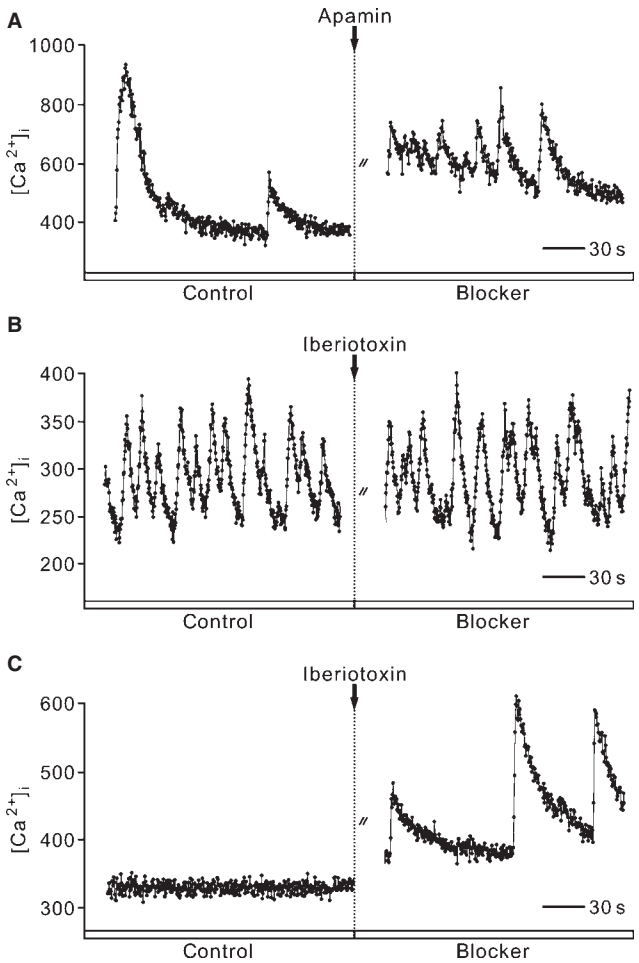

FIG. 3. Spontaneous Ca^{2+} transients are modulated by SKs, but not by BKs. The SK antagonist apamin (100 nM in standard saline with 1 mM Ca^{2+}, 10 min of preincubation, n = 41) increased the frequency of Ca^{2+} transients and the baseline $[Ca_{2+}]_i$ in 93% of all active cells (A). Application of 100 nM iberiotoxin (10 min of incubation, n = 31), the BK antagonist never affected spontaneous Ca^{2+} transients or baseline Ca^{2+} levels in active cells (B). However, in inactive cells, iberiotoxin always induced Ca^{2+} transients and increases in baseline $[Ca_{2+}]_i$ in all cells tested (n = 26).

frequency of Ca^{2+} transients did not change. When the SK antagonist apamin (100 nM) was added to saline containing 1 μM extracellular Ca^{2+}, baseline $[Ca^{2+}]_i$ and the superimposed oscillation frequency strongly increased in almost all cells (Fig. 4B). In the presence of apamin, increasing the extracellular Ca^{2+} concentration from 1 μM to 1 mM silenced the cells, and baseline $[Ca^{2+}]_i$ decreased (Fig. 4B) in approximately 76% of the cells (n = 86). This silencing of activity resulted from the opening of BKs, because it could be eliminated by additional treatment with 100 nM iberiotoxin (Fig. 4B). These experiments demonstrated that, in the continuous presence of 100 nM apamin, the increase in extracellular Ca^{2+} concentration from 1 μM to 1 mM caused the opening of BKs. This protocol was combined with subsequent addition of 20 μM nifedipine or 50 nM ω-agatoxin IVA. This should determine whether BKs couple to specific VACCs. The L-type VACC antagonist nifedipine was ineffective, and did not mimic the effects of 100 nM iberiotoxin (n = 16) (Fig. 4C). Thus, L-type VACCs did not couple to BKs. In contrast, in approximately 28% of tested cells (n = 36), subsequent application of ω-agatoxin IVA activated the cells and increased baseline $[Ca^{2+}]_i$, suggesting that BKs failed to open. The combination of ω-agatoxin IVA and iberiotoxin resulted in a further increase in the amplitude of Ca^{2+} transients (Fig. 4D). These results provide evidence for at least partially selective coupling of BKs to P/Q-type VACCs.

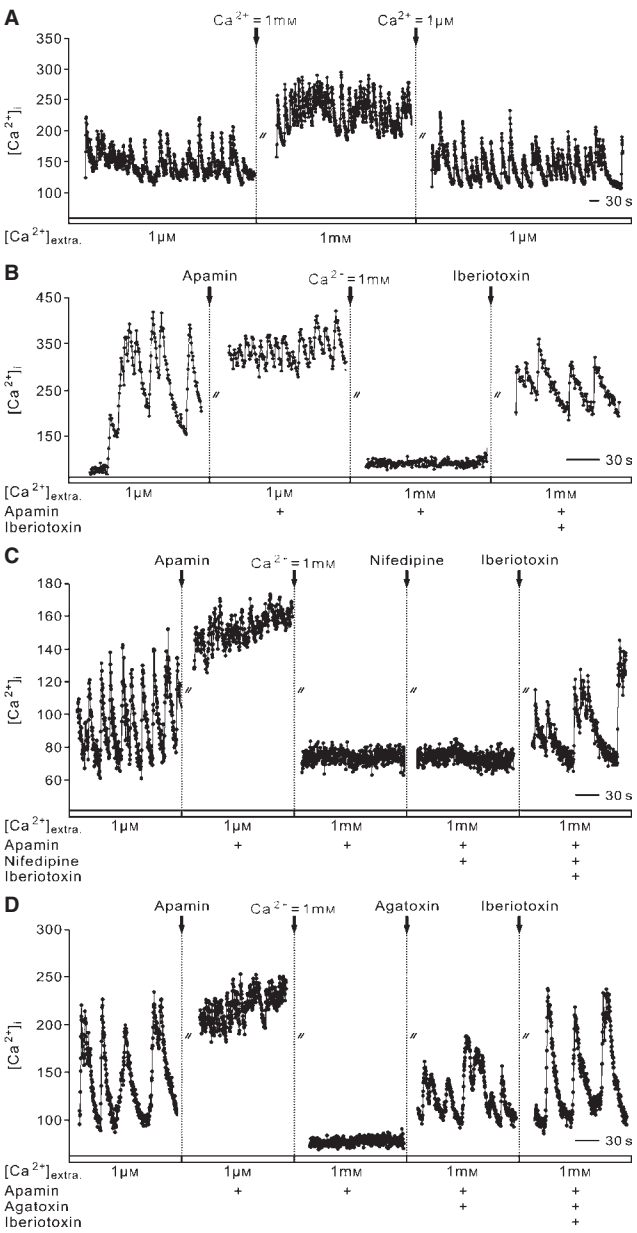

FIG. 4. P/Q-type but not L-type VACCs couple to BKs. Increasing the external Ca^{2+} concentration from 1 μM to 1 mM elevated the $[Ca_{2+}]_i$ (41%, $n = 116$) (A). After application of the SK antagonist apamin (100 nM), an increase in the external Ca^{2+} concentration silenced the cells and decreased baseline $[Ca^{2+}]_i$ (76%, $n = 86$). Additional application of the BK antagonist iberiotoxin (100 nM) induced Ca^{2+} transients (B). The L-type VACC antagonist nifedipine (20 μM) could not activate silenced cells in increased external Ca^{2+} concentrations in the presence of 100 nM apamin ($n = 16$). In contrast, activation occured after additional treatment with 100 nM iberiotoxin (28%, $n = 36$) (C). The P/Q-type VACC antagonist ω-agatoxin IVA (50 nM) activated silenced cells, similarly to iberiotoxin application. However, iberiotoxin-induced Ca^{2+} transients showed higher amplitudes (D).

Discussion

Pacemaker neurons of the insect circadian pacemaker center, the aMe in the brain's optic lobes, express spontaneous activity not only on a circadian time scale of 24 h but also in the gamma frequency range of 20–70 Hz (Schneider & Stengl, 2005, 2006, 2007). These spontaneous gamma band oscillations are a prerequisite for temporal encoding of fast (millisecond scale) information changes in the attentive vertebrate brain (Singer & Gray, 1995; Nadasdy, 2010; Hong *et al.*, 2012). Thus, we predicted that insect circadian pacemakers not only time 24-h physiological rhythms, but also employ temporal encoding in the millisecond time range (Schneider & Stengl, 2005, 2006, 2007). As a first step towards testing this hypothesis with Ca^{2+} imaging combined with pharmacology, we examined Ca^{2+}-dependent ion channels underlying fast spontaneous activity in aMe neurons of the Madeira cockroach, an established circadian pacemaker model system. Previously, Schneider & Stengl (2007) have shown that the inward Na^+ current of the cockroach aMe neurons is very sensitive to TTX. Previous studies indicated that Ca^{2+} channels and BKs in cockroach neuronal cells are sensitive to mibefradil (Benquet *et al.*, 2000, 2002), nifedipine (Mills & Pitman, 1997; Benquet *et al.*, 2002), ω-agatoxin IVA (Benquet *et al.*, 1999), and iberiotoxin (Gautier *et al.*, 2008). Although the HCN channel and SK genes have been identified in insects, to our knowledge no thorough pharmacological characterisations of DK-AH 269 and of apamin have been described in insects so far (Krieger *et al.*, 1999; Marx *et al.*, 1999; Littleton & Ganetzky, 2000; Gisselmann *et al.*, 2003). Therefore, and because the genome of the Madeira cockroach has not yet been characterised, we cannot exclude the possibility that the antagonists employed affected more than one class of ion channel. Nevertheless, all of the antagonists employed influenced Ca^{2+} transients of the Madeira cockroach aMe neurons in a dose-dependent manner (for details, see Table 1).

The TTX-sensitive spontaneous Ca^{2+} transients of active circadian pacemaker neurons correlate with TTX-sensitive spontaneous spiking activity. Evidence has been provided that LVA VACCs and HCN cation channels coupled to SKs are the predominant channels underlying fast Ca^{2+} transients. In contrast, we hypothesise that P/Q-type VACCs are activated only during input-dependent depolarisations. The P/Q-type VACCs couple to BKs, which appear to override pacemaker channels and promote rebound transient inhibition of spontaneous activity.

Ion channels employed for the control of spontaneous activity

This study concentrated on the analysis of pacemaker channels involved in the generation of subthreshold membrane potential oscillations affecting baseline Ca^{2+} levels. In addition, the Ca^{2+}-permeable ion channels that accompany APs were examined in insect circadian pacemaker neurons. In the Madeira cockroach, the LVA VACCs, HCN channels, and, in fewer cases, sustained, slow inactivating Na^+ pacemaker channels (not shown) open at hyperpolarised resting potentials (Fig. 5). They provide an influx of Ca^{2+}, Na^+, and K^+. They drive the resting potential to spike threshold, and they elicit Na^+-dependent APs. The rapidly rising potential during the upstroke of the Na^+ spikes then activates L-type HVA VACCs. In addition, the rising intracellular Na^+ concentration appears to close mibefradil-sensitive LVA VACCs, counteracting further influx of Ca^{2+}. Furthermore, the increased $[Ca^{2+}]_i$ and the rapid depolarisation activate SKs as well as other voltage-dependent K^+ channels (not shown), which repolarise the cell back to resting potentials (Fig. 5). Finally, pumps return intracellular Ca^{2+} and Na^+ concentrations back to baseline. Then, the opening of the pacemaker channels starts a new oscillation cycle in intracellular voltage and Ca^{2+}, K^+ and Na^+ concentrations. Cycles of intracellular anions were not taken into consideration in this study, and await further investigation.

Thus, in the Madeira cockroach, apparently all circadian pacemaker neurons express LVA VACCs and at least 60% coexpress HCN pacemaker channels mediating spontaneous depolarisations and Ca^{2+} influx at rest. In contrast to vertebrate circadian pacemaker neurons in the SCN, the large majority of Madeira cockroach pacemaker cells do

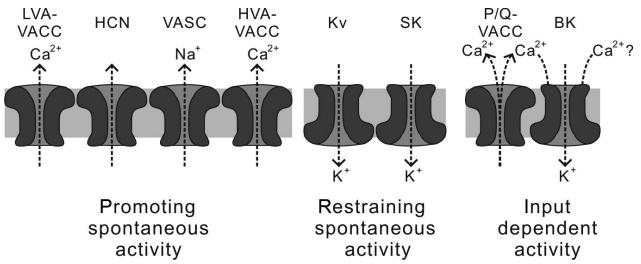

FIG. 5. Ion channels proposed to control the activity of circadian pacemaker neurons in the Madeira cockroach. LVA VACCs and HCN channels appear to be the predominant pacemaker channels promoting spontaneous Ca^{2+} transients. The spontaneous depolarisation could activate VASCs and HVA VACCs, with accompanying spontaneous APs. In contrast, voltage-gated (Kv) and SKs are necessary for restraining spontaneous excitability of the neurons. BKs appear to be selectively coupled to P/Q-type VACCs, and are hypothesised to be involved in input-dependent activity.

not employ sustained, slow inactivating TTX-sensitive Na^+ channels as pacemaker channels, as TTX did not decrease baseline Ca^{2+} levels (Jackson *et al.*, 2004; Kononenko *et al.*, 2004, 2008; Colwell, 2011; Kononenko, 2011). Whether LVA VACCs and HCN channels only elicit subthreshold membrane potential oscillations via coupling to K^+ channels or whether they also drive spontaneous APs without involvement of HVA VACCs cannot be resolved, as mibefradil also affects HVA VACCs to some extent (Benquet *et al.*, 2000). However, as there are also several L-type Ca^{2+} channels known in the vertebrate circadian clock that can act as pacemaker channels driving spontaneous AP rhythms, it is likely that different HVA VACCs also underlie spontaneous activity in the Madeira cockroach (reviews: Brown & Piggins, 2007; Kononenko, 2011; Colwell, 2011; Tuckwell, 2012). In contrast to reports in SCN neurons, the spontaneous Ca^{2+} transients in the Madeira cockroach are nifedipine-sensitive and are not affected by nimodipine (review: Kononenko, 2011). However, as increasing TTX concentrations blocked spontaneous Ca^{2+} transients in the Madeira cockroach clock cells, AP upstrokes activate further HVA VACCs coupled to SK channels. The voltage-dependent BKs require much stronger increases in the $[Ca_{2+}]_i$ than SKs (Hille, 2001), which appear not to occur during spontaneous activity in the absence of inputs. As was suggested here, BK opening appears to be coupled to stimulus-dependent gated P/Q-type HVA VACCs. Then, the BK opening suppresses spontaneous activity. This hypothesis and our data are consistent with the finding that blockers of P/Q-type VACCs elevated spontaneous activity. Also in vertebrates, P/Q-type VACCs are typically synaptic ion channels (Tuckwell, 2012). Interestingly, in circadian pacemakers of the Madeira cockroach, extracellular sodium ions appear to block Ca^{2+}-permeable cation channels, and therefore also affect baseline $[Ca_{2+}]_i$ and spontaneous activity. Balke & Wier (1992) showed that removal of external Na^+ could induce the phosphorylation of L-type Ca^{2+} channels and thereby increase the baseline $[Ca_{2+}]_i$ concentration. The ion channel type that accounts for the high Ca^{2+} baseline level and high-frequency Ca^{2+} oscillation in the Na^+-free saline, and its functional significance, remain to be elucidated. In addition, future studies will examine which role non-specific cation channels and different types of K^+ channel play in the generation of spontaneous activity in Madeira cockroach circadian pacemaker neurons.

Spontaneous activity and temporal encoding

There is an ongoing debate about what role temporal encoding plays in the brains of both humans and animals, and how single neuron firing properties allow for different encoding schemes (Hong *et al.*, 2012). Frequency encoding (rate encoding) implies that the AP frequency of a neuron encodes information on the quantity and time course of an external stimulus, whereas encoding of stimulus quality depends on the specific type of neuron (e.g. an olfactory receptor neuron expressing a specific type of odor receptor). For temporal encoding, the overall frequency of the AP response is not relevant; what counts is the timing, i.e. the phase of the first stimulus-dependent AP in relation to other APs elicited by other neurons in the brain (Nadasdy, 2010). Thus, a spontaneously active neuron that expresses subthreshold membrane potential oscillations acts as a temporal filter. It is sensitive to the time course of its input (e.g. to excitatory postsynaptic potentials). If input-dependent depolarisations occur at the same time (i.e. the same phase) as endogenous depolarisations, both depolarisations add up and the neuron reaches AP threshold and fires a spike. However, if excitatory postsynaptic potentials are not phase-synchronous with endogenous depolarisations, no AP response is elicited. In the present study, we clearly showed that the cockroach aMe neurons generate TTX-sensitive spontaneous Ca^{2+} transients in the absence of synaptic input, and can therefore be considered to be endogenously active neurons that act as temporal filters on the millisecond time scale. The spontaneous gamma band oscillations allow timing of outputs on the millisecond time scale in vertebrate and invertebrate brains alike. They are a prerequisite for temporal encoding, apparently also in the circadian system. Importantly, information is encoded not only in a single neuron, but also in an ensemble of phase-coupled neurons that spike synchronously, as was measured in electroencephalograms of the human cortex (Singer & Gray, 1995). Also in the aMe of the Madeira cockroach, synchronous oscillations in the gamma frequency range can be recorded (Schneider & Stengl, 2005). It remains to be determined what the significance is of temporal encoding on the millisecond time scale for circadian pacemaker neurons in vertebrates and invertebrates.

Gamma band spontaneous activity and circadian timing

Circadian pacemaker neurons change their spontaneous AP activity with periods of 24 h to time circadian outputs via neuropeptide release and, at the same time, express gamma band spontaneous activity (Schneider & Stengl, 2005). Not only circadian pacemaker neurons of the Madeira cockroach but also vertebrate circadian pacemakers of the SCN express spontaneous activity in the gamma frequency range (Colwell, 2011; Kononenko, 2011). Thus, this seems to be a widespread property of circadian pacemaker neurons with unknown relevance. Another characteristic of pacemaker cells of the Madeira cockroach, as well as SCN circadian pacemaker neurons, is their abundance of partly colocalised neuropeptides (Petri *et al.*, 1995; Reischig & Stengl, 1996, 2003b, 2004; Maywood *et al.*, 2007; Soehler *et al.*, 2007, 2008, 2011; Colwell, 2011; Schulze *et al.*, 2012). In the aMe of the Madeira cockroach, neuropeptidergic circadian pacemakers form ensembles of phase-coupled synchronously spiking neurons (Schneider & Stengl, 2005). As application of the neuropeptide pigment-dispersing factor triggered a transient peptide-dependent ensemble of synchronously spiking cells, it is assumed that a specific peptide-dependent ensemble gates a specific output of the circadian clock (Schneider & Stengl, 2005). The observation of gamma band oscillations of synchronous ensembles suggests that circadian control of neuropeptide release gates circadian clock outputs with a precision in the millisecond time range, as employed in other brain areas. Therefore, we hypothesise that the circadian clock has a ‘short hand’ and a ‘long hand’ to employ temporal encoding in the millisecond,

minute and hour time ranges. Preliminary recordings are consistent with this hypothesis (Schneider & Stengl, 2007). In future behavioral and physiological experiments, we will test our hypothesis by employing VACC antagonists to interfere with subthreshold membrane potential oscillations without blocking stimulus-dependent AP activity in circadian clock cells. As recent studies have shown that adult-specific electrical silencing of pacemaker neurons in the fruit fly obliterates circadian outputs but maintains circadian cycling of clock gene expression in the nucleus, it was concluded that AP activity does not feed back into the nuclear clockwork (Depetris-Chauvin *et al.*, 2011). However, in future studies, it still remains to be examined whether subthreshold oscillations in the Ca^{2+} concentration based on VACCs couple to nuclear clock oscillations coupled to changes in intracellular second messenger levels.

Acknowledgements

We are grateful to Dr Wolfgang W. Schwippert for critical reading of the manuscript. We thank Christa Uthof for expert technical assistance with primary cell cultures and Gisela Kaschlaw for animal maintenance.

Abbreviations

aMe, accessory medulla; AP, action potential; BK, large-conductance Ca^{2+}-dependent K^+ channel; $[Ca^{2+}]_i$, intracellular Ca^{2+} concentration; Fura-2 AM, Fura-2 acetoxymethyl ester; HCN, hyperpolarisation-activated, cyclic nucleotide-gated; HVA, high-voltage-activated; LVA, low-voltage-activated; SCN, suprachiasmatic nucleus; SK, small-conductance Ca^{2+}-dependent K^+ channel; SS, standard saline; TTX, tetrodotoxin; VACC, voltage-activated Ca^{2+} channel; VASC, voltage-activated Na^+ channel.

References

Atkinson, S.E., Maywood, E.S., Chesham, J.E., Wozny, C., Colwell, C.S., Hastings, M.H. & Williams, S.R. (2011) Cyclic AMP signaling control of action potential firing rate and molecular circadian pacemaking in the suprachiasmatic nucleus. *J. Biol. Rhythms*, **26**, 210–220.

Balke, C.W. & Wier, W.G. (1992) Modulation of L-type calcium channels by sodium ions. *Proc. Natl. Acad. Sci. USA*, **89**, 4417–4421.

Benquet, P., Guen, J.L., Dayanithi, G., Pichon, Y. & Tiaho, F. (1999) ω-agatoxin IVA -sensitive (P/Q-type) and -resistant (R-type) high-voltage activated Ba^{2+} currents in embryonic cockroach brain neurons. *J. Neurophysiol.*, **82**, 2284–2293.

Benquet, P., Frere, S., Pichon, Y. & Tiaho, F. (2000) Properties and development of calcium currents in embryonic cockroach neurons. *Neurosci. Lett.*, **294**, 49–52.

Benquet, P., Guen, J.L., Pichon, Y. & Tiaho, F. (2002) Differential involvement of Ca^{2+} channels in survival and neurite outgrowth of cultured embryonic cockroach brain neurons. *J. Neurophysiol.*, **88**, 1475–1490.

Brown, T.M. & Piggins, H.D. (2007) Electrophysiology of the suprachiasmatic circadian clock. *Prog. Neurobiol.*, **82**, 229–255.

Cloues, R.K. & Sather, W.A. (2003) Afterhyperpolarization regulates firing rate in neurons of the suprachiasmatic nucleus. *J. Neurosci.*, **23**, 1593–1604.

Colwell, C.S. (2011) Linking neural activity and molecular oscillations in the SCN. *Nat. Rev. Neurosci.*, **12**, 553–569.

Depetris-Chauvin, A., Berni, J., Aranovich, E.J., Muraro, N.I., Beckwith, E.J. & Ceriani, M.F. (2011) Adult-specific electrical silencing of pacemaker neurons uncouples molecular clock from circadian outputs. *Curr. Biol.*, **21**, 1783–1793.

Fogle, K.J., Parson, K.G., Dahm, N.A. & Holmes, T.C. (2011) Cryptochrome is a blue-light sensor that regulates neuronal firing rate. *Science*, **331**, 1409–1413.

Gautier, H., Auger, J., Legros, C. & Lapied, B. (2008) Calcium-activated potassium channels in insect pacemaker neurons as unexpected target site for the novel fumigant dimethyl disulfide. *J. Pharmacol. Exp. Ther.*, **324**, 149–159.

Gisselmann, G., Warnstedt, M., Gamerschlag, B., Bormann, A., Marx, T., Neuhaus, E.M., Stoertkuhl, K., Wetzel, C.H. & Hatt, H. (2003) Characterization of recombinant and native *I*h-channels from *Apis mellifera*. *Insect Biochem. Mol. Biol.*, **33**, 1123–1134.

Grynkiewicz, G., Poenie, M. & Tsien, R.Y. (1985) A new generation of Ca^{2+} indicators with greatly improved fluorescence properties. *J. Biol. Chem.*, **260**, 3440–3450.

Harrisingh, M.C., Wu, Y., Lnenicka, G.A. & Nitabach, M.N. (2007) Intracellular Ca^{2+} regulates free-running circadian clock oscillation *in vivo*. *J. Neurosci.*, **27**, 12489–12499.

Helfrich-Forster, C. (1995) The period clock gene is expressed in central nervous system neurons which also produce a neuropeptide that reveals the projections of circadian pacemaker cells within the brain of *Drosophila melanogaster*. *Proc. Natl. Acad. Sci. USA*, **92**, 612–616.

Hille, B. (2001) *Ion Channels of Excitable Membranes*, 3rd Edn. Sinauer Associates, Sunderland, MA, USA.

Homberg, U., Reischig, T. & Stengl, M. (2003) Neural organization of the circadian system of the cockroach *Leucophaea maderae*. *Chronobiol. Int.*, **20**, 577–590.

Hong, S., Ratte, S., Prescott, S.A. & De Schutter, E. (2012) Single neuron firing properties impact correlation-based population coding. *J. Neurosci.*, **32**, 1413–1428.

Jackson, A.C., Yao, G.L. & Bean, B.P. (2004) Mechanism of spontaneous firing in dorsomedial suprachiasmatic nucleus neurons. *J. Neurosci.*, **24**, 7985–7998.

Kononenko, N.I. (2011) Searching membrane target for mammalian circadian clock responsible for circadian modulation of firing rate. In Golvkin, L. & Maliszkewicz, A. (Eds), *Circadian Rhythms: Biology, Cognition and Disorders*. Nova Science Publishers, NY, pp. 29–56.

Kononenko, N.I., Shao, L.R. & Dudek, F.E. (2004) Riluzole-sensitive slowly inactivating sodium current in rat suprachiasmatic nucleus neurons. *J. Neurophysiol.*, **91**, 710–718.

Kononenko, N.I., Honma, S., Dudek, F.E. & Honma, K. (2008) On the role of calcium and potassium currents in circadian modulation of firing rate in rat suprachiasmatic nucleus neurons: multielectrode dish analysis. *Neurosci. Res.*, **62**, 51–57.

Krieger, J., Strobel, J., Vogl, A., Hanke, W. & Breer, H. (1999) Identification of a cyclic nucleotide- and voltage-activated ion channel from insect antennae. *Insect Biochem. Mol. Biol.*, **29**, 255–267.

Littleton, J.T. & Ganetzky, B. (2000) Ion channels and synaptic organization: analysis of the *Drosophila* genome. *Neuron*, **26**, 35–43.

Lundkvist, G.B., Kwak, Y., Davis, E.K., Tei, H. & Block, G.D. (2005) A calcium flux is required for circadian rhythm generation in mammalian pacemaker neurons. *J. Neurosci.*, **25**, 7682–7686.

Marx, T., Gisselmann, G., Stortkuhl, K.F., Hovemann, B.T. & Hatt, H. (1999) Molecular cloning of a putative voltage- and cyclic nucleotide-gated ion channel present in the antennae and eyes of *Drosophila melanogaster*. *Invert. Neurosci.*, **4**, 55–63.

Maywood, E.S., O'Neill, J.S., Chesham, J.E. & Hastings, M.H. (2007) The circadian clockwork of the suprachiasmatic nuclei – analysis of a cellular oscillator that drives endocrine rhythms. *Endocrinolgy*, **12**, 5624–5634.

Mills, J.D. & Pitman, R.M. (1997) Electrical properties of a cockroach motor neuron soma depend on different characteristics of individual Ca components. *J. Neurophysiol.*, **78**, 2455–2266.

Moreaux, L. & Laurent, G. (2007) Estimating firing rates from calcium signals in locust projection neurons *in vivo*. *Front. Neural Circuits*, **1**, 1–13.

Moreaux, L. & Laurent, G. (2008) A simple method to reconstruct firing rates from dendritic calcium signals. *Front. Neurosci.*, **2**, 176–185.

Nadasdy, Z. (2010) Binding by asynchrony: the neuronal phase code. *Front. Neurosci.*, **4**, doi: 10.3389/fnins.2010.00051.

Nishiitsutsuji-Uwo, J. & Pittendrigh, C.S. (1968) Central nervous system control of circadian rhythmicity in the cockroach: III. The optic lobes, locus of the driving oscillation? *Z. Vgl. Physiol.*, **58**, 14–46.

Nitabach, M.N., Blau, J. & Holmes, T.C. (2002) Electrical silencing of *Drosophila* pacemaker neurons stops the freerunning circadian clock. *Cell*, **109**, 485–495.

Nitabach, M.N., Sheeba, V., Vera, D.A., Blau, J. & Holmes, T.C. (2005) Membrane electrical excitability is necessary for the free running larval *Drosophila* circadian clock. *J. Neurobiol.*, **62**, 1–13.

Park, J.H., Helfrich-Förster, C., Lee, G., Liu, L., Rosbash, M. & Hall, J.C. (2000) Differential regulation of circadian pacemaker output by separate clock genes in *Drosophila*. *Proc. Natl. Acad. Sci. USA*, **97**, 3608–3613.

Peschel, N. & Helfrich-Forster, C. (2011) Setting the clock – by nature: circadian rhythm in the fruitfly *Drosophila melanogaster*. *FEBS Lett.*, **585**, 1435–1442.

Petri, B. & Stengl, M. (1999) Presumptive insect circadian pacemakers *in vitro*: immunocytochemical characterization of cultured pigment-dispersing hormone-immunoreactive neurons of *Leucophaea maderae*. *Cell Tissue Res.*, **296**, 635–643.

Petri, B., Stengl, M., Wurden, S. & Homberg, U. (1995) Immunocytochemical characterization of the accessory medulla in the cockroach *Leucophaea maderae*. *Cell Tissue Res.*, **282**, 3–19.

Reischig, T. & Stengl, M. (1996) Morphology and pigment-dispersing hormone (PDH)-immunocytochemistry of the accessory medulla, the presumptive circadian pacemaker of the cockroach *Leucophaea maderae*: a light- and electron-microscopical study. *Cell Tissue Res.*, **255**, 305–319.

Reischig, T. & Stengl, M. (2003a) Ectopic transplantation of the accessory medulla restores circadian locomotor rhythms in arrhythmic cockroaches (*Leucophaea maderae*). *J. Exp. Biol.*, **206**, 1877–1886.

Reischig, T. & Stengl, M. (2003b) Ultrastructure of pigment-dispersing hormone-immunoreactive neurons in a three-dimensional model of the accessory medulla of the cockroach *Leucophaea maderae*. *Cell Tissue Res.*, **314**, 421–435.

Reischig, T. & Stengl, M. (2004) Pigment-dispersing hormone (PDH)-immunoreactive neurons form direct coupling pathways between the bilateral symmetric circadian pacemakers of the cockroach *Leucophaea maderae*. *Cell Tissue Res.*, **318**, 553–564.

Schneider, N.L. & Stengl, M. (2005) Pigment-dispersing factor and GABA synchronize cells of the isolated circadian clock of the cockroach *Leucophaea maderae*. *J. Neurosci.*, **25**, 5138–5147.

Schneider, N.L. & Stengl, M. (2006) Gap junctions between accessory medulla neurons appear to synchronize circadian clock cells of the cockroach *Leucophaea maderae*. *J. Neurophysiol.*, **95**, 1996–2002.

Schneider, N.L. & Stengl, M. (2007) Extracellular long-term recordings of the isolated accessory medulla, the circadian pacemaker center of the cockroach *Leucophaea maderae*, reveal ultradian and hint circadian rhythms. *J. Comp. Physiol. A.*, **193**, 35–42.

Schulze, J., Neupert, S., Schmidt, L., Predel, R., Lamkemeyer, T., Homberg, U. & Stengl, M. (2012) Myoinhibitory peptides in the brain of the cockroach *Leucophaea maderae* and colocalization with pigment-dispersing factor in circadian peacemaker cells. *J. Comp. Neurol.*, **520**, 1078–1097.

Sheeba, V., Sharma, V.K., Gu, H., Chou, Y.T., O'Dowd, D.K. & Holmes, T.C. (2008) Pigment dispersing factor-dependent and -independent circadian locomotor behavioral rhythms. *J. Neurosci.*, **28**, 217–227.

Singer, W. & Gray, C.M. (1995) Visual feature integration and the temporal correlation hypothesis. *Annu. Rev. Neurosci.*, **18**, 555–586.

Soehler, S., Neupert, S., Predel, R., Nichols, R. & Stengl, M. (2007) Localization of leucomyosuppression in the brain and circadian clock of the cockroach *Leucophaea maderae*. *Cell Tissue Res.*, **328**, 443–452.

Soehler, S., Neupert, S., Predel, R. & Stengl, M. (2008) Examination of the role of FMRFamide-related peptides in the circadian clock of the cockroach *Leucophaea maderae*. *Cell Tissue Res.*, **332**, 257–269.

Soehler, S., Stengl, M. & Reischig, T. (2011) Circadian pacemaker coupling by multi-peptidergic neurons in the cockroach *Leucophaea maderae*. *Cell Tissue Res.*, **343**, 559–577.

Stengl, M. & Homberg, U. (1994) Pigment-dispersing hormone-immunoreactive neurons in the cockroach *Leucophaea maderae* share properties with circadian pacemaker neurons. *J. Comp. Physiol. A.*, **175**, 203–213.

Tuckwell, H.C. (2012) Quantitative aspects of L-type Ca^{2+} currents. *Prog. Neurobiol.*, **96**, 1–31.

Chapter IV

Calcium responses of circadian pacemaker neurons of the cockroach *Rhyparobia maderae* to acetylcholine and histamine

Baz ES*, Wei HY*, Grosshans J, and Stengl M. 2012.
* Baz ES and Wei HY contributed equally
This manuscript has been submitted in J. Exp. Biol. on 01 September 2012

Calcium responses of circadian pacemaker neurons of the cockroach *Rhyparobia maderae* to acetylcholine and histamine

El-Sayed Baz*, Hongying Wei*, Johannes Grosshans, Monika Stengl
El-Sayed Baz and Hongying Wei contributed equally
Correspondence: Monika Stengl
FB 10, Biology, Animal Physiology, University of Kassel,
Heinrich Plett Str.40, 34132 Kassel, Germany

Short title: ACh & HA effects on circadian pacemaker
Keywords: Accessory Medulla; Acetylcholine; Calcium Imaging; Cockroach; Histamine; Neurotransmitters

Summary

The accessory medulla (aMe) is the pacemaker that controls circadian activity rhythms in the cockroach *Rhyparobia maderae.* The circadian pacemaker center receives photic input from the compound eye via unknown excitatory and GABAergic inhibitory entrainment pathways. In addition, non-photic neuropeptidergic inputs couple both bilaterally symmetric pacemaker centers. Not much is known about the classical neurotransmitters of input pathways to the cockroach circadian system, besides, possibly a histaminergic centrifugal neuron. It connects the aMe with projection areas in the protocerebrum and may provide non-photic inputs. To identify neurotransmitters of input pathways to the circadian clock with Fura-2-dependent Ca^{2+} imaging primary cell cultures of the adult aMe were stimulated with acetylcholine (ACh), as the most prominent excitatory, and histamine (HA), as a common inhibitory neurotransmitter. Application of ionotropic nicotinic receptor (nAChR)- and metabotropic muscarinic receptor (mAChR)-agonists and -antagonists revealed that only nAChRs are present in aMe neurons, next to HA receptors. Dose-dependently ACh-induced Ca^{2+} increases in the aMe cells were mediated by voltage-activated Ca^{2+} channels. HA application caused dose-dependent decreases in intracellular Ca^{2+} levels in only a subpopulation of circadian pacemaker neurons while ACh responses occurred in most of the aMe cells. These data suggest that ACh is a prominent neurotransmitter of the light entrainment pathway while HA is involved in a non-photic input pathway to the circadian clock of the Madeira cockroach.

Introduction

Circadian pacemakers coordinate daily physiological and behavioral rhythms in vertebrates and invertebrates alike (Pittendrigh, 1981; Jackson et al., 2001). Lesion and transplantation studies demonstrated that the optic lobes and, specifically, the accessory medulla (aMe), a small neuropil with about 250 associated neurons at the ventromedial edge of the medulla, is the pacemaker that controls circadian locomotor activity rhythms of the cockroach *Rhyparobia maderae* (Syn.: *Leucophaea maderae*), a well-established circadian clock model (Page, 1982; Stengl and Homberg, 1994; Reischig and Stengl, 2003). Antisera against neuropeptides located abundant, partly colocalized neuropeptides in specific subgroups of the aMe-associated neurons (Petri et al., 1995; Söhler et al., 2007; 2008; 2011). Among them three groups of pigment-dispersing hormone-immunoreactive (PDF-ir) circadian clock neurons were characterized best. In the fruitfly *Drosophila melanogaster* as well as in the Madeira cockroach the PDF-ir circadian pacemaker neurons are clock outputs and control locomotor activity rhythms connecting the circadian pacemaker center with different midbrain and optic lobe targets (reviews: Homberg et al., 2003; Yoshii et al., 2009). In addition, in the Madeira cockroach 4 of the PDF-ir neurons form input pathways to the circadian clock. They couple both bilaterally symmetric accessory medullae (aMae) with optic lobe neuropils as circadian coupling pathways (Reischig and Stengl, 2002, 2004; Söhler et al., 2011). However, little is known about the cellular and physiological nature of light entrainment pathways or other, non photic inputs into the circadian pacemaker of the Madeira cockroach. Apparently, only photoreceptors in or close to the compound eye are essential for photic entrainment with high intensity light dark (L:D) cycles (Roberts, 1965, 1974; Nishiitsutsuji-Uwo and Pittendrig, 1968). In addition, lesion experiments demonstrated that ipsi- and contralateral compound eyes provide light input into the aMe (Page et al., 1977; Page, 1978). The contralateral light inputs appear to be mediated via orcokinin-ir neuropeptidergic neurons projecting via the posterior optic commissure (Hofer and Homberg, 2006a, 2006b). With antibodies against histamine, the neurotransmitter of insect photoreceptors it was shown that there are no direct connections of compound eye photoreceptors with the aMe (Loesel and Homberg, 1999; reviews: Stuart, 1999; Homberg, 2002). Only one centrifugal histamine-ir neuron appeared to provide non-photic input into the circadian clock and connected the aMe with different midbrain targets (Loesel and Homberg, 1999). Thus, so far, only the GABA-ergic distal tract which connects the noduli of the aMe with the medulla and possibly also the lamina is the best candidate for a light entrainment pathway to the cockroach clock (Reischig and Stengl, 1996). Also, injection experiments combined with behavioral analysis revealed light-like phase response curves for GABA, consistent with a role of GABA in photic entrainment of the clock (Petri et al., 2002). However, next to inhibitory light inputs there is also evidence for excitatory photic inputs into the circadian pacemaker region (Loesel and Homberg, 2001). The respective neurotransmitters relaying excitatory photic input into the aMe are not known so far.

Classical insect neurotransmitters include acetylcholine, glutamate, γ-aminobutyric acid (GABA) and biogenic amines such as serotonin, dopamine, octopamine, tyramine and histamine (Kahsai et al., 2010; Kahsai and Winther, 2011). Not much is known about the role of these neurotransmitters in the cockroach circadian system. Thus, to determine possible input signals into the circadian clock of the Madeira cockroach we performed Fura-2-dependent Ca^{2+}- imaging with primary cell cultures of the adult aMe to measure neurotransmitter-dependent changes in intracellular Ca^{2+} levels. Here we focused on the study of acetylcholine (ACh) as a prominent excitatory and histamine (HA), as a prominent inhibitory neurotransmitter of insects. Since preliminary experiments with application of serotonin, dopamine and octopamine did not reveal any consistent results (n>150). It was found that ACh and HA receptors are present in aMe neurons of the Madeira cockroach. While ACh application triggered dose-dependent increases in intracellular Ca^{2+} in almost all aMe neurons, HA application caused dose-dependent decreases in intracellular Ca^{2+} levels in only a subpopulation of circadian pacemaker neurons. These data suggest that ACh may play a role in the light entrainment pathway and HA acts in a non-photic input pathway to the circadian clock.

Materials and Methods

Animals

Adult male cockroaches *Rhyparobia maderae* were used to generate primary cell cultures of the aMe. The animals were reared in a large tank at about 26°C, 60% humidity. A cycle of 12 h light/12 h dark regime (L:D = 12:12) was maintained to entrain the circadian system with the change from light to dark occurring at 08:00 AM.

Primary cell culture

The protocol for dissociation of aMe neurons has been described within detail in Petri and Stengl (1999). Briefly, the aMe was selectively excised using a glass capillary with a 200 µm tip diameter. To dissociate the single cells from the tissue, four aMae from two brains were incubated for 4 min at 37°C in 500 µl HBSS solution containing 1 mg/ml collagenase and 4 mg/ml dispase. The HBSS solution was supplemented with: 85% aqua purificata, 15% HBSS, 1% penicillin/streptavidin, 0.05 mg/ml Phenylthrourea, 0.025 mg/ml phenolrot. The mixture with cells was transferred in 10 ml Leibovitz`s L-15 medium (L-15) (PAA Laboratories Germany) with 2.8 mg/ yeastolate and 2.8 mg/ml lactalbumin. About 160 µl cell suspension was obtained after centrifugal sedimentation at 500 rpm for 5 min at 8°C. Each 40 µl cell suspension was dispersed on a concanavalin A coated glass cover slip in sterile plastic cell culture dish. After 2 h the cells were settled to the cover slip and the cell culture dish was filled with 1 ml cell culture medium. The cell culture medium was prepared from L-15 medium and additional salts: 200 mg/ml glucose, 80 mg/ml fructose, 35 mg/ml L-prolin, 6 mg/ml imidazol, 1% glutamin, 0.1% gentamicin, and 2.38 mg/ml hepes, pH

7.0 and osmolarity 360 mOsm adjusted with 5% NaOH and mannitol. The cell culture dishes were kept in darkness at 20°C in a humidified incubator. The chemicals were purchased from Sigma-Aldrich. The cells were processed for Ca^{2+}-imaging experiments after at least 24 h in culture. Cultures were prepared between about Zeitgeber time (ZT) 1:00 and 3:00. Since we do not know whether the culture procedure resets the circadian clock to a specific ZT we do not attempt to make a statement of ZT-dependency of neurotransmitter effects in our experiments.

Calcium Imaging

Before starting the Ca^{2+}-imaging experiments, the cells were loaded with 4 µM Ca^{2+} indicator Fura-2 acetoxymethyl ester (Fura-2 AM, Molecular Probes) dissolved in standard saline for 40 min in darkness at room temperature. The standard saline containing (in mM): 156 NaCl, 4 KCl, 1 $CaCl_2$, 10 hepes and 5 glucose (pH 7.1, osmolarity 380 mOsm). Following dye loading, the cover slip with dissociated cells was transferred to a recording chamber and thoroughly washed using standard saline continuously using a perfusion pump (REGLO Digital MS-2/6, Ismatec).

The Fura-2 loaded cells were viewed with a 20x objective of a fluorescence microscope (DMI3000 B, Leica Microsystems). The dual wavelength Ca^{2+}-sensitive indicator was excited alternately at 340 nm and 380 nm with 500 ms intervals via a monochromator Polychrome 5000 (Till Photonics) with exposure times of 30 and 15 ms, respectively. Images were captured with an EM-CCD camera iXON+ DU885KCS-VP (Andor) every 500 ms. The region of interest for each cell in the field of view was manually identified. The ratio of fluorescence at 340/380 nm was calculated using Live Acquisition software (Version 2.0.0.12, Till Photonics), which reflects the concentration of the intracellular calcium.

Stimulus solutions and application

ACh, nicotine (50 µM, nicotinic ACh receptor agonist), pilocarpine (50 µM, muscarinic ACh receptor agonist) mecamylamine (50 µM, nicotinic ACh receptor antagonist), and scopolamine (50 µM, muscarinic ACh receptor antagonist) (Wegener et al., 2004), Mibefradil (10 µM voltage activated calcium channels blocker) (Benquet et al., 2000), and HA were purchased from sigma and were dissolved in standard saline (= different stimulus solutions). The neurons were continuously superfused with normal standard saline (0.5 ml/min) except during stimulus presentation bath solutions were replaced by the respective stimulus solution. The responses to the stimulus were monitored by comparing changes in the intracellular calcium levels (Ca^{2+}) before and after application. The ACh and HA application were carried out during the subjective day.

For dose-response experiment, the ACh stimuli were applied carefully at different concentrations ranging from 10 nM to 1 mM via a syringe to obtain a homogeneous distribution of the stimulus in the bath. To stimulate as many cells as possible during one stimulus application syringe-stimulation was preferred over

picospritzer-stimulation which allows only controlled stimulation of a single cell. The volume ejected from the syringe was 1 ml for 60-90 s. Directly before the stimulus injection the standard saline in the chamber was completely removed, except for about 300 µl to avoid the dilution of the stimulus concentration. The neurons were continuously superfused with normal standard saline before and after stimulus presentation. Always, bath perfusion was stopped during stimulus presentation. To analyze the response to the ACh agonists and antagonists, ACh, nicotine and pilocarpine stimuli were applied, and then the neurons were incubated by 50 µM scopolamine or 50 µM mecamylamine for five minutes before being treated with ACh agonists solutions containing 50 µM from the same antagonist.

The HA stimuli were bath applied for 60 s at different concentrations (ranging from 100 nM to 1 mM) by an electronic 3-way valve (manufactured by Parker) connected to the perfusion system. The 3-way valve alternates the flow of the standard saline and the histamine solution. The valve and the pump were controlled by computer. The valve is suited for saline flow and is an excellent alternative to manual change of the stimulus. Following the neurotransmitter application, the cells were washed with the standard saline and were continuously superfused during the experiments.

Statistical analyses

Data are given as means ± standard error of the mean (S.E.M.). The magnitude and duration of the Ca^{2+} responses were calculated with Spike 2. Kolmogorov-Smirnov test was used for normality test. Analysis of variance (ANOVA) with Tukey's post hoc analysis was performed for statistical comparison. Data were analyzed with SPSS 19.0 statistical software.

Results

Effect of ACh on intracellular Ca^{2+} levels in primary cell cultures of the aMe

Application of ACh increased the intracellular Ca^{2+} level in a dose-dependent manner in about 96% of the tested aMe cells (*N*= 126 cells) (Fig. 1A, B). The threshold concentration for the ACh effect varied between 10 nM and 1 µM. The magnitude of the peak response was dose-dependent between 10 nM and 0.1 mM. In 55% of the ACh sensitive cells (*N*= 121 cells), desensitization was observed at the higher concentration (1 mM) (Fig. 1B, normalized response for 1 mM ACh application = 91.5%). The maximum response occurred within 20 s after the ACh application. At higher concentrations of ACh, intracellular Ca^{2+} level first increased but decayed quickly, suggesting that desensitization occurred immediately after the activation of the receptors. The increased Ca^{2+} level was accompanied by rapid Ca^{2+} oscillations in 88% of the recorded aMe cells (*N*= 121 cells) (arrows in Fig. 1A). After ACh washout from the bath solution, the intracellular Ca^{2+} level returned to control levels and the

ACh -dependent Ca^{2+} oscillations disappeared.

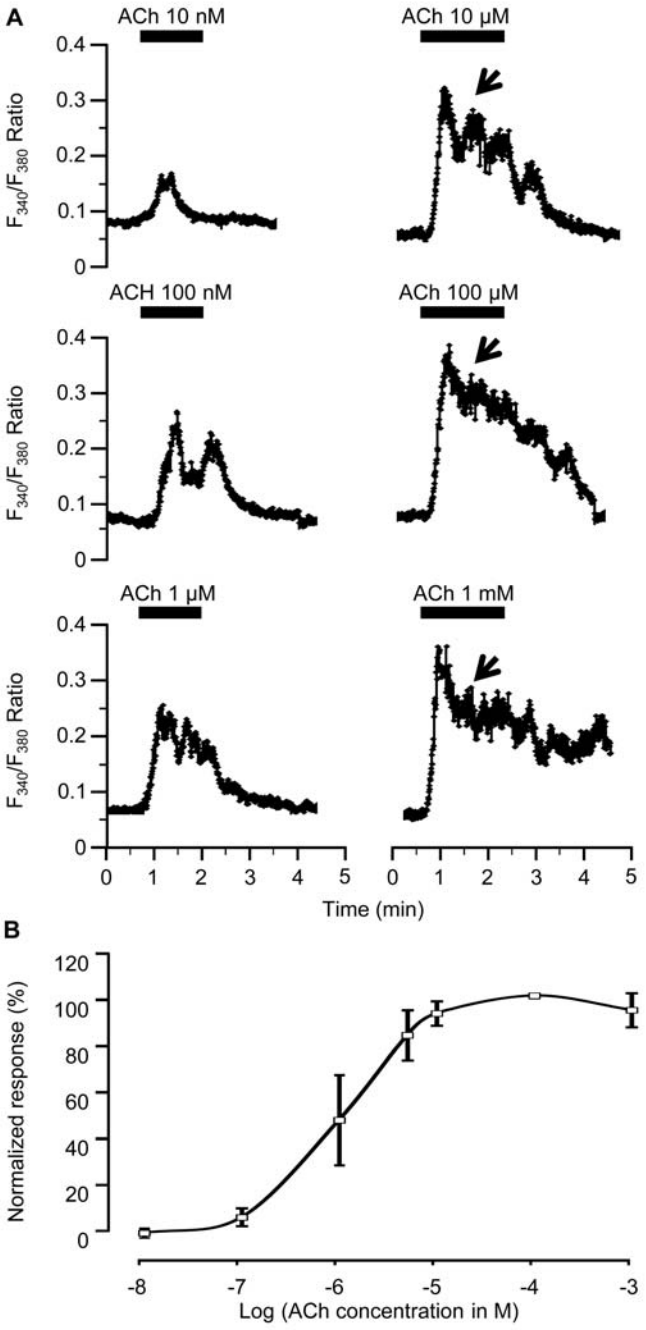

Figure. 1 Acetycholine (ACh) increased intracellular calcium levels in primary cultured cockroach circadian pacemaker neurons loaded with the Ca^{2+} indicator dye fura-2. (A) Response of an accessory medulla neuron to increasing concentrations of ACh. The intracellular calcium level increased immediately after ACh applications, accompanied by rapid Ca^{2+} oscillations. At higher concentrations of ACh, intracellular calcium level first increased but decayed afterwards (arrows). About 10 min interruption and washout of the ACh with standard saline between each concentration applied. The solid bars indicate the duration of the application. (B) Normalized ACh dose-response curve. Responses were normalized to the response at 100 µM ACh (=100%). Data were plotted as means ± S.E.M. The desensitization of the response occurred at 1 mM ACh.

ACh response is mediated by nicotinic receptors

ACh responses are mediated via cholinergic receptors, either via ionotropic nicotinic receptors (nAChR) or via metabotropic muscarinic receptors (mAChR) (Wegener et al., 2004). The nAChR and mAChR agonists were combined with their corresponding antagonists to determine the receptor types involved in the ACh

responses. As shown in Fig. 2A, responses to 50 μM nicotine (nAChR agonist) resembled responses to 100 μM ACh in all cells tested (*N*=31 cells). However, the cells showed no response to 50 μM pilocarpine (mAChR agonist) in all cells recorded (*N*=31 cells). Preincubation with 50 μM scopolamine (mAChR antagonist) did not block nicotine-responses in any of the recorded cells (*N*=11 cells). After blocking the nAChRs with 50 μM mecamylamine (nAChR antagonist), nicotine ceased to increase the intracellular Ca^{2+} level in any of the cells tested (*N*=23 cells). Pilocarpine did not affect the intracellular Ca^{2+} level in presence of scopolamine or mecamylamine. To further identify the receptor type, the effect of antagonists on ACh-induced Ca^{2+} increases were examined (Fig. 2B). Scopolamine did never affect the ACh-induced Ca^{2+} increase (*N*=20 cells), while mecamylamine blocked the ACh effect in all cells tested (*N*=20 cells). Therefore, the ACh responses of the aMe cells were mediated very likely by nAChRs, but not by mAChRs.

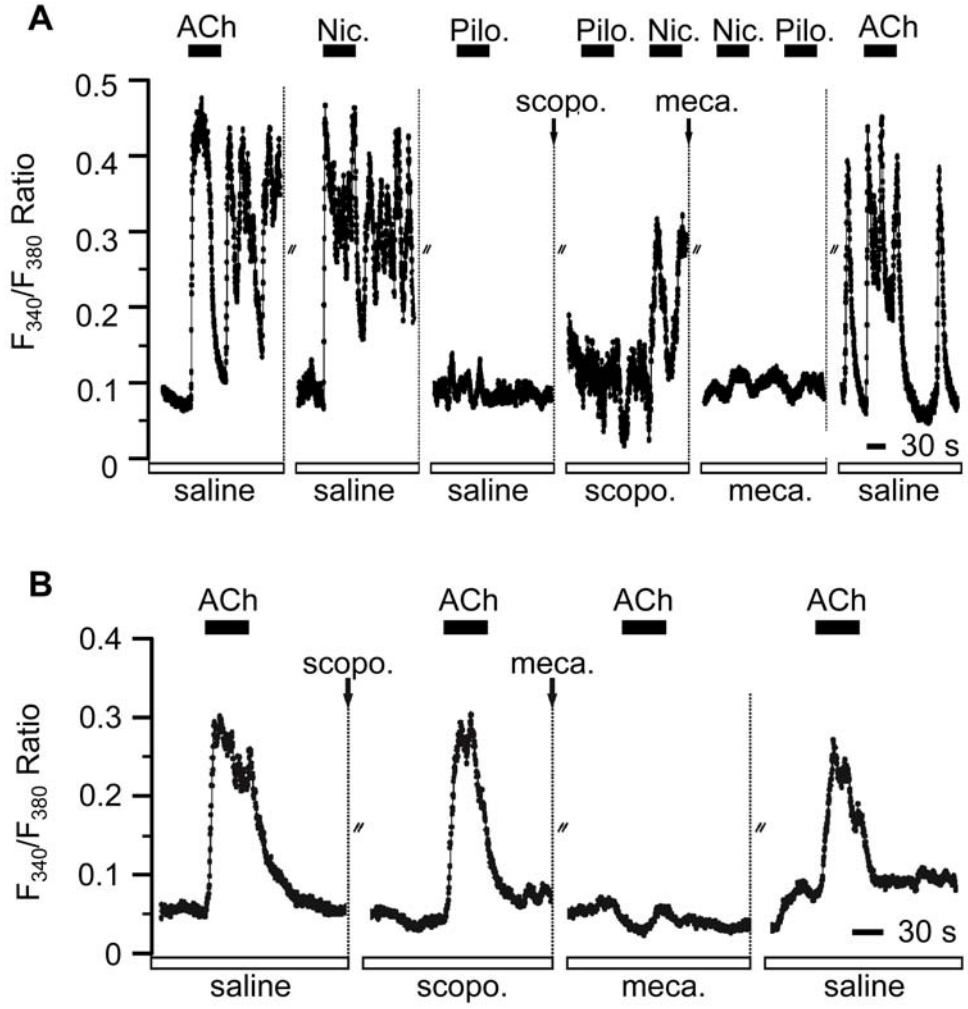

Figure. 2 Acetylcholine responses act via a nicotinic but not a muscarinic ACh receptor in primary cultured cockroach circadian pacemaker neurons loaded with fura-2. (A) Fluorescence traces recorded from single cell show the effect of acetylcholine (ACh), nicotinic receptor agonist {nicotine (Nic)} and antagonist {(mecamylamine (meca)}, muscarinic receptor agonist {pilocarpine (Pilo)} and antagonist

{scopolamine (scopo)}. The cell immediately showed increase in intracellular calcium concentration in response to 100 μM ACh or 50 μM nicotine application while no intracellular calcium concentration changes when applying 50 μM pilocarpine The aMe neurons incubated by 50 μM scopolamine or 50 μM mecamylamine for five minutes before measurements and during the time of the application. Scopolamine did not alter the increasing of intracellular calcium levels, while mecamylamine remarkably blocked increasing of intracellular calcium levels in response to Nicotine. No intracellular calcium concentration changes when applying pilocarpine in presence of scopolamine or mecamylamine. **(B)** Response to ACh application, before and during incubation by scopolamine or Mecamylamine, and after washout. The cell immediately showed increase in intracellular calcium concentration in response to 100 μM ACh application. The aMe neurons incubated by 50 μM scopolamine or 50 μM mecamylamine for five minutes before measurements and during the time of the application. Scopolamine did not affect the increasing of intracellular calcium levels, while mecamylamine remarkably stops increasing of intracellular calcium levels. About 10 min washout of the blocker with standard saline led to calcium increasing in response to ACh. The solid bars indicate the duration of the application.

ACh-induced Ca^{2+} increase is mediated by voltage-activated Ca^{2+} channels

In all recorded aMe cells, addition of 10 μM mibefradil (reversible voltage-activated Ca^{2+} channel blocker) reduced the intracellular Ca^{2+} level and blocked Ca^{2+} increases, which were induced by 100 μM ACh or 50 μM nicotine (*N*=22 cells) (Fig. 3). Therefore, the ACh-induced Ca^{2+} increase in the aMe cells was mediated by voltage-activated Ca^{2+} channels.

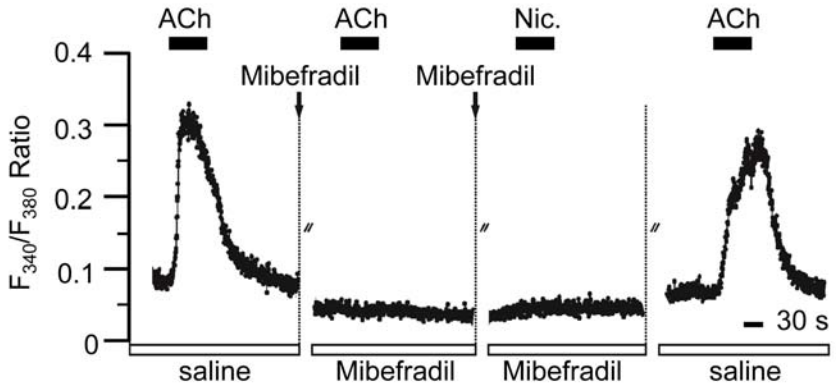

Figure. 3 Mibefradil, voltage activated calcium channels blocker, stops the calcium increasing of primary cultured cockroach circadian pacemaker neurons loaded with fura-2 in response to acetylcholine or nicotine. Cell immediately showed increase in intracellular calcium concentration following 100 μM ACh application. Incubation of aMe neurons by 10 μM mibefradil for five minutes before measurements and during the time of the application resulted in reduced intracellular calcium baseline levels as well as stopped the calcium increasing in response to 100 μM ACh or 50 μM nicotine (Nic). About 10 min washout of the blocker with standard saline led to calcium increasing in response to ACh. The solid bars indicate the duration of the application.

Effect of HA on intracellular Ca^{2+} levels in primary cell cultures of the aMe

Application of the HA solution (100 µM) for 60 s evoked three different types of response patterns (Fig. 4A). The response type I expressed a rapid decrease in the intracellular Ca^{2+} concentration following HA application. This decrease remained for 325.84±13.8 s (mean ± S.E.M.) after washout and, thereafter, it recovered to the control level. The response type II showed a sustained Ca^{2+} decrease. Even after washout it did not recover to the control level. The response type III summarized the irregular changes in the spontaneous calcium oscillations after HA application, which could be caused by homeostatic changes of the spontaneous active cells.

The percentages of each response pattern were calculated at different concentrations of HA, 1 µM, 10 µM and 100 µM (Fig. 4B). In 14.19% of the examined cells (*N*=191 cells) responses to 1 µM HA were observed (Type I=5.88% Type II=0% Type III=8.31%). In 30.79%, of the examined cells (*N*=311 cells) responses to 10 µM HA were observed (Type I=14.78% Type II=4.15% Type III=11.86%). In 48.65%, of the examined cells (*N*=266 cells) responses to 100 µM HA were observed (Type I=19.02% Type II=10.09% Type III=19.53%).

Finally, it was examined whether the HA response amplitude and duration for type I HA response patterns displays dose-dependency. The amplitude was measured from the control level to the maximum intracellular Ca^{2+} decrease and the duration of the responses were calculated from the beginning of the intracellular Ca^{2+} decrease up to recovery to the control level (Fig. 5). It was noted that the durations of the responses changed in a dose-dependent manner when applying increasing concentrations of HA, from 1 µM to 100 µM, while the response amplitude appeared to be saturated since it did not show significant dose- dependency ($P>0.05$, ANOVA). The threshold concentration for the HA effect varied between 100 nM and 1 µM. The responses were normalized to the response at 100 µM HA (=100%). A dose-response curve was constructed based upon the normalized duration of the response (Fig. 5B). The response duration increased with increasing concentrations of HA. Desensitization became apparent at higher concentrations of HA (1 mM, data not shown).

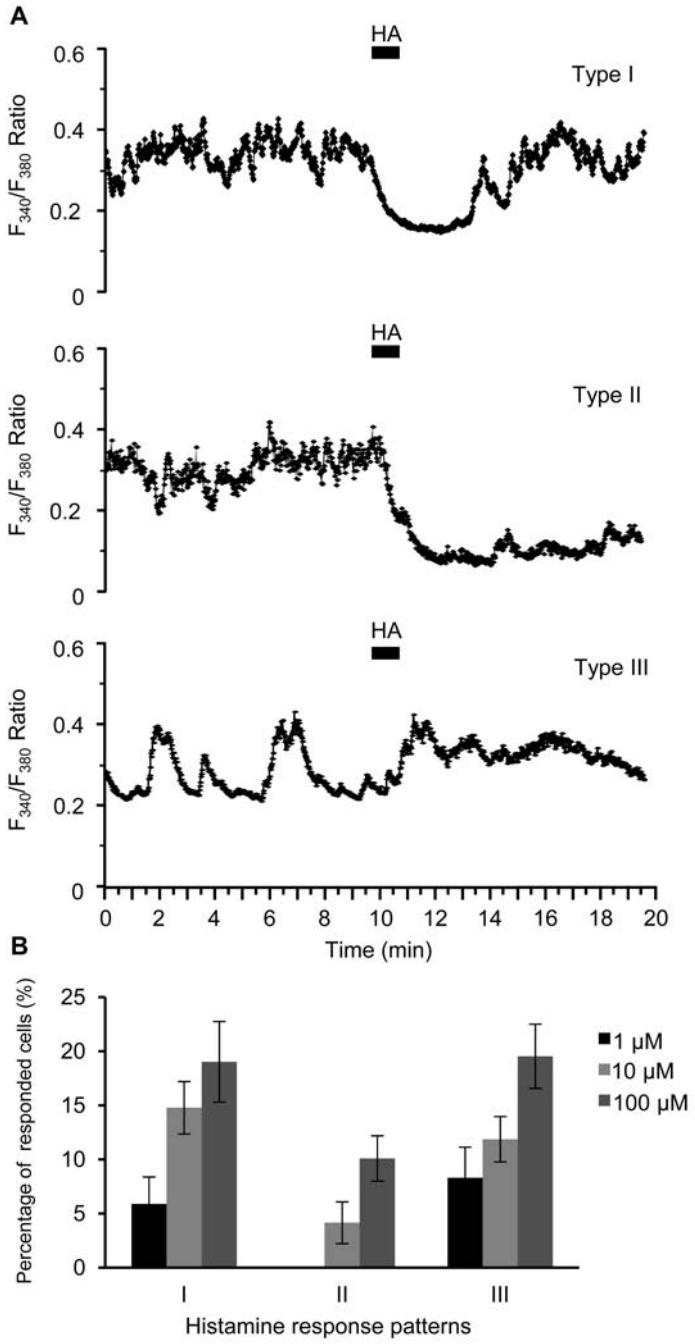

Figure. 4 Histamine (HA)-induced variations in fluorescence of primary cultured cockroach circadian pacemaker neurons loaded with the Ca^{2+} indicator dye fura-2. (A) Traces show fluorescence of three individual neurons in response to 100 μM HA application for 60 sec which is indicated by the solid bar. The HA response patterns are classified as the following: type I response; cell immediately showed decrease in intracellular calcium concentration following the HA application and thereafter it recovered to the control level after washout. Type II response; cell showed Ca^{2+} decrease but after washout did not recover to the control level. Type III response summarized the irregular changes in the spontaneous calcium oscillations after HA application, which could be caused by homeostatic changes of the spontaneous active cells. The solid bars indicate the duration of the application. (B) Comparison between the percentages of the histamine response patterns in response to different concentrations of HA, 1 μM, 10 μM and 100 μM. Data presented as mean ± S.E.M.

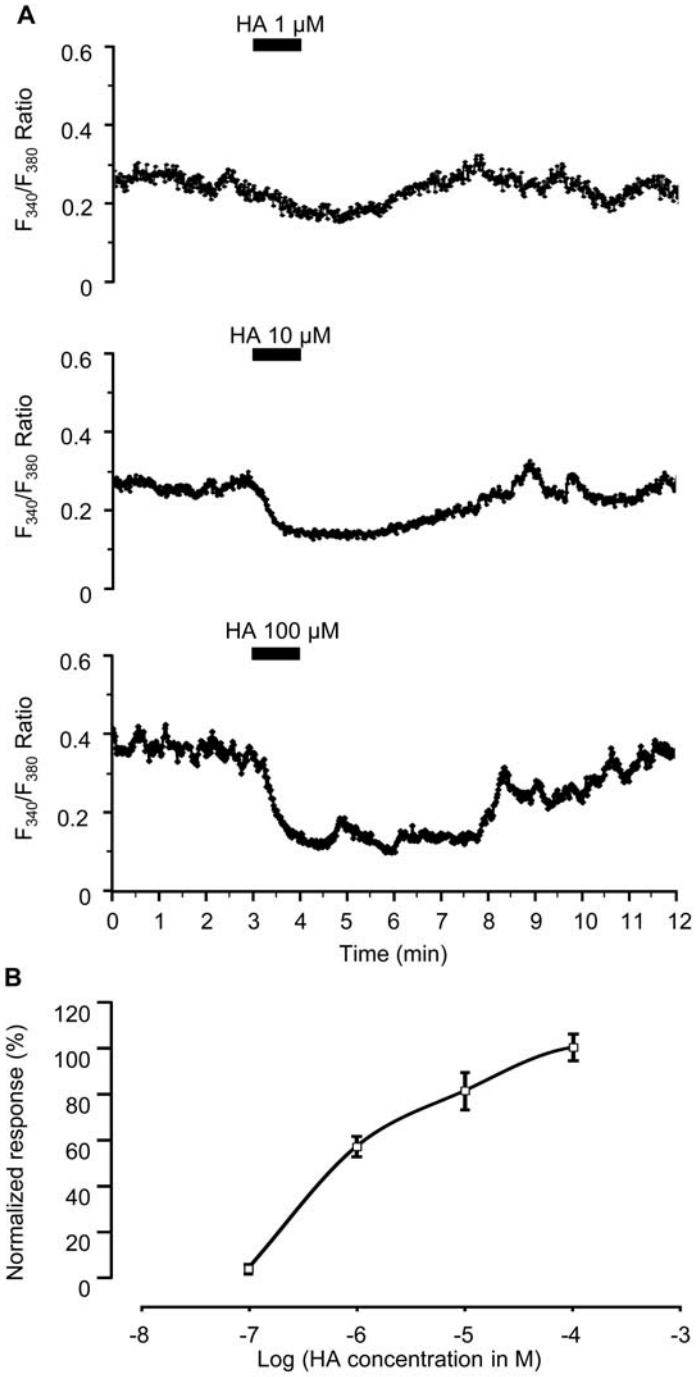

Figure. 5 Histamine (HA) decreased intracellular calcium levels in primary cultured cockroach circadian pacemaker neurons loaded with the Ca^{2+} indicator dye fura-2. (A) Response of accessory medulla neurons to increasing concentrations of HA (e.g. 1 µM, 10 µM and 100 µM). The intracellular calcium level decreased immediately after HA applications and after washout it remains for few minutes and thereafter it recovered to the control level. The solid bars indicate the duration of the application. (B) Normalized HA dose-response curve. Responses were normalized to the response at 100 µM HA (=100%). Data were plotted as means ± S.E.M. The desensitization of the response occurred at 1mM HA (Data not shown).

Discussion

To determine the general neurotransmitters of input pathways to the circadian clock of the Madeira cockroach we examined neurotransmitter effects in Ca^{2+} imaging experiments on primary cell cultures of adult aMe neurons. We provided evidence for the presence of nAChRs in most neurons of the aMe as well as HA-receptors in a subpopulation of circadian clock neurons.

ACh as a prominent neurotransmitter in the circadian clock

Several studies have provided strong evidence for ACh as a key player in the circadian pacemaker center both in mammals and in insects (Vijayalakshmi et al., 1977; Wegener et al., 2004; Hut et al., 2011; Keene et al., 2011; McCarthy et al., 2011; Lelito et al., 2012). In mammals, circadian fluctuation in the cholinergic system (e.g. ACh content, cholinergic enzyme activity, cholinergic receptor and vesicular acetylcholine transporter) has been biochemically demonstrated (Hanin et al., 1970; Schiebeler et al., 1974; Nordberg et al., 1980; Mash et al., 1985; Morley et al., 1990). Several immunocytochemistry-studies have located enzymes characteristic of cholinergic neurons within the SCN. The AChT- and AChE-positive cholinergic cells probably belong to the “simple bipolar” cells in the SCN, which are suggested to transfer light information (Hut et al., 2011). In the nervous system of the cockroach *Periplaneta americana*, the ACh content and AChE activity also showed inverse circadian rhythms (Vijayalakshmi et al., 1977).

In mammals, the distributions of mAChR and nAChR within the SCN were determined employing immunocytochemistry against the receptors, since antibodies against ACh are not available. However, immunoreactivity to the apparently few nAChRs was low and barely detectable (Van der Zee et al., 1991). Approximately all SCN neurons were immunopositive for mAChR, suggesting a more important role of the mAChR in the SCN cholinergic neurotransmission (Van der Zee et al., 1999; 2004). Also, the reverse-transcribed-PCR studies revealed expression of mRNA for all mAChR subtypes in the SCN (Yang et al., 2010). Excitatory effects of ACh or nicotine were determined *in vivo* (Miller et al., 1987; Nashmi and Lester, 2006). However, *in vitro*, the majority of SCN cells were inhibited by mAChR agonists, whereas some SCN cells were excited or not responsive (Yang et al., 2010). These multiple cholinergic responses could indicate that ACh could regulate the SCN neuron excitability differentially depending on the multiple receptors and the physiological phases of individual SCN cells. In contrast to these different effects in vertebrate circadian pacemaker neurons, ACh increased the activity of the large pigment-dispersing factor-immunoreactive ventrolateral neurons (PDF-ir l-LNvs) in the *Drosophila* brain via nAChRs, but not via mAChRs (McCarthy et al., 2011). In the circadian pacemaker neurons of the *Drosophila* larval brain, the expression of nAChRs were observed employing immunocytochemistry. In addition, larval circadian pacemaker neurons responded to ACh with increases in intracellular Ca^{2+}

concentration via nAChR *in vivo* as well as *in vitro* (Wegener et al., 2004).

Using Ca^{2+} imaging combined with pharmacology, here it was shown that ACh affected the aMe cells of the cockroach via nAChRs. Since the large majority of circadian pacemaker neurons of the aMe were ACh-sensitive ACh appears to be well suited to control the general response range of circadian pacemaker neurons. Thus, either it acts not stimulus-specific or, since photic input is most importantly for the circadian clock, ACh may mediate photic inputs. Future experiments will test this hypothesis.

HA as a neurotransmitter relaying apparently non-photic input to the circadian pacemaker neurons

Histamine (HA) was reported to be an important neurotransmitter and neuroregulatory compound in the nervous systems of a wide range of organisms (Schwartz et al., 1991; Fleck et al., 2012). Thus, HA was implicated in the regulation of CNS functions, such as behavioral states, biological rhythms, thermoregulation, feeding rhythms, energy metabolism, and learning and memory (Huang et al., 2011). The distribution of histaminergic profiles was mapped in the central nervous system of many insects species (e.g., Nässel et al., 1988; Pirvola et al., 1988; Homberg and Hildebrand, 1991; Pollack and Hofbauer, 1991; Nässel and Elekes, 1992; Buchner et al., 1993; Bornhauser and Meyer, 1997; Loesel and Homberg, 1999; Monastirioti, 1999; Ignell, 2001). The presence of HA-immunoreactivity in specific sets of neurons in the brain of different insect species suggests neurotransmitter or neuromodulatory roles of HA in numerous central circuits (Nässel, 1999). Importantly, HA serves as the neurotransmitter of photoreceptors in insects by directly activating a chloride channel in the postsynaptic cells (Hardie, 1989; Stuart et al., 2007). Thus, HA acts as a fast inhibitory neurotransmitter in the insect nervous system. Two histamine-gated chloride channels were described thus far in *D. melanogaster* (Gengs et al., 2002; Gisselmann et al., 2002; Zheng et al., 2002; Roeder, 2003; Pantazis et al., 2008). Application of HA to the first order interneurones caused an electrical response similar to that induced by light. A more detailed examination of this response using patch clamp techniques showed that application of HA caused an increase in the chloride permeability of the large monopolar cells. This increase in chloride permeability was attributed to a directly coupled HA receptor that caused the opening of a chloride channel (Hardie, 1987, 1988, 1989).

In mammals, a role for HA as a neurotransmitter in circadian entrainment was suggested (Stephan et al., 1981; Moore, 1983; Tuomisto, 1991). Histamine release in rats is under circadian control since its release during the dark period was significantly higher than during the light period (Mochizuki et al., 1992). Jacobs et al. (2000) suggested that HA receptors are the final gate at which both photic and non-photic entrainment mechanisms converge before sending a resetting signal to the intracellular biological clock of mammals (Jacobs et al., 2000). Furthermore, HA was reported to have different effects on shifting the circadian activity phase depending on

its circadian administration time (Itowi et al., 1991; Stehle, 1991). It is also reported that at the level of the SCN the direct excitatory effects of histamine on neuronal firing is mediated via H1 receptors and the inhibitory effects via H2 receptors (Liou et al., 1983; Stehle, 1991). However, *in vivo* studies suggested that HA is a neuromodulator of glutamatergic transmission via its effects on the NMDA receptor (Eaton et al., 1995, 1996).

Our results indicate that HA application inhibits aMe neurons possibly during the subjective day. Since we did not obtain ZT-dependent effects and since we cannot determine whether the culture procedures reset circadian clocks of aMe neurons, we cannot determine whether neurotransmitter sensitivity of aMe neurons is ZT-dependent. Since we always observed HA-dependent inhibitions, the observed HA effects on aMe neurons may be mediated via histamine-dependent chloride channels. In the Madeira cockroach HA-immunoreactivity in the AMe originated from a centrifugal neuron of the midbrain, but not from direct photoreceptor input to the clock (Loesel and Homberg, 1999). Thus, it is likely that HA serves a non-photic inhibitory input into the circadian clock. Future experiments have to determine the nature and function of this input.

References

Benquet, P., Frere, S., Pichon, Y. and Tiaho, F. (2000). Properties and development of calcium currents in embryonic cockroach neurons. *Neurosci. Lett.* 294, 49-52.

Bornhauser, B. C. and Meyer, E. P. (1997). Histamine-like immunoreactivity in the visual system and brain of an orthopteran and a hymenopteran insect. *Cell Tissue Res.* 287, 211-221.

Buchner, E., Buchner, S., Burg, M. G., Hofbauer, A., Pak, W. L. and Pollack, I. (1993). Histamine is a major mechanosensory neurotransmitter candidate in *Drosophila melanogaster*. *Cell Tissue Res.* 273, 119-125.

Eaton, S. J., Cote N. K. and Harrington, M. E. (1995). Histamine synthesis inhibition reduces light-induced phase shifts of circadian rhythms. *Brain Res.* 695, 227-230.

Eaton, S. J., Eoh, S., Meyer, J., Hoque, S. and Harrington, M. E. (1996). Circadian rhythm photic phase shifts are not altered by histamine receptor antagonists. *Brain Res. Bull*. 41, 227-229.

Fleck, M. W., Thomson, J. L. and Hough, L. B. (2012). Histamine-gated ion channels in mammals? *Biochem. Pharmacol.* 83, 1127-1135.

Geng, C., Leung, H. T., Skingsley, D. R., Iovchev, M. I., Yin Z., Semenov, E. P., Burg, M. G., Hardie, R. C., and Pak, W. L. (2002). The target of *Drosophila* photoreceptor synaptic transmission is a histamine-gated chloride channel encoded by ort (hclA). *J. Biol. Chem.* 277, 42113-20.

Gisselmann, G., Pusch H., Hovemann, B. T. and Hatt, H. (2002). Two cDNAs coding for histamine-gated ion channels in *D. melanogaster. Nat. Neurosci.* 5, 11-2.

Hanin, I., Massarelli, R. and Costa, E. (1970). Acetylcholine concentrations in rat brain: diurnal oscillation. *Science* 170, 341–342.

Hardie, R. C. (1987). Is histamine a neurotransmitter in insect photoreceptors? *J. Camp. Phvsiol.* A 161, 201-213.

Hardie, R. C. (1988). Effects of anatagonists on putative histamine receptors in the first visual neuropile of the housefly *Musca domestica. J. Exp. Biol.* 138, 221-241.

Hardie, R. C. (1989). A histamine-activated chloride channel involved in neurotransmission at a photoreceptor synapse. *Nature* 339, 704-706.

Hofer, S. and Homberg, U. (2006a). Evidence for a role of orcokinin-related peptides in the circadian clock controlling locomotor activity of the cockroach *Leucophaea maderae*. *J. Exp. Biol.* 209, 2794-2803.

Hofer, S. and Homberg, U. (2006b). Orcokinin immunoreactivity in the accessory medulla of the cockroach *Leucophaea maderae*. *Cell Tissue Res.* 325, 589-600.

Homberg, U. (2002). Neurotransmitters and neuropeptides in the brain of the locust. *Microsc. Res. Tech.* 56, 189-209.

Homberg, U. and Hildebrand, J. G. (1991). Histamine-immunoreactive neurons in the midbrain and subesophageal ganglion of the sphinx moth *Manduca sexta. J. Comp. Neural.* 307, 647-657.

Homberg, U., Reischig, T. and Stengl, M. (2003). Neural organization of the circadian system of the cockroach *Leucophaea maderae*. *Chronobiol. Int.* 20, 577-590.

Huang, Z. L., Urade, Y. and Hayaishi, O. (2011). Key roles of the histaminergic system in sleep-wake regulation. *Sleep Biol. Rhythm* 9, 34–37.

Hut, R. A. and van der Zee, E. A. (2011). The cholinergic system, circadian rhythmicity, and time memory. *Behav. Brain Res.* 221, 466-480.

Ignell, R. (2001). Monoamines and neuropeptides in antennal lobe interneurons of the desert locust, *Schistocerca gregaria*: an immunocytochemical study. *Cell Tissue Res.* 306, 143-156.

Itowi, N., Yamatodani, A., Mochizuki, T. and Wada, H. (1991). Effects of intracerebroventricular histamine injection on circadian activity phase entrainment during rapid illumination changes. *Neurosci. Lett.* 123, 53-56.

Jackson, F. R., Schroeder, A. J., Roberts, M. A., McNeil, G. P., Kume, K. and Akten, B. (2001). Cellular and molecular mechanisms of circadian control in insects. J*. Insect Phsyiol.* 47, 822–842.

Jacobs, E. H., Yamatodani, A. and Timmerman, H. (2000). Is histamine the final neurotransmitter in the entrainment of circadian rhythms in mammals? *Trends Pharmacol. Sci.* 21, 293-298.

Kahsai L., Martin J. R. and Winther A. M. (2010). Neuropeptides in the *Drosophila* central complex in modulation of locomotor behavior. *J. Exp. Biol.* 213, 2256–2265.

Kahsai, L., and Winther, A. M. (2011). Chemical neuroanatomy of the Drosophila central complex: distribution of multiple neuropeptides in relation to neurotransmitters. *J. Comp. Neurol.* 519, 290–315.

Keene, A. C., Mazzoni, E. O., Zhen, J., Younger, M. A., Yamaguchi, S., Blau, J., Desplan, C. and Sprecher, S. G. (2011). Distinct visual pathways mediate *Drosophila* larval light avoidance and circadian clock entrainment. *J. Neurosci.* 31, 6527-6534.

Lelito, K. R. and Shafer, O. T. (2012). Reciprocal Cholinergic and GABAergic Modulation of the Small Ventrolateral Pacemaker Neurons of Drosophila's Circadian Clock Neuron Network. *J. Neurophysiol.* 107, 2096-2108.

Liou, S. Y., Shibata, S., Yamakawa, K. and Ueki, S. (1983). Inhibitory and excitatory effects of histamine on suprachiasmatic neurons in rat hypothalamic slice preparation. *Neurosci. Lett.* 41, 109-113.

Loesel, R. and Homberg, U. (1999). Histamine-immunoreactive neurons in the brain of the cockroach *Leucophaea maderae*. *Brain Res.* 842, 408-418.

Loesel, R. and Homberg, U. (2001). Anatomy and physiology of neurons with processes in the accessory medulla of the cockroach *Leucophaea maderae. J. Comp. Neurol.* 439, 193-207.

Mash, D. C., Flynn, D. D., Kalinoski, L. and Potter, L. T. (1985). Circadian variations in radioligand binding

to muscarine receptors in rat brain dependent upon endogenous agonist occupation. *Brain Res.* 331, 35–38.

McCarthy, E. V., Wu, Y., Decarvalho, T., Brandt, C., Cao, G. and Nitabach, M. N. (2011). Synchronized bilateral synaptic inputs to Drosophila melanogaster neuropeptidergic rest/arousal neurons. *J, Neurosci.* 31, 8181-8193.

Miller, J. D., Murakami, D. M. and Fuller, C. A. (1987). The response of suprachiasmatic neurons of the rat hypothalamus to photic and nicotinic stimuli. *J. Neurosci.* 7, 978–986.

Mochizuki, T., Yamatodani, A., Okakura, K. and Horii A. (1992). Circadian rhythm of histamine release from the hypothalamus of freely moving rats. *Physiol. Behav.* 51, 391-394.

Monastirioti, M. (1999). Biogenic amine systems in the fruit fly *Drosophila melanogaster*. *Microsc. Res. Tech.* 45, 106-121.

Moore, R. Y. (1983). Organization and function of a central nervous system oscillator: the suprachiasmatic nucleus. *Fed. Proc*. 42, 2783-2789.

Morley, B. J. and Garner, L. L. (1990). Light-dark variation in response to chronic nicotine treatment and the density of hypothalamic alpha-bungarotoxin receptors. *Pharmacol. Biochem. Behav.* 37, 239–245.

Nashmi, R. and Lester, H. A. (2006) CNS localization of neuronal nicotinic receptors. *J. Mol. Neurosci.* 30, 181–184.

Nässel, D. R. (1999). Histamine in the brain of insects: a review. *Microsc. Res. Tech.* 44, 121-36.

Nässel, D. R. and Elekes, K. (1992). Aminergic neurons in the brain of blowflies and *Drosophila*: dopamine- and tyrosine hydroxylase-Cell immunoreactive neurons and their relationship with putative histaminergic neurons. *Cell Tissue Res.* 267, 147-167.

Nässel, D. R., Holmqvist, M. H., Hardie, R. C., Håkanson, R. and Sundler, F. (1988). Histamine-like immunoreactivity in photoreceptors of the compound eyes and ocelli of the flies *Calliphora erythrocephala* and *Musca domestica*. *Cell Tissue Res.* 253, 639-646.

Nishiitsutsuji-Uwo, J. and Pittendrigh, C. S. (1968). Central nervous system control of circadian rhythmicity in the cockroach: III. The optic lobes, locus of the driving oscillation? *Zeitschrift für vergleichende Physiologie* 58, 14-46.

Nordberg, A. and Wahlstrom, G. (1980). Diurnal fluctuation in striatal choline acetyltransferase activity and strain difference in brain protein content of the rat. *Acta. Physiol. Scand,* 108, 385–388.

Page, T.L. (1978). Interactions between bilaterally paired components of the cockroach circadian system. *J. Comp. Physiol. A* 124, 225-236.

Page, T. L. (1982). Transplantation of the cockroach circadian pacemaker. *Science* 216, 73-75.

Page, T. L., Caldarola, P. C. and Pittendrigh, C. S. (1977). Mutual entrainment of bilaterally distributed circadian pacemakers. *Proc. Natl. Acad. Sci. USA* 58, 14–46.

Pantazis, A., Segaran, A., Liu, C. H., Nikolaev, A., Rister, J, Thum, A. S., Roeder, T., Semenov, E., Juusola, M., and Hardie, R. C. (2008). Distinct roles for two histamine receptors (hclA and hclB) at the *Drosophila* photoreceptor synapse. *J. Neurosci.* 28, 7250-7259.

Petri, B. and Stengl, M. (1999). Presumptive insect circadian pacemakers in vitro: immunocytochemical characterization of cultured pigment-dispersing hormone-immunoreactive neurons of *Leucophaea maderae*. *Cell Tissue Res.* 296, 635–643.

Petri, B., Homberg, U., Loesel, R. and Stengl, M. (2002). Evidence for a role of GABA and Mas-allatotropin in photic entrainment of the circadian clock of the cockroach *Leucophaea maderae. J. Exp. Biol.* 205, 1459-1469.

Petri, B., Stengl, M., Wurden, S. and Homberg, U. (1995). Immunocytochemical characterization of the accessory medulla in the cockroach *Leucophaea maderae*. *Cell Tissue Res.* 282, 3-19.

Pirvola, U., Tuomisto, L., Yamatodani, A. and Panula, P. (1988). Distribution of histamine in the cockroach brain and visual system: an immunocytochemical and biochemical study. *J. Com.p Neurol.* 276, 514–526.

Pittendrigh, C. S. (1981). Circadian systems: General perspective. In Handbook of Behavioral Neurobiology, Biological Rhythms, ed. J. Aschoff, 4:57-80. New York: Plenum.

Pollack, I. and Hofbauer, A. (1991). Histamine-like immunoreactivity in the visual system and brain of *Drosophila melanogaster*. *Cell Tissue Res.* 266, 391–398.

Reischig, T. and Stengl, M. (2002). Optic lobe commissures in a three-dimensional brain model of the cockroach *Leucophaea maderae*: A search for the circadian coupling pathways. *J. Com.p Neurol.* 443, 388-400.

Reischig, T. and Stengl, M. (1996). Morphology and pigment-dispersing hormone (PDH)-immunocytochemistry of the accessory medulla, the presumptive circadian pacemaker of the cockroach *Leucophaea maderae*: a light- and electron-microscopical study. *Cell Tissue Res.* 255, 305-319.

Reischig, T. and Stengl, M. (2003). Ectopic transplantation of the accessory medulla restores circadian locomotor rhythms in arrhythmic cockroaches (*Leucophaea maderae*). *J. Exp. Biol.* 206, 1877–1886.

Reischig, T. and Stengl, M. (2004). Pigment-dispersing hormone (PDH)-immunoreactive neurons form direct coupling pathways between the bilateral symmetric circadian pacemakers of the cockroach *Leucophaea maderae*. *Cell Tissue Res.* 318, 553-564.

Roberts, S. K. (1965). Photoreception and entrainment of cockroach activity rhythms. *Science* 148, 958–959.

Roberts, S. K. (1974). Circadian rhythms in cockroaches. Effects of optic lobe lesions. *J. Comp. Physiol.* 88, 21–30.

Roeder, T. (2003). Metabotropic histamine receptors—nothing for invertebrates? *Eur. J. Pharmacol.* 466, 85-90.

Schiebeler, H. and von Mayersbach, H. (1974). Circadian variations of acetylcholine esterase (E.C.3.1.1.7) in rat brains. *Int. J. Chronobiol.* 2, 281–289.

Schwartz, J. C., Arrang, J. M., Garbarg, M., Pollard, H. and Ruat, M. (1991). Histaminergic transmission in the mammalian brain. *Physiol. Rev.* 71, 1-51.

Söhler, S., Neupert, S., Predel, R., Nichols, R. and Stengl, M. (2007). Localization of leucomyosuppressin in the brain and circadian clock of the cockroach *Leucophaea maderae*. *Cell Tissue Res.* 328, 443-452.

Söhler, S., Neupert, S., Predel, R. and Stengl, M. (2008). Examination of the role of FMRFamide-related peptides in the circadian clock of the cockroach *Leucophaea maderae. Cell Tissue Res.* 332, 257-269.

Söhler, S., Stengl, M. and Reischig, T. (2011). Circadian pacemaker coupling by multi-peptidergic neurons in the cockroach *Leucophaea maderae. Cell Tissue Res.* 343, 559-577.

Stehle, J. (1991). Effects of histamine on spontaneous electrical activity of neurons in rat suprachiasmatic nucleus. *Neurosci. Lett*. 130, 217-220.

Stengl, M., and Homberg, U. (1994). Pigment-dispersing hormone-immunoreactive neurons in the cockroach *Leucophaea maderae* share properties with circadian pacemaker neurons. *J. Comp.*

Physiol. A 175, 203-213.

Stephan, F. K., Berkley, K. J. and Moss, R. L. (1981). Efferent connections of the rat suprachiasmatic nucleus. *Neuroscience* 6, 2625-2641.

Stuart, A. E. (1999). From fruit flies to barnacles, histamine is the neurotransmitter of arthropod photoreceptors. *Neuron* 22, 431–433.

Stuart, A. E., Borycz, J. and Meinertzhagen, I. A. (2007). The dynamics of signaling at the histaminergic photoreceptor synapse of arthropods. *Prog. Neurobiol.* 82, 202–27.

Tuomisto, L. (1991). Involvement of histamine in circadian and other rhythms. In *Histaminergic neurons: Mophology and function* (ed. T. Watanabe and H. Wada), pp. 283-295. Boca Raton, FL: CRC Press.

Van der Zee, E. A., Biemans, B. A., Gerkema, M. P. and Daan, S. (2004). Habituation to a test apparatus during associative learning is sufficient to enhance muscarinic acetylcholine receptor-immunoreactivity in rat suprachiasmatic nucleus. *J. Neurosci. Res. 78*, 508-519.

Van der Zee, E. A. and Luiten, P. G. M. (1999). Muscarinic acetylcholine receptors in the hippocampus, neocortex and amygdala: A review of immunocytochemical localization in relation to learning and memory. *Prog. Neurobiol.* 58, 409–471.

Van der Zee, E. A., Streefland, C., Strosberg, A. D., Schroder, H. and Luiten, P. G. (1991). Colocalization of muscarinic and nicotinic receptors in cholinoceptive neurons of the suprachiasmatic region in young and aged rats. *Brain Res.* 542, 348–352.

Vijayalakshimi, S., Mohan, P. M. and Babu, K. S. (1977). Circadian rhythmicity in the nervous system of the cockroach, *Periplaneta americana*. *J. Insect Physiol.* 23, 195-202.

Wegener, C., Hamasaka, Y. and Nässel, D. R. (2004). Acetylcholine increases intracellular Ca^{2+} via nicotinic receptors in cultured PDF-containing clock neurons of *Drosophila*. *J. Neurophysiol.* 91, 912–923.

Yang, J. J., Wang, Y. T., Cheng, P. C., Kuo, Y. J. and Huang, R. C. (2010). Cholinergic modulation of neuronal excitability in the rat suprachiasmatic nucleus. *J. Neurophysiol.* 103, 1397–1409.

Yoshii, T., Wülbeck, C., Sehadova, H., Veleri, S., Bichler, D., Stanewsky, R. and Helfrich-Förster, C. (2009). The neuropeptide Pigment-dispersing factor adjusts period and phase of *Drosophila*'s clock. *J. Neurosci.* 25, 2597–2610.

Zheng, Y., Hirschberg, B., Yuan, J., Wang, A. P., Hunt, D. C., Ludmerer, S. W., Schmatz, D. M. and Cully, D. F. (2002). Identification of two novel *Drosophila melanogaster* histamine-gated chloride channel subunits expressed in the eye. *J. Biol. Chem.* 277, 2000-2005.

Chapter V

Photoperiod affects physiological responses of cultured circadian pacemaker neurons in the Madeira cockroach *Rhyparobia maderae*

Wei HY, Baz ES, and Stengl M. 2012. In preparation.
This manuscript will be submitted in J. Biol. Rhythms

Photoperiod affects physiological responses of cultured circadian pacemaker neurons in the Madeira cockroach Rhyparobia maderae

Hongying Wei, El-Sayed Baz, Monika Stengl
Correspondence: Monika Stengl
FB 10, Biology, Animal Physiology, University of Kassel,
Heinrich Plett Str.40, 34132 Kassel, Germany

Running head: photoperiod effects on physiological responses of circadian pacemaker neurons
Keywords: circadian pacemakers, photoperiod, spontaneous activity, acetycholine, brain plasticity, calcium.

Abstract

Little is known about photoperiod-dependent plasticity of the circadian system. In the cockroach *Rhyparobia maderae* circadian pacemaker neurons of the accessory medulla are spontaneously active being either activated or inhibited with rises of the extracellular Ca^{2+} concentration. Their spontaneous activity appears to be a prerequisite to neuropeptide-dependent ensemble-formation and gating of clock-outputs. Here, we searched for physiological changes in single, isolated circadian pacemaker neurons in cockroaches either raised in 12:12, 16:8, or 8:16 light: dark cycles. Using Ca^{2+} imaging, 7 different response types of spontaneously active circadian pacemaker neurons were distinguished in different extracellular Ca^{2+} concentrations. The percentage of different response types (type-percentage vectors) was highly photoperiod-specific and reproducible. It reliably predicted the different photoperiods and, thus, encoded short- and long-day information. No evidence for a photoperiodic change in responses to acetylcholine a hypothetical neurotransmitter of photic entrainment pathways was obtained. Thus, exposure to different photoperiods in development not only changes the network of the circadian clock, but also alters physiological responses of single circadian pacemaker neurons via so far unknown mechanisms. Currently, it is examined whether the observed plasticity of the circadian system can also be induced transiently in adult insects as an adaptive property to transient changes in the environment.

Introduction

While circadian clocks allow for anticipation of daily changes in light and dark, circannual clocks, such as a photoperiodic clock, regulate seasonal adaptation to changes in the photoperiod during the turn of the year (photoperiodism). It is agreed upon that both types of clocks the circadian and the circannual clocks are interdependent and may even share cellular components. However, the respective mechanisms and cellular nature of their respective interdependence are not resolved, yet (reviews: Bredshaw and Holzapfel 2010; Yoshii et al., 2012).

The circadian clock of the Madeira cockroach

The cockroach *Rhyparobia maderae* is a well established model system for the cellular and behavioral analysis of circadian rhythms research (Nishiitsutsuji-Uwo and Pittendrigh 1968; Page 1982; Homberg et al., 2003). Lesion and transplantation studies located the circadian pacemaker which controls locomotor activity rhythms to the accessory medulla (aMe) of the brain´s optic lobes ventromedially to the medulla (Page, 1978, 1982; Stengl and Homberg, 1994; Reischig and Stengl 2003a,b). The aMe is associated with 7 soma groups which connect it to different optic lobe neuropils as well as to various midbrain targets such as locomotor control centers. Photic entrainment via the compound eye reaches the aMe via GABAergic distal tract neurons and via suggested cholinergic excitatory interneurons (Reischig and Stengl 1996; Loesel and Homberg 2001; Wei, El-Baz, Stengl, submitted). Circadian pacemaker neurons of the aMe are astoundingly abundant of different neuropeptides (Petri et al. 1995; Reischig and Stengl 1996; Söhler et al., 2007, 2008, 2011). Best characterized are the pigment-dispersing factor-ir (PDF-ir) neurons which control locomotor activity rhythms in different insect species (reviews: Homberg et al. 2003; Yoshii et al. 2012).

Spontaneous activity-dependent temporal encoding in the circadian clock of the Madeira cockroach

Another characteristic of Madeira cockroach circadian pacemaker neurons is their spontaneous activity. They display fast, gamma-band (20-70 Hz) ultradian action potential rhythms superimposed on their circadian activity rhythms (Schneider and Stengl 2005, 2006, 2007). Gap junctions synchronize the spontaneously active aMe cells to fire with the same frequency. Mostly GABA-ergic interneurons control the phase of the spontaneous activity to generate ensembles (=assemblies) of cells which fire with the same frequency and same phase. Different ensembles maintain a constant phase difference to each other, apparently mediated via mostly inhibitory interneurons (Schneider and Stengl 2005, 2006). It was hypothesized that the insect circadian pacemaker center employs temporal encoding to control the phase of different outputs over the course of the day (Schneider and Stengl, 2005). It was suggested that circadian outputs are gated via peptide-dependent assembly

formation. Peptide-release at a defined time of day phase-shifts spontaneous activity rhythms. Thereby, the neuropeptides recruit an ensemble of phase-coupled pacemaker neurons to gate a specific output (Schneider and Stengl, 2005). A necessary prerequisite to this temporal coding scheme is the presence of spontaneous activity in pre- and postsynaptic cells which is in the same frequency range to allow for resonance coupling. Thus, tight phase- and frequency control of spontaneous activity of the neuropeptidergic circadian pacemaker neurons via external input signals is called for. Since spontaneous activity of the aMe circadian pacemaker neurons is generated mostly via Ca^{2+}-dependent ion channels spontaneous activity and, thereby, these mechanisms of input-dependent gating of aMe outputs strongly depend on the extracellular Ca^{2+} concentration (Wei and Stengl, 2012).

Does the circadian clock of the Madeira cockroach express photoperiod-dependent plasticity?

Under the assumption that different photoperiods are detected via the circadian clock it is expected that different photoperiods shape the response ranges of the circadian clock network. To search for photoperiod-dependent plasticity of the circadian clock of the Madeira cockroach, cockroaches were raised either in 12:12, 18:6 (long-day), or 6:18 (short-day) light-dark (L:D) cycles. As shown previously, raising cockroaches in different photoperiods changed the network of the PDF-ir neurons. The number of PDF-ir neurons as well as their branching patterns differed in short- versus long-day conditions. Therefore, some of the PDF-ir neurons appear to be activated directly or indirectly via light (Wei and Stengl, 2011).

Here, we want to know, whether changes in photoperiod not only change the network of PDF-ir circadian pacemaker cells but whether single aMe neurons also change physiological properties via raising cockroaches in different photoperiods. Since spontaneous activity is an important prerequisite to temporal encoding, we focused on the analysis of spontaneous activity as most critical physiological parameter. After characterizing/typing aMe neurons according to their spontaneous activity in three different extracellular Ca^{2+} concentrations we examined with FURA2-based Ca^{2+} imaging whether these physiological types differed between the three groups of cockroaches either raised in 12:12 (controls), short- or long-days. Indeed, the percentage of the different physiological types differed significantly between the three groups of cockroaches and could predict photoperiod.

Since acetylcholine (ACh) was shown to activate almost all aMe neurons it was suggested to either participate in the light-entrainment pathway to the clock or to set the general response range of aMe neurons to different inputs. Thus, also responses to ACh were compared in the different populations of cockroaches raised in different photoperiods. At the ACh concentration tested, no evidence for a change in ACh-sensitivity of cultured aMe cells by photoperiods was observed. Our results indicate that not only the PDF-ir network but also physiological parameters of single aMe neurons display photoperiod-dependent plasticity.

Materials and Methods

Primary cell culture

Adult male cockroaches *Rhyparobia maderae* were raised in different photoperiods of light/dark cycles (either LD 6:18, 12:12, or 18:6). The animals were reared in laboratory colonies at 26°C, 60% humidity. Their respective aMae with associated soma groups were excised and dispersed to obtain primary cell cultures of the circadian pacemaker neurons following established procedures (Petri and Stengl, 1999). The cells were plated on glass coverslips (no.1, Thermo Scientific) coated with concanavalin A (Sigma). They were maintained in cell culture for about 24h in a humidified incubator at 20°C in constant darkness and, then, were processed for Ca^{2+}-imaging experiments.

Calcium Imaging

The protocol for filling aMe cells with Fura-2 and the measurement of their intracellular Ca^{2+} concentration changes using the Till Photonic imaging system has been described within details in Wei and Stengl (2012). Briefly, the aMe cells were loaded with 4 µM Fura-2 acetoxymethyl ester (Fura-2 AM, Molecular Probes) for 40 min at room temperature, followed by a 10 min wash with standard saline using a perfusion pump (REGLO Digital MS-2/6, Ismatec.) The standard saline contains 156 mM NaCl, 4 mM KCl, 1mM $CaCl_2$, 10 mM Hepes and 5 mM glucose (PH 7,1; osmolarity, 380 mOsm).

To determine the effects of the extracellular Ca^{2+} concentration on the spontaneous activity, the aMe cells were exposed to extracellular salines were only the Ca^{2+} concentrations were changed, all other ions were the same as in the standard saline (Na^+, K^+, and Cl^-). Low Ca^{2+} saline (1 µM extracellular Ca^{2+} concentration $[Ca^{2+}]_{extra}$), standard saline (control 1 mM $[Ca^{2+}]_{extra}$) and increased Ca^{2+} saline (6 mM $[Ca^{2+}]_{extra}$) for 10 min each. Their corresponding intracellular Ca^{2+} activity ($[Ca^{2+}]_i$) was measured by calculating the ratio of fura-2 fluorescence excited at 340 nm and 380 nm (F_{340}/F_{380}). Spontaneous action potential activity is accompanied by fast Ca^{2+} concentration transients. Thus, only fast Ca^{2+} transients but not slow baseline Ca^{2+} concentration changes were evaluated in this study, as indication of action potential activity. To examine physiological responses to the hypothetical photic neurotransmitter acetylcholine (ACh) the ACh stimuli were bath applied via the superfusion system for 60 s at 3 different concentrations (1 µM, 10 µM and 100 µM). Following each ACh application, the cells were washed with the standard saline for 5 min.

Response types and type-percentage vectors

According to presence or absence of the spontaneous activity in 3 different salines, 8 different response types were distinguished. The aMe cells without activity under all 3

conditions were not included in the calculation of the percentage of the response types. Thus, aMe cells with intracellular Ca^{2+} activity from the same cockroach brain were assigned to the remaining 7 different response types. The percentage of the 7 response types for each cockroach brain was calculated.

To search for photoperiod-dependent plasticity the cockroaches were raised in 3 different photoperiods (stimuli, S = 1, 2, 3). For each experimental group (S), 20 cockroach brains with aMe cells were collected for analyses (animal, A = 1-20). The aMe cells from the same cockroach brain were assigned to 7 response types and the percentage of each types was calculated. Therefore, for each selected cockroach brain $A \in \{1,.....20\}$ from each photoperiod $S \in \{1,2,3\}$, the percentages of each response type $T \in \{1,.....7\}$ were determined, resulting in a 3D matrix type-percentage vectors P(*s,a,t*). The notation $Ps(a,t) \equiv P(s,a,t)\big|s \equiv S$ presents the percentages of all types from all animals for the same stimulus S.

Pearsons coefficient of correlation between pairs of type-percentage vectors

The correlation coefficient (CC) between pairs of type-percentage vectors from the same stimulus is given by

$$CC_{(i,m,x)(i,n,x)} = \frac{\frac{1}{N_T}\sum_{T=1}^{T}(P_{Si,Am}(T)-\overline{P_{Si,Am}})(P_{Si,An}(T)-\overline{P_{Si,An}})}{\sqrt{\frac{1}{N_T}\sum_{T=1}^{T}(P_{Si,Am}(T)-\overline{P_{Si,Am}})^2\cdot(P_{Si,An}(T)-\overline{P_{Si,An}})^2}}$$

The CC between pairs of type-percentage vectors from different stimuli is given by

$$CC_{(i,m,x)(j,n,x)} = \frac{\frac{1}{N_T}\sum_{T=1}^{T}(P_{Si,Am}(T)-\overline{P_{Si,Am}})(P_{Sj,An}(T)-\overline{P_{Sj,An}})}{\sqrt{\frac{1}{N_T}\sum_{T=1}^{T}(P_{Si,Am}(T)-\overline{P_{Si,Am}})^2\cdot(P_{Sj,An}(T)-\overline{P_{Sj,An}})^2}}$$

The CC analyses were calculated with self-written R programs. Pearson´s CC (-1 to +1) is sensitive to a linear relationship between to variables. The CC is a measure of "correlation" or "predictability" between two variables. The larger CC the better can one variable predict the other. Negative values indicate an inverse correlation: if one variable increases, the other decreases. Positive values indicated a direct correlation.

Statistical analyses

The peak amplitudes of the Ca^{2+} responses to ACh applications were normalized to baseline values ($\Delta R/R_{baseline}$). They were calculated with self-written software employing C++. The Kolmogorov-Smirnov test was used for normality test. The peak

amplitudes for cell cultures obtained from different photoperiods were compared by use of the ANOVA and factor analysis.

Results

In our search for photoperiod-dependent physiological plasticity in single, dispersed circadian pacemaker neurons of the Madeira cockroach, first the physiological parameters examined were defined. Then, these parameters were quantitatively analyzed in different cockroach colonies raised in different photoperiods with control 12:12h light: dark cycles, long- and short-day conditions. Analysis of spontaneous activity was the focus of this study since spontaneous activity is a prerequisite to temporal encoding schemes and non-Hebbian-type plasticity such as homeostatic scaling (Singer and Gray, 1995; Nadasdy, 2010; Hong et al., 2012).

Cultured aMe circadian clock neurons can be distinguished according to their spontaneous activity in different extracellular Ca^{2+} concentrations

Since the spontaneous activity of aMe circadian pacemaker neurons is maintained via Ca^{2+}-permeable and Ca^{2+}-dependently activated cation channels (Wei and Stengl 2012) the cells spontaneous activity strongly depends on the extracellular Ca^{2+}concentration. This property was used to distinguish different physiological response types of the cultured aMe neurons which cannot easily be distinguished according to morphological criteria *in vitro.* According to presence or absence of spontaneous activity in 3 different salines (with low, normal, or high $[Ca^{2+}]_{extra}$), 7 different response types from active aMe cells can be distinguished. The silent cells which did not express any spontaneous activity under all 3 conditions tested were excluded from analysis, since they could not be distinguished unequivocally from damaged, unresponsive cells. Types 1, 2, 3 showed spontaneous activity only in one of the three extracellular salines (Fig. 1). Type 1 was active only in low (1 µM), type 2 in normal (1 mM), and type 3 only in high (6 mM) $[Ca^{2+}]_{extra}$. In contrast, types 4, 5, 6 were silent only when they were exposed to either low (type 4), normal (type 5), or high (type 6) $[Ca^{2+}]_{extra}$ saline. Type 7 was spontaneously active in all of the 3 different Ca^{2+} salines (Fig. 1, Table.1). The photoperiod (stimulus)-dependent response type distribution could be described as mean percentages of response types calculated from 20 animals for each $\overline{Ps(a)} = \frac{1}{20}\sum_{a=1}^{20} Ps(a)$ (Table.1).

Table1. Photoperiod (light/dark cycle LD)-dependent spontaneous activity responses to 3 different salines (1 µM, 1 mM, or 6 mM extracellular calcium concentration $[Ca^{2+}]_{extra}$). The stars represent the presence of spontaneous activity.

type	$[Ca^{2+}]_{extra}$			percentage of response type		
	1 µM	1 mM	6 mM	LD 6:18	LD 12:12	LD 18:6
1	★			19 %	9 %	4 %
2		★		6 %	29 %	12 %
3			★	6 %	4 %	10 %
4		★	★	38 %	10 %	31 %
5	★		★	5 %	5 %	17 %
6	★	★		5 %	23 %	9 %
7	★	★	★	22 %	20 %	17 %

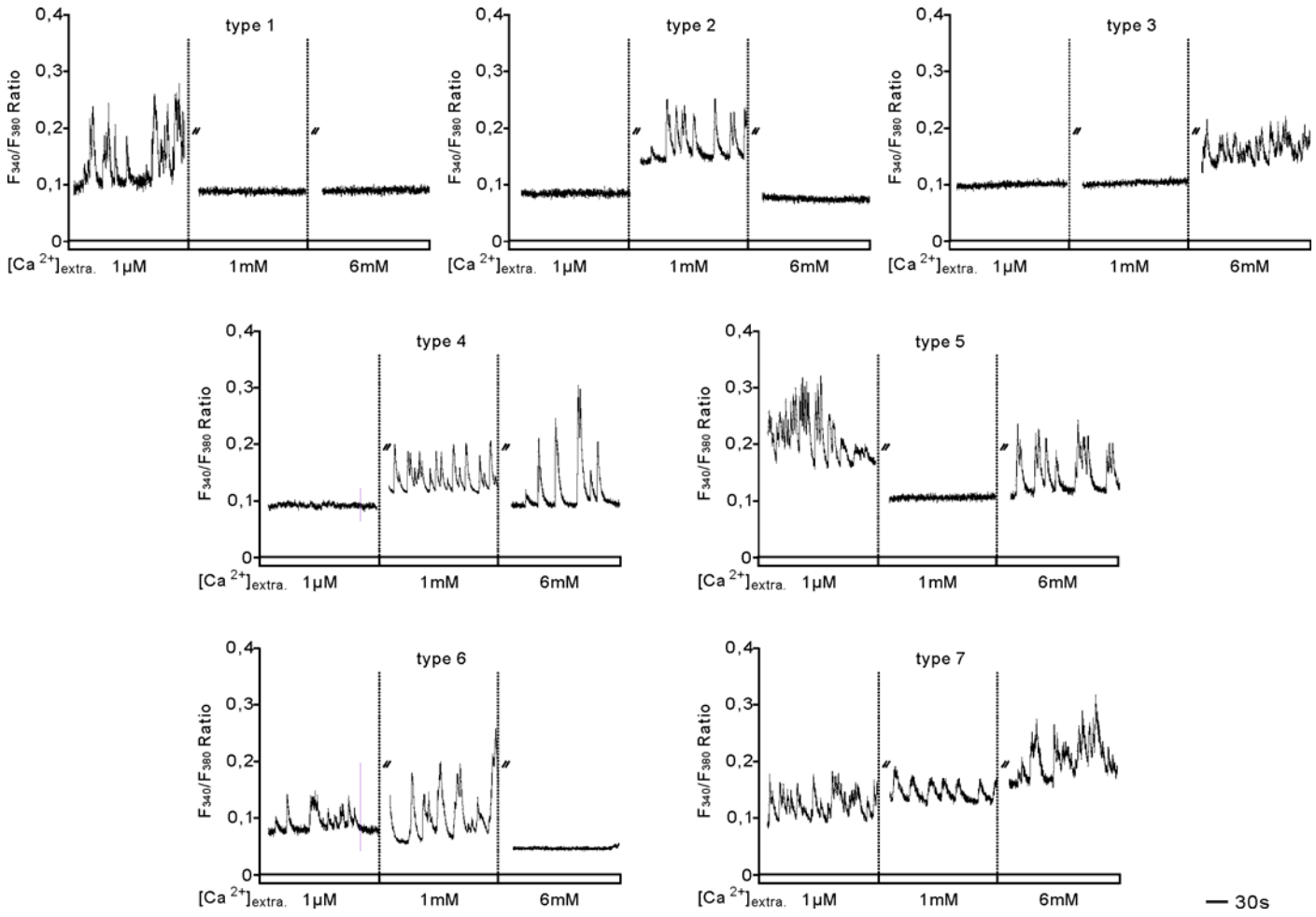

Figure 1. Physiological circadian pacemaker cell types distinguished according to presence or absence of the intracellular spontaneous activity in salines with low (1µM), normal (1mM) and high (6mM) extracellular calcium concentration ($[Ca^{2+}]_{extra}$).

Type-percentage vectors are highly reproducible and dependent on photoperiod

To test whether the type-percentage vectors of the aMe cells are photoperiod-specific, we calculated the CCs of type-percentage vectors for all possible pairs of animals and sorted them with respect to stimulus pairs. Comparing type-percentage vectors from animals reared in the same photoperiod stimulus, the CCs $_{(i,m,x)(i,n,x)}$ showed mean values of 0.789 ± 0.151 (LD 6:18), 0,772 ± 0.160 (12:12), and 0,752 ± 0.152 (18:6) for each photoperiod stimulus (Fig. 2). Thus, one variable could consistently predict the other. On the other hand, comparing type-percentage vectors from animals reared in the different photoperiod stimuli, the CCs $_{(i,m,x)(j,n,x)}$ showed distributions with smaller mean values of 0.329 ± 0.203 (6:18 / 12:12), 0.180 ± 0.217 (12:12 / 18:6), and 0.176 ± 0.234 (6:18 / 18:6), indicating that one variable could not predict the other (Fig. 3). The higher CCs between type-percentage vectors from the same stimulus and lower CCs from different stimuli indicated that the type-percentage vectors are highly photoperiod specific and reproducible for all photoperiod stimuli.

To test how accurately a photoperiod stimulus can be predicted by the type-percentage vectors of the aMe cells, we compared the test type-percentage vector (P_{test}) with template vectors ($P_{templates}$) for each photoperiod stimulus using the CCs. We selected one P_{test} and created $P_{templates}$ for each stimulus from remaining vectors. The predicted photoperiod stimulus ($S_{predict}$) is the stimulus of template vector ($S_{template}$), which is most similar to the test vector. The $S_{predict}$ was compared to the actual stimulus (S_{actual}) of the P_{test}, thus obtaining a true or false prediction. The type-percentage vectors could predict the photoperiod stimuli with a success rate of 68%. This demonstrated that the type-percentage vectors could serve as predictor for the photoperiod with certain accuracy, and therefore encoded information about the photoperiod the animals were raised in.

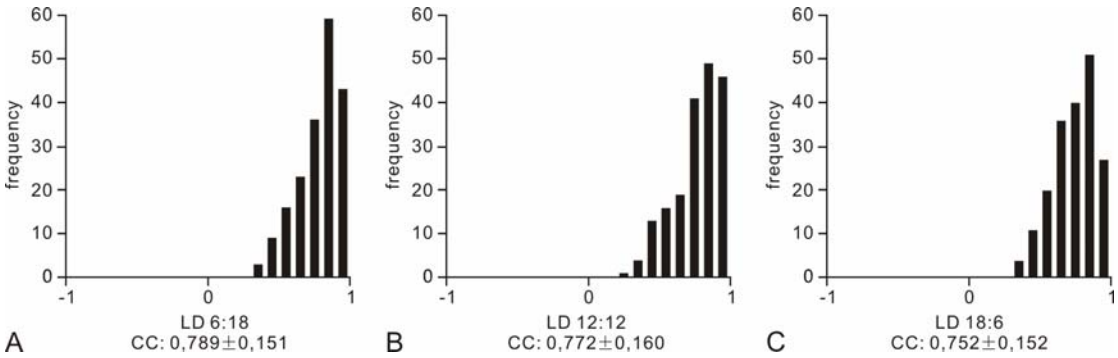

Figure 2. Distributions of correlation coefficients (CC) for type-percentage vectors from animals reared in the same photoperiod stimulus. The type-percentage vectors are highly reproducible. LD, light/dark regime.

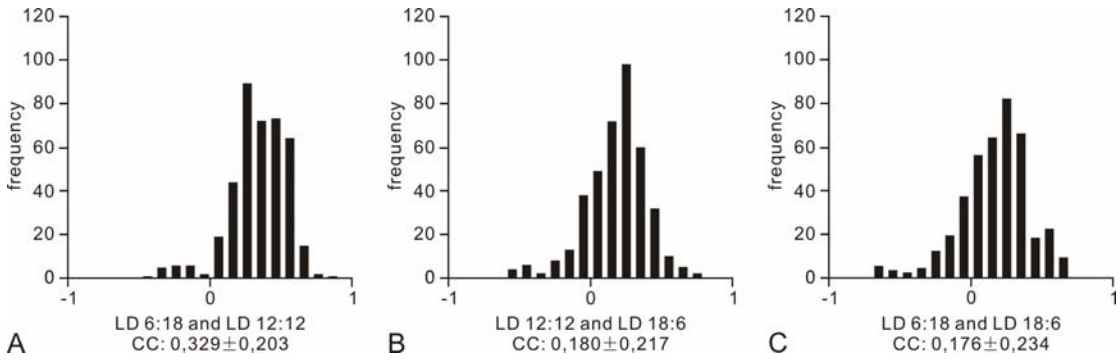

Figure 3. Distributions of correlation coefficients (CC) for type-percentage vectors from animals reared in the different photoperiod stimulus. The type-percentage vectors are photoperiod specific. LD, light/dark regime.

The photoperiodic function of ACh could not be confirmed

Previously it was shown that most aMe circadian pacemaker neurons respond to application of acetylcholine (ACh) with rises of intracellular Ca^{2+} (Baz, Wei and Stengl, submitted). Thus, it was assumed that photic information as the main excitatory sensory input into the circadian clock may be relayed via ACh. It was hypothesized that possibly the different photoperiods may change either the number of photosensitive neurons and/or the concentrations of ACh receptors in the membrane of single aMe pacemaker neurons. The peak amplitudes of the Ca^{2+} responses to ACh applications of aMe cells from cockroach raised in different photoperiods did not differ except for the highest ACh concentration tested (Fig. 4). The cultured aMe cells from cockroaches raised in LD 12:12 or 18:6 cycles showed a significant greater increase in intracellular Ca^{2+} levels after 100 µM ACh application as compared to LD 6:18 (ANOVA LSD $p<0.05$). However, using factor analysis, the Ca^{2+} responses to 100 µM ACh from the 3 experimental groups can be grouped into the same response type. The intracellular Ca^{2+} responses to 1 µM and 10 µM ACh application showed no significant difference among the 3 experimental groups.

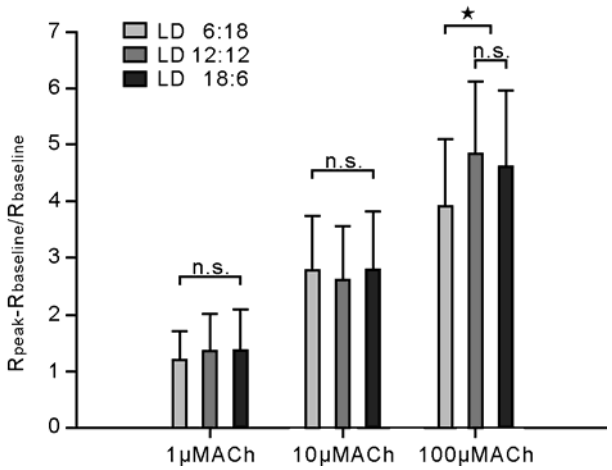

Figure 4. Normalized amplitudes (R_{peak}-$R_{baseline}$/$R_{baseline}$) of the Ca^{2+} responses to acetylcholine (ACh) applications of cultured accessory medulla (aMe) cell cultures from cockroach rearing in different photoperiods: light/dark (LD) 6:18, 12:12 or 18:6. The intracellular Ca^{2+} responses to 1μM and 10μM ACh application showed no significant difference among the 3 experimental groups. The cultured aMe cells from cockroaches raised in LD 12:12 or 18:6 cycles showed a significant greater increase in intracellular Ca^{2+} levels after 100μM ACh application as compared to those under LD 6:18 (ANOVA LSD $p<0.05$).

Discussion

To determine whether ionic mechanisms of cultured circadian pacemaker neurons are sensitive to photoperiod, the spontaneous activity changes of cultured aMe neurons from cockroaches raised in different photoperiods were investigated in response to increases in the $[Ca^{2+}]_{extra}$. The type-percentage vectors obtained from 7 responses types of active aMe neurons in the same cockroach were analyzed. It was found that this type-percentage vector is highly photoperiod-specific and reproducible. So far, comparison of the ACh effect on all tested aMe cells did not provide evidences for the change of ACh-sensitivity of cultured aMe cells by photoperiods. Future experiments will analyse which molecular mechanisms underlie photoperiod-dependent plasticity in the circadian system and whether it is induced transiently also in the adults.

The dual oscillator system and its adaptation to different photoperiods

The fruit fly *Drosophila melanogaster* expresses two locomotor activity peaks controlled via circadian oscillators, one anticipating lights-on in the morning and one anticipating lights-off in the evening. They are suggested to be controlled by a dual circadian oscillator system consisting of a morning oscillator (M-cells) and an evening oscillator (E-cells) which allows for adaptation to changing photoperiods (Pittendrigh and Daan 1976; Helfrich-Förster 2009; review Yoshii et al. 2012). The two separate oscillators respond differently to light and control the phase-relationship of the two daily locomotor activity peaks. The M-oscillator is advanced (accelerated, activated)

by light at dawn, thus expressing a short period. This oscillator controls the locomotor activity peak in the morning. The E-oscillator is delayed by light at dusk (decelerated, inhibited), thus expressing a longer period. It controls the phase (the onset) of the locomotor activity peak in the evening. Genetic manipulations combined with locomotor activity assays and immunocytochemical analysis identified the cellular nature of the respective oscillators in *D. melanogaster.* It was suggested that the M cells of the fruitfly are 4 small ventrolateral neurons (s-LNv) and CRYPTOCHROME (CRY)-positive neurons in posterior dorsal neuron group1 (DN_{1p}s) The E cells are three CRY-positive dorsal lateral neurons (LNd), the 5^{th} s-LNv and the CRY-negative DN_{1p}s. (Grima et al., 2004; Rieger et al., 2006; Stoleru et al., 2007; Helfrich-Förster, 2009; Sheeba et al., 2008; Yoshii et al., 2012). Under short photoperiods or in DD the M cells dominate and determine the phases of M- and E-dependent locomotor activity peaks. In contrast, under long photoperiods or LL the E cells control the phases of both peaks (Stoleru et al., 2007; review: Yoshii et al. 2012). However, newer data suggest that there are not necessarily specific M- and E-oscillator neurons but external stimuli may recruit overlapping cell groups either into M- or E-oscillators (review: Yoshii et al., 2012).

The role of ACh in light entrainment pathways to the insect circadian clock

The molecular mechanisms how light might recruit M- and E- circadian oscillators and how different photoperiods shape the insect circadian system remain largely unknown. However, various light entrainment pathways to circadian clock neurons are well established in *D. melanogaster*, while they are less defined in the Madeira cockroach (Rieger et al. 2003; Homberg et al. 2003). In the fruitfly entrainment via high light intensities and entrainment to short photoperiods requires the blue light photopigment cryptochrome (CRY), which is present in most circadian oscillator cells (Emery et al., 2000a,b; Rieger et al. 2003). Entrainment via lower light intensities and to very long- and short photoperiods appears to be signaled via the compound eye (Konopka et al., 1989; Helfrich-Förster et al., 2001; Rieger et al. 2003). Furthermore, Potdar and Sheeba (2012) suggested that the light-sensitive lLNvs enable flies to adjust to different photoperiods via maintaining the phase relationships between M and E-oscillators, possibly via direct connections to the sLNvs. In the blowfly *Protophormia terraenovae*, Shiga and Numata (2009) showed that s-LNvs themselves are necessary for photoperiodism, but it is not known whether they are directly light-sensitive. On the other hand, Saunders (2010) suggested that the photoperiodic clock and the circadian clock work in cooperation under control of TIMELESS, but they are physically separated and, thus, may not be located to light-sensitive sLNvs. Acetylcholine is the neurotransmitter of the larval Hofbauer-Buchner eyelet which brings light input into the larval circadian pacemaker center in the aMe of the fruitfly apparently contacting sLNvs directly (Wegener et al., 2004; Rieger et al., 2003; Veleri etal., 2007). Lelito and Shafer (2012) demonstrated excitatory responses of s-LNvs to acetycholine (ACh) via nicotinic receptors.

In the Madeira cockroach, light information is transmitted indirectly via interneurons from the photoreceptors to the aMe, because no direct inputs from histaminergic ommatidial photoreceptors into the aMe have been detected (Loesel and Homberg, 1999). The GABA-ir distal tract is a good candidate for the ipsilateral light entrainment pathway into the aMe, which occurs through suggested cholinergic excitatory interneurons (Reischig and Stengl 1996; Loesel and Homberg 2001). The excitatory effect of ACh on the circadian pacemaker neurons have been observed in most of the aMe cells (Baz, Wei and Stengl, submitted). Therefore ACh is suggested to be a prominent neurotransmitter of the light entrainment pathway and be involved in relaying the different photoperiodic information. Unfortunately, At the ACh concentrations tested, no evidences for a change in ACh-sensitivity of cultured aMe cells by photoperiods was detected. Although comparison of the ACh effect on all pooled aMe cells did not show any obvious difference between experimental groups, it could not be excluded that ACh could relay photoperiodic information only to a small group of cells which was overlooked via pooling all physiological response types. Other neurotransmitters, such as glutamate or GABA need to be tested in the future.

The role of light in the spontaneous activity-dependent temporal encoding in the circadian clock of the Madeira cockroach

The spontaneous Ca^{2+} activity in the cockroach circadian pacemakers accompany tetrodotoxin (TTX) blockable spontaneous action potentials (Wei and Stengl, 2012). They are prerequisite for temporal enconding, apparently also peptide-dependent assembly formation and the circadian behavioral and physiological rhythms (Schneider and Stengl 2005). It is still under debate whether and how electrical activity of the plasma membrane is coupled to circadian clock gene expression in the nucleus (Nitabach et al., 2005; Sheeba et al., 2008; Folge et al., 2011; Depetris-Chauvin et al., 2011). However, evidence is accumulating that electrical activity of circadian pacemaker neurons in not just an output of the molecular clockwork but is intricately connected in many feed-back circuits with clock gene rhythms and also with light-inputs. For example, Folge et al. (2011) showed that light-dependent excitation of large ventral lateral circadian clock neurons (l-LNvs) in *Drosophila* is mediated by potassium channels via the blue-light sensor CRYPTOCHROME (CRY). In addition, light regulates the degradation of the clock protein TIMELESS (TIM) via circadian CRY-TIM interactions (Tomioka and Matsumoto, 2010; Peschel and Helfrich-Förster, 2011). Several studies showed that TIM plays a key role not only in the circadian clock system, but also in the photoperiodic clock system (Goto and Denlinger, 2002; Shafer et al., 2004; Pavelka et al., 2003). In the flies, *Sarcophaga crassipalpis* and *Drosophila*, under long-day conditions, the mRNA or protein levels of *tim* are significantly lower than those measured under short-day conditions. Here, we showed that spontaneous activity with the corresponding ionic mechanisms of the aMe cells is dependent on the $[Ca^{2+}]_{extra}$. Seven different physiological aMe cell types could be distinguished and regulated by LD regimes. Therefore, we suggested that the photoperiod could affect the ion channel

composition of the cultured cockroach circadian pacemaker neurons.

The role of circadian pacemaker neurons in the photoperiodic clock system

Several models suggest the insect circadian pacemaker neurons are involved in the photoperiodic clock system controlling the insect photoperiodism (review: Vladimir, 2011). In the blow fly *Protophormia terraenovae*, Shiga and Numata (2009) showed the circadian clock PDF-ir s-LNvs are a component for the photoperiodic clock. In recent years, amply evidence suggests the circadian and photoperiodic system have the same output effectors: the neurosecretory cells in the *pars intercerebralis* (PI) and *pars lateralis* (PL) releasing various neurotransmitters and neuropeptides. Several studies showed the synthesis and release of insect hormones are strongly under circadian control (Hamanaka et al., 2005; Jackson et al., 2001; Zhao and Zera, 2004; Vafopoulou and Steel, 1996, 2009; Vafopoulou et al., 2007, 2010). Our previous study showed the photoperiod can regulate the number and branching patthern of PDF-ir aPDFMes in the cockroach brain, which play a key role as input to and outputs of the circadian clock system (Wei and Stengl, 2011). Here, the study presents, for the first time, some evidence that physiological responses of circadian pacemaker neurons are photoperiod sensitive. The synaptic connections between the circadian pacemaker neurons and the PI or PL in the cockroach brain, remains to be examined further. These results, together with the results of our previous anatomical studies, show raising Madeira cockroach *R. maderae* in different photoperiods changes the neuronal anatomy as well as the physiology of circadian pacemaker neurons. Our data suggest the circadian pacemaker system could serve as component of the photoperiodic clock, and has the plasticity and potential to allow for physiological adaptations to different photoperiods.

References

Baz ES, Wei HY, Grosshans J, and Stengl M (2012) Calcium responses of circadian pacemaker neurons of the cockroach Rhyparobia maderae to acetylcholine and histamine. J Exp Biol, submitted.

Bradshaw WE and Holzapfel CM (2010) What Season Is It Anyway? Circadian Tracking vs. Photoperiodic Anticipation in Insects. J Biol Rhythms 25:155-165.

Depetris-Chauvin A, Berni J, Aranovich EJ, Muraro NI, Beckwith EJ, and Ceriani MF (2011) Adult-specific electrical silencing of pacemaker neurons uncouples molecular clock from circadian outputs. Curr Biol 21: 1783-1793.

Emery P, Stanewsky R, Hall JC, and Rosbash M (2000a) *Drosophila* cryptochromes: A unique circadian-rhythm photoreceptor. Nature 404: 456–457.

Emery P, Stanewsky R, Helfrich-Förster C, Emery-Le M, Hall JC, and Rosbash M (2000b) *Drosophila* CRY is a deep brain circadian photoreceptor. Neuron 26: 493–504.

Fogle KJ, Parson KG, Dahm NA, and Holmes TC (2011) Cryptochrome is a blue-light sensor that regulates neuronal firing rate. Science 331: 1409-1413.

Goto SS and Denlinger DL (2002) Short-day and long-day expression patterns of genes involved in the

flesh fly clock mechanism: period, timeless, cycle and cryptochrome. J Insect Physiol 48: 803–816.

Grima B, Chelot E, Xia R, and Rouyer F (2004) Morning and evening peaks of activity rely on different clock neurons of the Drosophila brain. Nature 431, 869–873.

Hamanaka Y, Yasuyama K, Numata H, and Shiga S (2005) Synaptic connections between pigment-dispersing factor-immunoreactive neurons and neurons in the pars lateralis of the blow fly Protophormia terranovae. J Comp Neurol 491: 390–399.

Helfrich-Förster C (2009) Does the morning and evening oscillator model fit better for flies or mice? J Biol Rhythms 24: 259–270.

Helfrich-Förster C, Winter C, Hofbauer A, Hall JC, and Stanewsky R (2001) The circadian clock of fruit flies is blind after elimination of all known photoreceptors. Neuron 30:249-261.

Homberg U, Reischig T, and Stengl M (2003) Neural organization of the circadian system of the cockroach *Leucophaea maderae*. Chronobiol Int 20, 577-590.

Hong S, Ratté S, Prescott SA, and De Schutter E (2012) Single neuron firing properties impact corrlation-based population coding. J Neurosci 32(4): 1413-1428.

Jackson FR, Schroeder AJ, Roberts MA, McNeil GP, Kume K, and Akten B (2001) Cellular and molecular mechanisms of circadian control in insects. J Insect Physiol 47: 833–842.

Konopka RJ, Pittendrigh C, and Orr D (1989) Reciprocal behaviour associated with altered homeostasis and photosensitivity of *Drosophila* clock mutants. J Neurogenet 6:1-10.

Lelito KR and Shafer OT (2012) Reciprocal Cholinergic and GABAergic Modulation of the Small Ventrolateral Pacemaker Neurons of Drosophila's Circadian Clock Neuron Network. J Neurophysiol 107: 2096-2108.

Loesel R and Homberg U (1999) Histamine-immunoreactive neurons in the brain of the cockroach *Leucophaea maderae*. Brain Res 842: 408-418.

Loesel R and Homberg U (2001) Anatomy and physiology of neurons with processes in the accessory medulla of the cockroach *Leucophaea maderae*. J Comp Neurol 439, 193-207.

Nadasdy Z (2010) Binding by asynchrony: the neuronal phase code. Front Neurosci 4**:** 51.

Nishiitsutsuji-Uwo J and Pittendrigh CS (1968) Central nervous system control of circadian rhythmicity in the cockroach: III. The optic lobes, locus of the driving oscillation? Zeitschrift für vergleichende Physiologie 58: 14-46.

Nitabach MN, Sheeba V, Vera DA, Blau J, and Holmes TC (2005) Membrane electrical excitability is necessary for the free-running larval *Drosophila* circadian clock. J Neurobiol 62: 1–13.

Page TL (1978) Interactions between bilaterally paired components of the cockroach circadian system. J Comp Physiol A 124, 225-236.

Page TL (1982) Transplantation of the cockroach circadian pacemaker. Science 216, 73-75.

Pavelka J, Shimada K, and Kostal V (2003) TIMELESS: a link between fly's circadian and photoperiodic clocks? Eur J Entomol 100: 255–265.

Peschel N and Helfrich-Förster C (2011) Setting the clock by nature: circadian rhythm in the fruitfly *Drosophila melanogaster*. FEBS Lett 585: 1435-1442.

Petri B and Stengl M (1999) Presumptive insect circadian pacemakers in vitro: immunocytochemical characterization of cultured pigment-dispersing hormone-immunoreactive neurons of *Leucophaea maderae*. Cell Tissue Res 296: 635-643.

Petri B, Stengl M, Würden S, and Homberg U (1995) Immunocytochemical characterization of the accessory medulla in the cockroach *Leucophaea maderae*. Cell Tissue Res 282: 3-19.

Pittendrigh CS and Daan S (1976) A functional analysis of circadian pacemakers in nocturnal rodents V. Pacemaker structure: a clock for all seasons. J Comp Physiol 106: 333–355.

Potdar S and Sheeba V (2012) Large Ventral Lateral Neurons Determine the Phase of Evening Activity Peak across Photoperiods in *Drosophila melanogaster.* J Biol Rhythms 27: 267-279.

Reischig T and Stengl M (1996) Morphology and pigment-dispersing hormone (PDH)-immunocytochemistry of the accessory medulla, the presumptive circadian pacemaker of the cockroach *Leucophaea maderae*: a light- and electron-microscopical study. Cell Tissue Res 255, 305-319.

Reischig T and Stengl M (2003a) Ectopic transplantation of the accessory medulla restores circadian locomotor rhythms in arrhythmic cockroaches (*Leucophaea maderae*). J Exp Biol 206:1877-1886.

Reischig T and Stengl M (2003b) Ultrastructure of pigment-dispersing hormone-immunoreactive neurons in a three-dimensional model of the accessory medulla of the cockroach *Leucophaea maderae*. Cell Tissue Res 314:421-435.

Rieger D, Shafer OT, Tomioka K, and Helfrich-Förster C (2006) Functional analysis of circadian pacemaker neurons in *Drosophila melanogaster*. J Neurosci 26: 2531–2543.

Rieger D, Stanewsky R, and Helfrich-Förster C (2003) Cryptochrome, compound eyes, Hofbauer-Buchner eyelets, and ocelli play different roles in the entrainment and masking pathway of the locomotor activity rhythm in the fruit fly *Drosophila melanogaster*. J Biol Rhythms 18: 377–391.

Saunders DS (2010) Controversial aspects of photoperiodism in insects and mites. J Insect Physiol 56: 1491–1502.

Schneider NL and Stengl M (2005) Pigment-dispersing factor and GABA synchronize cells of the isolated circadian clock of the cockroach *Leucophaea maderae*. J Neurosci 25: 5138-5147.

Schneider NL and Stengl M (2006) Gap junctions between accessory medulla neurons appear to synchronize circadian clock cells of the cockroach *Leucophaea maderae*. J Neurophysiol 95: 1996-2002.

Schneider NL and Stengl M (2007) Extracellular long-term recordings of the isolated accessory medulla, the circadian pacemaker center of the cockroach *Leucophaea maderae*, reveal ultradian and hint circadian rhythms. J Comp Physiol A 193: 35-42.

Shafer OT, Levine JD, Truman JW and Hall JC (2004) Flies by night: effects of changing day length on Drosophila's circadian clock. Curr Biol 14: 424–432.

Sheeba V, Gu H, Sharma VK, O'Dowd DK, and Holmes TC (2008) Circadian- and light-dependent regulation of resting membrane potential and spontaneous action potential firing of *Drosophila* circadian pacemaker neurons. J Neurophysiol 99: 976-988.

Shiga S and Numata H (2009) Roles of PER immunoreactive neurons in circadian rhythms and photoperiodism in the blow fly, *Protophormia terraenovae*. J Exp Biol 212: 867-877.

Singer W and Gray CM (1995) Visual feature integration and the temporal correlation hypothesis. Annu Rev Neurosci 18: 555-586.

Soehler S, Neupert S, Predel R, Nichols R, and Stengl M (2007) Localization of leucomyosuppressin in the brain and circadian clock of the cockroach Leucophaea maderae. Cell Tissue Res 328: 443-452.

Soehler S, Neupert S, Predel R, and Stengl M (2008) Examination of the role of FMRFamide-related peptides in the circadian clock of the cockroach Leucophaea maderae. Cell Tissue Res 332: 257-269.

Soehler S, Stengl M, and Reischig T (2011) Circadian pacemaker coupling by multi-peptidergic neurons in the cockroach Leucophaea maderae. Cell Tissue Res 343: 559-577.

Stengl M and Homberg U (1994) Pigment-dispersing hormone-immunoreactive neurons in the cockroach

Leucophaea maderae share properties with circadian pacemaker neurons. J Comp Physiol A 175: 203-213.

Stoleru D, Nawathean P, Paz Fernandez M, de la Menet JS, Ceriani MF, and Rosbach M (2007) The Drosophila circadian network is a seasonal timer. Cell 129: 207–219.

Tomioka K and Matsumoto A (2010) A comparative view of insect circadian clock systems. Cell Mol Life Sci 67: 1397-1406.

Vafopoulou X and Steel CGH (1996) The insect neuropeptide prothoracicotropic hormone is released with a daily rhythm: re-evaluation of its role in development. Proc Natl Acad Sci USA 93: 3368–3372.

Vafopoulou X and Steel CGH (2009) Circadian organization of the endocrine system. In: Gilbert, L.I. (Ed.), Insect Development. Elsevier, Oxford, pp. 395–458.

Vafopoulou X, Steel CGH, and Terry KL (2007) Neuroanatomical relations of prothoracicotropic hormone neurons with the circadian timekeeping system in the brain of larval and adult Rhodnius prolixus (Hemiptera). J Comp Neurol 503: 511–524.

Vafopoulou X, Terry KL, and Steel CGH (2010) The circadian timing system in the brain of the fifth larval instar of Rhodnius prolixus (Hemiptera). J Comp Neurol 518: 1264–1282.

Veleri S, Rieger D, Helfrich-Förster C, and Stanewsky R (2007) Hofbauer-Buchner eyelet affects circadian photosensitivity and coordinates TIM and PER expression in *Drosophila* clock neurons. J Biol Rhythms 22: 29-42.

Vladimir K (2011) Insect photoperiodic calendar and circadian clock: independence, cooperation or unity? J Insect Physiol 57: 538-556.

Wegener C, Hamasaka Y, and Nässel DR (2004) Acetylcholine increases intracellular Ca2+ via nicotinic receptors in cultured PDF-containing clock neurons of Drosophila. J Neurophysiol 91: 912–923.

Wei H and Stengl M (2011) Light affects the branching pattern of peptidergic circadian pacemaker neurons in the brain of the cockroach Leucophaea maderae. J Biol Rhythms 26: 507–517.

Wei H and Stengl M (2012) Ca^{2+}-dependent ion channels underlying spontaneous activity in insect circadian pacemaker neurons. Eur J Neurosci. doi: 10.1111/j.1460-9568.2012.08227.x.

Yoshii T, Rieger D, and Helfrich-Förster C (2012) Two clocks in the brain – an update of the Morning and Evening oscillator model in *Drosophila.* Prog Brain Res 199: 59-82.

Zhao Z and Zera AJ (2004) The hemolymph JH titer exhibits a large-amplitude. morph-dependent, daily cycle in the wing-polymorphic cricket *Gryllus firmus*. J Insect Physiol 49: 137–148.

Chapter VI

Influence of the surface termination of ultrananocrystalline diamond/amorphous carbon composite films on their interaction with neurons

Voss A, Wei HY, Müller C, Popov C, Kulisch W, Ceccone G, Ziegler C, Stengl M, and Reithmaier JP. 2012.
This manuscript is published in Diamond and Related Materials 26: 60-65.

Diamond & Related Materials 26 (2012) 60–65

Contents lists available at SciVerse ScienceDirect

Diamond & Related Materials

journal homepage: www.elsevier.com/locate/diamond

Influence of the surface termination of ultrananocrystalline diamond/amorphous carbon composite films on their interaction with neurons ☆,☆☆

A. Voss [a], H. Wei [b], C. Müller [c], C. Popov [a], W. Kulisch [a,*], G. Ceccone [d], C. Ziegler [c], M. Stengl [b], J.P. Reithmaier [a]

[a] Institute of Nanostructure Technologies and Analytics, Center of Interdisciplinary Nanostructure Science and Technology (CINSaT), University of Kassel, Germany
[b] Department of Animal Physiology, Center of Interdisciplinary Nanostructure Science and Technology (CINSaT), University of Kassel, Germany
[c] Department of Physics and Research Center OPTIMAS, University of Kaiserslautern, Germany
[d] European Commission Joint Research Centre, Institute for Health and Consumer Protection, Ispra, Italy

ARTICLE INFO

Article history:
Received 16 September 2011
Received in revised form 14 April 2012
Accepted 17 April 2012
Available online 26 April 2012

Keywords:
Ultrananocrystalline diamond
Surface modification
Zeta-potential measurements
Surface cell interaction

ABSTRACT

Ultrananocrystalline diamond (UNCD) films have been deposited by microwave plasma chemical vapor deposition from 17% CH_4/N_2 mixtures. In order to change the original hydrogen termination of the UNCD surfaces, the films have subsequently been subjected either to the so-called UV/O_3 treatment which leads to OH-terminated surfaces, or to NH_3/N_2 plasmas which introduces NH_2 groups but also a certain amount of OH groups. These three types of surfaces have been characterized by X-ray photoelectron spectroscopy, contact angle and ζ-potential measurements. The contact angle measurements have shown that as-grown UNCD surfaces are highly hydrophobic but became highly hydrophilic after both treatments. The ζ-potential measurements revealed that the isoelectric point of the H-terminated as-grown surface is distinctively higher than that of either UV/O_3 or NH_3/N_2 plasma treated surfaces. Finally, the interactions of these surfaces with neurons of the cockroach *Leucophaea maderae* have been investigated. These studies have shown that especially the two treated surfaces allow for a fast, strong attachment of these cells without compromising their viability and without changing their normal physiological responses. These results will be discussed in terms of those obtained with the different surface characterization techniques.

1. Introduction

In recent times, diamond has attracted considerable interest as a material for applications in biology, biotechnology, and biomedicine [1–3]. This is, on the one hand, due to the outstanding biological properties of diamond. It is composed solely of carbon, the building element of biological structures; furthermore it is biocompatible [4] and, at least at low temperatures, chemically extremely stable [5,6]. On the other hand, it possesses quite a number of outstanding mechanical, vibrational, optical and electrical properties [7,8] which can be utilized in biological devices and sensors [1,2].

Diamond can be deposited in form of thin films by a number of deposition techniques on a great variety of substrate materials [9]. However, depending on the deposition conditions and the substrate, quite a number of different diamond materials can be obtained [10]. The span reaches from single crystalline over polycrystalline and nanocrystalline to ultrananocrystalline diamond films [11,12]. The latter possess the advantage of rather smooth surfaces as compared e.g. to PCD and NCD films while retaining to a large extent the extreme properties of diamond [11,13].

In most cases either hydrogen or oxygen terminated surfaces are used as a starting point for further processing towards biotechnological and biomedical applications [2,3]. As-grown films are hydrogen terminated while oxygen termination can easily be achieved by plasma or photochemical processes [2,3,14]. Both terminations can be achieved with a great cleanliness on different diamond surfaces such as single crystals, PCD and NCD films. Our previous investigations have shown that this also holds for UNCD films [14]. From a chemical, but also from a surface electrical point of view also NH_2 terminating surface groups are of interest [15,16]. But the techniques employed hitherto to reach such a termination suffer from a common problem: All techniques are able to remove the initial terminating hydrogen atoms but their place is not only occupied by NH_2 groups but also by oxygen containing species (most probably

☆ Prime novelty statement: The influence of the surface termination of ultrananocrystalline diamond films on their interaction with neuronal cells has been investigated.

☆☆ Authorship statement: The submission of the manuscript has been approved by all co-authors. This manuscript has not been published nor is it currently being considered for publication in any other journal.

* Corresponding author at: Institute of Nanostructure Technologies and Analytics, University of Kassel, Heinrich-Plett Str. 40, 34132 Kassel, Germany. Tel.: +49 561 804 4205.
E-mail address: wilhelm.kulisch@yahoo.de (W. Kulisch).

0925-9635/$ – see front matter © 2012 Elsevier B.V. All rights reserved.
doi:10.1016/j.diamond.2012.04.005

OH) [15–18] although these processes have been performed in nominal oxygen-free ambients. The ratios N/O reported are on the order of unity.

In previous publications [14,19,20] we have shown that UNCD surfaces can be modified to bear H, OH, and F functional groups by means of plasma processes and the so-called UV/O_3 treatment. Recently, NH_3/N_2 plasmas have been employed to attach NH_2 functional groups to the UNCD surface [21].

The aim of the present study was a comparison of the interaction of three types of these surfaces, namely H-, OH- and NH_2-terminated surfaces with neuronal cells, after a thorough characterization of these surfaces in view of their composition, hydrophobicity, and electrical properties. There are already a number of papers in the literature on neuron adhesion on different types of diamond [6,22–25]. It has been shown [24,26] that cell adhesion is the better the smaller the crystallite size. This makes an investigation of UNCD films with even smaller crystallite sizes promising. The question of surface termination has also been addressed [24,25] but aminated surfaces have not been investigated hitherto.

2. Experimental details

2.1. UNCD film deposition and properties

The UNCD samples used in this study have been prepared by means of microwave plasma chemical vapor deposition (MWCVD). Details of this process have been published previously [11,27]. The major process parameters were as follows: The gas mixture was 17% CH_4/N_2, the MW power 800 W, the working pressure 2.2 kPa, and the total gas flow 300 sccm.

Prior to the deposition, the 3 inch (100) Si wafers used as substrates were subjected to an ultrasonic pre-treatment for 1 h in a suspension of 80 mg ultradispersive diamond (UDD, grain size 3–5 nm) and 50 mg nanocrystalline diamond powder (NCD, 250 nm) in 75 ml n-pentane in order to enhance the nucleation density. The nucleation density obtained by this process was about 1×10^{10} cm^{-2} [28].

The bulk properties of these UNCD films have been studied thoroughly in a number of investigations; the major results—as far as they are of importance for the present study—can be summarized as follows [11,29,30]: The films consist of diamond nanocrystallites of 3–5 nm diameter; they are embedded in an amorphous carbon matrix of 1–1.5 nm width with a volume ratio of the two components of almost unity. The bulk films are composed mostly of carbon; the concentration of nitrogen and oxygen is below 1 at % each. The hydrogen content is about 8 at % in the film bulk but 12–14 at % at the surface of the films [31]. The biocompatibility of this type of UNCD films has been previously proven for four different types of cells [14].

2.2. Surface modification

Two processes have been used to modify the surface termination of these UNCD films which are hydrogen terminated after the growth [14]: i) the so-called UV/O_3 treatment [20] and ii) NH_3/N_2 plasmas. For the UV/O_3 treatment, the surfaces were exposed to the UV light of a 600 W mercury lamp (BHK, Claremont, CA; major emissions a.o. at 185 and 253.7 nm) at normal pressure in air. The size of the lamp was 12.5 cm × 12.5 cm, the distance between lamp and sample 4 cm.

A new process has been employed to attach NH_2 groups to UNCD surfaces. In our previous work, a NH_3/N_2 rf plasma has been used [21]. In the present study an inductively-coupled NH_3/N_2 plasma (ICP) was employed. The process parameters were as follows: gas flows 5 sccm NH_3 and 100 sccm N_2; pressure $1.8–2\times10^{-2}$ mbar; ICP power 150 W.

2.3. Surface characterization

X-ray photoelectron spectroscopy has been used to study the composition of the surfaces and to investigate their bonding environment. An Axis Ultra spectrometer (Kratos Analytical Ltd., UK) with a monochromatic Al K_α source was used for these measurements. The area of the analyses was 400×700 μm^2. Pass energies of 160 eV and 20 eV were used for the survey and core level spectra, respectively. A filament (I = 1.9 A, V = 3.2 V) inserted in the magnetic lens system acts as neutralizer for surface charge compensation. All core level spectra were shifted to a common binding energy of the hydrocarbon component of the C1s spectra of 285.0 eV.

2.4. Contact angle measurements

The contact angles were determined by a CAM 100 Contact Angle Meter (KSV Instruments). A drop of purified water of about 1 µl was deposited on the sample surface by a Hamilton syringe. After that the software of the device approximated the drop shape by adjusting the parameters of the Young–Laplace equation and calculated the left and right contact angles. For each sample at least four values were measured. In the following, only the arithmetic mean and the standard deviation were given.

2.5. Zeta-potential measurements

In order to determine the ζ-potential as a function of the pH value, two samples (size 20 mm × 10 mm) of the surface to be investigated were arranged plan-parallel in the cell by means of double-sided gluing tape and then exposed to a lateral flow of a 1 mM potassium chloride (KCl) solution under defined pressure conditions. In order to vary the pH value either 0.1 M HCl or 0.1 M NaOH was titrated to the solution. For each pH value, four measurements were performed with the flow direction changing after each of them. The two surfaces form a channel of small width (about 200 µm in the present study) (Fig. 1). The fluid flows through this channel and creates the pressure difference required. The instrument used for these measurements was the electrokinetic Analyzer EKA (Anton Paar, Austria). The software "Visiolab" was used to control the measurements and to evaluate them. The electrolyte is pumped with constantly increasing pressure through the gap while the streaming potential U is measured. The change of the streaming potential with increasing pressure dU/dp is proportional to the zeta-potential. The curves obtained were averaged and converted into ζ/pH plots. The errors given are the standard deviations. The zero of the zeta-potential as a function of pH determines the point of zero charge (PZC, also called isoelectric point IEP): the net charge is zero. On the left side of the PZC the surface carries a positive, on the right a negative charge.

2.6. Neuron cell culture, calcium imaging and neuronal viability tests

Primary cell cultures were obtained from the circadian pacemaker center, i.e. the accessory medulla, of adult males of the cockroach *Leucophaea maderae*. They were generated at Zeitgebertime ZT1:00 from cockroaches kept under 12:12 h light:dark cycles in own rearing facilities [32]. Excised accessory medullae with at least 250 associated neurons were dissociated into single cells according to established protocols [33]. The cell suspension was plated either on concanavalin

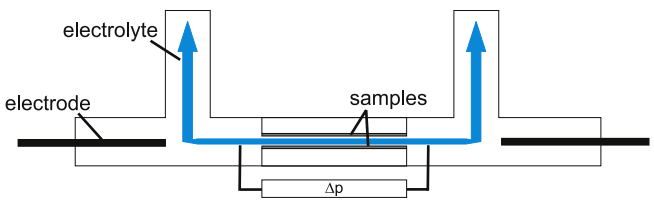

Fig. 1. Sketch of the experimental set-up for the measurement of the ζ-potential.

A (ConA, Sigma) coated glass cover slips kept in a sterile plastic cell culture dish (control, number of samples n = 16) or on NH_3/N_2 plasma (n = 14), UV/O_3 treated (n = 16), or on as-grown (n = 7) UNCD surfaces without any additional cell adhesion molecules. The cells were allowed to settle to the respective surfaces for about 20 min in a humidified incubator at 20° in constant darkness, before adding 1 ml cell culture medium. This cell culture medium was prepared from Leibovitz's L-15 medium (L-15) (PAA Laboratories Germany) and additional salts: 200 mg/ml glucose, 80 mg/ml fructose, 35 mg/ml L-prolin, 6 mg/ml imidazol, 1% glutamin, 0.1% gentamicin, and 2.38 mg/ml HEPES. A pH of 7.0 and an osmolarity of 360 mOsm were adjusted with 5% NaOH and mannitol.

About 24 h after the plating, cell adhesion and viability were evaluated by means of a live cell calcium imaging system (Ca^{2+}-imaging). The cells were loaded with 4 μM Fura-2 acetoxymethyl ester (Fura-2 AM, Molecular Probes) for 40 min at room temperature. The different types of surfaces with cells were transferred to a recording chamber, washed and incubated with a standard extracellular Ringer solution: (in mM) 156 NaCl, 4 KCl, 1 $CaCl_2$, 10 HEPES and 5 glucose (pH 7.1, osmolarity 380 mOsm). The recordings were carried out using a Ca^{2+}-imaging system (Till-Photonics, with an Examiner D1 microscope, 20× objective W N-Achroplan, NA 1.0, Zeiss, Germany). Two sets of fluorescence images were taken with a CCD camera (Andor 885) while switching the excitation light wavelength between 340 nm and 380 nm with 400 ms intervals from a monochromator (Polychrome 5000, Till-Photonics). The Fura-2 fluorescence ratio $R = F_{340}/F_{380}$ of cell bodies was measured. The fluorescence ratio in the imaging data was calculated using a Till-Photonics Software (TILLvisION 4.0). The autofluorescence of the background was subtracted from each image before calculation of the ratio.

The cell adhesion was evaluated by counting the number of attached cells in a defined area ($7\times10^4\,\mu m^2$) for each sample. During the viability-test, the intracellular Ca^{2+} concentration change in response to a 5 s pulse of 60 mM KCl extracellular solution introduced with a pump was expressed as percentage of the baseline ($\Delta R/R_{baseline}\times100\%$). To evaluate the electrical activity of the neurons, we observed the percentage of cells displaying spontaneous oscillations of the intracellular Ca^{2+} concentration.

All data are expressed as mean ± standard deviation. One-way analysis of variance (ANOVA) was performed to compare the neurons cultured on the control glass cover slips coated with ConA with neurons on as-grown as well as NH_3/N_2 plasma and UV/O_3 treated UNCD surfaces. All statistical studies were performed by using SPSS 13.0.

3. Results and discussion

3.1. Surface composition

The surface composition of the three types of UNCD films investigated in this study as revealed by XPS are summarized in Table 1. This table yields the following results: i) The as-grown surface is extremely clean. ii) The contents of oxygen and nitrogen are close to those observed for the film bulk; iii) As compared to the as-grown film, the oxygen content of the UV/O_3 treated surface has risen to about 8 at %. This is in good agreement with data obtained in a different UV/O_3 set-up [19]. But it has to be mentioned that with a direct O_2 MW plasma treatment even higher surface oxygen concentrations of up to 12 at % have been achieved [19]; iv) The surface composition of the NH_3/N_2 plasma treated surface contains about 5 at % nitrogen but also a slightly larger fraction of oxygen. This is in agreement with all literature data: It is possible to attach NH_2 groups to diamond surfaces but there is always a competition with the attachment of oxygen [15–17,21]. In a number of experiments we have observed that the atomic surface ratio of nitrogen and oxygen is always close to unity. Up to now, it was not possible to identify an optimum set of parameters to achieve a nitrogen concentration as high as possible. Most probably the scenario is as follows: During the NH_3/N_2 plasma treatment, the original H-termination is removed. Whether OH- or NH_2-groups occupy the dangling surface bonds, depends on the percentage or NH_x and oxygen species in the plasma. As the process is carried out nominally oxygen-free, hardly controllable parameters such as the water coverage of the chamber walls come into play. This is, as has already been pointed out, the common problem of all techniques to directly attach NH_2-groups to diamond surfaces.

In a further experiment it was investigated whether the oxygen content of the aminated surfaces is due to storage in air rather than to oxygenation during the process itself. It turned out that storing in air for two months slightly reduces the nitrogen content at the cost of oxygen from 5.1 to 4.5 at %. This leads us to the conclusion that part of the oxygen stems from the amination process, in agreement with literature [18]. Nevertheless, storage effects also play a role.

From the C 1 s spectra of these samples (not shown graphically) it is evident that both treatments lead to a slight graphitization of the surface as indicated by a small shoulder at 284.0 eV but this is only a minor effect.

Table 1
Surface composition obtained by XPS for the various surface treatments. The errors are ± 0.5% in the case of carbon and ± 0.2% in the case of O and N.

Surface	C	O	N
AG	97.0	2.2	0.8
NP	86.5	6.5	5.1
UV	90.0	8.1	0.7

3.2. Wettability of the surfaces

The contact angle θ_C against purified water of as-grown UNCD films is on the order of 75–85° which means that as-grown films are highly hydrophobic, in agreement with their hydrogen termination. The hydrophobicity of these surfaces can even be enhanced by post-deposition hydrogen microwave plasmas and fluorine containing rf plasmas (contact angles of 90° and >100°, respectively) [19].

The NH_3/N_2 and UV/O_3 treatments used in the present study render the UNCD surfaces completely hydrophilic. This can be seen from Fig. 2 where the contact angles are presented as a function of time for both processes. Both curves show the same principal behavior but there are also pronounced differences. In both cases an initial decrease of the contact angle is observed, followed by a stable plateau.

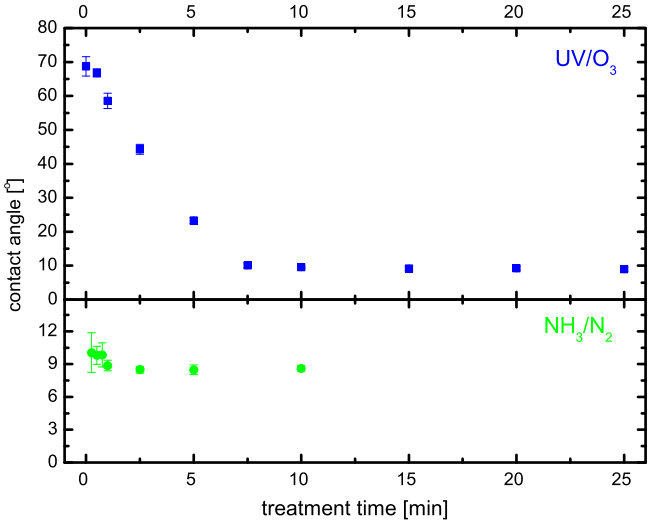

Fig. 2. Contact angles vs time for two different surface treatments: UV/O_3 treatment (top) and NH_3/N_2 plasma (bottom).

The final values are almost identical and hint at a very hydrophilic surface: $\theta_C = 8.5°$ for the NH_3/N_2 plasma treatment and $\theta_C \approx 10°$ for the UV/O_3 treatment. But from Fig. 2 it can also be seen that this final value is already reached after 1.5 min in the case of the NH_3/N_2 plasma but that about 7 min are needed for the UV/O_3 treatment. The treatment times for the samples for the ζ-potential studies and the cell interaction investigations have been chosen to lie in these plateaus.

The surfaces keep their hydrophobic and hydrophilic character, respectively, at least for a couple of months [20].

3.3. Zeta-potential measurements

Fig. 3 shows the results of the ζ-potential measurements performed with the three types of surfaces. For each of them two measurements are presented, one performed with titration with NaOH for the high pH range and one for the low pH region obtained by titration with HCl. Within the errors of these measurements, in each of the three cases the two parts fit together rather well.

The isoelectrical points obtained from these measurements are listed in Table 2, together with literature data. It can be seen that for the as-grown, i.e. hydrogen terminated surface the IEP is 4.0 ± 0.1, which is in rough agreement with the literature data. Here it has also to be taken into account that these literature data stem from a wide variety of diamond materials. These literature data predict a drastical decrease of the isoelectrical point for oxygen or OH-terminated surfaces to values below 2. A decrease of the IEP after the UV/O_3 treatment is indeed observed, but not to such low values as reported by e.g. Chakrapani et al. [34] and Härtl et at. [35]. But if one looks at the surface composition of this sample shown in Table 1 and also at the contact angle presented in Fig. 2, one can conclude that the UV/O_3 process performed in this study was not optimal. The surface oxygen concentration of about 8 at % is lower than the maximum of 12 at % reached by an O_2 microwave plasma. This is in agreement with the contact angles of about 10° as compared to values of about 5° observed after this plasma process.

The IEP of the NH_3/N_2 plasma treated sample is close to that of the UV/O_3 treated surface ($IEP = 3.5 \pm 0.1$). To our knowledge, there are no ζ-potential measurement data on this type of diamond surface in the literature. From the results presented in the previous sections it is evident that the surface is somewhat similar to the UV/O_3 treated sample: The surface is hydrophilic and contains OH-groups. The difference is the presence of NH_2 groups. Anyway, the question of the IEP of a purely NH_2-terminated surface has to remain open at this point.

Table 2
Literature data of isoelectrical points obtained from ζ-potential measurements with diamond surfaces.

Author	Ref	Material	IEP H	IEP O	IEP NH_2
Chakrapani	[34]	Diamond powder	8	1.2	
Härtl	[35]	Single crystalline	3–3.5	<1.5	
Jelinek	[36]	DLC	3.7		
Lee	[37]	Diamond particles	3.2		
This work		UNCD	4 ± 0.1	3.7 ± 0.1	3.5 ± 0.1

3.4. Interactions with neurons

The cockroach *L. maderae*, an established model system of circadian rhythms research, is a highly adaptive species which has survived since the carboniferous period. To analyze the self-organization of physiological processes between circadian pacemaker cells in response to changes in the environment, primary cell cultures of the cockroach circadian pacemaker center were established to allow for interfacing with transistors. When cultured on ConA-covered surfaces [38], the pacemaker neurons show an increase of the spontaneous activity *in vitro* as compared to *in vivo*, an indication for membrane potential shifts in the presence of ConA which appears to cause depolarization. To ensure better physiological conditions, we searched for inert surfaces which in addition allow a fast attachment, support viability and interfacing with engineered transistors.

In the present investigation, in a first step the cell densities on the surfaces were compared against each other: as controls ConA-coated cover slips and samples of the three differently terminated UNCD surfaces. Cell adhesion to the various diamond surfaces is more solid and thus more stable compared to ConA coated glass control with the adhesive protein, as the cells on the diamond surfaces did not detach as easily during exchanges of the extracellular media as those on ConA (not shown graphically). Twenty four hours after plating the cell density (Fig. 4) on as-grown UNCD surfaces did not differ from that on the controls (ANOVA LSD $p > 0.05$). In contrast, the NH_3/N_2 plasma and UV/O_3 treated samples showed a significantly higher cell density than the controls (ANOVA LSD $p < 0.05$), but no significant differences between them were observed (ANOVA LSD $p > 0.05$). This stronger attachment of primary neurons appeared to depend on the hydrophilic properties of the surfaces, which promotes cell adhesion.

To test the viability of the attached circadian pacemaker neurons, the intracellular Ca^{2+} concentration change in response to the addition of a 5 s pulse of 60 mM KCl solution was examined (Fig. 5). The

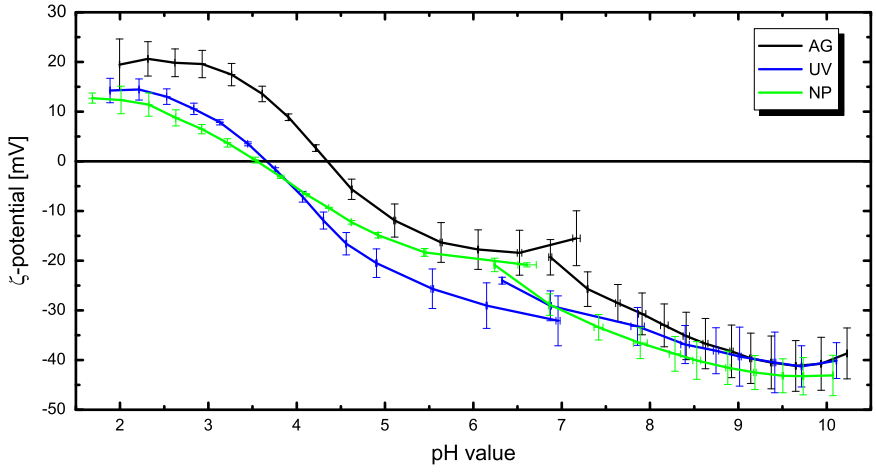

Fig. 3. Results of the ζ-potential measurements for all three surfaces. AG: as grown; UV: UV/O_3 treatment; NP: NH_3/N_2 plasma treatment.

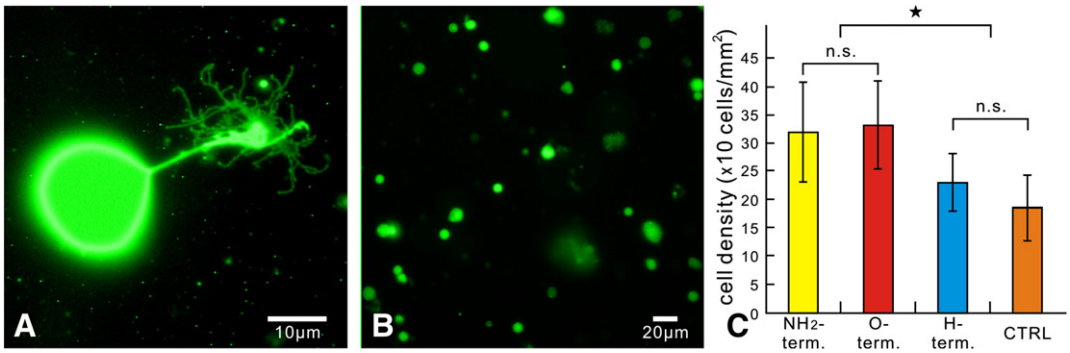

Fig. 4. A,B: Morphology of neurons loaded with calcium indicator Fura-2 grown on a NH_3/N_2 plasma treated surface. C: Cell density at 24 h after plating. The cell densities on NH_3/N_2 and UV/O_3 treated surfaces were significantly higher than the cell densities on as-grown and control surfaces (ANOVA LSD $p<0.05$). n.s. not significant.

high K^+ concentrations depolarize intact cell membranes and promote a voltage-dependent Ca^{2+} influx. Cells which are damaged or dying are already strongly depolarized and do not respond to KCl. The neurons grown on the various UNCD surfaces did not differ significantly from the controls in their responses to KCl stimuli (ANOVA LSD $p>0.05$). Therefore, these diamond surfaces did not interfere with the voltage-dependent, physiological response of the neurons. Instead the diamond structures expressed excellent biocompatibility as they did not compromise the cell viability.

Finally, we examined with Ca^{2+}-imaging whether the spontaneous activity of the circadian pacemaker neurons changes on UNCD surfaces (Fig. 6). Since circadian pacemaker neurons produce spontaneous action potentials, fast voltage-dependent Ca^{2+}-channels are activated which cause fast, transient fluctuations of the intracellular Ca^{2+} concentration. On cover-slips coated with ConA we had noticed that cultured circadian pacemaker neurons appear to be more depolarized than in the brain of intact cockroaches, since they expressed more spontaneous activity *in vitro* as compared to *in situ*. Therefore, we searched for non-organic surfaces which keep the cells more hyperpolarized and decrease the spontaneous activity without deleting it completely. Indeed, the NH_3/N_2 plasma and UV/O_3 treated UNCD surfaces slightly, but significantly decreased the spontaneous activity, as compared to the lectin control, while as-grown UNCD surfaces decreased the spontaneous activity even more strongly than the treated diamond surfaces.

To summarize these observations: The two types of treated diamond surfaces allow for a very fast, strong attachment without compromising the cell viability and without changing the normal physiological responses such as lectins are known to do [39]. Thus, they are preferable compared to the organic surfaces used before but also to as-grown UNCD films on which the cell density was lower and which suppressed the responses of the cells considerably. In future experiments it will be tested whether UNCD films coated on electrodes allow for improved electrical recording of cultured insect neurons to develop bio-sensors on engineered interfaces.

It has already been mentioned that UNCD surfaces are biocompatible, irrespective of their surface termination [14]. This is confirmed by the present study. None of the surfaces investigated are cytotoxic. In contrast, cell attachment and viability are similar or even improved as compared to the well-established ConA control. It is also clear that there are differences between the as-grown surfaces and the two types of treated surfaces. On the basis of the present knowledge it is not possible to explain these results in detail. But it is worth to point out that there are at least two differences between the treated and the as-grown surfaces: i) the first are hydrophilic, the latter are hydrophobic; ii) in all cases the surface charge is negative at pH = 7 at which the cell experiments have been performed but the charge is considerably lower for the as-grown sample. Both observations may serve as a starting point for further investigations.

4. Summary

Ultrananocrystalline diamond films have been deposited from 17% CH_4/N_2 mixtures by MWCVD. After deposition, the original H-termination has been rendered to OH- or a mixed NH_2/OH-termination by means of UV/O_3 or NH_3/N_2 plasma treatments, respectively. These three types of surfaces have been thoroughly investigated by XPS, contact angle and ζ-potential measurements. The XPS measurements showed that the surfaces are hydrogen terminated after growth while the UV/O_3 treatment leads to an OH-termination. In the case of the NH_3/N_2 plasma treatment, a mixed OH/NH_2-termination was achieved. The contact angle measurements proved the as-grown surfaces to be hydrophobic while both treatments led to highly hydrophilic surfaces.

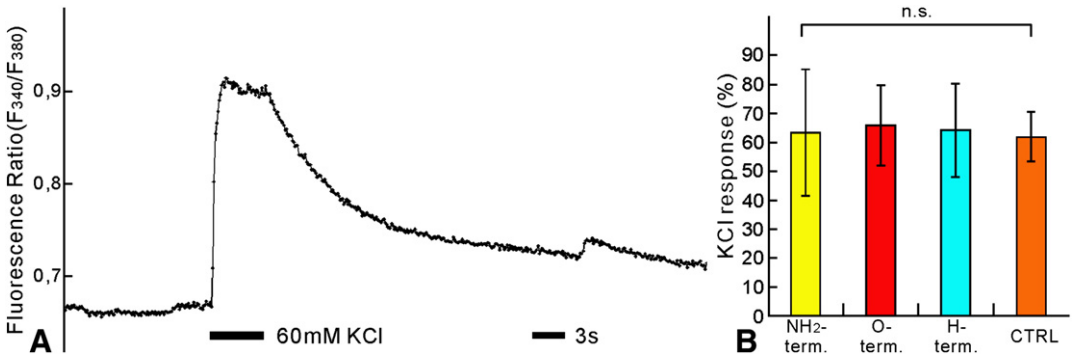

Fig. 5. A,B. Calcium imaging of insect circadian pacemaker neurons in response to 60 mM extracellular KCl solution. A: The increase of intracellular Ca^{2+} concentration from baseline was induced by a 5 s pulse of Ringer solution containing 60 mM KCl (black bars at the bottom). B: The responses were expressed as percentage of the baseline ($\Delta R/R_{baseline} \times 100\%$). The KCl responses of neurons on the four surfaces did not differ (ANOVA LSD $p>0.05$) significantly.

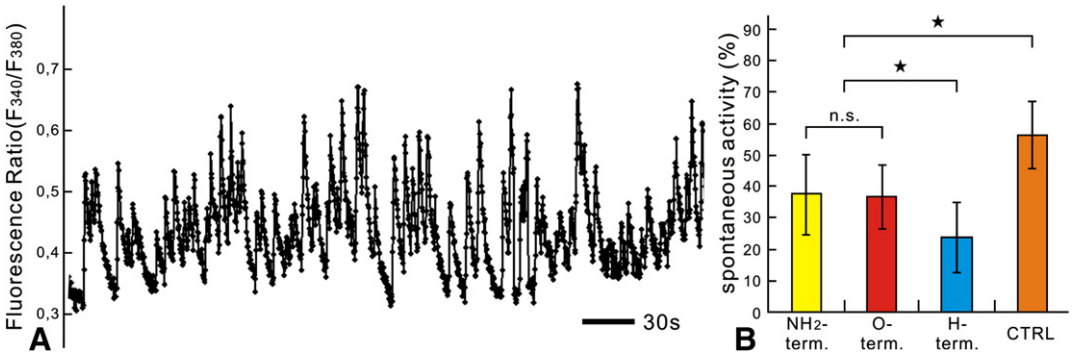

Fig. 6. A,B. Insect circadian pacemaker neurons grown on UNCD surfaces express a decreased spontaneous activity. A: In calcium imaging experiments the neurons grown on a control sample showed spontaneous, fast, transient rises of the intracellular Ca^{2+}-concentration. B: Percentage of cells displaying spontaneous activity in primary cell cultures. The percentages of active cells on the treated UNCD surfaces showed no significant difference (ANOVA LSD $p > 0.05$). However, they were significantly more active than cells on the as grown surfaces and less active than cells grown on the control surfaces (ANOVA LSD $p < 0.05$).

ζ-potential measurements have shown that the isoelectric point of as-grown samples is distinctly higher than those of the two treated surfaces. Studies of the interaction of these three types of surfaces with neurons showed that none of them is cytotoxic. Cell attachment was found to be best for the two treated surfaces. A slightly reduced cell activity as compared to ConA control samples may even be of advantage since it reflects a more natural hyperpolarized state of the cells.

References

[1] J.A. Carlisle, O. Auciello, Electrochem. Soc. Interface 12 (2003) 28.
[2] C.E. Nebel, B. Rezek, D. Shin, H. Uetsuka, N. Yang, J. Phys. D 40 (2007) 6443.
[3] S. Szunerits, R. Boukherroub, J. Solid State Electrochem. 12 (2008) 1205.
[4] L. Tang, C. Tsai, W.W. Gerberich, L. Kruckeberg, D.R. Kania, Biomaterials 16 (1995) 483.
[5] B.D. Thoms, M.S. Owens, J.E. Butler, C. Spiro, Appl. Phys. Lett. 65 (1994) 2957.
[6] C.G. Specht, O.A. Williams, R.B. Jackman, R. Schoepfer, Biomaterials 25 (2004) 4073.
[7] W. Kulisch, Deposition of Superhard Diamond–Like Materials, Springer Tracts on Modern Physics, Heidelberg Berlin, 1999.
[8] P.W. May, Philos. Trans. R. Soc. Lond. A 358 (2000) 473.
[9] P.K. Bachmann, W.v. Enckevort, Diamond Relat. Mater. 1 (1992) 1021.
[10] J. Butler, Electrochem. Soc. Interface 12 (2003) 22.
[11] W. Kulisch, C. Popov, Phys. Status Solidi A 203 (2006) 203.
[12] O.A. Williams, M. Daenen, J. D'Haen, K. Haenen, J. Maes, V.V. Moshchalkov, M. Nesladek, D.M. Gruen, Diamond Relat. Mater. 15 (2006) 654.
[13] D.M. Gruen, Annu. Rev. Mater. Sci. 29 (1999) 211.
[14] W. Kulisch, C. Popov, G. Ceccone, D. Gilliland, J.P. Reithmaier, F. Rossi, Surf. Coat. Technol. 206 (2011) 667.
[15] G.-J. Zhang, K.-S. Chong, Y. Nakamura, T. Ueno, T. Funatsu, I. Ohdomari, H. Kawarada, Langmuir 22 (2006) 3728.
[16] J.-H. Yang, K.-S. Chong, G.-J. Zhang, K.-S. Chong, M. Degawa, Y. Sasaki, I. Ohdomari, H. Kawarada, Langmuir 22 (2006) 11245.
[17] Y. Coffinier, S. Szunerits, B. Marcus, R. Desmet, O. Melnyk, L. Gengembre, E. Payen, D. Delabouglise, R. Boukherroub, Diamond Relat. Mater. 16 (2007) 892.
[18] S. Torrengo, A. Miotello, L. Minati, I. Bernagozzi, M. Ferrari, M. Dipalo, E. Kohn, G. Speranza, Diamond Relat. Mater. 20 (2011) 990.
[19] W. Kulisch, C. Popov, D. Gilliland, G. Ceccone, A. Ruiz, F. Rossi, Diamond Relat. Mater. 18 (2009) 745.
[20] W. Kulisch, C. Popov, D. Gilliland, G. Ceccone, J.P. Reithmaier, F. Rossi, Surf. Interface Anal. 42 (2010) 1152.
[21] H. Koch, W. Kulisch, C. Popov, R. Merz, B. Merz, J.P. Reithmaier, Diamond Relat. Mater. 20 (2011) 254.
[22] A. Thalhammer, R.J. Edgingt, L.A. Cingolani, R. Schoepfer, R.B. Jackman, Biomaterials 31 (2010) 2097.
[23] P. Ariano, A. Lo Giudice, A. Marcantoni, E. Vittone, E. Carbone, D. Lovisolo, Biosens. Bioelectron. 24 (2009) 2046.
[24] P. Ariano, O. Budnyk, S. Dalmazzo, D. Lovisolo, Ch. Manfredotti, P. Rivolo, E. Vittone, Eur. Phys. J. E 30 (2009) 149.
[25] Y.-C. Chen, D.-C. Lee, C.-Y. Hsiao, Y.-F. Chung, H.-C. Chen, J.P. Thomas, W.-F. Pong, N.-H. Tai, I.-N. Lin, I.-M. Chu, Biomaterials 30 (2009) 3428.
[26] K.F. Chong, K.P. Loh, S.R.K. Vedula, C.T. Lim, H. Sternschulte, D. Steinmüller, F.S. Sheu, Y.L. Zhong, Langmuir (2007) 5615.
[27] W. Kulisch, C. Popov, S. Bliznakov, G. Ceccone, D. Gilliland, L. Sirghi, F. Rossi, Thin Solid Films 515 (2007) 8407.
[28] W. Kulisch, C. Popov, T. Sasaki, L. Sirghi, H. Rauscher, F. Rossi, J.P. Reithmaier, Phys. Status Solidi A 208 (2011) 70.
[29] C. Popov, W. Kulisch, P.N. Gibson, G. Ceccone, M. Jelinek, Diamond Relat. Mater. 13 (2004) 1371.
[30] C. Popov, W. Kulisch, S. Boycheva, K. Yamamoto, G. Ceccone, Y. Koga, Diamond Relat. Mater. 13 (2004) 2071.
[31] W. Kulisch, T. Sasaki, F. Rossi, C. Popov, C. Sippel, D. Grambole, Phys. Status Solidi RRL 2 (2008) 77.
[32] H.Y. Wei, M. Stengl, J. Biol. Rhythms 26 (2011) 507.
[33] B. Petri, M. Stengl, Cell Tissue Res. 296 (1999) 77.
[34] V. Chakrapani, A.B. Anderson, J.C. Angus, AIChE Annu. Meet. Conf. Proc., 395c, 2005, p. 1.
[35] A. Härtl, J.A. Garrido, S. Nowy, R. Zimmermann, C. Werner, D. Horinek, R. Netz, M. Stutzmann, J. Am. Chem. Soc. 129 (2007) 1287.
[36] M. Jelinek, K. Smetana, T. Kocourek, B. Dvorankova, J. Zemek, J. Remsa, T. Luxbacher, Mater. Sci. Eng. B 169 (2010) 89.
[37] E. Lee, J. Choi, Surf. Coat. Technol. 148 (2001) 234.
[38] N.L. Schneider, M. Stengl, J. Neurosci. 25 (2005) 5138.
[39] S.J. Chen, C.C. Lin, W. Tuan, C. Tseng, R. Huang, J. Biomed. Mater. Res. 93 (2010) 1482.

ACKNOWLEDGEMENTS

First and foremost, I would like to thank my supervisor Prof. Dr. Monika Stengl for giving me the opportunity to stay in her laboratory for the PhD and for her constant encouragement and guidance in many aspects.

My special thank is addressed to Dr. Wolfgang W. Schwippert for helpful suggestions in many regards.

I also thank Prof. Dr. Charlotte Helfrich-Förster to take the part of the second referee of this thesis, and Prof. Dr. Jörg H. Kleinschmidt and Dr. Cyril Popov for their participation in the examination commission.

I extend my gratitude to El-Sayed Baz for the nice teamwork and critically reading of the thesis. I thank Alexandra Voss for the excellent cooperation

I thank Christa Uthof for her expert technical assistance.

I wish to express my most sincere thanks to husband Yi Zhang and my parent for their unconditional assistance and emotional support.